



COCORA 2011

The First International Conference on Advances in Cognitive Radio

April 17-22, 2011

Budapest, Hungary

COCORA 2011 Editors

Eugen Borcoci, Politehnica University of Bucharest, Romania

Pascal Lorenz, University of Haute Alsace, France

COCORA 2011

Foreword

The First International Conference on Advances in Cognitive Radio [COCORA 2011], held between April 17 and 22 in Budapest, Hungary, was an inaugural event dealing with various aspects, advanced solutions and challenges in cognitive (and collaborative) radio networks. It covered fundamentals on cognitive and collaborative radio, specific mechanism and protocols, signal processing (including software defined radio) and dedicated devices, measurements and applications.

Most of the national and cross-national boards (FCC, European Commission) have a series of activities in the technical, economic, and regulatory domains in searching for better spectrum management policies and techniques, due to spectrum scarcity and spectrum underutilization issues. Therefore, dynamic spectrum management via cognition capability can make opportunistic spectrum access possible (either by knowledge management mechanisms or by spectrum sensing functionality). The main challenge for a cognitive radio is to detect the existence of primary users reliably in order to minimize the interference to licensed communications. Optimized collaborative spectrum sensing schemes give better spectrum sensing performance. Effects as hidden node, shadowing, fading lead to uncertainties in a channel; collaboration has been proposed as a solution. However, traffic overhead and other management aspects require enhanced collaboration techniques and mechanisms for a more realistic cognitive radio networking.

We take here the opportunity to warmly thank all the members of the COCORA 2011 Technical Program Committee, as well as the numerous reviewers. The creation of such a broad and high quality conference program would not have been possible without their involvement. We also kindly thank all the authors who dedicated much of their time and efforts to contribute to COCORA 2011. We truly believe that, thanks to all these efforts, the final conference program consisted of top quality contributions.

Also, this event could not have been a reality without the support of many individuals, organizations, and sponsors. We are grateful to the members of the COCORA 2011 organizing committee for their help in handling the logistics and for their work to make this professional meeting a success.

We hope that COCORA 2011 was a successful international forum for the exchange of ideas and results between academia and industry and for the promotion of progress in the field of cognitive radio.

We are convinced that the participants found the event useful and communications very open. We also hope the attendees enjoyed the historic charm of Budapest, Hungary.

COCORA 2011 Chairs:

Hang Chen, Johnson C. Smith University - Charlotte, USA
Miguel Garcia Pineda, Polytechnic University of Valencia, Spain
Amer Hassan, Microsoft Corporation, USA
Ivana Maric, Aviat Networks - Santa Clara, USA

Amor Nafkha, SUPELEC, France

Homayoun Nikookar, Delft University of Technology, The Netherlands

Adrian Popescu, Blekinge Institute of Technology - Karlskrona, Sweden

Arnd-Ragnar Rhiemeier, Cassidian Electronics - Ulm, Germany

Qin Xin, Simula Research Laboratory, Norway

Tomohiko Taniguchi, Fujitsu Laboratories Limited, Japan

COCORA 2011

Committee

COCORA Advisory Chairs

Amor Nafkha, SUPELEC, France
Tomohiko Taniguchi, Fujitsu Laboratories Limited, Japan
Homayoun Nikookar, Delft University of Technology, The Netherlands
Hang Chen, Johnson C. Smith University - Charlotte, USA
Adrian Popescu, Blekinge Institute of Technology - Karlskrona, Sweden

COCORA Industry/Research Chairs

Amer Hassan, Microsoft Corporation, USA
Qin Xin, Simula Research Laboratory, Norway
Arnd-Ragnar Rhiemeier, Cassidian Electronics - Ulm, Germany
Ivana Maric, Aviat Networks - Santa Clara, USA

COCORA Publicity Chair

Miguel Garcia Pineda, Polytechnic University of Valencia, Spain

COCORA 2011 Technical Program Committee

Anwer Al-Dulaimi, Brunel University, UK
Ilham Benyahia, Université du Québec en Outaouais, Canada
Francisco Bernardo, Universidad de Sevilla, Spain
Hang Chen, Johnson C. Smith University, USA
Xiaoying Gan, Shanghai Jiao Tong University, China
Amer Hassan, Microsoft Corporation, USA
Abubakar Sadiq Hussaini, Instituto de Telecomunicações - Aveiro, Portugal
Insoo Koo, University of Ulsan, South Korea
Thomas D. Lagkas, University of Western Macedonia, Greece
Jia-Chin Lin, National Central University, Taiwan
Ivana Maric, Aviat Networks - Santa Clara, USA
Amor Nafkha, SUPELEC, France
Homayoun Nikookar, Delft University of Technology, The Netherlands
Dominique Noguét, CEA-LETI, France
Adrian Popescu, Blekinge Institute of Technology - Karlskrona, Sweden
Neeli R. Prasad, Aalborg University, Denmark
Arnd-Ragnar Rhiemeier, Cassidian Electronics - Ulm, Germany
Gonzalo Seco-Granados, Universitat Autònoma de Barcelona, Spain
Tomohiko Taniguchi, Fujitsu Laboratories Limited, Japan
Qin Xin, Simula Research Laboratory, Norway
Xiaochun Xu, University of Florida, USA
Liaoyuan Zeng, University of Limerick, Ireland

Copyright Information

For your reference, this is the text governing the copyright release for material published by IARIA.

The copyright release is a transfer of publication rights, which allows IARIA and its partners to drive the dissemination of the published material. This allows IARIA to give articles increased visibility via distribution, inclusion in libraries, and arrangements for submission to indexes.

I, the undersigned, declare that the article is original, and that I represent the authors of this article in the copyright release matters. If this work has been done as work-for-hire, I have obtained all necessary clearances to execute a copyright release. I hereby irrevocably transfer exclusive copyright for this material to IARIA. I give IARIA permission to reproduce the work in any media format such as, but not limited to, print, digital, or electronic. I give IARIA permission to distribute the materials without restriction to any institutions or individuals. I give IARIA permission to submit the work for inclusion in article repositories as IARIA sees fit.

I, the undersigned, declare that to the best of my knowledge, the article does not contain libelous or otherwise unlawful contents or invading the right of privacy or infringing on a proprietary right.

Following the copyright release, any circulated version of the article must bear the copyright notice and any header and footer information that IARIA applies to the published article.

IARIA grants royalty-free permission to the authors to disseminate the work, under the above provisions, for any academic, commercial, or industrial use. IARIA grants royalty-free permission to any individuals or institutions to make the article available electronically, online, or in print.

IARIA acknowledges that rights to any algorithm, process, procedure, apparatus, or articles of manufacture remain with the authors and their employers.

I, the undersigned, understand that IARIA will not be liable, in contract, tort (including, without limitation, negligence), pre-contract or other representations (other than fraudulent misrepresentations) or otherwise in connection with the publication of my work.

Exception to the above is made for work-for-hire performed while employed by the government. In that case, copyright to the material remains with the said government. The rightful owners (authors and government entity) grant unlimited and unrestricted permission to IARIA, IARIA's contractors, and IARIA's partners to further distribute the work.

Table of Contents

IPSAG Cognitive Radio Routing Protocol: Models and Performance <i>Cornelia-Ionela Badoi, Victor Croitoru, and Adrian Popescu</i>	1
Deployment Strategies in Competitive Wireless Access Networks <i>Dina Pamela Gonzalez Sanchez and Jens Zander</i>	7
A Routing Strategy for Cognitive Radio Networks Using Fuzzy Logic Decisions <i>Ali El Masri, Naceur Malouch, and Hicham Khalife</i>	13
An Application-Oriented Routing Protocol for Multi-hop Cognitive Radio Networks <i>Ba Lam To, Thuong Van Vu, Thi Mai Trang Nguyen, and Anne Fladenmuller</i>	19
Improving Spectrum Sensing Performance by using Eigenvectors <i>Roberto Garello and Yifan Jia</i>	26
Iterative Decision Feedback Equalization for Filter Bank Multicarrier Systems <i>Zsolt Kollar, Gabor Peceli, and Peter Horvath</i>	31
Impact of Control Channel Design on Cooperative Spectrum Sensing in Opportunistic Spectrum Access Networks <i>Marco Petracca, Franco Mazzenga, Remo Pomposini, Francesco Vatalaro, and Romeo Giuliano</i>	36
Broadcast Signaling for a Centralized Cognitive Radio Network with Distributed Control <i>Nicolas Bolivar and Jose Marzo</i>	42
A Flexible Bufferless H-ARQ Processor Based on Dataflow Scheduling <i>Pierre-Henri Horrein, Christine Hennebert, and Frederic Petrot</i>	48
Optimal Pilot Placement in Cognitive Radio Systems for Wiener Filtered MMSE Channel Estimation <i>Boyan Soubachov and Neco Ventura</i>	54
Deriving the Key Electrical Specifications for a Multi-Standard Radio Receiver <i>Silvian Spiridon, Florentina Spiridon, Claudius Dan, and Mircea Bodea</i>	60
Cyclostationarity Detection of DVB-T Signal: Testbed and Measurement <i>Matthieu Gautier, Marc Laugeois, and Philippe Hostiou</i>	64
A Censored and Ordered Sequential Evidence Theory Based Collaborative Spectrum Sensing Scheme for CRAHN <i>Nhan Nguyen-Thanh and Insoo Koo</i>	70

DVB-T Receiver Performance Measurements Under Secondary System Interference

75

Jussi Kerttula and Riku Jantti

Efficient Mid-end Spectrum Sensing Implementation for Cognitive Radio Applications based on USRP2 Devices

81

Daniel Denkovski, Vladimir Atanasovski, and Liljana Gavrilovska

IPSAG Cognitive Radio Routing Protocol: Models and Performance

Cornelia-Ionela Bădoi, Victor Croitoru
 Faculty of Electronics, Telecommunications and
 Information Technology
 “POLITEHNICA” University of Bucharest
 Bucharest, Romania
 e-mails: cbadoi@elcom.pub.ro,
croitoru@adcomm.pub.ro

Adrian Popescu
 School of Computing
 Blekinge Institute of Technology
 Karlskrona, Sweden
 e-mail: adrian.popescu@bth.se

Abstract—The paper is about performance evaluation of the IP Spectrum Aware Geographic routing protocol (IPSAG). IPSAG is an opportunistic cognitive routing protocol, which determines a source-destination route in a hop-by-hop manner, based on global and local information. Simulation results are reported for a particular case of IPSAG, where the cognitive radio (CR) nodes are uniformly distributed inside the cognitive radio network (CRN) and a two-dimensional random walk model is used to model the mobility of CR nodes. The results show that the IPSAG protocol is performing well in the case of a highly mobile CRN and that the source-destination path is successfully found in the majority of cases, especially when the network is highly populated.

Keywords—Cognitive Radio Network (CRN); IP Spectrum Aware Geographic (IPSAG) routing; random walk

I. INTRODUCTION

Cognitive Radios (CR) have been suggested as a solution to the problem of scarce spectrum resource, by giving the possibility for the secondary users to use the licensed users channels sensed to be free.

In relation to the existing wireless technologies, the CR technology has a revolutionary character by providing new functions. The most representative functions are:

- *Sensing function*: the CR terminal is able to sense the entire environment and accordingly change the behavior.
- *Sharing function*: the CR users must respect the primary users priority regarding the channel access and, at the same time, must be able to share the free channels with other CR users.

The new features have a strong impact on the routing function. Due to the unstable nature of CRNs, regarding both node mobility and channel availability in time, a very dynamic routing protocol is needed. In this direction, especially when the channel availability period is much lower than the CR transmission duration, there is need for a totally opportunistic routing [1].

Today, a large number of suggested CR routing are based on existing routing algorithms for ad-hoc networks, adjusted to respond to CR demands. Most of the solutions are based on the Ad Hoc On-Demand Distance Vector protocol (AODV), while limiting the broadcast area of the Route Request (RREQ) message [2].

Furthermore, in order to avoid the network flooding with control messages, source/destination based routing solutions are advanced. In this case, the needed information is obtained with the help of Common Control Channel (CCC) [1].

Along with the traditional factors (delay, interference, throughput), the routing metrics also include the fluctuation of the link availability. The vacant channels are selected based on probabilistic information [3] or by considering the switching frequency from one channel to another [4].

Within this context, the IP Spectrum Aware Geographic routing protocol (IPSAG) was advanced as a solution to routing in CRNs [5]. IPSAG uses the IP principle of step-by-step forwarding with respect to the channel availability status, QoS features and CR node geographic positions.

The paper evaluates the IPSAG behavior in different mobility conditions, from stationary to high CR mobile nodes. The CRN model is implemented and tested in Java.

The rest of the paper is as follows. Section II describes the IPSAG protocol functionality. Section III presents the advanced CRN model to test IPSAG correctness. Sections IV and V provide the obtained results of IPSAG simulation in a one-cell and a seven-cells CRN, respectively. Section VI concludes the paper.

II. IPSAG PROTOCOL DESCRIPTION

The IPSAG protocol is a highly opportunistic protocol for CRN routing. IPSAG is inspired by the IP flexibility regarding the route selection process. The path is determined step-by-step according to a position-based approach, which also considers the channels availability and the Quality of Service (QoS) features.

The characteristics of the protocol are as follows [5]:

- The next-hop decision process is an individual one, taken by each CR node on the source-destination path. No previous determined route is used when forwarding the data packet. This is the basic concept of IP.
- The spectrum opportunities of CR nodes are considered when constructing the step-by-step path: a link between two CR nodes can be part of the source-destination route if the corresponding CR nodes have at least one joint channel sensed to be free; i.e., IPSAG is a spectrum aware routing protocol.

- QoS elements in the form of signal-to-noise ratio (SNR) are considered in determination of a channel between two arbitrary nodes. Hereby, a channel sensed to be free is allocated only if the channel has the SNR above a given threshold.
- Geographical routing principles are used to reach the CR destination node. Given the CR neighbors with common spectrum opportunities (SOP) with QoS, the CR node selects the next-hop to be the one closest to the destination.

The local decision process regarding the next-hop election is as follows (see Figure 1):

- Each CR node determines its geographical neighbors inside a circle (with the node at the center and variable radius, usually selected to be equal with the transmission range).
- Within the neighborhood, the CR node determines the neighbors with which it has common SOP (also satisfying the QoS demands);
- The next-hop is the closest node to the destination between the pre-determined neighbors.

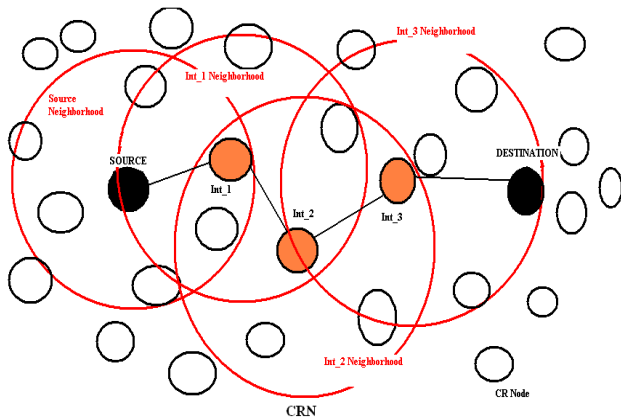


Figure 1. IPSAG routing example [5]

For instance, in Figure 1, the Source is running IPSAG inside its neighborhood and chooses node Int_1 as the next hop to forward the packet. Similarly, node Int_1 selects node Int_2, and Int_2 selects Int_3 to be the next-hops. Finally, node Int_3 determines that the destination is located in its neighborhood and forwards the packet [5].

III. SIMULATIONS MODELS

In order to analyze the IPSAG performance for mobile CR nodes, a CRN model has been created in Java. The elements that provide the CRN simulation environment are:

- *Channel class*, which models the primary radio channel. The channel is characterized by an availability status and a variable SNR. It also has an index based on which it is identified in the corresponding cell. In our simulations the channel status is considered to vary between “available/unavailable” with a probability of 0.5 at each IPSAG iteration.
- *Cell class*, which models the radio cell. This class extends the Polygon Java class and it is described by the

set of radio channels that can be utilized on its area. Also, in each cell, the available radio channels at a given time, which correspond to a required SNR threshold, can be determined.

- *Node class*, which models the CR node. Each node is able to determine and maintain a table with its neighbors, and it can choose the next-hop when running IPSAG. The neighborhood radius along which the node discovers its neighbors can be varied. The CR node can determine the cell in which it is located at a given time. It is identified by a global index in the CRN. Initially, the CR nodes are uniformly distributed along the network and each CR node moves across CRN according to the two-dimensional random walk model in a discrete manner [6]. At each IPSAG iteration, the CR node has the possibility to move with a probability of 0.5 at left/right and up/down, respectively. The random walk implementation avoids the CR nodes exceeding the CRN perimeter. The case when a CR node crosses the border is not considered.
- *Network class*, which models the CRN. The user can set the simulation parameters. These are: total number of CR nodes, number of cells that form the CRN, number of radio channels per cell, geographical dimensions of the radio cell, number of the channels belonging to the Industrial, Scientific and Medical (ISM) band used for inter-cells routing and the random-walk step where the nodes are moving.

Two CRN models are used in our simulations, namely one cell CRN and seven cells CRN (see Figure 2).

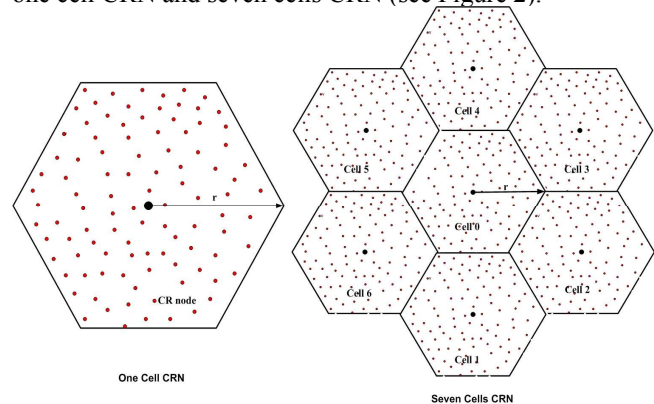


Figure 2. The CRN models used in simulations

In the first case, the IPSAG routing is used inside the cell. In the second case, the IPSAG routing is extended for inter-cells routing, with the difference that the channels are allocated from the ISM band.

In all simulation cases we consider a number of 120 radio channels per cell. This corresponds to the spectrum reutilization scheme factor of $N=3$, for the 800 MHz band (62 carriers for each uplink/downlink communications direction) [7]. As mentioned above, the channel availability is varied at each IPSAG iteration with a 0.5 probability.

Furthermore, the cell radius is considered to be 2 000 m, which is a common value.

IV. SIMULATIONS RESULTS – ONE CELL

The IPSAG simulations focus on the probability to successfully find a source-destination route. Also, the probability of not finding the route from the first attempt is analyzed in different conditions. According to [8], this is the first performance criteria when evaluating a total opportunistic routing protocol. At the same time, the number of intermediary nodes between source and destination is observed. In this case, the results are reported with a confidence interval of 95 %.

The parameters considered in the simulations are:

- The *random walk step*, from the stationary case to a step value around the transmission range of 533 m [9];
- The *number of CR nodes*, which gives information about the manner in which IPSAG is performing in a poorly/highly populated CRN;
- The *neighborhood radius value* of the circle, inside which a CR node determines its neighbors.

Our results are as follows.

A. Experiments regarding the random walk step

For this simulation type, different movement situations are considered (random walk step values of 50, 100, 250, 350 and 500 m, respectively) such as to analyze the influence on the IPSAG behavior. The number of CR nodes is maintained constant (100 nodes), a value that is very close to the number of radio channels (120).

As we observe in Figure 3, the average number of intermediary nodes grows with the random walk step.

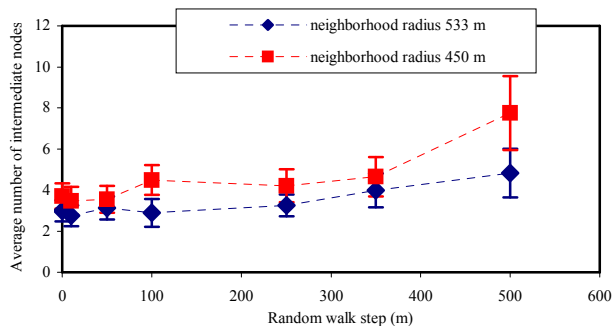


Figure 3. The CR nodes random walk step influence on the number of intermediate nodes

At the same time it can be observed that a higher value for the neighborhood radius decreases the number of intermediary nodes along the path. This is because a higher number of CR nodes means a higher number of next-hop candidates, influencing thus the optimum next-hop selection.

We compare our protocol with two other CR protocols. These are Cognitive On-Demand Distance Vector (CAODV), which is an improvement of AODV protocol for CRN [10], and Opportunistic Service Differentiation Routing Protocol (OSDRP), which chooses the “minimum delay-maximum stability” route based on the channels availability issues [11]. The performance of these protocols has been observed to be similar to the IPSAG one cell case,

for 100 CR nodes. Thus, if IPSAG gives an average hop count number of 2.5, respectively of 4 [see Figure 3], COADV offers an average hop count of 3.5/4 (see Figure 8 in [10]) while OSDRP gives a total number of 3 to 8 intermediary CR nodes (see Figure 4 in [11]), depending on the particular simulations parameters.

An important advantage is that, in a highly mobile CRN, IPSAG has a larger probability to find the source-destination route from the first attempt compared with the stationary case (see Figure 4). In other words, regarding the path determination, IPSAG is performing better in a mobile environment than in a stationary case.

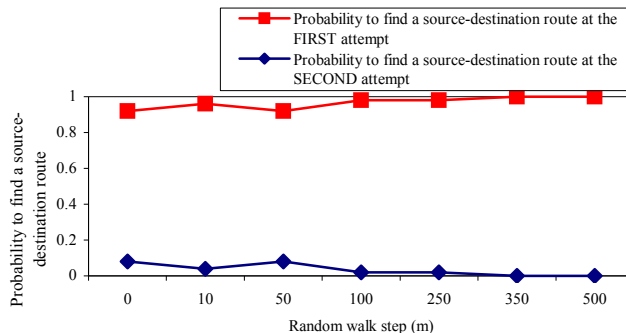


Figure 4. Probability to find the source-destination route (533 m neighborhood radius)

A small degradation in finding the path at the first attempt is observed when decreasing the neighborhood radius. However, this still has a better behavior at a high random-walk steps (see Figure 5).

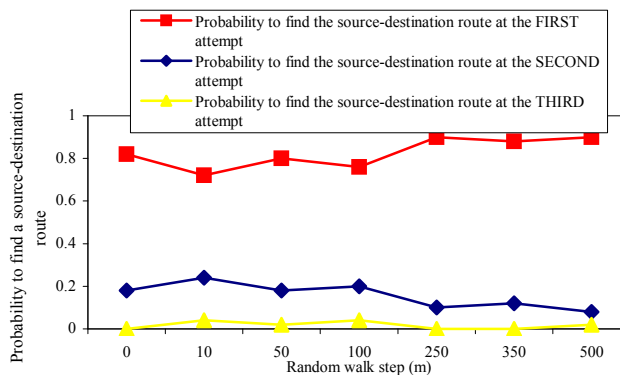


Figure 5. Probability to find the source-destination route (450 m neighborhood radius)

These results show therefore that IPSAG is performing very well in the case of mobile CR nodes. The neighborhood radius value can however diminish the performance at lower values or improve it at higher values, which are approaching the transmission range.

B. Experiments regarding the number of CR nodes

These experiments focus on the number of CR nodes and the influence on the IPSAG behavior. In the previous

simulations the number of CR nodes was maintained constant, but in this case it varies between 50 and 200. Also, the neighborhood radius is preserved at an optimum value, represented by the transmission range (533 m).

The simulation results show that, in a highly populated network, IPSAG is behaving better than in a poorly populated CRN. As it can be observed in Figure 6, the average number of intermediary nodes is bigger when there are only few CR nodes inside CRN. The simulation results confirm the previous results according to which the average number increases with the random walk step (see Figure 2).

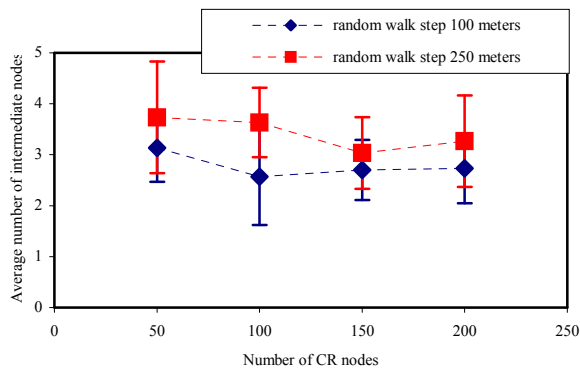


Figure 6. The number of CR nodes influence on the average number of intermediate nodes in the source-destination path

The probability of finding the route from the first attempt is approximately maximum when the CRN is very populated, and significantly decreases (0.7) for a lower number of CR nodes (see Figure 7).

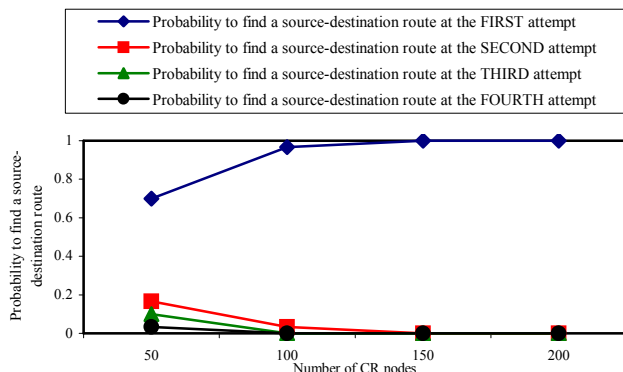


Figure 7. Probability of finding the source-destination route (random walk step 100 m)

The probability of successfully finding the route is considerably low when the CR numbers and the random walk step have small values. The worse case scenario is considered for 50 CR nodes and a random walk step of 100 m, when this probability is going to be approximately 0.6 (see Figure 7). When the CR nodes are stationary, this probability becomes lower than 0.6.

This decrease is however improved in a highly mobile environment (see Figure 8). If, at a 100 m value for the

random walk step, the probability to find the route at the first attempt is around 0.7, for a 250 m step this probability increases at 0.8. This result confirms the good performance of IPSAG in a highly mobile network.

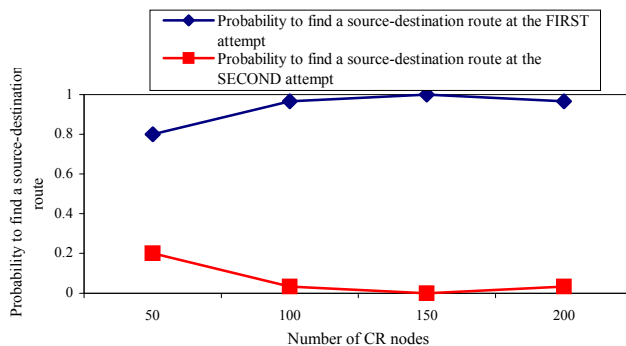


Figure 8. Probability of finding the source-destination route (random walk step 250 m)

Thus, the results clearly show that a populated CRN improves the IPSAG performance.

V. SIMULATIONS RESULTS – SEVEN CELLS CLUSTER

The conditions considered in Section 4 remain valid. A number of 120 radio channels and a cell radius of 2000 m, respectively, are maintained for each cell. Also, the average number of intermediary nodes along the path and the probability to successfully find the route are considered in evaluating IPSAG. In addition, the average number of inter-cells routing is analyzed.

A. Experiments regarding the random walk step

The average number of intermediary nodes between the source and destination increases with the growth of the random walk step. A lower neighborhood radius value also increases this parameter (see Figure 9). This is because, in a highly mobile environment, the IPSAG geographical selection of the next-hop (closest neighbor to the destination) does not have the accuracy of the stationary case.

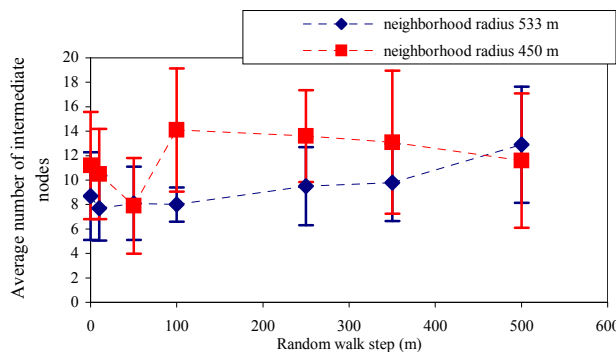


Figure 9. The influence of the step of random walk on the average number of intermediate nodes

At the same time, the average number of inter-cell routing steps has a similar behavior as in the case of average

number of intermediary nodes on the path, but with a smaller dependence (see Figure 10). The low dependence can be explained by the fact that the next-hop is determined at each IPSAG iteration while an inter-cell routing step is done only when the destination is located in another cell.

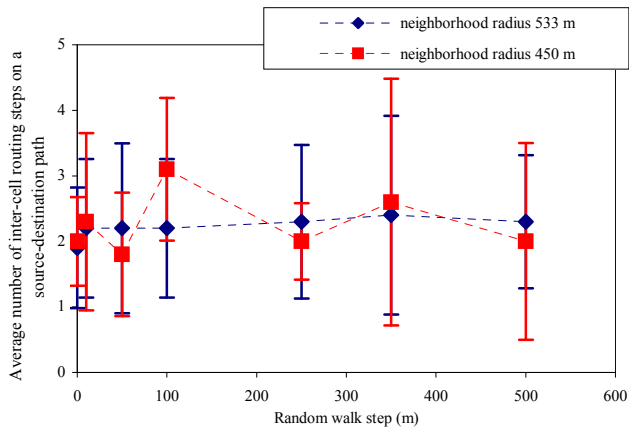


Figure 10. The influence of the step of random walk on the average number of inter-cell routing steps

As it can be observed in Figure 11, the probability of finding the route from the first attempt is good, with the remark that, relative to the one-cell CRN instance, it presents a higher variability. Also, the good behavior of IPSAG for high mobility is maintained. This is because, when CRN is very dynamic, the current node always has neighbors that satisfy the IPSAG conditions. The price is in form of a longer route, given that the number of intermediary nodes increases with the mobility degree.

When the neighborhood radius is reduced, the number of neighbors for a given CR node is also reduced and thus, the probability of finding the route at the first attempt decreases. Furthermore, the tentative number for successfully finding the route increases (see Figure 12).

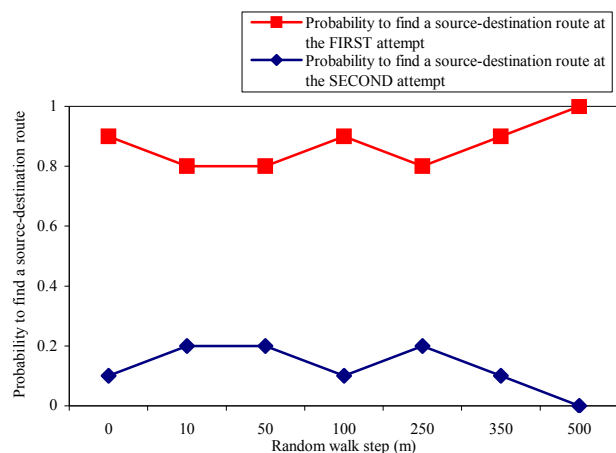


Figure 11. Probability to find the source-destination route (533 m neighborhood radius)

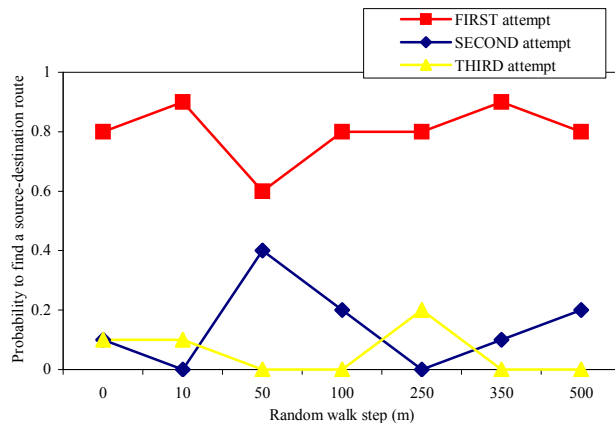


Figure 12. Probability to find the source-destination route (450 m neighborhood radius)

The simulations show therefore that IPSAG is performing well in a high mobility environment, even when the CRN area is broader, with a perceptible deterioration when the neighborhood radius is decreased.

B. Experiments regarding the number of CR nodes

In this experiments set the neighborhood radius is maintained constant (533 m).

As showed in the one-cell CRN case, the increase of the CR nodes number inside the CRN improves the IPSAG performance. When the CRN grows from one cell to a seven cells area, the number of intermediary nodes suffers a 2/3 orders increase (see Figure 13).

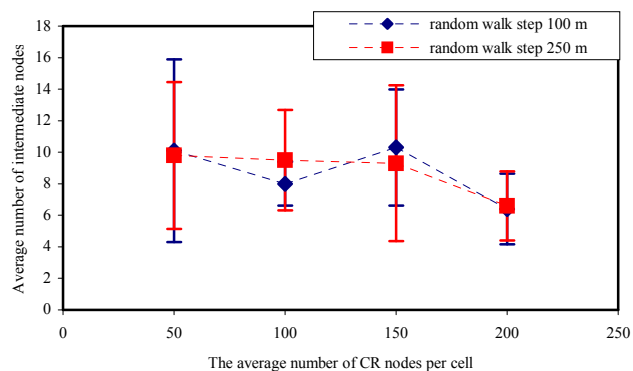


Figure 13. The influence of the number of CR nodes on the average number of intermediate nodes on the source-destination path

Note. Given that the CR nodes are uniformly distributed along the CRN area and they are moving according to the random walk model, the number of CR nodes may be different from one cell to another. This is the reason of using the parameter “average number of CR nodes per cell”.

As expected, a similar behavior shows the average number of inter-cell routing steps with the CR nodes density growth. As shown in Figure 14, this parameter decreases with the increase of the random walk step, which implies a short path.

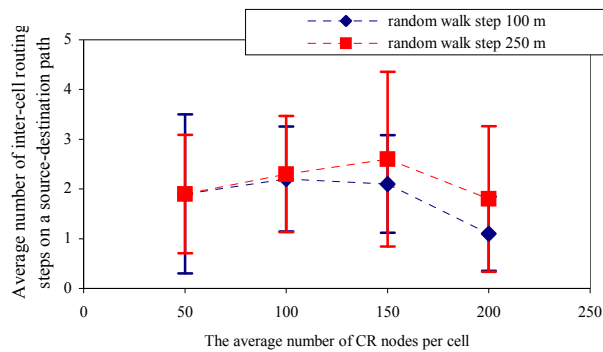


Figure 14. The influence of the number of CR nodes on the average number of inter-cell routing steps on the source-destination path

Similar to the case of a one cell CRN, the probability of finding the path has a high value in a populated CRN (see Figure 15).

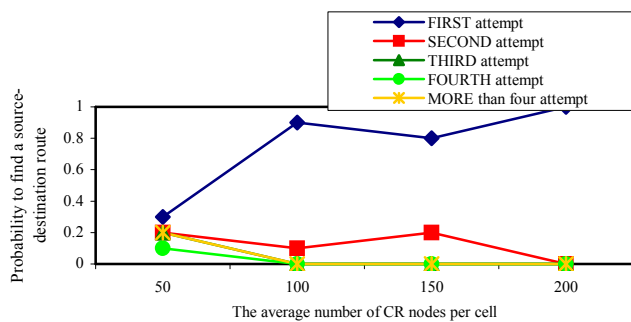


Figure 15. Probability of finding the source-destination route (random walk step 100 m)

Also, there are no major differences for a random walk step variation from 100 m to 250 m (see Figure 16).

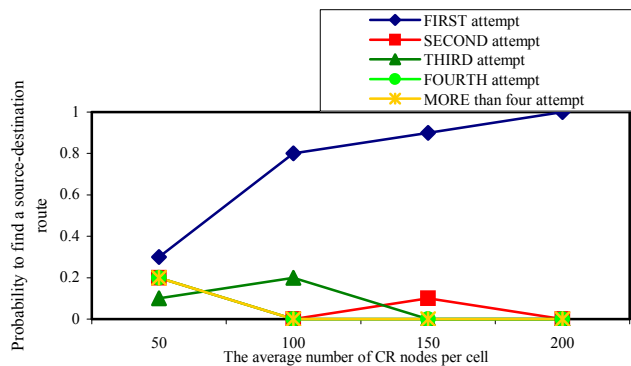


Figure 16. Probability of finding the source-destination route (random walk step 250 m)

Therefore, IPSAG has been proved to perform well even when the CRN area increases.

VI. CONCLUSION AND FUTURE WORK

The paper has focused on evaluating the performance of IPSAG – a new suggested CR routing protocol.

A simple CRN simulator has been developed in Java. The experiments have focused on the IPSAG performance in different mobility conditions. In this respect, a two dimensional random walk model was implemented for the CR nodes.

The simulation results showed that IPSAG is well performing at high random walk steps. The path was successfully found in the majority of cases from the first attempt, with the drawback of a longer route in terms of intermediary nodes between source and destination. Also, it was observed that the IPSAG performance improves in a high populated network and diminishes through the neighborhood radius decrease below the transmission range.

The conclusion is therefore that IPSAG responds very well to the CRN highly dynamism. This good behavior can be explained by the total opportunistic character of the protocol in finding the path.

The future work will focus on the IPSAG performance in large areas, by splitting the network into clusters.

ACKNOWLEDGMENT

The work has been funded by the Sectoral Operational Programme Human Resources Development 2007-2013 of the Romanian Ministry of Labour, Family and Social Protection through the Financial Agreement POSDRU/6/1.5/S/16.

REFERENCES

- [1] H. Khalife, N. Malouch, and S. Fdida, "Multihop cognitive radio networks: to route or not to route", *IEEE Network*, vol. 23, pp. 20–25.
- [2] X. Zhou, D. Zhou, X. Kong, and Q. Sheng, "ACK Signal Based On-Demand Routing Algorithm in Cognitive Radio Networks", *PacRim 2009*, August 2009, pp. 774 – 779.
- [3] H. Khalife, S. Ahuja, N. Malouch, and M. Krunz, "Probabilistic Path Selection in Opportunistic Cognitive Radio Networks", *IEEE Global Telecommunications Conference*, 2008, pp. 1-5.
- [4] S. Krishnamurthy, M. Thoppian, S. Venkatesan, and R. Prakash, "Control channel based MAC-layer configuration, routing and situation awareness for cognitive radio networks", *MILCOM 2005*, pp. 455 – 460.
- [5] C. I. Bădoi, V. Croitoru, and R. Prasad, "IPSAG: An IP Spectrum Aware Geographic Routing Algorithm Proposal for Multi-hop Cognitive Radio Networks", *COMM 2010*, June 2010, pp. 491-496.
- [6] W. Wang, "Modeling and Management of Location and Mobility", in *Wireless Information Hayways*, D. Katsaros, A. Nanopoulos, and Y. Manolopoulos, IRM Press, 2005, pp. 177-212.
- [7] T. Rappaport, "Wireless Communications: Principles and Practice", *Prentice Hall Communications Engineering and Emerging Technologies Series*, 2nd Edition, 2001.
- [8] C. Siva Ram Murthy and B. S. Manoj, "Ad Hoc Wireless Networks – Architectures and Protocols", *Prentice Hall Communications Engineering and Emerging Technologies Series*, 2004, pp. 191-226.
- [9] T. Ohta, K. Ogasawara, and Y. Kakuda, "End-to-End Transfer Rate Adjustment Mechanism for VANET", *IEEE Third International Conference on Dependability*, July 2010, pp. 1-6.
- [10] A. S. Cacciapuoti, C. Calcagno, M. Caleffi, and L. Paura, "CAODV: Routing in mobile ad-hoc cognitive radio networks", *Wireless Days (WD)*, October 2010, pp. 1-5.
- [11] K. C. How, M. Ma, and Y. Qin, "An Opportunistic Service Differentiation Routing Protocol for Cognitive Radio Networks", *GLOBECOM 2010*, December 2010, pp. 1-5.

Deployment Strategies in Competitive Wireless Access Networks

Pamela González Sánchez^{1,2}, Jens Zander¹

¹The Royal Institute of Technology KTH, Radio Communication Systems, 164 40 Kista, Sweden

²National University of Engineering UNI, P.O. Box5595, Managua, Nicaragua

Emails: dpgs@kth.se, jenz@kth.se

Abstract—The rapid growth of mobile internet traffic has forced wireless service providers to deploy increasingly higher capacity in their wireless broadband access systems. The flat rate revenue streams in combination with the rapidly growing costs associated with conventional access deployment is usually referred to as the “revenue gap”. In this context, various schemes for infrastructure sharing to reduce unnecessary duplication of infrastructure present an interesting solution. Besides explicit cooperation, competitive sharing (“coopetition”) where various access providers provide partially overlapping coverage is one interesting sharing mechanism. In this paper, we analyze such a scheme and study how the operator should deploy their networks, striking a balance between areas of exclusive coverage, where each provider has a monopoly situation, and overlap areas with provider competition, to achieve maximal profitability. The competition is based on the proportionally fair auction scheme. The users behave selfishly as they bid for the various access providers. The access providers compete with each other by selecting the so called reservation price. Results are expressed in terms of Nash equilibrium solutions, which are numerically derived for some sample scenarios. Results indicate that the fraction of coverage overlap does play an important role for both the performance of the system and the profitability of the service providers. As the level of overlap between the two networks increases the revenue that each base station gets decreases significantly. In addition, the user experienced throughput degrades considerably for low demand but the cost per transferred Megabyte is not greatly affected. Further, we conclude that a win-win situation for both users and access providers can be achieved with a suitable overlap coverage by two networks.

Index Terms—Wireless access markets; coverage overlap; competition; resource allocation; Nash equilibrium

I. INTRODUCTION

A. Overview

The rapid increase of mobile internet traffic has put the spotlight on how the future wireless broadband access systems should be deployed and operated at significant lower costs per transmitted bit than today. The flat rate revenue streams in combination with the rapidly growing costs associated with conventional access deployment is usually referred to as the “revenue gap. Nowadays, closing this “gap” is on top of the priority list of wireless mobile service providers. Low cost deployment and more efficient utilization of existing resources are key solutions to be investigated.

The traditional way of infrastructure deployment has been that every service provider offers his own access system in all locations, i.e., achieving “full” coverage by himself. This

has been possible in most mobile phone systems due to the relatively low costs and high profit margins. As the increasing data rates require a much denser (and more expensive) network of base stations, full coverage is no longer an option to most service providers. Instead *Infrastructure sharing*, where providers share infrastructure in low user density areas is one possible alternative to offer better coverage and quality of service (QoS) in a cost efficient manner [1].

The sharing of wireless infrastructure, however, raises the question of how resources and revenues should be divided when multiple subsystems, managed by potentially competing actors, are involved in delivering the access service. An alternative would be to share the infrastructure implicitly by establishing an open wireless access market wherein networks not only compete for users on a long-term time-scale, but also on a much shorter time-base. This could be realized with an architecture where autonomous trade-agents, that reside in terminals and access points (APs) or base stations (BSs), manage the resources through negotiations [2]–[5].

In competitive multi-user networks, services are provided to users that are assumed to be rational, choosing strategies in order to maximize their own utility. This resource management problem can be expressed as a noncooperative game and the system performance can be analyzed in terms of the Nash equilibrium, i.e., a set of optimal bids such that no single user wishes to deviate from its bid given that the bids of the other users remain the same and cannot further improve their utility [6]–[8].

B. Prior Work

In [2], the authors developed a framework for studying demand-responsive pricing in contexts where access points (APs) with fully overlapping coverage compete for users. Resources are partitioned through a proportional fair divisible auction and they investigated if, and when, an open market for wireless access can be self-sustained. They showed that in scenario where access providers (APs) compete an open access market results in better services at lower price, compared to a case where APs cooperate. They utilized an architecture where autonomous trade-agents manage the resources through negotiations.

In [4], a market-based framework for decentralized radio resource management in environments populated by multiple,

possibly heterogeneous, APs and the service provided to the users is of file transfers, was introduced. The problem addressed for the user is to determine how much resources it should purchase from the different APs in order to maximize its utility (“value for money”).

In [7], Maheswaran et al. introduced a bidding mechanism for allocation of network resources among competing agents, and study it from a game-theoretic perspective. Although they proved the existence and the uniqueness of Nash equilibrium in a decentralized manner, the user’s performance (QoS) and service providers’ revenue have not been studied.

C. Our problem

In this work we study how competitive sharing (“coopetition”), where various access providers provide partially overlapping coverage in a competitive fashion, can reduce cost.

The scenarios studied can be illustrated as in Figure 1. We analyze how the balance between areas of exclusive coverage, where the provider has a monopoly situation, and overlap areas with provider competition affects the profitability of the access providers. We also analyze how the user’s QoS is affected by this level of overlap among networks and by traffic load variation. A game-theoretic approach and the proportionally fair auction mechanism [9]–[11] are used aiming to answer the following questions:

- How is the operator revenue affected by the level of overlap and the traffic load variations in the system?
- Is the user quality of service, QoS, in terms of available data rate and cost per Megabyte affected by these two parameters?

The rest of the paper is organized as follows. In Section II, we introduce our basic assumptions and describe the wireless architecture-scenario, resource allocation mechanism, and user demand model. Section III gives a thorough overview of the user game. Section IV outlines the service providers’ strategy. In Section V we show the numeral results from simulation and in Section VI we present out the conclusion.

II. SYSTEM MODEL

The system model with the basic assumptions, a description of the scenario under consideration and the resource allocation mechanism applied in this work are introduced in the following.

A. Basic Assumptions - Scenario

Given the network deployment illustrated in Figure 1, the problem for each BS is to select a reservation price, ϵ , so that its expected revenue is maximized. When the user is in a non-overlapping area, this user can only bid for resources from the single BS that provides coverage of this area. This user faces a monopolistic market, since the BS can charge any price due to the absence of a competitor. Both, in overlapping and

nonoverlapping coverage the users may choose not to utilize a specific BS if the price is too high.

Figure 1 illustrates the basic scenario under investigation, where $s_{i,j}^m$ denotes the bid, in monetary units, that user j places in auction i at BS m , in order to get a portion of the available transmission time $x_{i,j}$ for a file transfer (Note that we have assumed a purely time division multiplexed link). The link $user-SP$ indicates the link provided by access provider who dominates the market in this area (i.e., the access providers who provide coverage) and it is to this BS that users should send a positive bid in order to be served.

We model a file download service, specifically, the download time in a wireless TDMA system with N selfish competing users and m BSs with overlapping coverage areas. The BSs are assumed to be identical in transmit power, system bandwidth, minimum received signal to noise ratio requirement, etc.

The resources that we focus on are downlink transmission slots. These slots are allocated to different users in order to share the downlink throughput among them. Allocation of the resource is done through a proportional fair divisible auction. We assume that the resource is infinitesimally divisible and that the cost associated with the file transfer depends on the total time-duration and the monetary expenditure required for the complete file download.

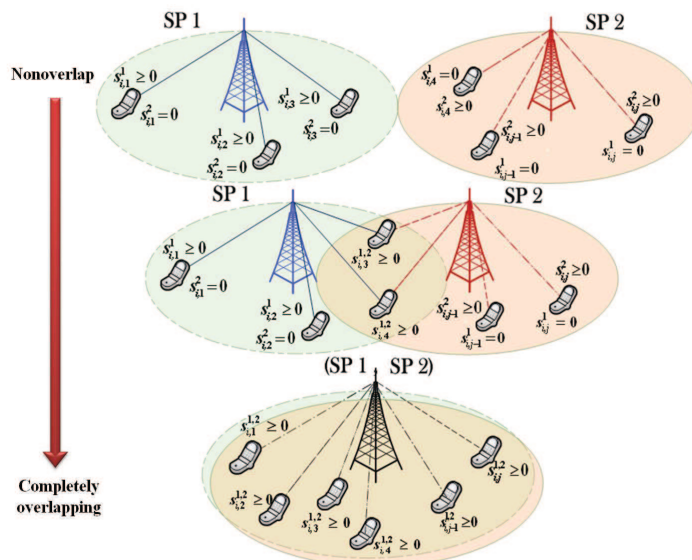


Fig. 1. Basic scenario - Illustration of a wireless network architecture with different percentages of overlap, which represents a system with different levels of competition

As in [2] [4], we investigate a trade-agent-based model for the auction bidding process. The trade-agents are entities located in the BSs, who act selfishly on behalf of their users. The main objective of each trade-agent is to maximize its user’s utility (here computed as value for money). The portion of the transmission time allocated to user j can be expressed

as follows:

$$x_{i,j}(s) = \frac{s_{i,j}}{s_{i,j} + S_{i,-j}} \in [0, 1), \quad (1)$$

where $S_{i,-j}$ represents the strategies (bids) of all the opponents' trade-agents and it is equal to $\sum_{k \neq j} s_{i,k} + \epsilon$ where the reservation price $\epsilon \in [0, \epsilon_{max})$. The reservation price is a nonzero price floor below which the resource will not be sold. Note that by definition the price floor must be nonzero as if it were zero, then there would be no price floor.

Assuming that the peak data-rate of a single user j on whose behalf the trade-agent j is acting, remains unchanged during the entire file transfer and that this applies for all the users, i.e., $R_{i,j} = R_{z,j} \forall i, z$, the total demand associated with the other trade-agents, thus $\sum_{k \neq j} s_{i,k} = \sum_{k \neq j} s_{z,k} \forall i, z$.

Note that z is the last round of the auction. Due to these assumptions, each trade-agent will place identical bids in all the auctions.

B. Resource Allocation Mechanism - Proportionally Fair Divisible Auction

As described in the previous section, the total transmission time is divided via employing a proportional fair divisible auction. In a proportional share allocation scheme each user is characterized by a parameter that expresses the relative share or amount of the resource that it should receive. Hereafter, the bid that the user submits to the BS is used to express the user's share. In this work a dynamic system has been modeled in which users are assumed to dynamically join and leave the competition (game). Therefore, the portion of the resource depends on both the number of users that enter the game and the level of competition at different times. On light of this, this mechanism allows flexibility, since the users can decide when to join or leave the competition, and ensures fairness, which follows from the fact that the users always get a share of the resource proportionally to their bids (as expressed in Equation 1).

The auction process is held by an auctioneer located in the BS (thus since the users' trade-agents are also allocated in the BS all the communication between the trade-agents and the auctioneer is strictly local to the BS). This concept was introduced in [9] and analyzed later in competitive environments for networks with fully overlapping coverage in [2], [4]. We examine the case where the file transfer requires z auctions to complete, i.e., $i = \{1, \dots, z\}$ (see Figure 2).

Figure 2 illustrates the auction procedure associated with a file transfer [4]. In this example trade-agent j initiates a file transfer in auction 1.

Since, at the beginning of each allocation cycle, an interrupt is generated in the system, too short a cycle may cause a large overhead in the system, in the long run (i.e., in Operating Systems each allocation cycle is in the order of milliseconds).

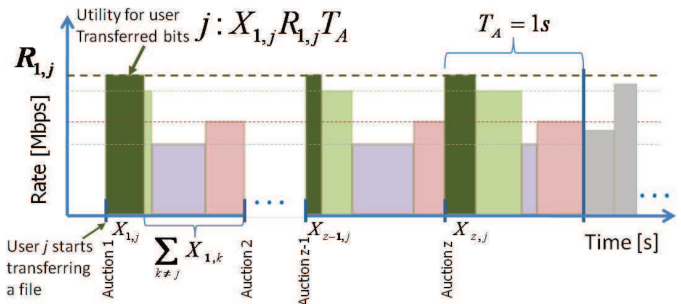


Fig. 2. Illustration of auction procedure associated with a file transfer

On the other hand, a cycle of too long duration (i.e., cycles of one minute) may induce a large delay for the file download, thus, a degradation in the user QoS.

In our analysis, we assume that each auction is carried out every one second [2], [4]. This means that each auction determines the allocation of resources for the time after the conclusion of the auction and that a new auction starts every second. Note that the auction can proceed in parallel with the usage of the link resources for downloading, but this usage is according to the resource allocation determined by the last auction. For simplicity of the analysis, we neglected the overhead that can occur in a real system application.

In a proportional fair resource allocation mechanism, a user knows exactly how much it has to “pay” over any interval of time while this is active, considering that they choose how much they will bid for the resource. The user cannot, however, predict how much service time it will actually receive. This is because the fraction of the resource, and therefore the service time the user will receive, may change at any time depending on the level of competition for the resource [10].

In each auction, user j is allocated a portion $x_{i,j}$ of the total available transmission time during each auction T_A (where $T_A = 1$ second), and depending on its peak data-rate $R_{i,j}$ the agent will be able to transfer a total of $x_{i,j} R_{i,j} T_A$ bits. After participating in z auctions the file transfer is completed and the trade-agent j awaits for a new request from its user to enter the competition again.

C. User Demand Model

A demand function that consists of files with an expected size q in Megabits is considered. Each file arrives to the system of BSs according to a Poisson process characterized by an intensity, λ .

D_0 represents the potentially offered load, which can be defined as $D_0 = q\lambda$, and it is assumed that the aggregate demand is perfectly known for all BSs [2].

III. USER GAME - UTILITY MAXIMIZATION

We focus in finding the Nash Equilibrium Point (NEP) for the reservation price of the resource, ϵ , considering the two

games (competition among users for resources and among BSs for users) in the competition area for different levels of coverage overlap. This NEP is related to the Best Response from the trade-agents (acting on behalf of the users). In the monopolist area (non-overlapping coverage) only competition among users is observed.

By obtaining the NEP we are able to analyze the BS's expected revenue with different levels of competition. These results enable us to predict the users' performance (in terms of throughput and monetary expenditure per transferred file).

The users compete against each other for resources - while trying to maximize their utility function in order to transfer a file. This game is expressed later in Equation (2). For our analysis, we assume that the file size is finite (and identical), $q = 1$ Megabyte.

$$\begin{aligned} \varphi(s_{-j}) &= \arg \max_{s_j} U_{i,j}(s_j, S_{-j}) \\ \forall j \in \{1, \dots, N\}, m \in \{1, 2\}. \end{aligned} \quad (2)$$

In the above equation $U_{i,j}(s_j, s_{-j})$ is related to the throughput, $x_{i,j}R_{i,j}$, associated with user j and is defined as:

$$U_{i,j} = \sum_{m=1}^2 \max \left[0, x_{i,j}R_{i,j}^m - s_{i,j}^m \right]. \quad (3)$$

Deriving the first order solution (i.e., as a linear equation) of Equation (3) with respect to $s_{i,j}^m$ we can obtain the best response (BR), which describes how trade-agent j should react to the strategies (optimal bid that the trade-agent should submit the BSs) of all the other trade-agents in order to maximize its user's utility. This would be expressed as follows:

$$s_{i,j}^m = \sqrt{R_{i,j}^m \left(\sum_{k \neq j} s_{i,k}^m + \epsilon_m \right)} - \sum_{k \neq j} s_{i,k}^m + \epsilon_m. \quad (4)$$

Since the peak transfer rate for all of the users is the same over all auctions, and they all have to transfer the same size file, then giving each user the whole channel (i.e., all of the time slots) enables this user to complete and leave the system, hence leaving all of the remaining resources for the *remaining* users.

The monetary expenditure, E^m , incurred by user j is given by the summation of the bids submitted in all the auctions, z_j , required to download the file, as indicated in:

$$E_j^m = \sum_{i=1}^{z_j} s_{i,j}^m \quad (5)$$

IV. BASE STATION STRATEGY-REVENUE MAXIMIZATION

A. Open Access Market-Competing BSs

This game take place among BSs, who selfishly, try to maximize their own expected revenue per second, as defined in Equation (6).

$$\phi_m(\epsilon_{-m}) = \arg \max_{\epsilon_m} \Phi(\epsilon_m, \epsilon_{-m}), \quad (6)$$

where $\phi_m(\epsilon_{-m})$ represents the best response (BR) function associated with BS m . Equation (7) describes the NEP, which is the solution to the competitive game among BSs.

$$\epsilon_m^* = \phi_m(\epsilon_{-m}^*) \quad \forall m \in M. \quad (7)$$

The stability and uniqueness of the NEP for the games have been calculated through successive iterations (negotiation) between the BSs and users via mean of simulation. It has been proved that symmetric wireless systems with proportional share resource allocation mechanism converge to the NEP reaching the nearest optimal performance [2]–[4], [6], [12].

V. NUMERICAL RESULTS

The requests of the files to be downloaded by the users arrive according to a Poisson process and the resources are allocated once per second based on the NEP. In this work we characterize the user's performance (QoS) by using the average user throughput and monetary expenditure per Megabyte. The BSs' performance is quantified by the average revenue per second. The pathloss has been modeled as expressed below:

$$L(d) = 35.3 + 38 \log_{10}(d) \quad \text{in units of dB}, \quad (8)$$

where d denotes the distance between the BS and the mobile terminal. In our experiment we have neglected shadow fading and modeled interference as coming from constantly transmitting BSs. As in [2], we use a truncated version of the Shannon bound that has been adjusted to include efficiency losses, leading to the peak data-rate:

$$R_{i,j} = \min \left(W \log_2 \left(1 + \frac{\Gamma_{i,j}}{2} \right), R_{max} \right), \quad (9)$$

where $W = 3.84$ MHz is the channel bandwidth, $\Gamma_{i,j}$ represents the signal to interference and noise ratio and R_{max} denotes the maximum bit-rate that can be achieve by the user.

A. Simulation Settings

Extensive simulations in MATLAB were carried out with a granularity of one second (auction cycle) for two wireless access providers. Table. I summarizes the simulation parameters that were used. These values have been taking from the prior analysis introduced in [2].

TABLE I
SIMULATION PARAMETERS VALUES

Parameters - with units in square brackets	Value
BS Transmit Power (P) [W]	20
Users distribution	Uniform
Cell Radius [meters]	440
Number of Competing BSs (M)	2
File size (q) [Megabyte]	1
Maximum bite-rate (R_{max}) [Mbit/s]	7

B. Simulation Results

Figure 3 shows the BR function for the non-cooperative game under different levels of competition where there, in average, 0.4 packets/BS/s enter the system. In this figure A represents the percentage of overlap of the two wireless access networks coverage.

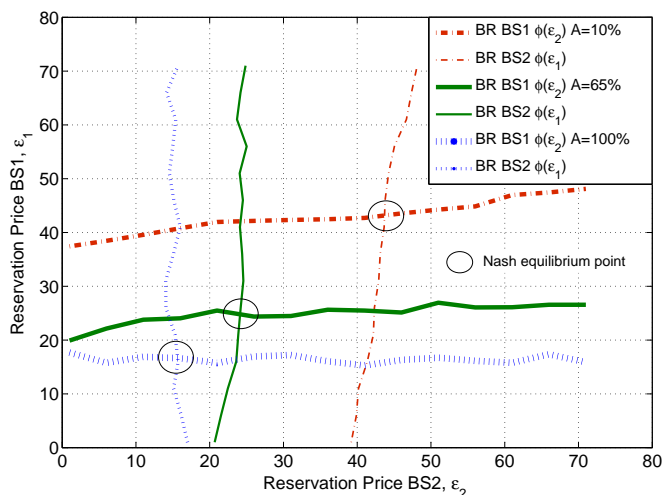


Fig. 3. Average revenue per BS as a function of the reservation price, ϵ .

Based on the results in Figure 3 we observe that there exist at least one NEP in the system.

1. User Performance The experienced users' QoS in terms of throughput and average price per transferred file as a function of the potentially offered load, D_0 , is shown in Figure 4. These depend on the load demand density and are affected by the level of competition introduced with the coverage overlap between networks (representing different levels of competition).

It can be observed that for low load demand, the throughput experienced by users degrades considerably as the level of competition increases. This is due to the fact that the fraction of the resource that each user gets decreases as more users fall in the competition area (in the overlapping coverage).

When the load density increases (2.4 Megabits/second and higher, from $\lambda=0.3$ files/s) the throughput degradation is slightly smaller leading to less negative impact on the user's experienced QoS, compared to fully overlapping coverage.

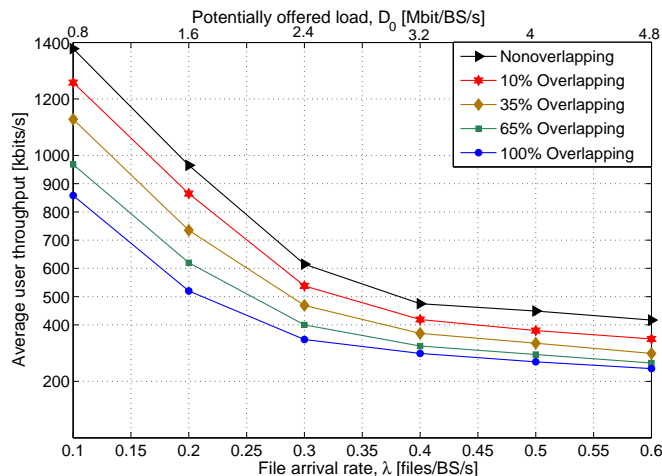


Fig. 4. Average throughput experienced by users for different levels of overlapping coverage as a function of the potentially offered load, D_0 , (file arrival rate λ).

Figure 5 shows the average price per transferred Megabyte experienced by users. We observe that an architecture where BSs compete and share their resources implicitly, combined with autonomous trade-agents acting on behalf of the users, has the potential to reduce price. For networks with low demand density the average price per transferred Megabyte is affected (small increment) in a low scale.

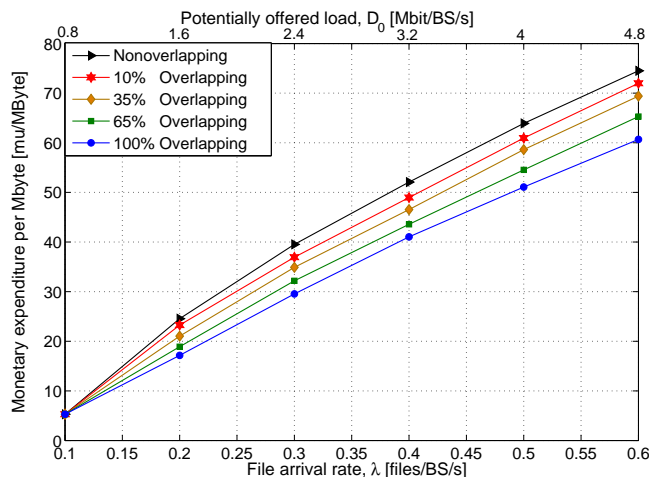


Fig. 5. Average price, p , per transferred Megabyte of data for different levels of overlapping coverage as a function of the potentially offered load, D_0 , (file arrival rate λ).

As illustrated in Figure 5, the resulting user's monetary expenditure per Megabyte increases rapidly as a function of the potentially offered load, D_0 , and on a slightly basis as the level of overlap (competition) is reduced.

2. Base Station's Revenue; The average revenue associated with the BS game for different levels of coverage overlap can be observed in Figure 6. As the overlapping area by the two wireless networks increases so does the level of competition and more

users experience an *open access market*. The reservation price for the resource decreases as a consequence of the competition leading to lower BS's revenue.

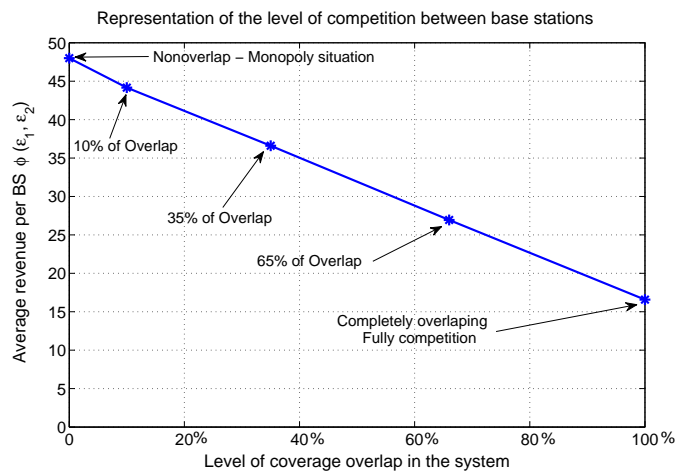


Fig. 6. Average base station's revenue per second and slot associated with the BS game as a function of the level of coverage overlap. On average 0.4 files/s arrive to each BS, each file is of size $q = 8$ Megabits.

Figures 4 and 5 show that the experienced user's QoS is affected for low demand density. However, we can notice that for load density higher than 3.2 Megabits/second ($\lambda=0.4$ files/s) the degradation is slightly smaller leading to less impact on the user's experienced QoS and providing a great gain (more than 50%) in the BS's revenue.

Generally, our results indicate that both users and access providers can benefit when a suitable overlap coverage by two networks is achieved. According to our results a proper percentage of overlap might be approximately 35% based on the interest or objective function of all the involved parties. We investigated the behavior of the system by considering only two wireless networks in order to get insight on to which extent competition can be beneficial for both providers and users.

VI. CONCLUSION

In this paper, we analyzed a competitive sharing scheme ("cooperation") where two access providers provide partially overlapping coverage in a competitive fashion as an option to maximize their revenue. We study how the balance between areas of exclusive coverage and overlap areas with provider competition affects the profitability of the access providers.

Access providers with symmetric wireless networks that overlap partially in coverage compete with each other by selecting a reservation price. It has been shown that, under our assumptions, the system converges to a unique Nash equilibrium point. Results indicate that the fraction of coverage overlap does play an important role for both the performance of the system and the profitability of the access providers.

We observe that as the level of overlap increases the revenue that each base station decreases significantly. In addition, the user's experienced throughput degrades considerably for low demand density meanwhile the cost per transferred Megabyte is affected in a low scale. Further, we conclude that a win-win situation for both users and access providers can be achieved with a suitable coverage overlap by two networks.

ACKNOWLEDGMENT

The authors would like to thank the Swedish International Development Agency (SIDA), and VINNOVA (MODyS project) for their partial support of this work. We would also like to acknowledge Professor Gerald Q. Maguire for his valuable comments, which have helped us to improve this paper. The contributions from initial discussions with Dr. Ki Won Sung, Saltanat Khamit and Dr. Johan Hultell are hereby acknowledged.

REFERENCES

- [1] J. Markemdhahl, Östen Mäkitalo, J. Werding, and B. G. Mölleryd, "Business innovation strategies to reduce the revenue gap for wireless broadband services," *Communications and Strategies Journal*, vol. 1, no. 75, 2009. [Online]. Available: <http://econpapers.repec.org/RePEc:idt:journl:cs7502>
- [2] M. Blomgren and J. Hultell, "Demand-responsive pricing in open wireless access markets," in *Proceedings of the IEEE Vehicular Technology Conference VTC-Spring*, 2007.
- [3] R. T. Maheswaran and T. Başar, "Nash equilibrium and decentralized negotiation in auctioning divisible resources," *Group Decision and Negotiation Journal*, vol. 12, no. 5, 2003.
- [4] M. Blomgren and J. Hultell, "Decentralized market-based radio resource management in multi-network environments," in *Proceedings of the IEEE Vehicular Technology Conference VTC-Spring*, 2007.
- [5] R. T. Maheswaran and T. Başar, "Coalition formation in proportionally fair divisible auctions," 2003.
- [6] D. Fudenberg and J. Tirole, *Game Theory*, 1991.
- [7] R. T. Maheswaran and T. Başar, "Decentralized network resource allocation as a repeated noncooperative market game," in *Proceedings of the 40th IEEE Conference on Decision and Control*, vol. 5, 2001.
- [8] D. Niyato and E. Hossain, "Radio resource management games in wireless networks: an approach to bandwidth allocation and admission control for polling service in IEEE 802.16," *Wireless Communications, IEEE Journal*, vol. 14, no. 1, 2007.
- [9] I. Stoica, H. Abdel-Wahab, K. Jeffay, S. Baruah, J. Gehrke, and C. Plaxton, "A proportional share resource allocation algorithm for real-time, time-shared systems," in *Proceedings of the 17th IEEE Real-Time Systems Symposium*, 1996.
- [10] I. S. Hussein, H. Abdel-wahab, and K. Jeffay, "On the duality between resource reservation and proportional share resource allocation," in *Proceedings of Multimedia Computing and Networking*, 1997.
- [11] L. Abeni, G. Lipari, and G. Buttazzo, "Constant bandwidth vs. proportional share resource allocation," vol. 2, 1999.
- [12] J. Hultell, "Access selection in multi-system architectures: cooperative and competitive contexts," *Licentiate Thesis in Telecommunications*, Kungliga Tekniska Högskolan KTH, Sweden 2007.

A Routing Strategy for Cognitive Radio Networks Using Fuzzy Logic Decisions

Ali El Masri
Troyes University of Technology
Troyes, France
Email: ali.el_masri@utt.fr

Naceur Malouch
Université Pierre et Marie Curie (UPMC)
Paris, France
Email: Naceur.Malouch@lip6.fr

Hicham Khalifé
University of Bordeaux
Bordeaux, France
Email: hicham.khalife@labri.fr

Abstract—We design a novel routing procedure for multihop cognitive radio networks composed of adequate metrics and a strategy to combine these metrics. In cognitive radio networks, channels are not permanently available. The objective is then to increase channel availability when the routes are established. Two global metrics are defined. The stability metric evaluates the utilization efficiency of channels by capturing their sporadic availability to cognitive users. The predicted power metric estimates the spectrum capabilities for the on-going transmission without interrupting licensed users. We use fuzzy logic theory to compute and combine these metrics in order to make suitable routing decisions. Numerical analysis and simulation results show that our procedure is able to find the route that goes through the nodes with better channel conditions. Fuzzy logic seems then to be an appropriate technique to decide the routes to establish in multihop cognitive radio networks.

Keywords-Cognitive Radio Networks; Routing; Fuzzy Logic;

I. INTRODUCTION

Cognitive Radio is an emerging and promising technology that aims to increase the overall utilization of radio resources by enabling dynamic allocation of portions of the wireless spectrum. Unlicensed users, through cognitive radio devices, can opportunistically operate over the current unused parts of licensed bands called white spaces, spectrum holes, or spectrum opportunity [1]. The unlicensed users should be equipped with new smart and programmable radios that sense large portions of the spectrum, learn their surrounding environment, analyze and make intelligent decisions, identify the instantaneous unused channels, use multiple channels in parallel, dynamically reconfigure their transmission parameters to adapt to the current unused parts of the licensed bands.

Proposed traditional routing solutions in multi-channel multihop ad hoc and mesh networks are not appropriate for cognitive radio networks (CRN). First, in CRN no static spectrum allocation is possible hence nodes cannot assume permanent access to the channels. Therefore, the channel selection must be part of the routing decisions and must be taken at the network layer jointly with the MAC (Medium Access Control) layer. Second, the transmission of unlicensed users on a channel can be interrupted by the licensed users activity thus forcing cognitive radios (CR) to look for instantaneously available opportunities. As a direct result, the

unlicensed users should permanently scan the spectrum and choose the appropriate route to follow before starting the transmission. The established path should avoid, if possible, route handover. Third, the unlicensed users should adapt their transmission power to avoid any interference with licensed users operating over the primary radios (PR), which have the absolute priority of using the channels.

In this paper, we introduce a novel routing procedure based on the inferred behavior of licensed users. Each channel at each node is evaluated by two metrics. First, the stability metric aims to reflect the utilization efficiency of the spectrum by studying the sporadic availability of the licensed bands to the unlicensed users. Second, the transmission power estimation metric aims to characterize allowed transmission power and its variation over time. We use the fuzzy logic theory [2] to combine these metrics in order to make good routing decisions. In general, fuzzy logic allows the partial membership of a variable x in a set A . The degree of membership is specified using membership functions and linguistic variables. Fuzzy logic theory is an adapted technique to solve the uncertainty, the heterogeneity, and the information incompleteness of routing problems in cognitive radio environment. Particularly, even if the properties of channels are well identified, it is still difficult to assess with certainty the impact of these properties on the performance of a given route.

The contribution of this paper is twofold. First in presenting routing metrics that characterize the dynamic and unstable aspects of cognitive radio networks and second in proposing a technique that avoids combining these parameters through inflexible methods similar to the weighted sum. Indeed, the fuzzy logic allows partial membership of a channel to a metric and a metric to a path thus capturing the dynamic and uncertain behavior observed in cognitive radio networks. Besides, we validate our metrics and routing procedure with simulations and show that our routing ensures long term stability by implicitly accounting for instantaneous channels variations.

II. PROBLEM FORMULATION

A. Routing in Cognitive Radio Networks

Because in Cognitive Radio Networks channels are not permanently available, proposed routing techniques for multi-channel multi-hop ad hoc or mesh networks cannot be reused for CRNs. Any proposed routing strategy in CRNs should

Part of this work was supported by the grant ANR-10-VERS-005-03

characterize the non-permanent availability and describe the sporadic accessibility of the spectrum bands. Other CRN routing proposals address the above issue by simply computing the percentage of availability for each channel [3] [4].

B. Objective

We consider a multihop cognitive radio network where data is forwarded through multiple cognitive radio nodes between a source and a destination. Cognitive nodes try to share several channels occupied by licensed users belonging to different networks and thus having different properties. The objective is then to design an appropriate routing strategy that builds a single path from a source node to a destination using only cognitive radio nodes as intermediate relays. The steps of the design are as follows:

- 1) Given a multihop cognitive radio network, find the best routing metrics that best characterize the availability and usability of the channels.
- 2) Given a number of computed metrics, propose a flexible method of combining parameters able to capture uncertainty and variations of the computed metrics.
- 3) Given the metrics and their combination, find the best path between a source node and a destination. The path is composed of an aggregated set of channels on every hop.

III. ROUTING METRICS

We describe in this part the proposed routing metrics and their combination using fuzzy logic. We first emphasize on the stability metric and the transmission power estimation. Then, a channel weight is computed for every link by the means of a fuzzy logic controller.

A. Stability

The goal of the stability metric is to capture the activity behavior of PR nodes over the licensed channels and hence the sporadic availability of these channels to CR nodes. In other words, the stability aims to describe how the availability of channels is distributed over time. The distribution model of channels availability can be described by the number of periods during which channels are available to CR transmissions and the manner these periods are disposed in time, such as the distance between two successive periods and the difference in their durations. We call a channel stable when it switches between long available periods and/or long unavailable periods. When unavailable periods are small the channel is of course excellent to use, but long unavailable periods also provide us a good information which is avoiding to use the channel for sure. An unstable channel switches quickly between availability and unavailability. The degree of stability can be specified according to its position between a channel that is almost static and a highly unstable channel.

In this work, we use 3 parameters to compute the stability of channels. The frequency of transitions between availability and unavailability, the deviation in the duration of available periods and the deviation in the duration of unavailable periods. In

the following, we describe the impact of each parameter on the stability. Figure 1 shows an example of the impact of the frequency of transitions between available and unavailable periods on the stability of channels. It is clear that for the same percentage of channel availability, the degree of stability decreases proportionally with the increase of the frequency of transitions.

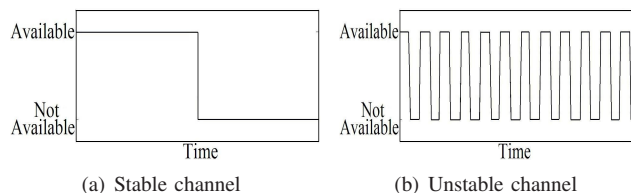


Fig. 1. Impact of frequency of transitions on the stability

Figure 2 shows that two channels with the same percentage of availability and the same frequency of transitions can have two different degrees of stability. This can be captured by the deviation of available periods. We notice that when the value of deviation in the duration of available periods increases, the distribution model of channel availability is more similar to the stable case. In fact, the availability of the channel in Figure 2(a) is composed of one long and several short available periods. The long period is similar to the long available period in the original stable case in Figure 1(a) and the short periods are almost not useful and can offer in the rest of the time the same performance as the long unavailable period in Figure 1(a). Similar remarks can be made about the unavailability periods deviation where the increase of the unavailable periods duration increases the system stability.

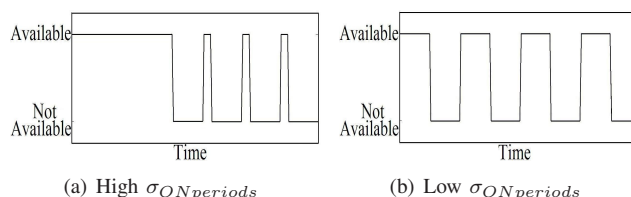
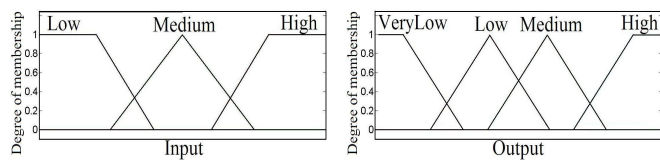


Fig. 2. Impact of availability deviation $\sigma_{ONperiods}$ on the stability

To compute the degree of stability of each channel, we combine the 3 parameters using the Fuzzy Logic Controller FLC 1. The FLC 1 consists of 3 inputs linguistic variables (frequency of transitions between availability and unavailability (*input1*), deviation in the duration of available periods (*input2*), and deviation in the duration of unavailable periods (*input3*)). FLC 1 inputs are characterized by the membership functions depicted in Figure 3(a), whereas its output linguistic variable (*Stability*), is characterized by the membership function depicted in Figure 3(b). Each input linguistic variable is specified by a term of three fuzzy sets, $T(input) = [Low, Medium, High]$. The output linguistic variable is characterized by a term of four fuzzy sets, $T(output) = [VeryLow, Low, Medium, High]$.



(a) Input: Frequency of transitions, $\sigma_{ONperiods}$, or $\sigma_{OFFperiods}$ (b) Output: Stability

Fig. 3. Membership functions of FLC1

The output is a value between 0 and 100. In order to obtain the channel stability, we define the fuzzy Rule Base shown in Table I. This table is a proposal for the FLC 1 determined via the analysis in the previous section but also by observations during simulations. Note that the rule base is malleable enough so that other researchers can argue and propose different rules for different reasons. For instance, if the frequency of transitions is medium and the deviations are very high, one can consider that the stability is high rather than medium.

TABLE I
FLC1 FUZZY RULE BASE

IF			THEN
Frequency of transitions	$\sigma_{ONperiods}$	$\sigma_{OFFperiods}$	stability
High	High	High	Low
High	High	Medium	Low
High	High	Low	Low
High	Medium	High	Low
High	Medium	Medium	VeryLow
High	Medium	Low	VeryLow
High	Low	High	VeryLow
High	Low	Medium	VeryLow
High	Low	Low	VeryLow
Medium	High	High	Medium
Medium	High	Medium	Medium
Medium	High	Low	Medium
Medium	Medium	High	Medium
Medium	Medium	Medium	Low
Medium	Medium	Low	Low
Medium	Low	High	Low
Medium	Low	Medium	Low
Medium	Low	Low	Low
Low	High	High	High
Low	High	Medium	High
Low	High	Low	High
Low	Medium	High	High
Low	Medium	Medium	High
Low	Medium	Low	High
Low	Low	High	High
Low	Low	Medium	High
Low	Low	Low	High

B. Transmission Power Estimation

The stability metric characterizes the spectrum holes to be used by cognitive radio transmissions. Nevertheless in order to exploit these white spaces, CRs must judiciously compute their transmission power in a way not to disturb primary radios activity. Moreover, since interference at PRs is additive, the estimated transmission power should also account

for neighboring CRs activity over the channel. Consequently every CR should continuously estimate the maximum allowed transmission power P_{max} over every available channel. Practically, the estimated transmission power dictates the set of CR receivers on every channel i.e the obtained CRN topology.

The predicted P_{max} to be considered for next transmissions can be computed based on a set of previously measured values of P_{max} , in addition to the current measured value. Many methods exist in the literature to predict the next value of random variables such as regression models or Kalman filters. The appropriate prediction method to use is out of the scope of this work. We rather focus on how we can benefit from the results obtained from the prediction method by considering a general output from the prediction module. We assume in this work that any considered estimation technique, provides the predicted value $P_{Predicted}$ of P_{max} and the confidence interval $[P_{Predicted} - \beta, P_{Predicted} + \beta]$, where β is the error level.

By means of the Fuzzy Logic Controller FLC2 each CR node computes the final predicted power ($FinalPredictedPower$) for each channel based on the two outputs of the prediction method ($P_{Predicted}, \beta$).

The FLC2 consists of two linguistic variables inputs ($P_{Predicted}$ and β) characterized by the membership functions depicted in Figure 4(a) and 4(b), and one output linguistic variable ($FinalPredictedPower$), characterized by the membership function depicted in Figure 4(c). $P_{Predicted}$ is characterized by a term of three fuzzy sets, $T(P_{Predicted}) = [Low, Medium, High]$, and β is characterized by one fuzzy set, $T(\beta) = [High]$. The output linguistic is characterized by $T(output) = [VeryLow, Low, Medium, High]$. The exact output power can be computed in Watts by normalization however this operation is not necessary since the objective in our metric is the comparison between channels.

Finally, note that $FinalPredictedPower$ is the maximum allowed transmission power beyond which primary users are disturbed. It is not necessarily the power that is going to be used when transmitting. Clearly, the used power can be optimized based on the location of the receiver node.

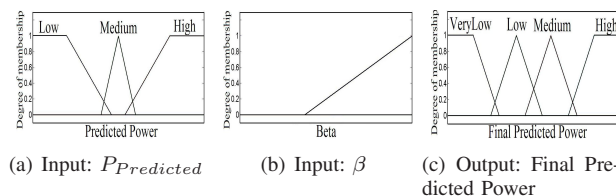


Fig. 4. Membership functions of FLC2

The policy of FLC2 is based on six simple rules shown in table II. Rules 1, 3, and 5 indicate that the final result of the predicted power ($FinalPredictedPower$) is proportional to the value of $P_{Predicted}$. Rules 2, 4, and 6 point that the final result of the predicted power of a channel with a high value of β must be lower than a channel with a comparable value of $P_{Predicted}$ and smaller value of β .

TABLE II
FLC2 FUZZY RULE BASE

n	IF		THEN
	$P_{Predicted}$	β	$FinalPredictedPower$
1	High		High
2	High	High	Medium
3	Medium		Medium
4	Medium	High	Low
5	Low		Low
6	Low	High	VeryLow

TABLE III
FLC3 FUZZY RULE BASE

Stability	IF		THEN
	$FinalPredictedPower$	Channel Grade	
High	High	VeryHigh	
High	Medium	Medium	
High	Low	VeryLow	
Medium	High	High	
Medium	Medium	Medium	
Medium	Low	Low	
Low	High	Low	
Low	Medium	Low	
Low	Low	Low	

C. Channel grade

The Fuzzy Logic Controller FLC3 depicted in Figure 5 combines these two routing metrics to compute the grade of each channel at each node. The best channel is the most stable channel with a high $final$ predicted value of P_{max} (greater than the minimum needed for transmission). The higher the final predicted power, the higher the number of neighbors and thus the higher the route possibilities to select. Also, a higher final predicted power provides a security margin before violating it. Membership functions are depicted in Figure 5, while other finer rules are summarized in table III.

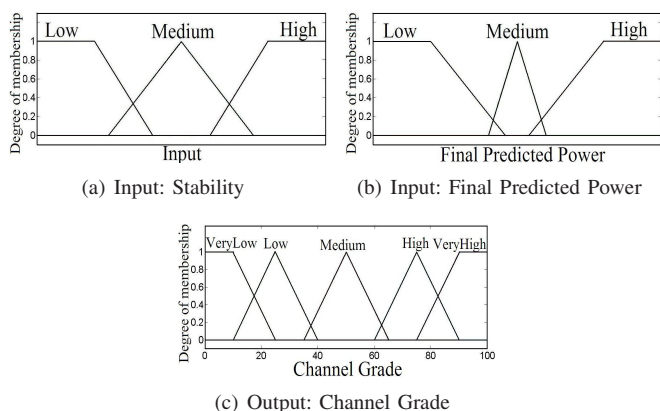


Fig. 5. Membership functions of FLC3

IV. ROUTE CONSTRUCTION

The computation of the routing metrics must take place for each channel in all the routes from the source to the destination. The grade of a link between two CR nodes (a value between 0 and 100) is equal to the sum of the grades of all channels that are going to be used for transmission

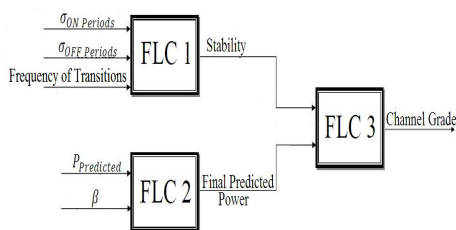


Fig. 6. The global FLC of the channel grade computation

between these two nodes. As for the grade of a route we aim at including in the final grade also the number of hops. To do so, the link grades are inverted, then the final grade is the inverse of their sum. The route with the highest grade is the best route from the source to the destination since the *lowest* sum of the inverted link grades tends intrinsically to reduce the number of hops in addition to considering links with high grades.

More formally, if we denote by R the set of all routes between a source node S and a destination D , and by n_r the number of links that constitute route r , $r \in R$, then computing the best route based on the grades of routes between S and D can be written as

$$\max_{r \in R} \left(\sum_{l=1}^{n_r} 1/g_l^r \right)^{-1} \tag{1}$$

where g_l^r is the grade of link l in route r ($l \in 1 \dots n_r$, $r \in R$).

When the source wants to establish a connection, it is possible to incorporate the computation of the route grades in an AODV-like [5], [3] or a DSR-like [6] routing protocol that allows also to reach the destination.

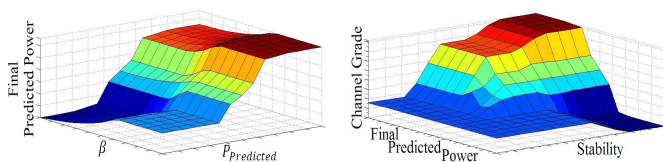
The predicted maximum allowed power for transmission should be updated while the route is constructed towards the destination. This is because the addition of a channel to the route activates the channel for transmission and will add possibly an interference at PR receivers. The predicted power is then possibly reduced for the same channel of next links in the route. This update cannot use the recent measured powers received from the sensing module of the cognitive radio since the transmission is not yet started. The deployment of a procedure that updates the maximum power during route construction is challenging and increases the complexity of the route establishment especially that it would require message exchange between CR nodes and distributed power computations. However, in our case, channels with higher maximum power are chosen first, which reduces the probability of violating the interference condition if more than one CR node use the same channel in the route. Practically, this will not affect PR activity but establishes a route where some CR nodes will not be able to transmit as predicted. Designing a lightweight procedure to update the maximum power dynamically is one of our future work.

V. PERFORMANCE EVALUATION

A. Metrics Validation

Before simulating the whole routing procedure, we first validate the effectiveness of using the fuzzy logic within the proposed metrics. Since our proposed metrics are based on IF-THEN rules and not on mathematical equations, we show how these metrics change with the variation of the FLCs inputs. We consider here a simple one hop network since the objective is to show that the developed metrics capture efficiently the cognitive radio environment. All simulations were conducted using MATLAB.

Figure 7(a) represents how the output of the FLC2 ($FinalPredictedPower$) changes as a function of its two inputs ($P_{Predicted}$ and β). It is clear that the Final Predicted Power is proportional to the $P_{Predicted}$ obtained through the prediction operation. However, if a CR node compares between two channels, the channel that has the highest value of $P_{Predicted}$ is not always selected. For instance, if two channels have close values of $P_{Predicted}$, a CR node chooses the channel which has the lowest value of β . In other words, the chosen channel is the one whose operation of prediction gives the highest level of confidence. Such result cannot be obtained through the classical $P_{Predicted} - \beta$ function.



(a) Final Power as a function of Predicted Power and prediction error (b) Channel Grade as a function of Stability and Final Predicted Power

Fig. 7. Stability and power estimation validation

Figure 7(b) shows how the channel grade varies based on the stability and the $FinalPredictedPower$. Note that if the stability is very low, the channel grade is also low regardless of the $FinalPredictedPower$ value. However, if the stability is high, the channel grade switches between very high and very low levels and it is highly dependent on the $FinalPredictedPower$. The two previously obtained results typically express the relation between the stability and the $FinalPredictedPower$. In fact, a **stable** channel should be selected based on the $FinalPredictedPower$ since the current state of the channel will mostly continue in the future for a significant period of the time. On the other hand, an unstable channel will probably switch several times between availability and unavailability during a short period, and then the impact of the current state on channel selection is widely reduced. It is also remarkable that during unavailability periods, an unstable channel is preferred over a stable one since the former allows starting the transmission faster than the latter one and provides at least some throughput guarantee even with intermittent connectivity. This example shows again the flexibility provided by the fuzzy logic to control carefully

the channel selection. Such figure cannot be obtained using a traditional weighted sum equation.

B. Routes Construction Simulations

In order to simulate the routing procedure, we use 64 nodes placed in a grid topology (Figure 8). The source node is the node placed in the top left corner of the grid while the destination node is the one placed in the bottom right corner. There are 6 licensed channels between every two nodes. For all the simulations, all channels have 50% availability ratio in the long term. We simulate three types of channel models corresponding to different degrees of stability. These types are placed in the network in order to create three regions of channels as shown in Figure 8. The channels of the bottom region behave following a high stability scheme, channels of the top region behave as a low stability scheme whereas the channels of the middle region behave as a medium stability scheme. Schemes are similar to Figures 1 and 2 and they are created randomly. This configuration will show clearly how routes are chosen through different links with different conditions.

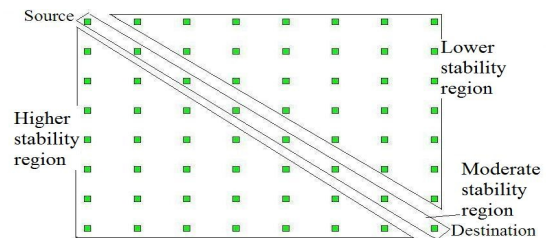


Fig. 8. Simulated network topology

First, we run the routing algorithm to find the best route from the source to the destination. Figure 9(a) shows the route constructed through links with highest grades. It also highlights that the number of hops is considered in the route construction, for this reason the route is close to the moderate stability region. Hence, the chosen route is a good tradeoff between the quality of links and the route hop count.

Second, we continue running the algorithm between the same source and the same destination but for new connections up to 9 routes which is the maximum possible in this topology. We repeat this operation several times while varying randomly and uniformly the starting time of each route establishment. The obtained routes can be categorized into two types. Examples of these successive routes are shown in Figures 9 and 10. In Figure 9, we notice that the first four constructed routes are in the bottom region of the topology where the stability is higher, routes 5, 6, and 7 are hybrid between the higher and the moderate stability region, and finally the last two routes are totally in the lower stability region. This types of routes looks indeed intuitive and validates the routing algorithm in contrast to the second type shown in Figure 10.

In Figure 10, we highlight a different scenario observed during our simulations. In some cases, the first established routes in the network start surprisingly from the unstable

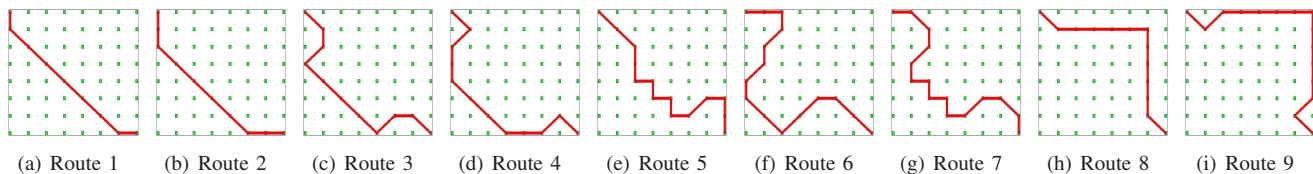


Fig. 9. The case where the first constructed routes start from the high stability region of the network

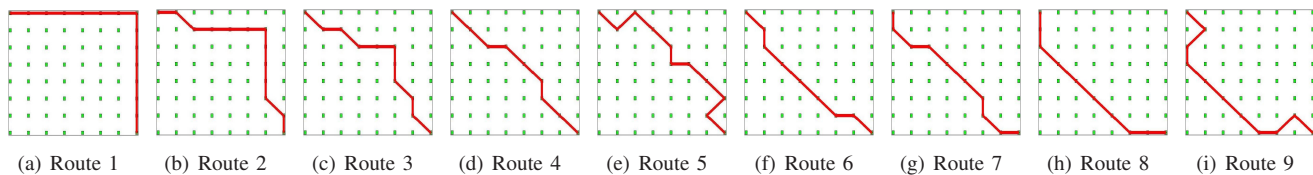


Fig. 10. The case where the first constructed routes start from the low stability region of the network

region and they finish in the stable one. In fact, the routes with stable channels have very low grades when the predicted power is low and/or β is high. These routes were indeed established when the final predicted allowed power is too low or does not allow transmission. Although the unstable links have low grades, these grades are still greater than the grades of stable ones during periods where the channels are not really available for transmission. Here, among bad quality routes, our strategy selects the less worse one.

VI. RELATED WORK

Some routing techniques for cognitive radio networks were proposed in the literature. Sharma *et al.* proposed in [7] a way to integrate the interference temperature into routing decisions. Routing metrics are combined using a simple weighted sum. Yet, this way is not flexible enough and it was not evaluated by simulation or models. Akyildiz *et al.* proposed in [3] STOD-RP an on-demand routing protocol based on clustering approach. In STOD-RP, a single channel is used within each cluster and a recovery mechanism is provided to tolerate spectrum loss. However, the throughput is much reduced within each cluster and the cluster heads become quickly *bottleneck* links. A new routing metric was proposed in [8] based on a probabilistic definition of the available capacity of channels in order to find the route with the higher probability of availability. After the route establishment, new channels are added until the throughput demand is satisfied. Probabilistic throughput computation is adequate to increase the long term availability but it may not be adapted for short connections. In [9], a new routing scheme was proposed in order to reduce the power consumption. This usually leads to select the nearest neighboring node, and then the number of hops in the route is significantly increased. Authors in [4] present SAMER a new routing scheme to provide a tradeoff between the local spectrum conditions at the forwarding nodes and the global spectrum view of the entire routing path. However, the complex distribution of channels availability is simply presented by a general average of availability.

Our work differs from previous proposals in two aspects: First, by presenting a new flexible and efficient way to

combine routing metrics in cognitive radio networks. Second, by proposing new routing metrics able to capture the uncertain, dynamic and sporadic availability of licensed bands.

VII. CONCLUSION AND FUTURE WORK

This paper proposes a new routing approach for multihop cognitive radio networks based on the sporadic availability of channels. Two routing metrics are defined based on the power allocation at cognitive radio nodes. These metrics are computed and combined using the fuzzy logic theory. Numerical analysis and simulations show that our routing procedure is able to exploit adequately all types of channels whenever there are available spaces. The established routes achieve a good tradeoff between availability, transmission ability and stability.

Based on our results, further investigations can be made including especially experimenting other fuzzy rules that can be tuned for specific application requirements. It is also interesting to estimate the benefit from designing a distributed update of the maximum allowed power during the construction of the route.

REFERENCES

- [1] I. Akyildiz, W. Y. Lee, and K. Chowdhury, "CRAHNs: Cognitive Radio Ad hoc Networks," *Ad Hoc Networks – Elsevier Science*, vol. 7, no. 5, pp. 810–836, 2009.
- [2] W. Pedrycz and F. Gomide, *An Introduction to Fuzzy Sets: Analysis and Design*. MIT Press, 1998.
- [3] G. Zhu, M. Felice, and I. Akyildiz, "STOD-RP: A Spectrum-Tre Based On-Demand Routing Protocol for Multi-Hop Cognitive Radio Networks," in *Proceedings of the IEEE GLOBECOM Conference*, Nov. 2008.
- [4] I. Pefkianakis, S. Wong, and S. Lu, "SAMER: Spectrum Aware Mesh Routing in Cognitive Radio Networks," in *Proceedings of the IEEE DySPAN Conference*, Oct. 2008.
- [5] P. C., R. E., and D. S., "Ad hoc on demand distance vector (aodv) routing," IETF, RFC 3561, 2003.
- [6] Johnson D., Hu Y. and Maltz D., "The Dynamic Source Routing Protocol for Mobile Ad Hoc Networks for IPv4," IETF, RFC 4728, 2007.
- [7] H. Sharma, M. Krunz, and O. Younis, "Channel Selection under Interference Temperature Model in Multi-hop Cognitive Mesh Networks," in *Proceedings of the IEEE DySPAN Conference*, Apr. 2007.
- [8] H. Khalife, S. Ahuja, N. Malouch, and M. Krunz, "Probabilistic Path Selection in Opportunistic Cognitive Radio Networks," in *Proceedings of the IEEE GLOBECOM Conference*, Nov. 2008.
- [9] C. Pyo and M. Hasegawa, "Minimum Weight Routing based on a Common Link Control Radio for Cognitive Wireless Ad hoc Networks," in *Proceedings of the IEEE IWCMC Conference*, Aug. 2007.

An Application-Oriented Routing Protocol for Multi-hop Cognitive Radio Networks

Ba-Lam To*, Thuong-Van Vu*, Thi-Mai-Trang Nguyen* and Anne Fladenmuller*

* University of Pierre and Marie Curie (UPMC)

Laboratory of Computer Science of Paris 6 (LIP6)

4 place Jussieu, 75005 Paris, France

Email: {Ba-Lam.To, Thi-Mai-Trang.Nguyen, Anne.Fladenmuller}@lip6.fr, Thuong-Van.Vu@phare.lip6.fr

Abstract—A challenge for routing in cognitive radio networks is the intermittent connection due to the occupying and releasing licensed channels of primary users. To solve this problem, the routing protocol will choose the most stable channel (the channel with the longest average length of idle period) to build up the stable path. This approach, however, can lead to the increase of channel competition between cognitive users since the most stable channels are preferred to be utilized by all cognitive users. In this paper, an application-oriented routing protocol is proposed. The main motivation is to reduce the channel competition between cognitive users by finding the appropriate path according to the application of cognitive users. Simulation results show that our proposed routing protocol reduces the loss ratio and increases the throughput significantly.

Index Terms—cognitive radio; application-oriented; routing; stability

I. INTRODUCTION

In wireless communication, the most valuable resource is the radio spectrum. However, according to recent studies[1][2], while the assigned spectrum (licensed spectrum) is under-utilized in various geographical locations and time, the unlicensed spectrum is always overloaded because of the growth of wireless services. To reduce the waste of licensed spectrum usage and provide more available spectrum resource for unlicensed users, an efficient way is allowing unlicensed users to opportunistically access the licensed spectrum without penalizing Quality of Service (QoS) of licensed users. Cognitive Radio (CR) [3] is envisaged as the sufficient technology that aims to flexibly use wireless radio spectrum. Each node in the Cognitive Radio Network (CRN) is equipped with a cognitive radio which has capabilities of sensing the busy channel, reconfiguring the radio parameters and switching to another channel. Due to the information collected during the sensing process, the CR users will use the idle licensed channel during vacant time and immediately release the channel whenever CR users detect any use of licensed users on this channel.

One of the most important problems in routing in multi-hop CRN is the intermittent connection. Unpredicted operation of primary users (PU) prevents secondary users (SU) from having a stable usage of the licensed spectrum. The intermittent connection will lead to frequent route corruptions whose consequence is that the re-routing process must be called

several times, increasing transmission delay and packet loss. Although there are many routing protocols proposed for CRN, only few of them tackle the intermittent connection problem. There are two possible methods used to solve the problem of intermittent connection: corruption avoidance method and corruption reaction method. In the corruption reaction method [4][5], the proposed routing protocols define mechanisms to recover the route in case that the route is corrupted. Therefore, network can avoid the performance degradation whenever the route is corrupted due to the coming back of primary users. In the corruption avoidance method, the proposed routing protocols [6]-[11] define mechanisms to select the most stable route in order to avoid frequent changes of route and improve network performances. By considering the spectrum stability as the metric in the routing protocol, nodes will select the most stable link for each hop and obtain the most stable route.

The above channel selection algorithm [6]-[11] is designed with cross layer approach in which the channel information is collected by lower layers and used by network layer for routing decision. Even though this channel selection algorithm can help nodes to choose the most stable channel, it still leads to some problems. Firstly, by forcing all CR nodes in an area to operate over the most stable channel, the competition among CR nodes for the same channel resources will cause contention and collision problems in which the consequence will be an increase of end-to-end delays or a decrease of throughput. Secondly, the stable-channel approach will under-utilize the ability of operating on different channels which cognitive radio offers. Therefore, a novel spectrum allocation strategy is needed to provide better spectrum utilization in CRN.

As each application has its own traffic pattern which decides the transmission behaviour, the channels can be allocated to CR users according to their application types. For example, with Constant Bit Rate (CBR) Voice over IP (VoIP) applications or Delay Tolerant Network-like applications in which the transmissions usually happen in short period of time, the channels which are not stable and often idle will be the appropriate candidate channels. Therefore, taking into account the type of applications, we can provide better channel allocation strategy in which the channel competition or interference

will be reduced. In this paper, we introduce the Application-Oriented Stability (AOS) metric which helps nodes using unreliable and non-elastic delay applications to choose the channels which can be used more frequently even though these channels are not stable. The most stable channel (the channel with the longest average length of idle period) will be reserved to the nodes using reliable and elastic delay applications. By this channel allocation strategy, radio spectrum resource is utilized more efficiently and network performance will be improved.

The remainder of this paper is organized as follows. In Section II, we discuss works related to stable routing in cognitive radio network. Section III will study channel usage pattern according to application and describe the network model. In Section IV, we analyse the Application-Oriented Stability metric in detail and present the application-oriented routing protocol. Simulation results are illustrated in Section V. Finally, Section VI concludes this paper and figures out the future work.

II. RELATED WORK

Some stability routing techniques in cognitive radio network already exist. In [8], the authors first define the maximum link hold-time as the maximum length of available period before a cognitive link is considered to be failed. After that, the authors expressed the link hold-time as a function of the maximum link hold-time and the primary user usage pattern. The route hold-time then will be derived as the accumulated hold-time of links which compose the route. Finally, the routing metric based on the route hold-time and end-to-end throughput is proposed. Sharma *et al.* propose in [7] a new routing metric for multihop cognitive networks. This new metric includes the stability factor, also known as the average channel availability time which is calculated as weighted moving average of previously measured availability times and the time measured in the current measurement duration. Same remarks apply on [9][10], where the proposed routing metric is based on the channel utilization which depends on the average duration of available period of the channel. [6] proposes a collaborative strategy for route and spectrum selection in cognitive radio networks. The routing metric includes the spectrum stability factor used to gauge the variation of the spectrum. In [11], the authors use a threshold to decide whether the channel is stable. The channel will be considered as stable if its average available time is larger than the threshold. Otherwise all unstable channels will be excluded from the spectrum opportunity.

Our work differs from the previous proposals in two aspects: first, taking into account the application of cognitive users when allocating the channel using our stability parameter, and second, considering the length variance of idle periods which can lead to the wrong channel selection.

III. NETWORK MODEL AND TRAFFIC ANALYSIS

A. Network Model

We consider a cognitive radio network composed of primary users and cognitive users. Primary users are nodes which

hold licenses for specific spectrum bands, and can occupy their assigned spectrum. Therefore, primary users will be provided a reliable communication environment regardless of time and space. Cognitive users use opportunistically the licensed channels to send their data when they detect the disappearance of primary users. We assume that all cognitive users are equipped with cognitive radios which have abilities of reconfiguring transmission parameters and scanning the channels for opportunistic transmission.

We also consider that each primary channel will follow an ON-OFF model in which channel alternates between state ON (active) and state OFF (inactive) [12]. An ON/OFF state models a time slot in which the primary user is or is not occupying a channel. The cognitive users can utilize the OFF time slot to transmit their own signals. Suppose that each channel changes its state independently. The ON-OFF channel model is depicted in Figure 1. The channels are assumed to

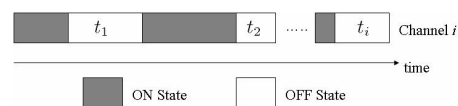


Fig. 1. The channel state for i th channel

be organized in two separate channel sets: a common control channel (CCC) and a set of data channels. All cognitive users in the network will use the CCC to send packets for contending the data channel or to exchange local information and routing control information. The set of data channel is used for data communication. Each data channel has bandwidth w . We also assume that all sensing information are accurate.

B. Traffic Analysis

In this section, Voice over IP (VoIP) on behalf of unreliable and non-elastic delay applications and File Transfer Protocol (FTP) on behalf of reliable and elastic delay applications will be studied through different topologies and channel patterns in order to find the most appropriate channel pattern for each type of application.

To study the impact of channel idle time on the performance of VoIP and FTP, we deploy different test cases which are different in the number of nodes (Figure 2). The detail of basic parameters used in each test case are described in Table I. Beside that, in each test case, ON-OFF model is used to model the channel availability at each node.

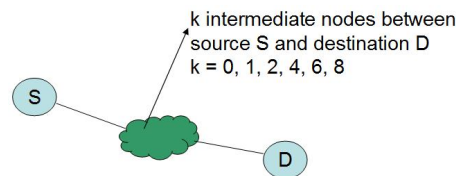


Fig. 2. Network topology of test cases

In each test case, we first create an UDP/CBR(VoIP) connection from source node to destination node and keep data

TABLE I
SIMULATION PARAMETERS

Parameter	Value	Comments
Flat Grid	1000x1000	Simulation space. Here, a flat field 1000mx1000m
Node	MobileNode	The PU/SU that is recognized in ns-2 as a mobile wireless node
Bandwidth	2Mbps	The bandwidth of wireless network
Stack delay	9.5-10.5ms	A delay that allows a packet to go through OSI stack at node in ns-2
Propagation model	Two-Ray Ground	A propagation model supported by ns-2 to simulate the signal propagation
Interference model	Thermal Threshold	If a packet power is lower than a minimum threshold (set fixed), packet will get dropped
UDP/CBR rate	64kbps	Rate for application UDP/CBR
TCP/FTP	varied	Rate which claims as much as possible from the remained bandwidth
Duration	300s	A runtime for data transfer in a test case
Protocol overhead	5%-10%	Extra information exchanged between nodes besides data transfer (e.g. routing packets of Routing layer used to establish path for data from source to destination)
Data in UDP packet	160 bytes	Data in each UDP packet
UDP loss ratio accepted	3%	Loss ratio is acceptable to application
MAC layer	AOS-MAC	A modified version of $MAC_{s02.11}$ supported by ns-2. AOS-MAC is implemented to allow the secondary users to transfer data on the licensed channel transparently to primary users
UDP traffic	UDP/CBR	UDP constant bit rate at 64kbps
Data in TCP packet	512 bytes	Data in each TCP packet
TCP traffic	TCP/FTP	The rate of FTP traffic is varied (FTP claims the bandwidth as much as possible)

transferring continuously in 300ms. All nodes in the network will choose the channel using the same criteria (e.g. the most stable channel which its length of idle time is varied for testing purpose) for data transmission. After that, we vary the length of channel idle time and observe the network performance which is shown through the throughput. We then create TCP/FTP connection and follow the same procedure as we did in case of UDP/CBR(VoIP) connection. The simulation is repeated 20 times for each test case.

The results are shown in Figure 3. The length of channel idle period (the OFF period) is varied from 2.1ms to 18.7ms. From Figure 3(a), two observations are deduced. Firstly, the network throughput will reach its maximum value and keep stable when the length of channel idle time reaches a threshold value. For instance, in the case there are 6 cognitive hops in the network, the network throughput will achieve its maximum value (78kps) when the length of channel idle time reaches the value of 15ms. Then the network throughput still stay at the maximum value even though the length of channel idle time continues to increase. Secondly, the threshold value of length of the channel idle time will be increased when there are more cognitive users in the networks. If cognitive users

use the stability metric for channel selection, there are more channel competition when there are more cognitive users in the network. Hence, the consequence is that the length of channel idle time need to be increased in order to achieve the maximum value of network throughput.

The above observations are also applicable in case that application is FTP (Figure 3(b)). However, there is a difference between both cases. The difference is that, to achieve the threshold value of network throughput, the length of channel idle time in case of FTP need to be much longer than the length of channel idle time in case of VoIP. For example, from Figures 3(a) and 3(b), in the case of there are 2 cognitive users in the network, network throughput will achieve the maximum value when the length of channel idle time in case of VoIP and in case of FTP is equal to or greater than 4ms and 16ms respectively. In case there are 6 cognitive users in the network, the length of channel idle time in case of VoIP needs to be equal to the threshold value of 17ms for the convergence of network throughput. With FTP, the length of channel idle time must be much longer.

With the above observations, it is obvious that the channels composed to built up the path should be allocated according to the application of cognitive users.

IV. APPLICATION-ORIENTED ROUTING

In this Section, the Application-Oriented Stability (AOS) parameter is described in detail, and a routing protocol using AOS as a routing metric is provided.

A. Application-oriented stability

This section will present the AOS parameter. The objective of AOS is to help CR nodes to find appropriate channels for transmitting data according to CR nodes' application type. For FTP application, CR nodes will look for the most stable channel. For VoIP application, CR nodes will look for the channel which are idle frequently even though these channels are not the most stable channel.

The AOS parameter is composed by two components: stability S and total idle time I . The stability S describes the average length of idle time period in which the unlicensed users can access the channel. This component presents the stability of the channel. The total idle time I is calculated by summing up all the idle periods of channel from the time when CR node joins the network, starts to sense the surrounding environment and obtains the available information about the channel. By considering the total idle time I in conjunction with the stability S , we can identify the channels which are vacant frequently and has biggest total idle time. If we have a channel pattern as Figure 1, the stability S and the total idle time I will be derived as follow:

The stability:

$$S = \alpha S + (1 - \alpha)t_i \quad (1)$$

where t_i is the length of the i th idle period of the channel in the current measurement duration and α is the smooth factor. The average available time of the channel S is calculated as the weighted sum of the past S and the current measured

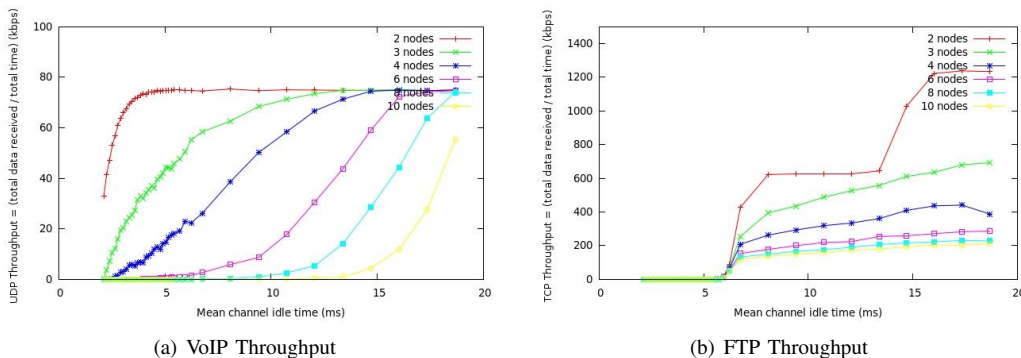


Fig. 3. The relationship between the throughput of VoIP, FTP and the idle length of channel

length of the idle time period of the channel. Each time the channel changes from the OFF state to the ON state, the value of stability component is re-calculated and updated. The most stable channel will have the largest value of S

The total idle time:

$$I = \sum_{i=1}^N t_i \tag{2}$$

where t_i is the length of the i th idle period of the channel. N is the number of idle period from the time when CR node joins the network, starts to sense the surrounding environment and obtains the available information about the channel until the current measurement.

The total idle time of the channel I is calculated as the total idle time from the time when node joins the network, senses the surrounding environment and obtain the first information about the channel until the measurement time. Each time the channel changes from the OFF state to ON state, the value of idle level component is re-calculated and updated.

As the objective of AOS parameter is helping CR nodes to choose the appropriate channel according to CR nodes' application type, the AOS parameter will be defined as follow:

$$AOS = \left[\frac{c}{S} + \frac{1-c}{\frac{1}{S} \ln I} \right] + \sqrt{\frac{1}{N} \sum_{i=1}^N (t_i - S)^2}, \quad S \geq S_{threshold} \tag{3}$$

where c is the application indicator. c will equal to 0 if the application is VoIP and equal to 1 if the application is FTP. $S_{threshold}$ is the lower bound for S . The lower bound of S will guarantee that the channel will be normally available in a period of time that is enough to ensure CR nodes will transmit a packet successfully

The first part of AOS is defined to find the most appropriate channel for applications. With FTP application ($c = 1$), the most stable channels will be preferred. With VoIP application ($c = 0$), the preferred channels are the channels which are less stable than the most stable channels, but the idle frequency is high. The second part of AOS is used to avoid the variation in length of channel idle periods. Otherwise, the large variation

in length of channel idle periods can cause the wrong channel selection.

Based on the AOS parameter, path metric will be derived as follow:

$$M = \sum_{i \in P, j \in C_i} AOS_{ij} \tag{4}$$

Where P is the end-to-end path. M is the path metric. C_i is the set of available channels for Cognitive Node i belonging to the path P

B. Application-Oriented Routing

In this section, we introduce our protocol using on-demand routing approach. When an application of CR node demands to transmit data, CR source node will initiate route discovery by broadcasting route request packet on CCC. After that, each intermediate node along the routes to destination will add the AOS information of channels into the route request packet in sequence. Whenever route request packets reach the destination node, destination node will use AOS information of channels to calculate the metric of each path and choose the path with minimum metric as the route of source node to the destination node.

Based on Ad-hoc On-Demand Distance Vector (AODV) routing protocol in NS-2 (version 2.31) [13] and CRN Simulator [14], Application-Oriented Routing Protocol (AORP) is implemented. Route REQuest (RREQ) packet format, route discovery and route selection are modified to implement AORP

1) *Route Request Packet Format*: To implement AORP, the RREQ packet needs to be modified to carry all information along the path which allow destination node to choose the appropriate path for source node. Each RREQ will contain complete information about a path between the source node and destination node: the address of intermediate node, the incoming channel used to communicate with its precedent node, the outgoing channel used to communicate with its successor node and the AOS value of the path associated with the intermediate node's outgoing channel. Beside that, the source node or intermediate nodes use neighbour IP address to send RREQ packets to its neighbours. In addition, the

application indicator c is also added to help intermediate node and destination node calculate the value of AOS and choose the appropriate path for source node according to the source node's application. The format of RREQ packet is depicted in Figure 4.

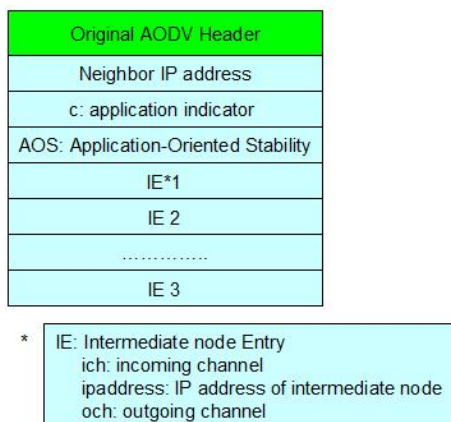


Fig. 4. Route Request Packet Format

2) *Route Discovery*: When an application of CR node demands to transmit data and CR node has not the route to the destination, source node will initiate multiple RREQ packets and send a RREQ packet to each neighbours on CCC. Each RREQ packet will contain the AOS value of the channel which has the minimum value of AOS among the common channels between source node and its neighbour. Whenever each intermediate node along the paths to destination receives a RREQ packet, it uses the Intermediate node Entry (IE) to check whether the RREQ packet is already forwarded by it. If the RREQ packet is not forwarded by the intermediate node yet, the intermediate node will create multiple the RREQ packets. The number of RREQ packets is equal to the number of its neighbours. For each pair of intermediate node and its neighbour, the intermediate node adds its address into the RREQ packet, puts the channel used to communicate with its precedent node in the incoming channel field of RREQ packet, puts the channel with the minimum value of AOS in the outgoing channel field of RREQ packet and updates the AOS value. Finally, the intermediate node sends the RREQ packets to its neighbours on CCC.

3) *Route Selection*: When the destination node receives a new RREQ packet, it will follow the below procedure to handle this packet:

Step 1: If there does not exist a path from the source node to destination node, then choose the route stored in RREQ and go to step 3, else go to step 2.

Step 2: If there exist a path from the source node to destination node, then compare the AOS value of existing path with the AOS value stored in the arrived RREQ. If the AOS value of existing path is less than or equal to the AOS value stored in RREQ, then ignore the RREQ packet, else update the path from source node to destination node to the new path stored in the arrived RREQ.

Step 3: Destination node sends ROUTE REPLY packet on licensed channel in unicast mode.

V. SIMULATION RESULTS

We study the proposed metric Application-Oriented Stability (AOS) through a simulation using ns2. The ON-OFF model and the AOS metric will be implanted in the MAC layer and Routing layer respectively. A MAC (named AOS-MAC) is modified from MAC IEEE 802.11 supported by ns2. AOS-MAC is implemented to allow secondary users (SUs) to transfer data on the channel transparently to primary users (PUs). In order to do this, SUs only send traffic in OFF periods and do not access the licensed channel in ON periods when PUs are present.

Two test cases are designed to validate the proposed ON-OFF model and the AOS metric. Throughout the simulations, we consider all topologies created in a flat area of $1000m \times 1000m$. In each test case, a number of intermediate nodes are placed between source node and destination node. Each intermediate nodes has its own accessible channel list. In addition, two connections TCP/FTP and UDP/VoIP are kept to maintain data transfer during the running time of the scenario.

To evaluate the performance of AORP, together with AORP, we will implement another routing protocol S-AODV. S-AODV is a modified version of AODV in which the most stable channel will be selected for data transmission. The routing metric of S-AODV is $\frac{1}{S}$ (S is presented in Formulation (1)). We then compare the network performance in the case that routing protocol is AORP with the network performance in the case that routing protocol is S-AODV.

Initially, test cases will be executed by using the S-AODV and then, will be run again by using AORP. The numerical results are collected, computed and analysed to deduct the performance obtained by using S-AODV and AORP. The performance of test cases are evaluated by two parameters throughput and packet loss. These parameters are mainly affected by the end-to-end (e2e) delays between source and destination because throughput is calculated by total packets in bytes over the duration of data transfer, while packet loss is counted by a delay time-out mechanism in TCP/FTP or a play-out delay threshold in UDP/VoIP application. In summary, the e2e delay affects directly to total packets sent successfully in a duration of data transfer which is set fixed (300s) in test cases. When e2e delay increases, less packets can reach to the destination. For ease to follow, below is the topologies of all test cases. Nodes in orange are source node and destination node of VoIP connection and nodes in blue are source node and destination node of FTP connection while the other nodes in white are the intermediate nodes. VoIP application is run with constant bit rate 64kbps. FTP is run with variable rate which claims the bandwidth (maximum 2Mbps) as much as possible. Channels with odd identifiers (1, 3, 5, etc.) should be preferred by VoIP application while channels with even identifiers (2, 4, 6, etc.) should be preferred by FTP application. In the work of AORP, the quality of channel will be associated to AOS.

Typically, the smaller the identifier is, the better the quality of the channel is.

Details for each test case result will be provided from Figure 7 to Figure 8 and Table II

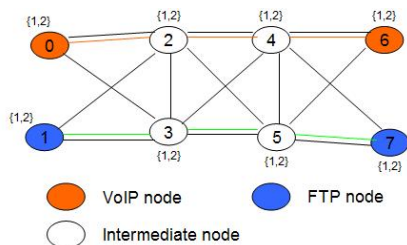


Fig. 5. 2 connections VoIP and FTP with less channel diversity in data flow

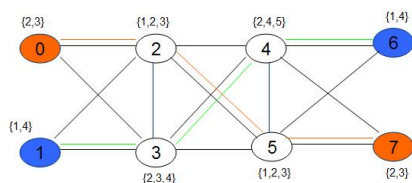


Fig. 6. 2 connections VoIP and FTP with channel diversity in data flow

TABLE II
TRAFFIC FLOW IN EACH TEST CASE

Test case	Traffic flow in case that routing protocol is AORP
Test case 1	VoIP traffic from node 0 to node 6 through node 2, 4 via channel 1 FTP traffic from node 1 to node 7 through node 3, 5 via channel 2
Test case 2	VoIP traffic from node 0 to node 7 through node 2, 5 via channels 3-1-3 FTP traffic from node 1 to node 6 through node 3, 4 via channels 4-2-4

In test case 1 and test case 2 (Figures 5 and 6), the performance of S-AODV is improved by AORP. This happens because by using S-AODV, all applications will try to use the most stable channels which have the largest average idle periods. Therefore, due to the AOS-MAC, all nodes have to compete with one another to take the channel and send the packet on the same channel. As the consequence, some packets might wait for a certain time before MAC is free again for being sent. This drawback could introduce the additional processing delay and increase the e2e delay, thus, increase the packet loss and reduce the performance for both VoIP connections and FTP connections. Compared to case with AOS, the applications will try to use the channels which are preferred to their needs. With the difference of preferred channel, nodes will not need to compete channels for data transmission and packets will not wait much for MAC to get free. Consequently, the AOS could lead both types of connection (VoIP and FTP) to the better performance.

However, in the concern of AORP, the diversity of channels could also give benefit to packets from the same flow. The throughput in Test case 2 (Figure 8(b)) is better than the throughput in Test case 1 (Figure 7(b)) because the path chosen in Test case 2 is composed by different channels while the path chosen in Test case 1 is composed by the same channel. The packets on path composed by different channels can avoid the channel competition and intra-flow interference caused by the transmission of packet belonging to the same flow. The channel competition and intra-flow interference would also introduce the additional processing delay, thus, reducing the throughput as shown in Test case 1.

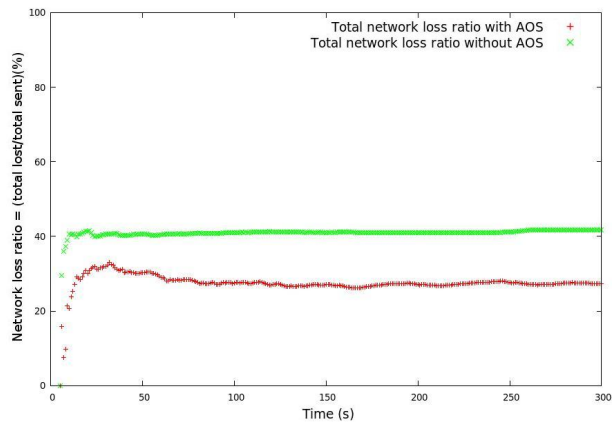
Regarding the total packet loss (Figure 7(a) and Figure 8(a)), the number of total lost packets is reduced significantly by using the AORP routing protocol instead of S-AODV. In case of S-AODV, all cognitive nodes are forced to use the most stable channel. In addition, the VoIP application is set to run with a low bit rate 64kbps while FTP application is set to claim the bandwidth as much as it can. According to this configuration, the packets of VoIP application would be sent out the channel later than packets of FTP application. As the consequence, these packets suffered from the additional processing delay (mentioned in previous paragraphs) and the packet e2e delay will exceed the play-out delay threshold of VoIP application. This play-out delay violation will cause packets to get dropped at destination and hence increase the packet loss of VoIP application, resulting in the increase in the total number of lost packets. On the contrary, in case of AORP, VoIP traffic and FTP traffic are separated on flows which have different interest of channels. By this way, there is no channel competition between nodes relaying VoIP traffic and nodes relaying FTP traffic. Therefore, the total packet loss is reduced dramatically.

VI. CONCLUSION AND FUTURE WORK

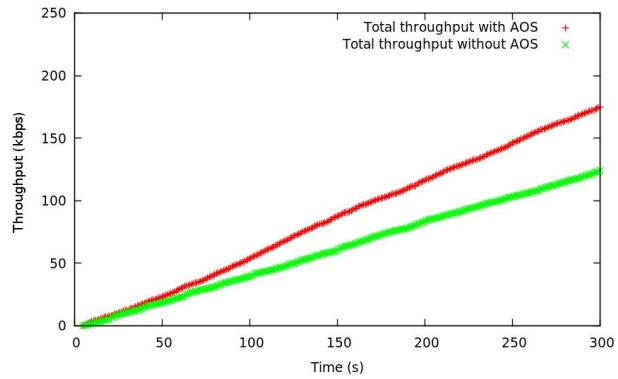
In this paper, we have proposed an application-oriented routing protocol in cognitive radio network. We studied the transmission behaviour of VoIP and FTP applications to figure out the appropriate channel for each type of application. Based on this study, the application-oriented stability metric and application-oriented routing protocol are proposed to find an appropriate path according to the application running in cognitive nodes. Through simulations, the application-oriented routing protocol was shown to outperform S-AODV. In the future, we envisage to investigate more applications' transmission behaviour to provide more efficient channel allocation and route composition schemes. We also consider channel bandwidth in conjunction with application-oriented stability parameter to find path satisfying the demand of cognitive users' applications. Additionally, the scenarios with more concurrent traffic flows will be examined to verify the scalability of AORP.

ACKNOWLEDGEMENTS

This work is supported by the internal project LIP6-ENST proposed to enhance the research collaboration between Uni-

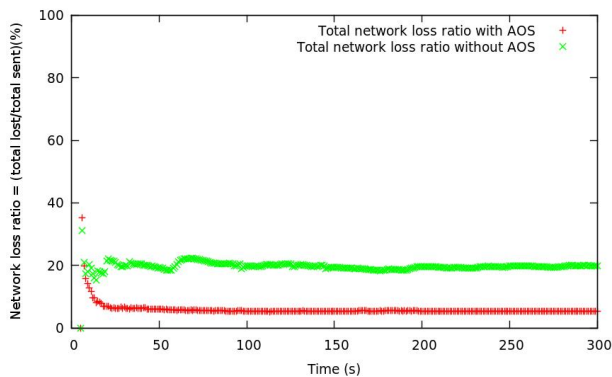


(a) Test case 1 - Loss

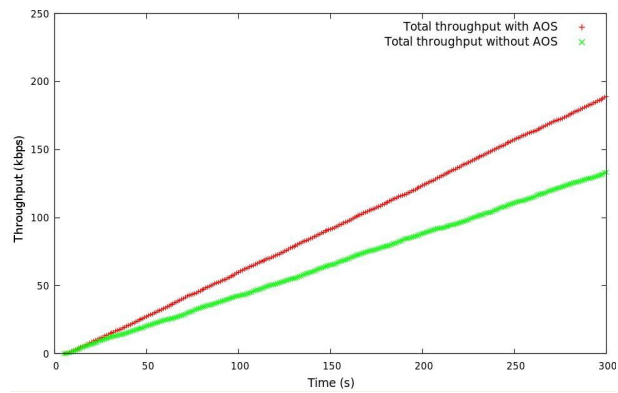


(b) Test case 1 - Throughput

Fig. 7. Test case 1 - No channel diversity



(a) Test case 2 - Loss



(b) Test case 2 - Throughput

Fig. 8. Test case 2 - Channel diversity

versity of Pierre and Marie Curie and Telecom ParisTech. Authors would like to thank Associate Professor Naceur Malouch from University of Pierre and Marie Curie for his valuable discussions about the routing techniques in CRN. Our thanks go also to Professor Philippe Martins from Telecom ParisTech for his remarks on spectrum sensing techniques and MAC layer aspects in CRN.

REFERENCES

[1] FCC, "Spectrum policy task force report", ET docket no. 02-155, November 2002.
 [2] FCC, "Notice for Proposed Rulemaking (NPRM 03 322): Facilitating Opportunities for Flexible Efficient, and Reliable Spectrum Use Employing Spectrum Agile Radio Technologies", ET docket no. 03 108, December 2003.
 [3] J. Mitola, "Cognitive Radio: an integrated agent architecture for software defined radio", PhD dissertation, Computer Communication System Laboratory, Department of Teleinformatics, KTH, Stockholm, Sweden, May 2000.
 [4] A. Sampath, L. Yang, L. Cao, H. Zheng, and B.Y. Zhao, "High Throughput Spectrum-aware Routing for Cognitive Radio Based Ad-hoc Networks", Third International Conference on Cognitive Radio Oriented Wireless Networks and Communications, May 2008.
 [5] G. Zhu, M.D. Felice, and I.F. Akyildiz, "STOD-RP: a spectrum-tree based on-demand routing protocol for multi-hop cognitive radio networks", IEEE Global Telecommunication Conference, pp. 1-5, November 2008.

[6] S. Deng, J. Chen, H. He, and W. Tang, "Collaborative Strategy for Route and Spectrum Selection in Cognitive Radio Networks", Future Generation Communication and Networking, pp. 168-172, December 2007.
 [7] M. Sharma, A. Sahoo, and K. D. Nayak, "Channel Selection under Interference Temperature Model i Multi-hop Cognitive Mesh Networks", IEEE Symposium on New Frontiers in Dynamic Spectrum Access Networks, pp. 133-136, April 2007.
 [8] G. Lei, W. Wang, T. Peng, and W. Wang, "Routing Metrics in Cognitive Radio Networks", IEEE International Conference on Circuits and Systems for Communications, pp. 265-269, May 2008.
 [9] L. Gong, S. Deng, W. Tang, and S. Li, "Anti-intermittence source routing protocol in distributed cogive radio network", International Conference on Wireless Communications, Networking and Mobile Computing, pp. 1-6, October 2008.
 [10] H. He, L. Gong, W. Tang, J. Wang, and S. Li, "Spectrum-aware Anti-intermittence Routing in Distributed Cognitive radio Network", International Conference on Communication, Circuit and System, pp. 236-240, July 2009.
 [11] L. Qin, J. Wang, and S. Li, "Stability-Driven Routing And Spectrum Selection Protocol in Cognitive Radio Networks", IEEE International Conference on Communication Technology and Applications, pp. 269-273, October 2009.
 [12] H. Su and X. Zhang, "Opportunistic MAC Protocols for Cognitive Radio Based Wireless Networks", The 41st Annual Conference on Information Sciences and Systems, pp. 363-368, March 2007.
 [13] The network simulator NS-2. <http://www.isi.edu/nsnam/ns>. August 2010.
 [14] Cognitive Radio Cognitive Network Simulator. <http://stuwweb.ee.mtu.edu/~ljialian/>. August 2010.

Improving Spectrum Sensing Performance by using Eigenvectors

Roberto Garello, Yifan Jia
 Department of Electronic (DELEN)
 Politecnico di Torino
 Turin, Italy

Email: garello@polito.it, yifan.jia@polito.it

Abstract—In this paper we present a method to improve the performance of eigenvalue-based detection, facilitated with eigenvectors of the sample covariance matrix. We focus on the multi-sensor detection of a single source case. If the channel is constant over adjacent sensing slots, it can be blindly estimated by using the eigenvector associated to the largest eigenvalue on condition of the source's presence. We introduce a new test where the eigenvector value, computed over some previous auxiliary slots, is properly used by the detection algorithm. The ROC curves show that the new test is able to outperform popular algorithms like the Roy Largest Root Test and the Energy Detection for both PSK and Gaussian sources, and to approach the optimal Neyman-Pearson performance with a very small number of auxiliary slots.

Keywords-largest eigenvector; spectrum sensing; cognitive radio; signal detection

I. INTRODUCTION

In Cognitive Radio (CR) scenario, secondary users can use multiple spectrum sensing techniques to enhance the detection performance of primary user's absence or presence, i.e., making a decision between the alternative hypothesis of pure noise (\mathcal{H}_0) or signal plus noise (\mathcal{H}_1). The new CR systems and standard will impose tight constraints on the detection algorithm performance. As an example, the IEEE 802.22 WRAN (Wireless Regional Area Networks) standard [1] requires very low values for the false alarm (P_{fa} lower than 0.1) and high detection probability (P_d no less than 0.9). These requirements may be difficult to be obtained with the popular energy detection (ED) [2], which simply compares the energy of the received signal against the noise level. ED performs very well in normal situations, but it can be unable to match stringent requirements in some extreme (but important) cases, like for example hidden nodes, where the signal-to-noise ratio (SNR) may be -10 dB or lower.

For this reason, several eigenvalue-based detection algorithms have been proposed in recent years, aiming to improve the performance of ED. Non-parametric methods, i.e., without a complete knowledge of all the system (signal, noise and channel) parameters can be generally categorized as (i) blind detectors, without knowledge of any parameter - to name a few, the Generalized Likelihood Ratio Test (GLRT) [3] and the Eigenvalue Ratio Test (ERT) [4]; (ii) semi-blind detectors, where some parameters are known

- such as the Roy Largest Root Test (RLRT) [5] which resorts to the noise level knowledge; (iii) trained detectors, where some parameters are estimated outside the sensing slots. These algorithms can be compared by studying the ROC (Receiver Operating Characteristics) curves, plotting the P_d as the function of P_{fa} . Most systems compute the test threshold as a function of P_{fa} (to guarantee Constant False Alarm Rate - CFAR). Then, a system outperforms another if it achieves a higher P_d at the parity of a certain P_{fa} .

It is known that, among all possible detection tests, an optimal solution exists. The likelihood ratio test derived according to the Neyman-Pearson (NP) lemma [6] for an alternative hypothesis, is the uniformly most powerful test. Unfortunately, the NP test is a parametric method requiring strong knowledge of the signal, noise, and channel parameters. For the case of semi-blind detectors with known noise level but unknown channel, the RLRT test is proved to be the best algorithm [7]. However, as can be observed by comparing their ROC curves, the gap between the NP and the RLRT is rather large. This penalty is essentially due to the gain/lack of the channel knowledge.

In single source case, if the channel is constant within adjacent sensing slots, it can be blindly estimated (i.e., without any use of pilot symbols) by using the eigenvector associated to the largest eigenvalue of the sample covariance matrix of the signal slots. The idea of this paper is to exploit this to enhance the detection performance of eigenvalue-based tests. To do this we propose a new test, called EigenVEctor (EVE) test, that explicitly employs the eigenvector in the test statistic. Simulation results shows the EVE test performs at least as good as the RLRT and with increased prior available auxiliary signal slots, is able to significantly cover the gap between the NP and the RLRT test. The paper is arranged as follows: The adopted model is presented in Section II. NP and RLRT tests are reviewed in Section III. The new EVE test is introduced in Section IV and its performance is analyzed in Section V. The practical consideration and future works are described in Section VI and Section VII.

II. MODEL

Denote by K the number of antennas or cooperative sensors and by N the number of samples per sensing slot.

We focus on a single source scenario, which is of interest for many detection problems, including cognitive radio. The $K \times 1$ received vector at time n collects the baseband complex (I/Q) samples from the K antennas:

$$\mathbf{y}(n) = [y_1(n) \dots y_k(n) \dots y_K(n)]^T.$$

We have:

$$\mathbf{y}(n) = \begin{cases} \mathbf{v}(n) & \mathcal{H}_0 \\ \mathbf{h}s(n) + \mathbf{v}(n) & \mathcal{H}_1 \end{cases}$$

where \mathbf{v} is a $K \times 1$ circularly symmetric complex Gaussian (CSCG) vector of noise samples with zero mean and variance σ_v^2 , i.e., $\mathbf{v}(n) \sim \mathcal{N}_{\mathbb{C}}(\mathbf{0}_{K \times 1}, \sigma_v^2 \mathbf{I}_{K \times K})$. All the noise vectors $\mathbf{v}(n)$ are assumed to be statistically independent.

The channel complex vector $\mathbf{h} = [h_1 \dots h_K]^T$ is assumed constant and memoryless within all the sensing window.

The signal samples $s(n)$ are assumed to have constant probability density function, zero mean and variance σ_s^2 . In the following, we will focus on two case studies, where signal samples $s(n)$ are independent Gaussian or PSK samples.

Under \mathcal{H}_1 , we define the average SNR at the receiver as

$$\rho \triangleq \frac{\mathbb{E} \|\mathbf{h}s(n)\|^2}{\mathbb{E} \|\mathbf{v}(n)\|^2} = \frac{\sigma_s^2 \|\mathbf{h}\|^2}{K \sigma_v^2} \quad (1)$$

Given the $K \times N$ received matrix

$$\mathbf{Y} \triangleq [\mathbf{y}(1) \dots \mathbf{y}(n) \dots \mathbf{y}(N)]. \quad (2)$$

and the $K \times K$ sample covariance matrix

$$\mathbf{R} \triangleq \frac{1}{N} \mathbf{Y} \mathbf{Y}^H \quad (3)$$

we will denote by $\lambda_1 \geq \dots \geq \lambda_K$ the eigenvalues of \mathbf{R} sorted in decreasing order and by $\mathbf{e}_1, \dots, \mathbf{e}_K$ the corresponding normalized eigenvectors.

III. KNOWN TEST STATISTICS

To make the decision between \mathcal{H}_0 and \mathcal{H}_1 , a test statistic compares a quantity T against a pre-defined threshold t : if $T > t$ \mathcal{H}_1 is selected, otherwise \mathcal{H}_0 is chosen. The test performance is evaluated by the false alarm probability $P_{fa} = \Pr(T > t | \mathcal{H}_0)$ and the detection probability $P_d = \Pr(T > t | \mathcal{H}_1)$. In practical, the decision threshold t is typically computed as a function of the target P_{fa} , to guarantee the aforementioned CFAR property.

The Neyman Pearson (NP) test is given by the following likelihood ratio:

$$T_{NP} = \frac{p_1(\mathbf{Y}; \mathbf{h}, \sigma_s^2, \sigma_v^2)}{p_0(\mathbf{Y}; \sigma_v^2)}. \quad (4)$$

and is known to be optimal, i.e., to achieve the maximum possible P_d for any given value of P_{fa} .

As an example, under the considered model, if the signal samples are independent Gaussian samples, the NP test is obtained by using [3]:

$$p_0(\mathbf{Y}; \sigma_v^2) = \frac{1}{(\pi \sigma_v^2)^{NK}} \exp\left(-\frac{N \text{tr} \mathbf{R}}{\sigma_v^2}\right)$$

and

$$p_1(\mathbf{Y}; \mathbf{h}, \sigma_s^2, \sigma_v^2) = \frac{1}{(\pi^K \det \Sigma)^N} \exp[-N \text{tr}(\mathbf{R} \Sigma^{-1})].$$

where $\Sigma = \sigma_v^2 \mathbf{I}_K + \sigma_s^2 \mathbf{h} \mathbf{h}^H$.

The NP test requires the exact knowledge of both the channel vector \mathbf{h} and the noise variance σ_v^2 . As pointed out in [7], if only the noise variance is known and the SNR is above the identifiability threshold:

$$\rho_{\text{crit}} = \frac{1}{\sqrt{KN}} \quad (5)$$

the best statistical test is the RLRT [5], which compares the largest eigenvalue of the sample covariance matrix against σ_v^2 :

$$T_R = \frac{\lambda_1}{\sigma_v^2}. \quad (6)$$

The RLRT outperforms all the other algorithms belonging to the class of semi-blind algorithms [8], i.e., where the noise level is assumed to be known, including the popular ED, which is given by:

$$T_{ED} = \frac{1}{KN \sigma_v^2} \sum_{k=1}^K \sum_{n=1}^N |y_k(n)|^2 \quad (7)$$

Despite of the superiority in its class, the gap between the RLRT and the NP test is not negligible, as it can be seen by observing the ROC curves reported in Figure 2. The scope of this paper is to cover the gap between RLRT and NP. To do this, we intend to use the eigenvector of the sample covariance matrix.

IV. THE NEW EVE TEST

Since the RLRT is the best test within the class of semi-blind algorithms, the performance differences with respect to the NP test must be due to the lack of channel knowledge. The method proposed in this paper works for a static channel, or at least a channel that can be considered as flat fading not only for the sensing slot but for some adjacent sensing slots. Clearly, this prevents its application to any kind of mobility. Despite of this, the results are extremely interesting for all the cases where the channel can be considered as static for some time because, as we will see, the new method is indeed able to approach the NP optimal performance.

The starting idea of the new test is that, given a \mathcal{H}_1 slot, the eigenvector \mathbf{e}_1 associated to the largest eigenvalue λ_1 provides an estimation of the channel vector \mathbf{h} . Given N_{aux} signal slots available before the current sensing slot, let us denote by \mathbf{e}_{aux} the normalized (i.e., with unitary energy) eigenvector computed by using $N_{aux} \cdot N$ samples. Now, the problem is how to properly use \mathbf{e}_{aux} during the current sensing slot. To do this we want to introduce a new statistical test that (i) uses \mathbf{e}_{aux} , (ii) is at least as strong as the RLRT, (iii) is able to approach the NP test when N_{aux} increases. Given the matrix \mathbf{Y} received in the current sensing slot, let

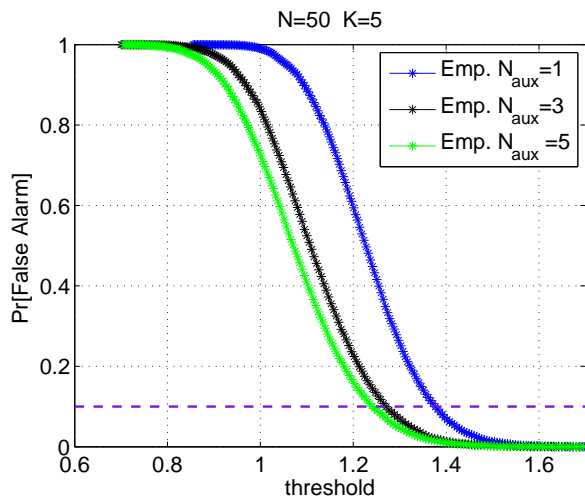


Figure 1. False Alarm Probability

us compute the sample covariance matrix R and the largest eigenvector e . Suppose that the quantity e_{aux} computed over N_{aux} previous signal slots is available, the proposed statistical test, called the EigenVEctor (EVE) test, is defined as:

$$T_{EVE} = \frac{N_{aux} [e_{aux}^H R e_{aux}] + [e^H R e]}{\sigma_v^2 (N_{aux} + 1)} \quad (8)$$

Note that if $N_{aux} = 0$, the test reduces to

$$T_{EVE} = \frac{e^H R e}{\sigma_v^2} = \frac{\|e\|^2 \lambda_1}{\sigma_v^2} = \frac{\lambda_1}{\sigma_v^2} \quad (9)$$

and has the same statistical power of the RLRT. We will now show that, for increasing N_{aux} , the test outperforms the RLRT and is able to cover the gap with respect to the NP test.

V. THE PERFORMANCE OF THE EVE TEST

Fixed a given threshold γ , the behavior of the false alarm probability is shown in Figure 1 for $N = 50$, $K = 5$ and $N_{aux} = 1, 3, 5$. These curves can be used to compute the threshold necessary to achieve a given false alarm rate. For example, the threshold values corresponding to $P_{fa} = 0.1$ are identified in the figure.

The ROC curves of the EVE test are plotted in Figure 2, 3, and 4 for $N = 50$, $K = 5$, $SNR = -10dB$, $N_{aux} = 1, 3, 5$, and compared against those of the Neyman-Pearson, the RLRT, and the Energy Detection. We can observe that (i) the new EVE test significantly outperforms the RLRT test and (ii) the EVE test approaches the Neyman-Pearson test even with a limited number of auxiliary slots.

Given a false alarm probability value $P_{fa} = 0.1$ and chosen the threshold γ according to it, fixed the SNR value, the behavior of the detection probability as a function of the number of antennas is reported in Figure 5, 6, and 7. It can

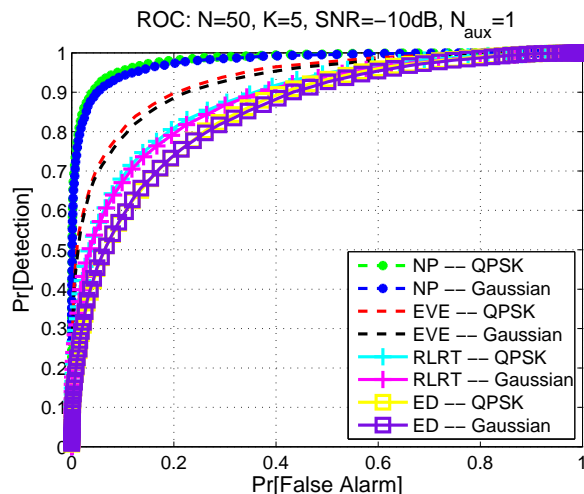


Figure 2. ROC curve

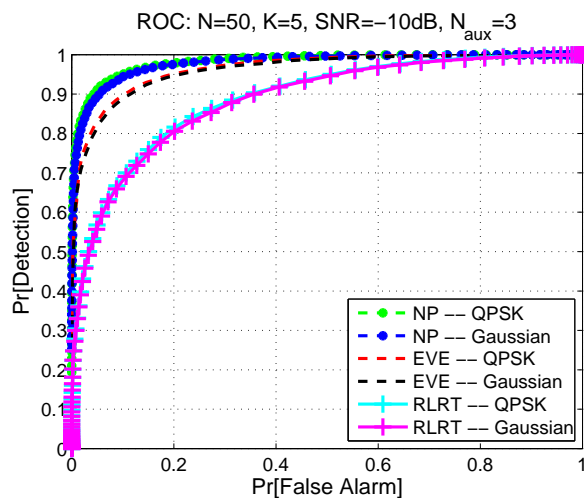


Figure 3. ROC curve

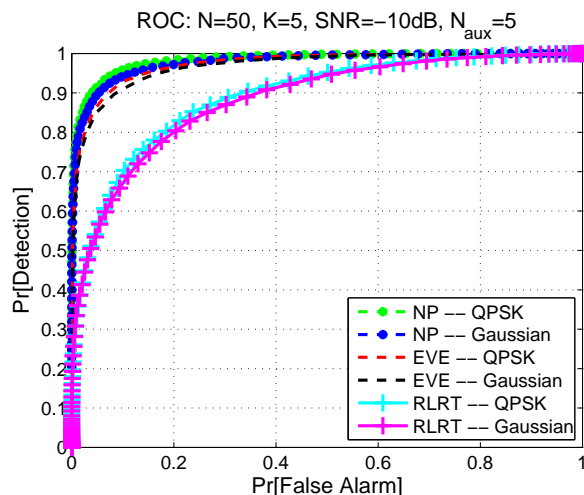


Figure 4. ROC curve

be observe that, at the parity of P_{fa} and P_d values, the EVE test requires a much lower number of antennas to achieve the same performance.

Given a false alarm probability value $P_{fa} = 0.1$ and chosen the threshold γ according to it, the behavior of the detection probability as a function of the signal-to-noise ratio is reported in Figure 8, 9, 10, and 11. By fixing a P_d value (for example 0.9 in the figures) it is possible to appreciate the improvement achieved by the EVE test in terms of received SNR at the parity of P_{fa} and P_d values. In the figures, a gain up to 2 dB is observed with respect to the RLRT, and up to 4 dB with respect to ED.

VI. PRACTICAL CONSIDERATIONS: ADJACENT SLOTS AND UNKNOWN NOISE VARIANCE

For practical applications, it is interesting to note that the test does not really require dedicated training slots. The eigenvectors can be computed by using the samples from the slots marked as \mathcal{H}_1 by the running sensing algorithm with a high reliability. Moreover, the EVE test can be modified to cover the case of unknown noise variance. As an example, the following modified test

$$T'_{EVE} = \frac{N_{aux} [e_{aux}^H R e_{aux}] + [e^H R e]}{\left(\frac{1}{K-1} \sum_{i=2}^K \lambda_i\right) (N_{aux} + 1)} \quad (10)$$

Since $\frac{1}{K-1} \sum_{i=2}^K \lambda_i$ represents the Maximum Likelihood estimation of the noise variance [9], the test is equivalent to the GLRT for $N_{aux} = 0$ and is able to improve it for increasing N_{aux} .

VII. CONCLUSIONS AND FUTURE WORKS

A new test using the eigenvector of the sample covariance matrix has been presented and evaluated in this paper. The test requires the channel to be constant over a number of adjacent slots, so it can be used only for constant or slowly changing channels. The improvement obtained with respect to the popular RLRT and ED tests is significant and the performances rapidly approach the optimal NP curves. Future research will focus on the computation of closed-form analytical formulas for the false alarm and detection probability.

REFERENCES

[1] IEEE 802.22, "Draft Standard for Wireless Regional Area Networks Part 22: Cognitive Wireless RAN Medium Access Control(MAC) and Physical Layer(PHY) Specifications: Policies and Procedures for Operation in the TV Bands," IEEE P802.22-D1.1, July 2008.

[2] H. Urkowitz, "Energy Detection of Unknown Deterministic Signals," Proc. IEEE, vol. 55, pp. 523-531, April 1967.

[3] P. Bianchi, M. Debbah, M. Maida, and J. Najim, "Performance of Statistical Tests for Source Detection using Random Matrix Theory," <http://arxiv.org/abs/0910.0827>. Last check: January 2011

[4] Y. Zeng and Y.-C. Liang, "Maximum-Minimum Eigenvalue Detection for Cognitive Radio," Proc. 18th Annual IEEE Intern. Symposium on Personal, Indoor and Mobile Radio Communication (PIMRC) '07, pp. 1-5, September 2007.

[5] S. N. Roy, "On a heuristic method of test construction and its use in multivariate analysis," Ann. Math. Stat., vol. 24, no. 2, pp. 220-238, 1953.

[6] J. Neyman and E. Pearson, "On the Problem of the Most Efficient Tests of Statistical Hypotheses," Philosophical Transactions of the Royal Society of London, Series A, vol. 231, pp. 289-337, 1933.

[7] S. Kritchman and B. Nadler, "Non-Parametric Detections of the Number of Signals: Hypothesis Testing and Random Matrix Theory," IEEE Trans. on Signal Processing, vol. 57, no. 10, pp. 3930-3941, 2009.

[8] Y. Zeng, Y.-C. Liang, A. T. Hoang, and R. Zhang, "A Review on Spectrum Sensing for Cognitive Radio: Challenges and Solutions," EURASIP Journal on Advances in Signal Processing, vol. 2010, pp. 1-15, January 2010.

[9] M. Wax and T. Kailath, "Detection of Signals by Information Theoretic Criteria," IEEE Trans. on Acoustics, Speech and Signal Processing, vol. ASSP-33, no. 2, pp.387-392, April 1985.

[10] I. M. Johnstone, "On the distribution of the largest eigenvalue in principal component analysis," Annals of Statistics, vol.29, no.2, pp.295-327, 2001

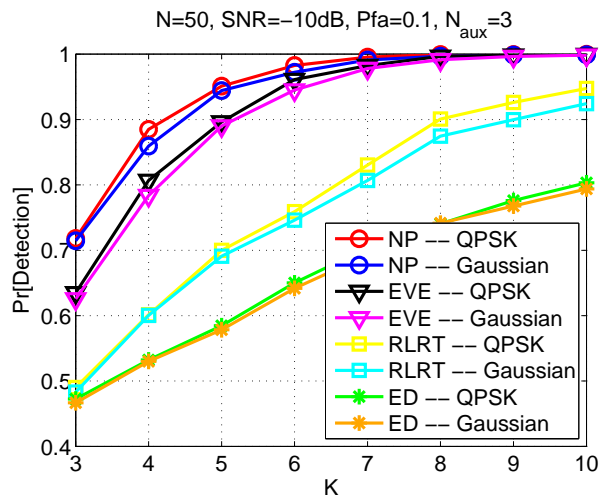


Figure 5. Antenna Gain

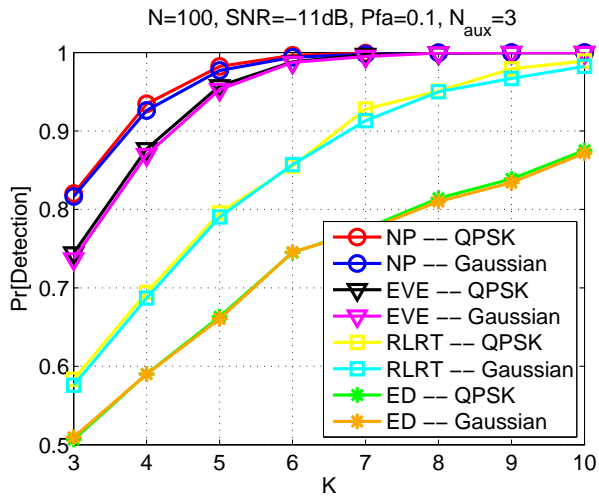


Figure 6. Antenna Gain

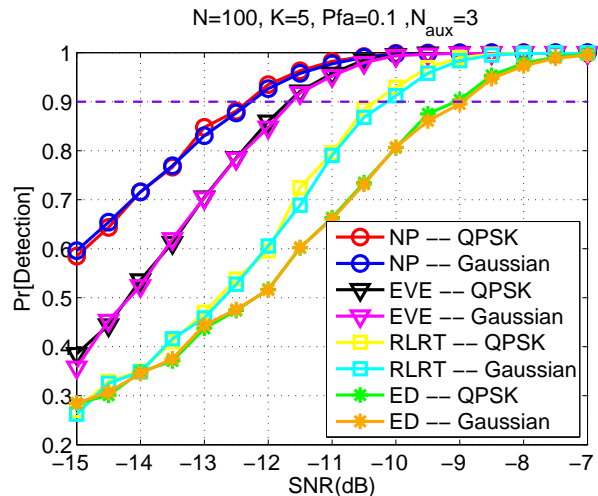


Figure 9. SNR Gain

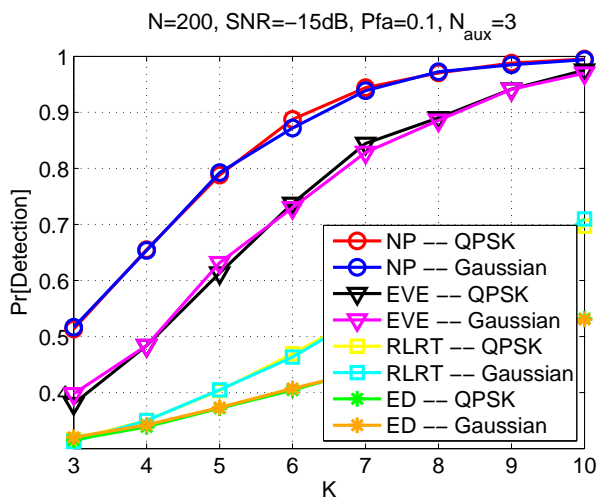


Figure 7. Antenna Gain

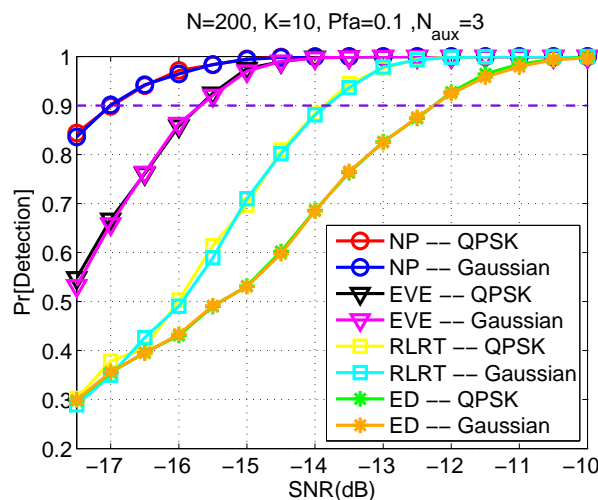


Figure 10. SNR Gain

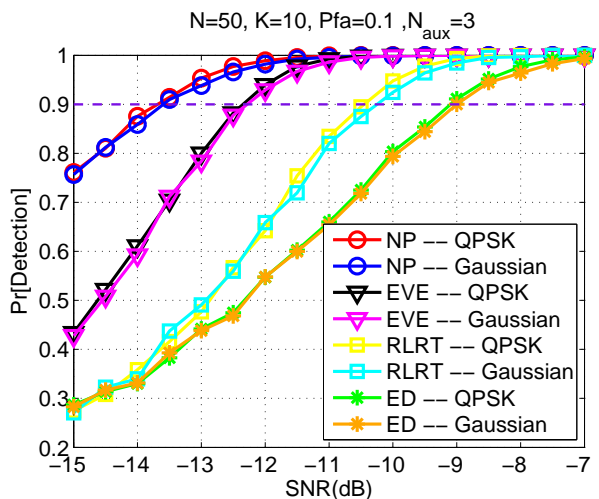


Figure 8. SNR Gain

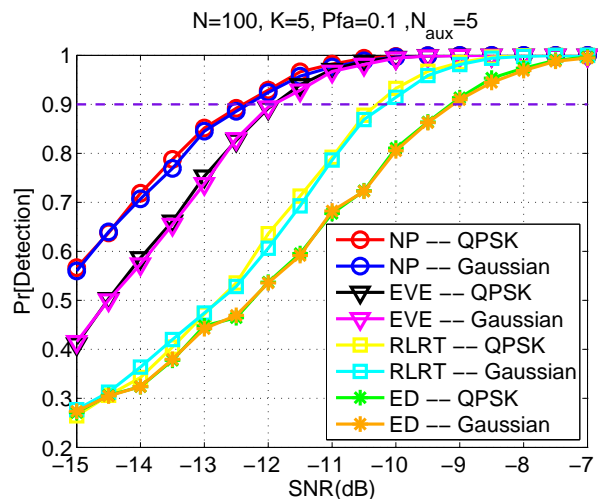


Figure 11. SNR Gain

Iterative Decision Feedback Equalization for Filter Bank Multicarrier Systems

Zsolt Kollár and Gábor Péceli

Department of Measurement and Information Systems
Budapest University of Technology and Economics
Budapest, Hungary
Email: {kollarzs,peceli}@mit.bme.hu

Péter Horváth

Department of Broadband Infocommunications
and Electromagnetic Theory
Budapest University of Technology and Economics
Budapest, Hungary
Email: hp@mht.bme.hu

Abstract—Filter Bank Multicarrier (FBMC) systems are a class of multicarrier modulation schemes for high speed wireless communication. These systems are known for their low adjacent channel leakage. In this paper we focus on the problem of channel equalization for FBMC systems. Most solutions in the literature use a per subcarrier equalization suffering from an error floor at high signal-to-noise ratios (SNR) caused by the residual inter-symbol-interference (ISI). We investigate a simple per subcarrier channel equalization method with ISI minimization and an averaging based ISI cancelation technique. We also introduce an iterative decision feedback scheme which outperforms the other known equalization methods. The presented methods are validated using simulation. The results are compared to the performance of Orthogonal Frequency Division Multiplexing (OFDM) systems with cyclic prefix (CP).

Keywords-FBMC; iterative; channel equalization; decision feedback.

I. INTRODUCTION

The introduction of Cognitive Radio (CR) triggered a new interest for researching alternatives of OFDM multicarrier systems [1]. In this paper, we focus on the FBMC systems as a major candidate competing with OFDM in CR scenarios. OFDM is a widely adopted modulation scheme due to its simple modulation/demodulation using IFFT/FFT block and a channel equalization with low complexity. Despite its many advantages it has some significant drawbacks which must be taken into consideration during the design.

These disadvantages include sensitivity to nonlinear distortions – due to the fluctuations in the instantaneous amplitude of the transmitted signal – as well as sensitivity to frequency offsets caused by local oscillator mismatch. Another important aspect is its spectral properties, especially the out of band radiation which is considered moderate in case of OFDM, but in this respect FBMC has a much better performance. The transmission data rate will be higher due to the fact that FBMC does not apply a CP. On the other hand, the channel equalization is more complex compared to OFDM due to the ISI caused by the multipath channel. In this paper, we focus on channel equalization for FBMC and OFDM systems. The basic problem of equalization for FBMC systems is presented in [2] and [3].



Figure 1. Block diagram of the OFDM transmitter

The paper is structured as follows. In Section II the OFDM and FBMC modulation schemes are described. In Section III we present the baseband signal model. In Section IV we introduce the channel equalization schemes that we intend to analyze in four subsections: first the basic per subchannel Zero Forcing (ZF) and Minimum Mean Square Error (MMSE), then the modified MMSE which minimizes the ISI and the averaged MMSE technique. In the last subsection, we present a new decision feedback equalization technique. In Section V we verify the channel equalization techniques for FBMC systems via bit error rate simulations and we assess their performance by comparing them to OFDM employing MMSE equalization. Finally, the conclusion is drawn.

II. OFDM AND FBMC MODULATION SCHEME

A. OFDM

In this section, we give only a short description of the OFDM modulation scheme. A general block diagram of an OFDM system can be seen in Fig. 1. First the bits are mapped to constellation symbols X . The time domain samples of an OFDM symbol are generated using IFFT as

$$x_n = \sum_{k=0}^{N-1} X_k e^{j\frac{2\pi}{N}nk}, \quad n = 0 \dots N-1, \quad (1)$$

where X_k is the complex modulation value for the k^{th} subcarrier. The CP is added to the OFDM symbol to form the transmitted signal s_n .

B. FBMC

FBMC systems are derived from the orthogonal lapped transforms [4] and filter bank theory [5]. The block diagram of one possible implementation of an FBMC transmitter can be seen in Fig. 2. Similar to OFDM the bits are first mapped to symbols X drawn from a complex constellation. Then the

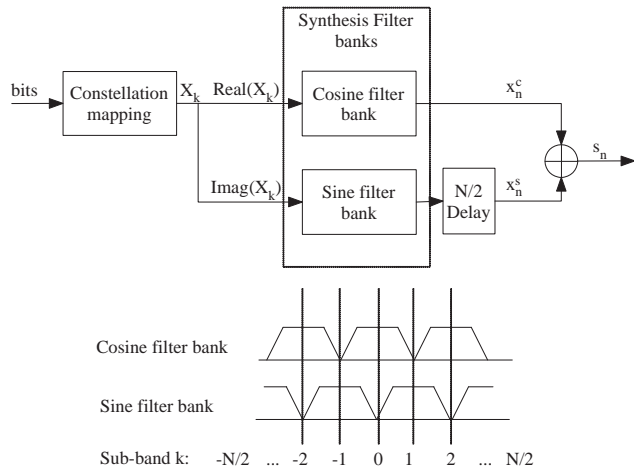


Figure 2. Block diagram of the FBMC transmitter, with the spectral structure of the cosine and sine filterbanks

real parts are modulated by a cosine filter bank where only the even-index subbands are used and the imaginary parts are modulated by a sine filter bank where only the odd-index subbands are modulated. An offset of half of the symbol overlapping $N/2$ duration is applied to the output of the sine filter bank – similarly to the offset quadrature amplitude modulation technique. The basic structure of the filter banks can be also seen in Fig. 3. First the frequency domain data is spread over M subcarriers forming a subband, then it is filtered by a prototype filter of the k^{th} subband $F_k(z)$ which is designed so that it fulfils the Nyquist criterion. In FBMC applications these filter bank structures are implemented in a computationally efficient manner using an N-IDFT and a polyphase network [5]. The filter bank yields symbols that span $N * M$ samples each. In order not to lose data rate they will overlap by a factor M – due to the Nyquist criteria, the symbols can be separated in the receiver and a perfect reconstruction is possible –. For example if $M = 4$ then 4 FBMC symbols overlap. This can be seen in Fig. 4 where the signal structure of FBMC is compared to the signal structure of the OFDM signal. The FBMC signal is given for an overlapping/oversampling factor of $M = 4$. The resulting transmitted signal is the sum of overlapping FBMC symbols generated by the filter banks.

III. BASEBAND TRANSCEIVER CHAIN

The applied baseband model for the transceiver chain can be seen in Fig. 5. The discrete received signal r_n can be expressed as

$$r_n = x_n * h_n + w_n, \quad (2)$$

where x_n , h_n and w_n are the samples of the transmitted signal, channel impulse response and AWGN noise respectively. We will use this model when dealing with the equalization algorithms, where the samples of the channel

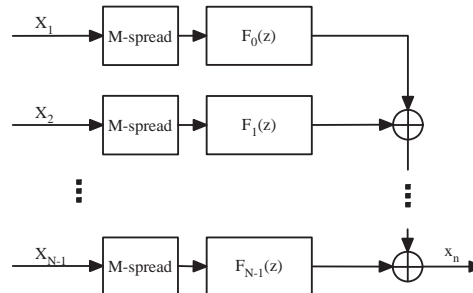


Figure 3. Basic structure of the filter bank with an oversampling ratio of M .

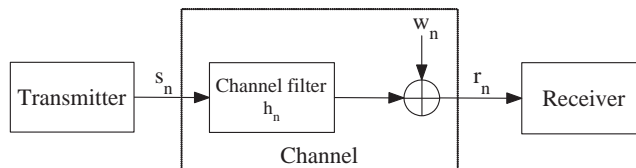


Figure 5. Model of the baseband transceiver chain.

impulse response are Rayleigh distributed, and the following expression is valid

$$\sum_{n=0}^{L-1} |h_n|^2 = 1. \quad (3)$$

where L is the length of the channel impulse response. In case of OFDM systems, if the CP is longer than the channel impulse response (2), after removing the cyclic prefix we can write for an OFDM symbol

$$Y_k = X_k H_k + W_k, \quad k = 0 \dots N - 1, \quad (4)$$

where Y_k is the N-FFT of r_n , belonging to one OFDM symbol. X_k , H_k and W_k are also an N-FFT of the signal x_n , h_n and w_n respectively. For FBMC systems the frequency domain description is more complicated due to ISI from the neighboring symbols. One of the implications of this ISI is that FBMC systems will require different equalization strategies.

IV. CHANNEL EQUALIZATION

A. ZF and MMSE

Zero forcing is known to be the simplest method for channel equalization in the frequency domain. We simply assume that the received noise is zero in equation (4), so the transmitted complex constellation value on the k^{th} subcarrier can be simply calculated as

$$\hat{X}_k^{\text{ZF}} = \frac{Y_k}{H_k}. \quad (5)$$

The MMSE technique gives a better result if we also take the information about the AWGN noise also into account. The problem of ZF occurs if H_k is small, the noise values will be

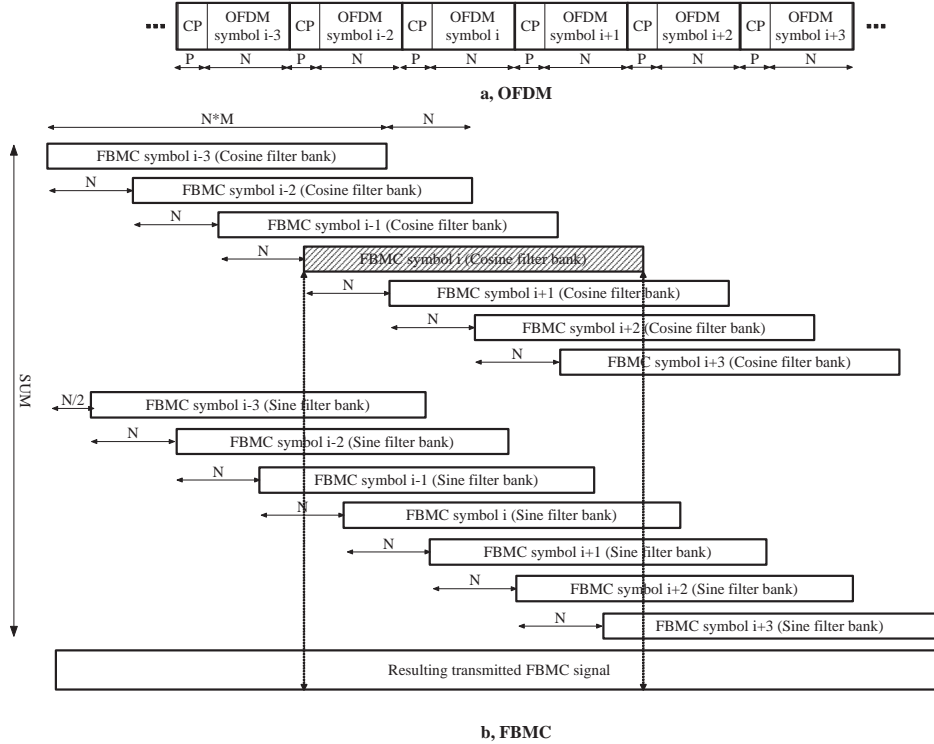


Figure 4. The structure of the transmitted (a) OFDM signal (with a symbol length N and a CP with a length P samples) and the (b) FBMC signal with an overlapping ratio of $M = 4$.

also amplified. The equalization coefficient $H_k^{\text{MMSE}} = \frac{1}{C_k}$ for the k^{th} subcarrier is calculated through the minimization the following expression:

$$\min_{C_k} E \left\{ \sum_{k=0}^{N-1} |X_k H_k - C_k Y_k|^2 \right\}, \quad (6)$$

where $E\{\cdot\}$ denotes the expected value of the argument. Using equation (4) the resulting channel compensation value for the k^{th} subcarrier is calculated according to [6] as

$$C_k = \frac{1}{H_k^{\text{MMSE}}} = \frac{H_k^*}{|H_k|^2 + \frac{N_0}{E_s}}, \quad (7)$$

where N_0 is the noise power and E_s is the signal power. It can be seen that with small $\frac{N_0}{E_s}$ values the MMSE solution is equal to the ZF. In case of FMBC and per-subcarrier equalization, (7) has to be modified in order to consider the ISI stemming for adjacent symbols similar to [7][8][9] as

$$\frac{1}{\hat{H}_k^{\text{MMSE}}} = \frac{H_k^*}{|H_k|^2 + \frac{N_0 + I}{E_s - I}} \quad (8)$$

where I is the power of the ISI, for which we present the following equation

$$I = E_s \sum_{n=0}^{L-1} \frac{n}{N} |h_n|^2. \quad (9)$$

Finally, the MMSE estimate results in

$$\hat{X}_k^{\text{MMSE}} = \frac{Y_k}{\hat{H}_k^{\text{MMSE}}}. \quad (10)$$

B. Modified MMSE I.

Observing (9) more closely, we have also concluded that the ISI can be minimized by moving the observation window along all possible positions of the channel impulse response to minimize the following equation

$$\min_{\Delta n} \{I(\Delta n)\} = \min_{\Delta n} \left\{ E_s \sum_{n=0}^{L-1} \frac{|n-\Delta n|}{N} |h_{|n-\Delta n|}|^2 \right\}, \quad (11)$$

$$\Delta n = 0 \dots L-1,$$

After finding the sample value Δn which minimizes equation (11), the observation window – where we perform the channel equalization – has to be moved by Δn samples and also the channel impulse response has to be circularly shifted, respectively as

$$\hat{X}_k^{\text{MIN}} = \frac{Y_k(\Delta n_{\min})}{\hat{H}_k^{\text{MMSE}}(\Delta n_{\min})}. \quad (12)$$

C. Modified MMSE II.

To further minimize the ISI we introduce the idea of the Averaged MMSE equalizer. The averaged MMSE is driven by the idea that the ISI can be also considered as

a noise, which can be eliminated by averaging. So based on the idea of moving the observation window, we perform the demodulation and MMSE equalization for each Δn positions of the possible L observation windows and then we average all complex modulation values belonging to the same subband

$$\hat{X}_k^{\text{AVG}} = \frac{1}{L} \sum_{\Delta n=0}^{L-1} \hat{X}_k^{\text{MMSE}}(\Delta n) = \frac{1}{L} \sum_{\Delta n=0}^{L-1} \frac{Y_k(\Delta n)}{\hat{H}_k^{\text{MMSE}}(\Delta n)} \quad (13)$$

With this calculation we can minimize the ISI.

D. Iterative decision feedback equalization

In this section we will introduce a novel iterative decision feedback scheme where the most reliable decision values are fed back after the decision to minimize the ISI in the received signal. This decision feedback scheme is shown in Fig. 6. The basic idea is to regenerate the transmitted signal, but only the subbands which are reliable, and filter it with the known channel filter. The idea is visualized in Fig. 4: If we want to make a decision for the shaded i^{th} FBMC symbol of the cosine filter bank, then we reconstruct as much as possible from the surrounding symbols $i-3, i-2 \dots i+3$ which overlap with it (both sine and cosine) based on the selection criteria. Then, during the decision on the i^{th} FBMC symbol the ISI of the known neighboring symbols can be subtracted, reducing the noise stemming from the ISI, leading to better performance. The selection criteria is defined based on the constellation diagram, we take confidence interval around each constellation point. The complex modulation symbols which fall inside this interval are considered as reliable. During the iteration process the interval can be enlarged as the ISI is minimized.

V. SIMULATION RESULTS

To verify the previously described equalization schemes, simulations were performed. The simulation parameters for both OFDM and FBMC system are summarized in Table I. In order to enable a proper comparison of the two different modulation schemes the SNR is defined as

$$\text{SNR}_{\text{dB}} = 10 \log_{10} \left(\frac{E_b}{N_0} \right) \quad (14)$$

$$= 10 \log_{10} \left(\frac{E_b N_c D}{(N+P) N_0} \right), \quad (15)$$

where E_b is the bit energy, N is the number of the subcarriers/subbands available and N_c is the number of subcarriers/subbands used. P is the length of the CP and D is the number of bits transmitted by one subcarrier/subband. During the simulations we have averaged the results of 10 channel realizations.

The simulated bit error rate (BER) for the proposed 3 MMSE equalization schemes can be seen in Fig. 7. For comparison we have also plotted the results for the AWGN channel without multipath propagation. For low SNR values

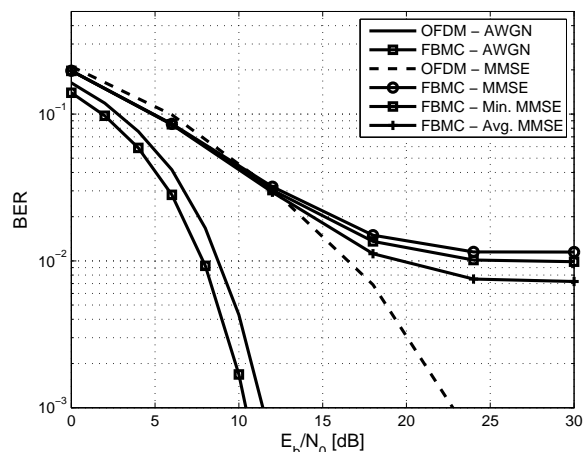


Figure 7. Bit error rate in function of SNR for the three MMSE-FBMC equalization schemes.

Table I
SIMULATION PARAMETERS FOR OFDM AND FBMC SYSTEM

Parameter	OFDM	FBMC
CP	16	-
N	64	64
M	1	4
Modulation (D)	16-QAM (4)	16-QAM (4)
Modulated subcarrier/subbands	48	48
Channel length L	16	16

the FBMC system has a very small gain over OFDM system in the BER results. It can be observed that OFDM outperforms FBMC at higher SNR value (SNR > 12 dB) the FBMC system when only an MMSE equalizer is applied. When introducing the minimized MMSE and the averaged MMSE, a small performance gain becomes apparent for large SNR values in favour of FBMC. This small difference will be crucial for the iterative decision feedback technique. These bit error rates can be considered as the starting values for the iterative algorithm.

The BER results for the iterative decision feedback technique is depicted in Fig. 8. The BER results for the 5. iteration step is plotted together with the initial starting values for the initial iteration. It can be observed that the averaged MMSE performs the best, the minimized MMSE has a similar result and finally the original MMSE has the worst BER.

VI. CONCLUSION

In this paper, we have investigated channel equalization schemes for FBMC system which were compared to the result of CP-OFDM system using MMSE equalization. First, modifications of the MMSE equalization technique suited for FBMC distorted by ISI were presented and the results were verified via simulation. We have also presented a decision

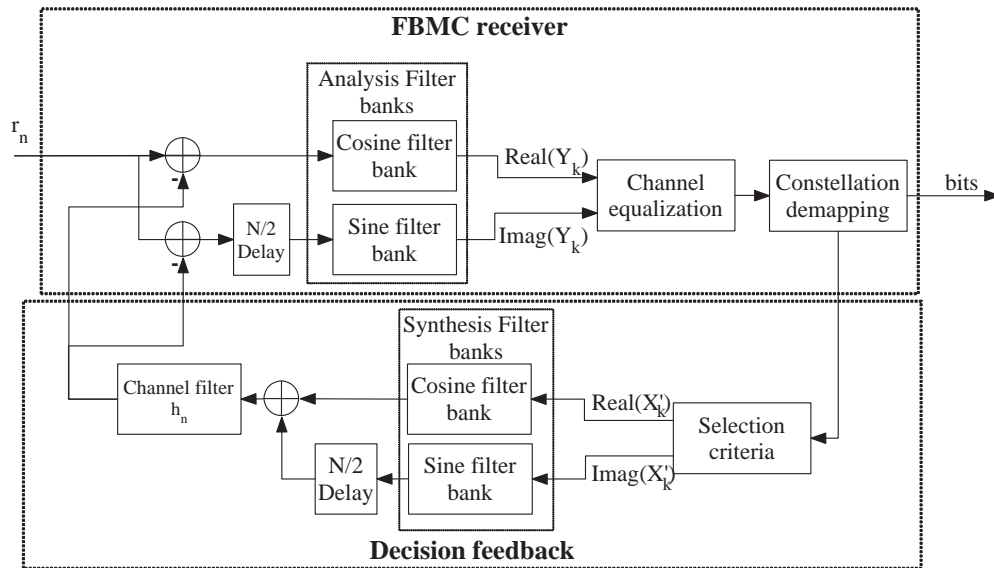


Figure 6. Model of the FBMC receiver with decision feedback loop.

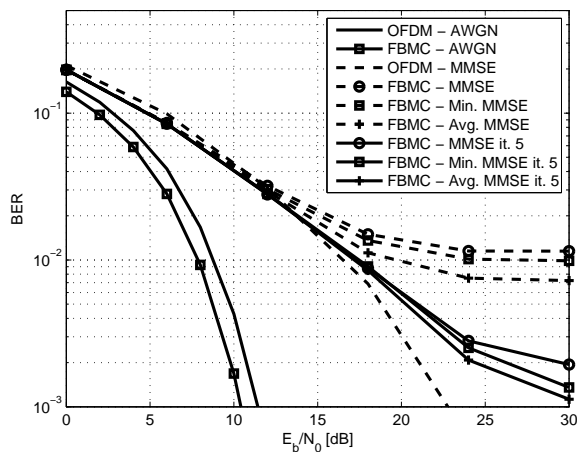


Figure 8. Bit error rate in function of SNR for the three MMSE-FBMC equalization schemes with decision feedback.

feedback scheme, which has a much better performance compared to the simple MMSE methods. The results show that FBMC is a very good candidate for competing with OFDM systems over multipath channels. The criteria for selecting the confidence interval around the constellation points requires further investigation, but the simulation provide promising results.

ACKNOWLEDGMENT

The research leading to these results was derived from the European Community’s Seventh Framework Programme (PF7) under Grant Agreement number 248454 (QoS MOS).

REFERENCES

- [1] Zs. Kollár and P. Horváth, “Modulation schemes for cognitive radio in white spaces,” *Radioengineering*, vol. 19, no. 4, pp. 511–517, Dec. 2010.
- [2] M. Renfors, H. Xing, A. Viholainen, and J. Rinne, “On channel equalization in filter bank based multicarrier wireless access systems,” in *Vehicular Technology Conference, 1999. VTC 1999 - Fall. IEEE VTS 50th*, vol. 1, Sep. 1999, pp. 228–232.
- [3] A. Viholainen, J. Alhava, J. Helenius, and J. Rinne, “Equalization in filter bank based multicarrier systems,” *IEEE Int. Conference on Electronics, Circuits and Systems*, Sep. 1999.
- [4] H. S. Malvar, “Extended lapped transforms: Properties, applications, and fast algorithms,” *IEEE Trans. on signal processing*, vol. 40, no. 11, pp. 2703–2714, Nov. 1992.
- [5] P. P. Vaidyanathan, *Multirate systems and filter banks*. Prentice-Hall Inc., 1993.
- [6] J. van de Beek, M. Edfors, M. Sandell, S. Wilson, and P. Borjesson, “On channel estimation in OFDM systems,” *Proc. IEEE Veh. Technol. Conf.*, vol. 2, pp. 815–819, Jul. 1995.
- [7] T. Ihalainen, T. H. Stitz, and M. Renfors, “Efficient per-carrier channel equalizer for filter bank based multicarrier systems,” in *Proceedings of IEEE International Symposium on Circuits and Systems (ISCAS '05)*, May 2005, pp. 3175–3178.
- [8] T. Ihalainen, T. H. Stitz, M. Rinne, and M. Renfors, “Channel equalization in filter bank based multicarrier modulation for wireless communications,” *EURASIP Journal Appl. Signal Process.*, Jan 2007.
- [9] A. Ikhlef and J. Louveaux, “Per subchannel equalization for MIMO FBMC/OQAM systems,” *Proc. of the conference IEEE PACRIM09*, Aug. 2009.

Impact of Control Channel Design on Cooperative Spectrum Sensing in Opportunistic Spectrum Access Networks

Marco Petracca, Franco Mazzenga, Remo Pomposini, Francesco Vatalaro
 University of Rome Tor Vergata, Italy
 E-mail: {petracca,mazzenga,pomposini,vatalaro}@ing.uniroma2.it

Romeo Giuliano
 RadioLabs, Rome, Italy
 E-mail: romeo.giuliano@radiolabs.it

Abstract—In Opportunistic Spectrum Access (OSA) networks, Secondary unlicensed Users (SUs) need a common Control Channel (CC) to identify the spectrum opportunities, i.e., common spectrum holes unused by licensed Primary Users (PUs). Typically, an *interference-free* CC is unrealistically assumed in the literature. In this paper we evaluate the impact of the availability and the characteristics of the CC on the performance of cooperative spectrum sensing. We deal with the dimensioning of an underlay Ultra-wideband (UWB) signalling network for the exchange of sensing data among secondary Cognitive Radio (CR) nodes avoiding harmful interference to PUs. To this aim, we analyse the trade-off between the connectivity degree of a multi-hop underlay UWB signalling network, directly related to the possibility to perform cooperative sensing, and its coexistence with PUs. It is observed that the correct dimensioning of the UWB signalling network allows to achieve high accuracy of PU detection without compromising primary systems.

Keywords - Cognitive Radio; Opportunistic Spectrum Access; Ultra-wideband; Control Channel.

I. INTRODUCTION

A lot of experimental studies prove the inefficient use of the radio spectrum [1], [2]. This result does not comply with the general belief that the available spectrum resources are not sufficient to meet the needs of the next generation wireless networks. Within the Cognitive Radio (CR) context [3], fixed spectrum allocation policy could be replaced by innovative forms of dynamic use, referred to as Dynamic Spectrum Access (DSA) [4]. Among the DSA options it is of great interest the so-called Hierarchical Access model (HAM) [5], according to which an unlicensed secondary CR user (SU) can access the spectrum licensed to a primary user (PU), provided that harmful interference is avoided.

In the literature, mainly two HAM approaches have been proposed [6]: “Spectrum Underlay”, also called horizontal sharing since based on spreading signals transmitted by SUs, for example by means of Ultra Wide Band (UWB) techniques; “Spectrum Overlay”, also known as Opportunistic Spectrum Access (OSA), according to which secondary nodes access the unused portion of band in a vertical way.

In order to guarantee protection to PUs [7], the underlay approach imposes SU transmission power below the required

maximum interference tolerance. This condition does not allow to provide SUs with high data rate services for medium and long range communications. The impossibility to make the best use of the unused spectrum resources prevents the underlay solution from achieving high values of spectral efficiency.

Conversely, OSA is the most performing solution in terms of achievable throughput, but it requires adaptive techniques accounting for the state of transmission of the PUs in order to allow the secondary nodes to identify the so-called “spectrum opportunity” [6], i.e., common white spaces, at a given location and time, agreed by a pair of SUs for communication. The spectrum opportunity identification requires a dedicated control channel (CC) to implement efficient signalling protocols for realizing OSA among SUs. More in general, a coordination among SUs is needed to improve the performance in terms of detection probability of PUs by means of cooperative spectrum sensing techniques [8]. Such methods assume particular relevance for detecting the spectrum occupancy when wireless channels are affected by shadow fading [9]. For these reasons the CC plays a fundamental role in OSA networks. Nevertheless, typically an *interference-free* CC is unrealistically assumed in the literature. Indeed, the allocation of a separate fixed CC for exchanging information on spectrum opportunities is very likely unavailable on PU networks with fast varying spectrum usage [10], and anyway it can entail waste of spectrum resources only for signalling data.

An interesting promising solution is represented by the usage of an underlay UWB channel for sharing spectrum sensing information, as proposed in [11]. Usually signalling channels require low bit-rates and this feature permits to extend the UWB radio coverage even for low transmission power. This satisfies the double target of ensuring as wide signalling coverage as possible with minimal interference to PUs, allowing to continuously perform coordination for white spaces exploitation. However, in [11], the authors consider just one licensed transmitter in the area without facing the problem of dimensioning the signalling network. Indeed, this issue entails to take into account the trade-off between the amount of sensing data exchanged on the secondary network and the interference caused to the PUs by the underlay signalling.

In this paper, we propose to exploit the benefits of both

Work performed within the project SANDRA, funded by the European Community's Seventh Framework Programme.

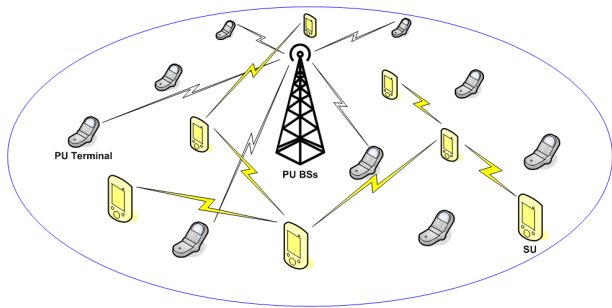


Figure 1. Interference scenario for secondary CR nodes and primary users.

HAM strategies by designing a *two-tier* OSA network, in which overlay spectrum access for data transmissions is driven by an underlay signalling network. We evaluate the impact of the availability and the characteristics of the CC on the performance of the OSA network in terms of cooperative detection probability. To this aim, we analyse the trade-off between the bit-rate of the CC and the connectivity degree of the underlay network for the exchange of sensing data among SUs. We also assess the maximum allowable density of the UWB devices such that the coexistence with primary systems is ensured, i.e., the interference caused by the signalling network does not compromise the performance of PUs.

The paper is organized as follows. In Section II, we describe the interference scenario for evaluating the performance of the underlay network in terms of accuracy of cooperative sensing and coexistence with PUs. The model for the analysis is detailed in Section III. Simulation results are reported in Section IV. Finally, conclusions are drawn in Section V.

II. INTERFERENCE SCENARIO

The interference scenario is shown in Figure 1. SUs can opportunistically access the spectrum for sensing information exchange provided that the interference level to PUs does not exceed a predefined threshold. We assume that the technology used by all the PUs in the scenario is the Global System for Mobile Communications (GSM). We considered three co-sited Base Stations (BSs) situated at the center of an area of 0.64 km^2 in a suburban environment. We assume that both PU terminals served by the BSs and SUs are randomly distributed within the area in accordance to an uniform spatial distribution. We suppose that BSs transmit at maximum power, whereas PU terminals implement power control mechanisms. This downbeat case is considered to demonstrate the capability of SUs to perform spectrum sensing sharing on the UWB underlay network even when hard interference conditions occur. For the same reason, we disregard traffic statistics of PUs and SUs by assuming that all the devices continuously transmit on their frequency band. Hence, more conservative results are expected by introducing a model accounting for users activity.

For the propagation model among devices in the area, we

considered the following expression for path loss calculation:

$$L(d) = \frac{MCL}{G_{tx} \cdot G_{rx}} \cdot \left(\frac{d}{d_0} \right)^\gamma \quad (1)$$

where $d > d_0$ is the distance (in m) between transmitter and receiver, $MCL > 0$ is the minimum coupling loss for $d_0 = 1$ m, γ is the path loss exponent and G_{tx} and G_{rx} are the antenna gains related to the transmitter and the receiver, respectively. According to values in [12], we conservatively set $\gamma = 2.5$ for outdoor propagation among UWB devices, while a path loss exponent equal to 3 is assumed for both PU links (between terminal and BS) and attenuation among PUs and SUs.

III. ANALYSIS

In this section we describe the proposed procedure to evaluate the density of SUs in the area such that a connectivity degree is reached guaranteeing the required level of protection to PUs at the same time. This trade-off depends on the bit-rate of the signalling channel. Then we provide an expression for calculation of cooperative detection probability accounting for the availability of the CC for exchanging sensing information among SUs.

A. UWB signalling network connectivity and coexistence

We characterize the availability of the CC in terms of the *Outage Probability* of the secondary underlay signalling network, given by:

$$P_{out} = Prob \{ SINR < \rho_0 \} \leq \alpha \quad (2)$$

$$s.t. \ 0 \leq P_{SU} \leq P_{max}$$

where ρ_0 is the required QoS level for the sensing information exchanging, α is the target outage probability and *SINR* is the *Signal-to-Noise plus Interference Ratio* expressed by the following formula:

$$SINR = \frac{E_b}{I_0 + \eta_0} = \left[\left(\frac{E_b}{I_{PU,0}} \cdot \frac{B_{UWB}}{B_{PU}} \right)^{-1} + \left(\frac{E_b}{\eta_0} \right)^{-1} \right]^{-1} =$$

$$= \left(\frac{C}{\eta} \right) \cdot \left[1 + (I_{BS} + I_T) \cdot \frac{R_b}{B_{UWB}} \right]^{-1} \quad (3)$$

where C is the received signal, R_b and B_{UWB} are the bit-rate and the bandwidth of the UWB devices, respectively, and η is the thermal noise power given by:

$$\eta = \eta_0 \cdot B_{UWB} \cdot N_F$$

where $\eta_0 = -174 \text{ dBm/Hz}$ is the noise PSD and N_F is the corresponding noise figure. As indicated in (2), the outage probability depends on both the interference from the active PUs and the propagation conditions. Furthermore, it is constrained on the transmission power of SUs, i.e., P_{SU} , which can not exceeds the maximum allowed power P_{max} .

Since the control traffic exploits an underlay channel known by each CR node of the OSA network, the exchange of sensing data among SUs does not cause interference to the overlay communications. According to this assumption, in (3) we can

neglect the interference due to the other UWB nodes and we only consider the interference caused by PU links, which is defined as:

$$I_{PU} = I_{PU,0} \cdot B_{PU} = I_{BS} + I_T \quad (4)$$

where B_{PU} is the bandwidth of the PU receiver and $I_{PU,0}$ is the interference spectral density on UWBs due to the PUs. $I_{PU,0}$ is composed of two main interference contributions to SUs due to PU BSs and PU terminals. These are given by the following expressions:

$$I_{BS} = \sum_{i=1}^{N_{BS}} \frac{P_{BS_i}}{L(d_i)} \quad (5)$$

$$I_T = \sum_{i=1}^{N_T} \frac{P_{T_i}}{L(d_i)} \quad (6)$$

where N_{BS} and N_T are the number of PU BSs and PU Terminals, respectively, d_i is the distance between the i -th PU (BS or terminal) and the considered SU, while P_{BS_i} and P_{T_i} are the transmission power of the i -th PU BS and PU terminal, respectively. As shown in (3), the interference terms are reduced by the ratio R_b/B_{UWB} , which represents a factor accounting for the signalling requirements and the characteristics of the UWB devices. It means that for a given UWB bandwidth and a fixed transmission power, the higher the bit-rate the worse the outage probability.

The proposed methodology for dimensioning a HAM cognitive network can be synthesized as follows:

- 1) given the considered scenario (e.g., the propagation characteristics, the number of interferers, the maximum allowed transmission power, etc.), calculate the outage probability of the signalling network under these conditions;
- 2) verify if the obtained outage probability is above the defined threshold α :
 - 2.1 if *yes*, we obtain the maximum UWB SUs transmission power satisfying constraints that fulfill the outage requirements;
 - 2.2 if *no*, the transmission power of the UWB devices is incremented in accordance to the regulatory restrictions.
- 3) calculate the maximum coverage range of UWB SUs;
- 4) determine the connectivity of the UWB signalling network with the obtained coverage. This metric is defined as the probability that a SU can reach all the other SUs of the signalling network according to a multi-hop architecture.
- 5) for a required connectivity degree, verify if the correspondent density of SUs in the area is compliant with the maximum number of UWB devices that guarantee the established level of protection to PUs. This is accounted for by the *Probability of Coexistence*, related to the interference to PUs from the underlay secondary network and calculated as:

$$P_{coex} = Prob\{I_{UWB} < I_{th}\} \quad (7)$$

I_{UWB} is the average interference caused to PUs (BSs or terminals) by the number N_{SU} of transmitting SUs, defined as:

$$I_{UWB} = \sum_{i=1}^{N_{SU}} \frac{P_{SU_{i,0}}}{L(d_i)} \cdot B_{PU} = \beta \sum_{i=1}^{N_{SU}} \frac{P_{SU_i}}{L(d_i)} \quad (8)$$

where:

$$P_{SU_{i,0}} = \frac{P_{SU_i}}{B_{UWB}}, \quad \beta = \frac{B_{PU}}{B_{UWB}}$$

are the PSD of DS-UWB devices and the ratio between the bandwidths of PUs and UWB SUs, respectively. This latter parameter is defined since the flat spectrum approximation, valid for narrowband PU, is assumed [13]. In (7) I_{th} is the allowable interference threshold. It is directly derived from the *Signal-to-Noise Ratio (SNR)* degradation, r , expressed as [13]:

$$r = \frac{\eta + I_{UWB}}{\eta} \quad (9)$$

This parameter measures the impact of the UWB interference on the *SNR* with respect to the thermal noise power N of the PU receiver chain. Once determined the maximum allowed value for the *SNR* degradation, namely r_{max} , the allowable interference threshold can be easily calculated as:

$$I_{th} = (r_{max} - 1) \cdot \eta \quad (10)$$

- 6) verify if the obtained probability of coexistence respects the required level of protection to PUs:
 - 6.1 if *yes*, the desired density of SUs is admitted. Hence the connectivity degree is accepted.
 - 6.2 if *no*, the bit-rate of the underlay signalling channel should be decreased up to match both the coexistence and connectivity requirements.

As shown by results presented in the next section, the described methodology allows to find a set of admissible pairs of values for the number of SUs and the bit-rate, all providing a desired connectivity degree subject to constraints on both the maximum transmission power of SUs and the interference to PUs.

B. Cooperative Detection Probability

Cooperative spectrum sensing techniques have been proposed to increase detection probability of PUs especially in shadowed or deeply faded channels. However, in order to perform cooperative sensing a CC is required for the exchange of sensing data among SUs. Typically an *interference-free* CC is assumed in the literature, but actually the unavailability of such a channel can reduce the cooperative sensing performance. Hence the characteristics of the signalling channel should be considered in the expression of the cooperative detection probability.

We assume that a number of Cognitive Cluster Head Nodes (CCNs) have been elected in the secondary network in accordance to a distributed algorithm using the UWB signalling

channel. CCNs are responsible for collecting sensing data from the SUs within their coverage and processing these data to decide on the availability of the spectrum holes. We also assume that SUs associated with a CCN are in the same PU activity area and that measurements taken by SUs are independent. Then, by considering the *AND* decision rule, that is a PU is considered idle only if an available band is detected out of all sensing data, the detection probability associated to the CCN decision is given by [14]:

$$P_D(k) = 1 - (1 - p_d)^{k+1}, \quad k \geq 0 \quad (11)$$

where k is the number of sensing data collected from the single CCN, which corresponds to the number of SUs within its coverage, while p_d is the detection probability of the single SU. Note that we assume a collaborative CCN which performs spectrum sensing together with the other SUs. The expression in (12) is valid if a channel among the CCN and the k SUs is available. Hence the average detection probability in cooperative spectrum sensing can be defined as:

$$\bar{P}_D(\delta_{SU}) = \sum_{k=0}^{N_c} P_D(k) \cdot Prob\{k|\delta_{SU}\} \quad (12)$$

where N_c is the number of SUs within the coverage range of the considered CCN, δ_{SU} is the density of SUs in the area and $Prob\{k|\delta_{SU}\}$ represents the probability of having at least k SUs within the CN coverage with which to perform cooperative spectrum sensing. It takes into account for the availability and the characteristics of the UWB CC for sensing information exchange among SUs. In other words, the cooperative detection probability is strictly related to the connectivity of the SU signalling network and its coexistence with primary systems, as shown in the next section.

The average missed detection probability of cooperative spectrum sensing can be then calculated as:

$$\bar{P}_{MD}(\delta_{SU}) = 1 - \bar{P}_D(\delta_{SU}) \quad (13)$$

IV. RESULTS

We carried out several simulations to assess the dimensioning of a SU underlay signalling network accounting for the trade-off between the level of protection to PUs and the connectivity degree of the SUs. We also evaluate the accuracy of the cooperative detection of PUs with respect to both the characteristics of the signalling network and its coexistence with primary systems. Results have been obtained using a Monte Carlo-based approach. The values assumed for the simulation parameters are reported in Table I. We assume a maximum tolerance on the outage probability of the UWB signalling data $\alpha = 5\%$. Omni-directional antennas are considered for both UWB SUs and PU terminals. We also suppose that each PU BS transmits on 14 carrier frequencies. As discussed in previous sections, typically low data rate are needed for signalling channels. Hence we performed simulations by assuming bit-rate ranging from 1 to 10 kbit/s.

In Figure 2 we report both the connectivity degree and the probability of coexistence of the multi-hop underlay signalling

	SUs	PU BSs	PU Terminals
B [MHz]	3000	0.4	0.4
f_c [MHz]	3100	1805 ÷ 1825	1775 ÷ 1785
P_{max} [dBm]	-6	43	33
γ	2.5	3	3
ρ_0 [dB]	4.5	9	9
G_{rx} [dBi]	1	12	1
G_{tx} [dBi]	1	12	1
N_f [dB]	5	9	9

Table I
VALUES FOR THE SIMULATION PARAMETERS

network as a function of the density of SUs in the area. It is observed that the signalling bit-rate R_b impacts on the percentage of connectivity among UWB devices. This can be explained by looking at the formula in (3), where the term R_b acts as a scaling factor reducing interference from the PUs to the SU receiver. Hence, the lower the CC bit-rate the higher the connectivity among UWB SUs. In other words, a higher density of UWB devices in the area is needed to obtain a required connectivity degree if the bit-rate increases due to the smaller coverage range. Moreover, the reduction of the SU SINR due to an increased number of active PUs implies a lower percentage of connectivity, as highlighted in Figure 2. As regards the probability that the underlay UWB signalling

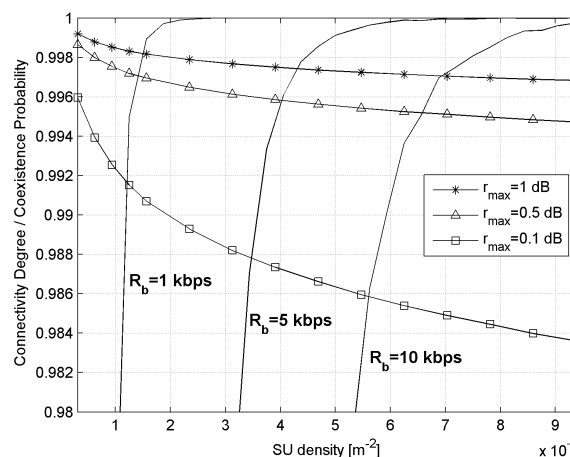


Figure 2. Connectivity degree and Probability of Coexistence vs density of SUs in the area (with 300 PU terminals and 3 co-sited BSs).

network causes harmful interference to primary systems, the obtained curves give an indication on the maximum allowed number of SUs in the considered scenario. We consider different values of the maximum interference tolerance r_{max} with respect to PU terminals. The coexistence only depends on the parameter β regardless of the bit-rate of the CC, as indicated in (7) and (8). As expected, for a given density of SUs in the area the higher the allowable interference threshold the lower the probability to harm PU performance.

As we explained in Section III, the proposed methodology allows to dimension the underlay UWB signalling network such that a predefined protection degree to PUs is guaranteed. As an example, starting from the curves in Figure 2 related

to $r_{max} = 0.1$ dB and considering a coexistence requirement of $P_{coex} \geq 98.6$ %, up to about 350 SUs can be tolerated for the considered scenario. As shown by the connectivity curves, this density of UWB devices implies a maximum percentage of connectivity of about 98.3 % for a signalling bit-rate of 10 kbit/s. If a completely connected UWB network is required, we have to decrease the bit-rate to 5 kbit/s. It is

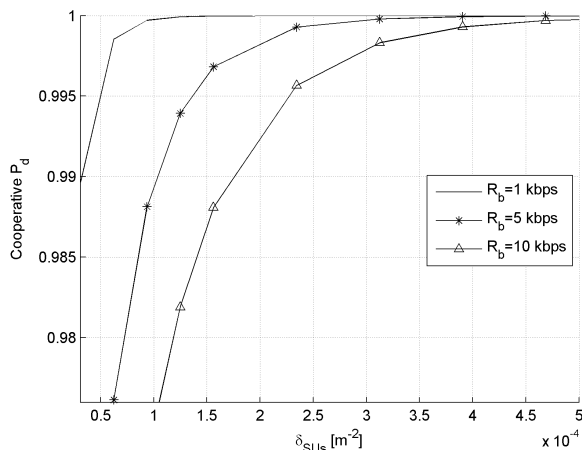


Figure 3. Performance of cooperative sensing in terms of detection probability vs density of SUs of the underlay signalling network (150 PU terminals, 3 co-sited PU BSs, $P_d=0.9$).

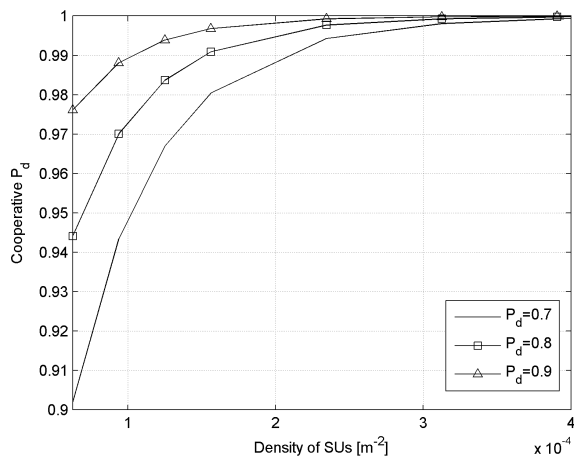


Figure 4. Performance of cooperative sensing in terms of detection probability vs density of SUs of the underlay signalling network (150 PU terminals, 3 co-sited PU BSs, $R_b=5$ kbps).

worthwhile to remind that, by assuming collaborative spectrum sensing among SUs, the percentage of connectivity of the underlay network is directly related to the detection probability performance, and consequently to an efficient usage of spectral resources. This is shown in Figure 3 and Figure 4, where we report the cooperative detection probability as a function of the density of UWB SUs in the area. Given a coverage range and a detection probability of the single SU, the higher the density of SUs in the area the more accurate the probability of

detecting PUs activity. When the bit-rate of the CC increases, the lower coverage leads to a decrease of the cooperative detection probability. This is due to the lower probability of finding CR nodes within the coverage of the CCN in order to maintain the same availability of the CC. Evidently, for a given bit-rate an increased detection probability of the single SU results in better cooperative detection performance.

In Figure 5 and Figure 6, we report the performance of cooperative sensing in terms of probability of missed detection as defined in (13). By taking into account for the availability and the parameters of the CC, it is observed that the values related to the expression of traditional cooperative sensing, i.e., $P_D(k)$, are obtained when the density of SUs in the considered scenario is sufficient to guarantee the maximum probability of finding at least k SUs within the coverage of the CCN. The

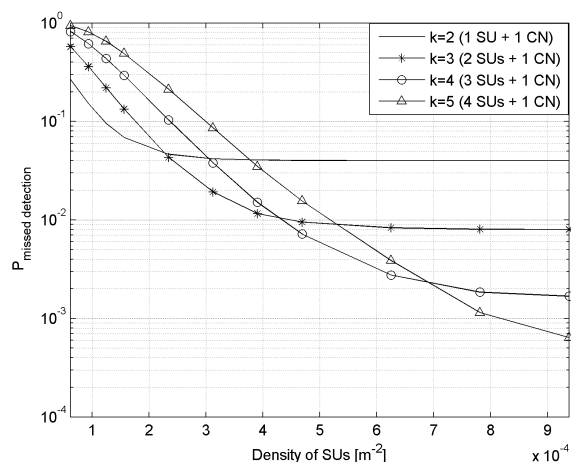


Figure 5. Performance of cooperative sensing in terms of probability of missed detection vs the density of SUs of the underlay signalling network (200 PU terminals, 3 co-sited PU BSs, $R_b=5$ kbps, $P_d=0.8$).

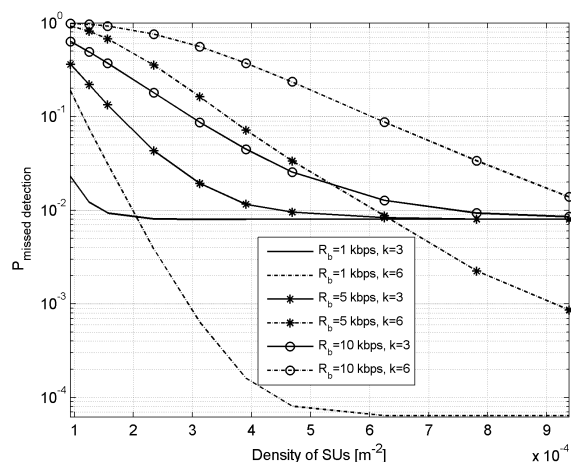


Figure 6. Performance of cooperative sensing in terms of probability of missed detection vs the density of SUs of the underlay signalling network (200 PU terminals, 3 co-sited PU BSs, $P_d=0.8$).

trends of the curves related to the different values of k can

be explained looking at the Figure 7, where the *probability density function* of k is reported for different number of SUs. Given the outage probability of the signalling network, the maximum transmission power of UWB nodes and the bit-rate of the CC, and then the CCN coverage range, when more sensing data are desired to perform cooperative detection, the probability of having at least k SUs within the CCN coverage, i.e., $Prob\{k|\delta_{SU}\}$, increases with the increase of the SU density. Hence, with the increase of the SU density a CCN can actually exploit more sensing data, so achieving a more accurate detection, up to reach the asymptotic value imposed by the terms $P_D(k)$. In other words the number k of SUs with

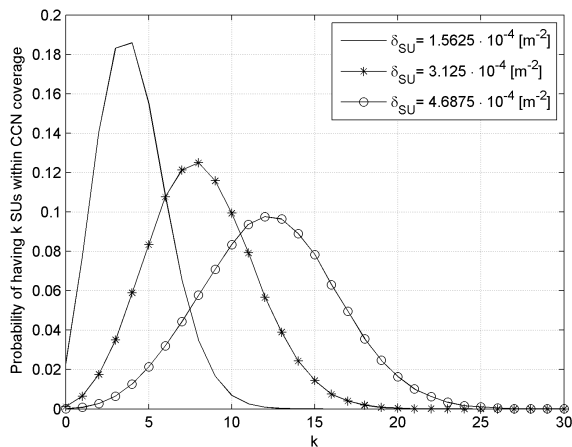


Figure 7. Probability of having k SUs within the coverage of the CCN vs k (150 PU terminals, 3 co-sited PU BSs, $R_b=5$ kbps).

which to decide of performing cooperative spectrum sensing depends on the density of SUs in the considered scenario. For a lower bit-rate of the CC, the resulting increase in CCN coverage leads to a minor density of SUs needed to obtain the target performance in terms of detection probability, as shown in Figure 6. In Figure 8 the cooperative detection probability is plotted as a function of the probability that the proposed UWB signalling network coexists with the primary systems in the considered scenario. As expected, a more stringent requirement on the maximum interference tolerance r_{max} entails a more rapid degradation of detection performance. Furthermore, the reduction in CC bit-rate allows to obtain better accuracy of PU detection while maintaining the same coexistence probability.

V. CONCLUSIONS AND FUTURE WORKS

In this paper, we faced the problem of the design of the control channel in OSA networks. We proposed to exploit the DS-UWB technology to realize an underlay signalling network for spectrum opportunity identification and cooperative spectrum sensing. We defined a cooperative detection probability accounting for the availability and the parameters of the control channel. We proved that the correct dimensioning of the proposed signalling network can provide SUs with a high

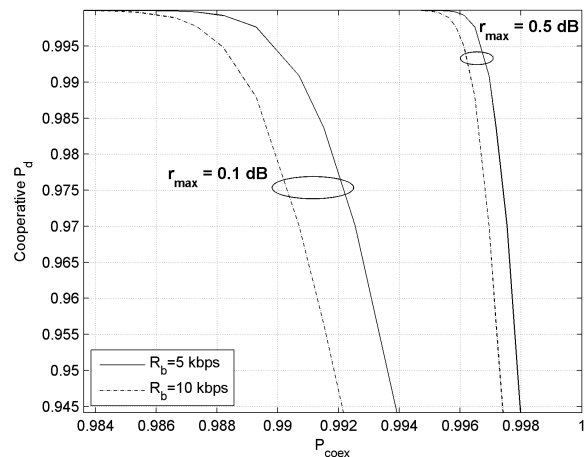


Figure 8. Cooperative detection probability vs coexistence probability of the underlay signalling network (150 PU terminals, 3 co-sited PU BSs, $P_d=0.8$).

availability of sensing data, thus increasing the accuracy of PU detection while avoiding harmful interference to PUs.

Future research can pertain to the design of suitable signalling protocol over the proposed underlay UWB CC to optimize the throughput in OSA networks.

REFERENCES

- [1] FCC, "Spectrum policy task force report", Tech. Rep. 02-135, Nov. 2002.
- [2] V. Valenta, Z. Fedra, R. Marsalek, G. Baudoin, M. Villegas, "Towards cognitive radio networks: Spectrum utilization measurements in suburban environment", IEEE Radio and Wirel. Symp., pp. 352-355, Jan. 2009.
- [3] J. Mitola III and G. Q. Maguire Jr., "Cognitive radio: making software radios more personal", IEEE Pers. Commun., pp. 13-18, Aug. 1999.
- [4] I. F. Akyildiz, W.Y. Lee, M. C. Vuran, S. Mohanty, "NeXt generation/dynamic spectrum access/cognitive radio wireless networks: A survey", Computer Networks, vol. 50, pp. 2127-2159, May 2006.
- [5] A. Ben Hadj Alaya-Feki, B. Sayrac, A. Le Cornec, E. Moulines, "Semi dynamic parameter tuning for optimized opportunistic spectrum access", IEEE 68th Vehic. Technol. Conf., pp. 1-5, Sept. 2008.
- [6] Q. Zhao and B. Sadler, "A survey of Dynamic Spectrum Access", IEEE Sign. Proces. Mag., pp. 79-89, May 2007.
- [7] Federal Communications Commission, "Revision of part 15 of the commissions rules regarding ultra-wideband transmission systems, first report and order", Washington, DC, ET Docket 98-153, FCC 02-48, 2002.
- [8] J. Unnikrishnan and V. V. Veeravalli, "Cooperative sensing for primary detection in cognitive radio", IEEE Jour. Sel. Topics Signal Process., vol. 2, no. 1, pp. 18-27, Feb. 2008.
- [9] A. Ghasemi and E. S. Sousa, "Opportunistic spectrum access in fading channels through collaborative sensing, IEEE Jour. Comm., vol. 2, no. 2, pp. 71-82, Mar. 2007.
- [10] P. Pawelczak, S. Pollin, H.-S.W. So, A. Bahai, R.V. Prasad, R. Hekmat, "Performance Analysis of Multichannel Medium Access Control Algorithms for Opportunistic Spectrum Access", IEEE Trans. on Vehic. Technol., vol. 58, no. 6, pp. 3014-3031, Jul. 2009.
- [11] M. E. Sahin and H. Arslan, "System design for cognitive radio communications", in Proc. CrownCom, Jun. 2006.
- [12] IEEE P802.15 Working Group for Wireless Personal Area Networks, "UWB Channel Characterization in Outdoor Environments", Aug. 2004.
- [13] R. Giuliano and F. Mazzenga, "On the coexistence of power-controlled ultrawide-band systems with UMTS, GPS, DCS1800, and fixed wireless systems", IEEE Trans. on Vehic. Technol., Vol. 54, NO. 1, pp. 62-81, Jan. 2005.
- [14] Won-Yeol Lee and I.F. Akyildiz, "Optimal spectrum sensing framework for cognitive radio networks", IEEE Transactions on Wireless Communications, vol. 7, no. 10, pp. 1536-1276, Oct. 2008.

Broadcast Signaling for a Centralized Cognitive Radio Network with Distributed Control

Nicolás Bolívar and José L. Marzo

Broadband Communications and Distributed Systems Group (BCDS)

Universitat de Girona

Girona, Spain

E-mail: nbolivar@eia.udg.edu, jose Luis.marzo@udg.edu

Abstract—For signaling and controlling a centralized Cognitive Radio Network (CRN) with users operating in different sets of channels, a dedicated common control channel is not a useful approach. Different strategies have been studied for this CRN control, some of them using time division mechanisms. This is because employing a channel per each Cognitive Radio User (CRU) for simultaneously controlling them is not efficient. However, for signaling specific events to all CRUs in a CRN, the Central Cognitive Base Station (CCBS) needs to communicate to all the operating devices in the CRN domain. Reducing the number of broadcast signaling channels is then a need for good performance and energy efficiency of the CRN. In this paper, for the solution of this broadcasting signaling problem, each CRU is represented by an array considering its channel usability. Using this array, a static evaluation of the problem is initially performed. Then, the dynamic characteristics of CRNs are included to find an acceptable number of channels to communicate to every user in a specific CRN.

Index Terms— *Broadcasting; Cognitive Pilot Channel; Cognitive Radio Networks; Dynamic Spectrum Access*

I. INTRODUCTION

Cognitive Radio Networks (CRNs) have been appointed as a solution to the apparent wireless spectrum scarcity problem [1-3]. This is because Cognitive Radio (CR) systems are able to detect free frequency spaces (bands) in the spectrum and to allocate communications in those spaces by using Dynamic Spectrum Access (DSA) mechanisms. CRN allow secondary users, i.e. CRU with partial Access to use specific bands of the wireless spectrum, to use free frequency bands while the Primary Users (PU), i.e. licensed users of specific bands, are absent.

In general, a CRN should be able to perform 4 tasks efficiently, spectrum sensing, spectrum decision, spectrum sharing, and spectrum mobility [2]. This means that have the ability of sensing, recognizing and adapting to specific characteristics of the environment. One of the CRNs most important characteristics is the ability for the Cognitive Radio Users (CRU) to dynamically access the spectrum. However, CRUs might be also capable of recognizing patterns of occupancy, to reduce the energy used for sensing, signaling and transmission. For this reason, Cognitive Radio technology has been also considered as an alternative to reduce energy consumption for wireless communications [4].

Several CR MAC protocols have been developed from Multi-channel MAC protocols. These MAC protocols can be

categorized in dedicated control channel, split phase, common hopping, and default hopping [5]. Some specific CR MAC protocols use a dedicated common control channel [6, 7]. However, heterogeneous CRU devices that do not share this control channel are not able to communicate in this CRN. Other than the aforementioned dedicated control channel approach, the other three approaches can be considered for efficient spectrum utilization because the CRN must operate in different frequency bands. On the other hand, these multi-channel MAC protocols need some kind of user synchronization to determine the control channel beforehand. Furthermore, in multi-channel MAC protocols, all CRU must be able to use the same frequency channels, which is not always the case in heterogeneous systems.

A cognitive pilot channel (CPC) is a solution proposed in the E2R project for enabling communication among heterogeneous wireless networks. The CPC consists on controlling frequency bands in a single or various “pilot” channels [8-11]. In [12], we have presented a basic model for a Centralized CRN that uses CPCs for signalization and control. The main idea was to introduce a control signal, basically periodical beacons, to announce channel availability and the necessity of leaving a frequency slot if that one was occupied. The basic model of the CRN provides signalling through CPCs distributed in every available channel or frequency slot. The control is performed by using frequency-division and time-division multiplexing techniques. This control, as expected, permits the utilization of the CRN by heterogeneous CRU devices.

In terms of energy, transmitting through every available channel would be inefficient. This is because the entire wireless spectrum channels would be occupied in a specific moment. Considering this problem, new alternatives should be explored to reduce the energy used for signaling CRUs channel availability. For reducing the energy, in [13], we used the characteristics of the time/frequency combined to approach for the CCBS to signal a new available channel only when a CRU that was not transmitting is requesting communication. We also considered the benefits of using a distributed control and a centralized database for reducing the amount of energy used to signal this availability in the CRN.

The CCBS, however, still needs to broadcast signals to its users in some specific moments. Signals that must be broadcasted by the base station include periodical beacons, alarms, among others [14]. Several broadcasting problems such as the minimum broadcasting energy problem [15] and the allocation for broadcasting heterogeneous data in multiple channels [16-17], among others have been studied. To the

best of the authors’ knowledge, none of the broadcasting studies deal with the problem of broadcasting availability through a minimum number communication channels, in general; not for CRNs, in particular. The channel allocation/frequency assignment problem, however, has been studied in static and dynamic environments. We refer to [18] and [19] for an overview of models and solutions of the frequency assignment problem in those environments, respectively. One of the main considerations for studies in frequency assignment problems is that a channel can generate interference in adjacent channels. In our scenario, since the broadcast signaling is transmitted the same for each channel and only in a couple of a large number of sub-channels [12-13], we can assume that using adequate modulation/coding schemes, interference among adjacent channels is non-existent [19].

The problem of obtaining the minimum number of channels for a base station, e.g. the CCBS, to transmit to all the users in its network is an optimization problem. For solving this problem, the dynamic characteristics of the CRN that include not only the entrance and departure of CRUs, but also external factors, the presence of PUs must be considered. However, several approaches that use algorithms to solve general optimization and broadcasting problems such as reduce the Greedy Algorithm, Satisfiability (SAT) theory [20], among others, might be adapted to solve this problem. In this paper, an adaptation of the greedy algorithm is proposed to solve the minimum number of channels problem, when this number of channels is low.

The rest of this paper is divided as follows: In Section II, the model of the CRN and the description of the solution are depicted. In Section III, basic considerations for the algorithm are shown. In Section IV, early results of the minimum channel algorithm obtained by using the strategies are presented. In Section V, the results and future work are discussed.

II. MODEL

The basic model of the CRN used in this work is shown in Fig. 1. A Central Cognitive Base Station (CCBS) controls CRU communication so that these CRU do not interfere each other or a Primary User (PU). For modeling the CCBS, in this paper, we consider that the spectrum is continuously and perfectly sensed. We also consider that for each frequency band, a threshold is decided to determine if a user is already using that channel. A logical “1” is then assigned if a communication exists in a frequency slot; otherwise, a logical “0” is assigned. This information is stored as a vector in a database, which also stores information from the channel control and data communications.

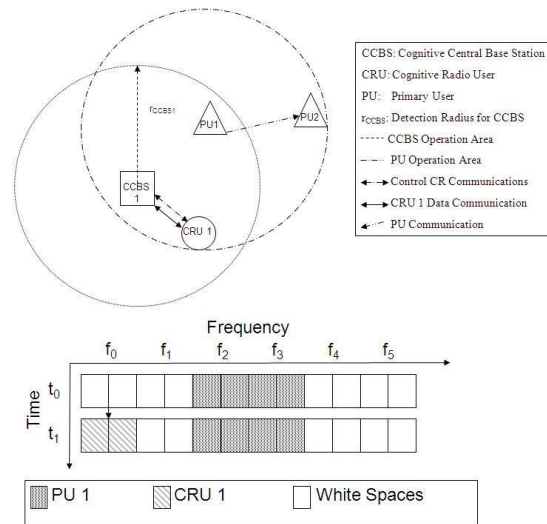


Fig. 1. CRN Model

In Fig. 1, CRU1 is communicating with its corresponding CCBS (CCBS1), while PU1 is communicating with PU2. PU1 transmission is within the range of the CCBS1 and CRU1. This means that the communication between CRU1 and CCBS1 must be performed in a different frequency slot than the one used for PU1-PU2 communication. A frequency/time representation of the corresponding scenario is also shown. In the proposed architecture, we assume that the management of the network is performed in the CCBS, which permits to reduce the amount of processes from the CRUs’ terminals and therefore, keeping those terminals simple while using today’s available technologies. We also assume that the CCBS decides which channel to assign for each CRU, according to the available channels and characteristics of the CRU.

The basic model of the CRN provides signaling through cognitive pilot channels (CPCs) distributed in every available channel or frequency slot. The control is performed by using frequency-division and time-division multiplexing techniques. This control, as expected, permits the utilization of the CRN by heterogeneous cognitive radio user (CRU) devices. Frequency sub-slots are used by the CCBSs and CRUs to exchange both control and data information. The CCBS is responsible of controlling which CRUs are communicating and the frequency slots used, by assigning CRUs free frequency slots to communicate. This information is sent in a vector to the CRUs, while kept in the CCBS database. Fig. 2 shows the division in frequency and sub-frequency slots.

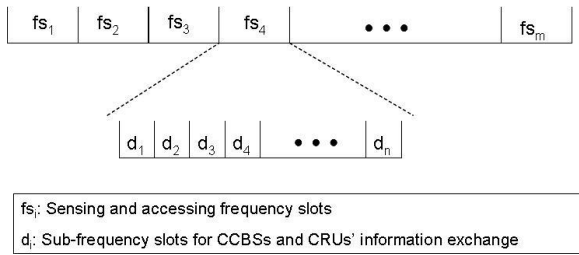


Fig. 2. Frequency and sub-frequency slot division of the spectrum

The basic algorithm for each frequency slot was defined by Fig. 3. The database was mainly used for keeping into memory the location of CRUs and PUs in the frequency bands. The main energy reduction is accomplished by reducing signalization transmissions.

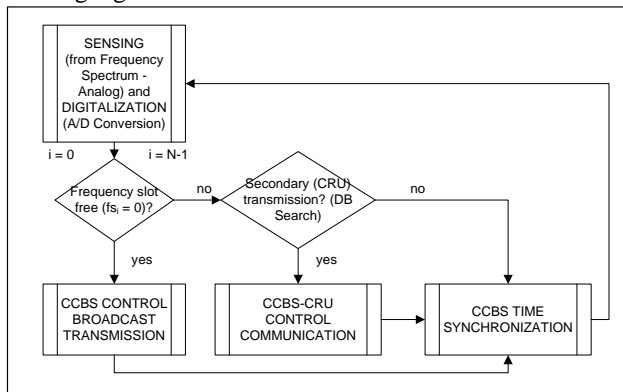


Fig. 3. CCBS Algorithm per each frequency slot i (fs_i)

When a CRU data communication is already established, and since PU communication can enter at any moment, a time-based approach is implemented in order to discover PU presence. This frequency and time system allows the elimination of a dedicated control channel for spectrum sharing. Using the slotted predefinition, if a transmission is received in a moment no transmission should be performed, we assume that a PU is communicating and, then, the channel is evacuated and the process of assigning a channel restarts, keeping into memory the last information that was going to be transmitted. The time slot division used for the CRN MAC presented in [12], as shown in Fig. 4, will be also used to reduce the signalization.

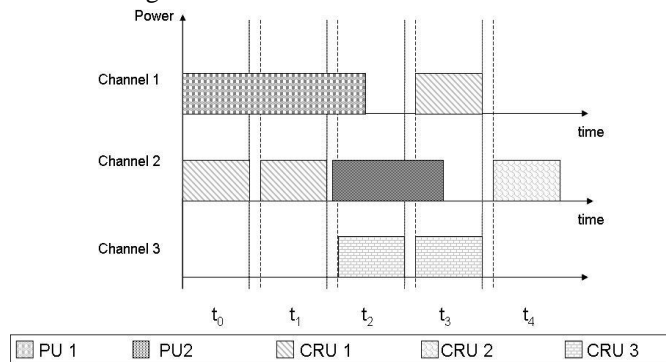


Fig. 4. Frequency slot utilization by both PU and CRUs (in time)

In Fig. 4, an example of the CRU admission in the CRN is shown. CRU 3, which has three channels for communications, “senses” its environment. Channel 1 is being used by a PU, so this channel is unavailable to CRU transmission. Channel 2 is occupied by CRU1. This makes the channel unavailable for CRU 3 use, but CRU 3 can detect the time slot position using CRU 1 transmission. Using that information, CRU 3 can access Channel 3 in time t_2 .

In [13], two additional characteristics are added to the CRN model of [12] to reduce broadcast transmissions. The first one is that CRU synchronization will be performed as follows: Since CRUs know the duration of the time slot, the CRU will search during a time slot in its channels for continuous transmission. If a CRU finds a PU-free channel, the device will send a signal for announcing that this CRU wants to access the network. A channel occupied by a CRU will be identified because of the time slots used for control, so this scheme will not introduce collisions among CRUs. The second reduction consists on using the ability the CCBS has to identify the channels every CRU in the network is able to use. In this manner, the CCBS will only send a new broadcast transmission for each channel petition. This means that now, the entire wireless frequency spectrum considered for the CRN domain will not be used at several moments, and the number of periodical broadcast beacon transmission will be also reduced.

In [13], we also showed that eliminating CCBS broadcasting transmission channels means a reduction in terms of energy per unit of time of approximately (number of available channels) x (broadcasting transmission time) x (power used for beacon transmission). Results indicated that a reduction in energy transmission due to signalization can be achieved by using the basic CRU sensing properties. Since the CRU can only detect values above a specific threshold for a determined period of time, the CRU might detect PU transmission due to its continuity, and CRU transmission due to its periodicity. Using that property, broadcasting transmissions, which contribute to energy waste, are reduced. Another advantage of using this property is that the CCBS is already aware of the available channels of each CRU. This is because in the admission process, each CRU has already indicated its characteristics. Considering that the CCBS has this knowledge, direct channel assignation can be performed, so broadcast transmission is also reduced. Then, the idea is to find the minimum number of broadcasting channels for the CCBS needed broadcasting transmission.

Considering again that the CCBS has knowledge of the channels each of the CRUs is able to use, for finding this minimum number of the broadcast transmission channels needed in a specific moment, a matrix called availability matrix is included. The relation among the frequency slots (channels) and CRUs in a specific time is shown in Fig. 5.

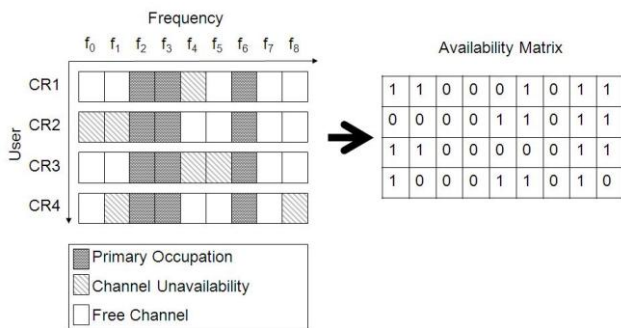


Fig. 5. Frequency slot utilization by both PU and CRUs (in time)

In Fig. 5, the availability matrix per CRU (A) in a specific time is presented. A channel is unavailable to a CRU due to two reasons: a PU is using an available channel for the CRU or the CRU cannot communicate through that channel. Using this information, each CRU is represented by a row and each channel, by a column. Each element represents then the availability of a channel to a CRU in a specific moment. A logical ‘1’ is assigned in this case if the channel is available to the user and a ‘0’ if the channel is unavailable.

In the availability matrix represented in Fig. 5, the eighth column, corresponding to f7, is a unitary column. This means that using that channel (f7), the CCBS can broadcast communication to all the users in its CRN during that period of time. In Fig. 6, a case where more than one channel is needed for the CCBS to broadcast is shown.

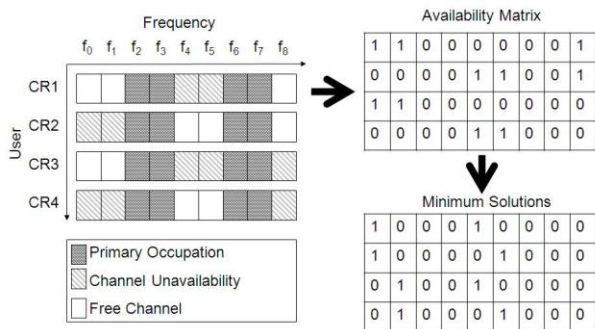


Fig. 6. Frequency slot utilization by both PU and CRUs (in time)

In the case presented in Fig. 6, the availability matrix shows that at least the CCBS needs two channels to communicate with all the CRUs in the network. The matrix composed with all the vectors that use the minimum channels for the CCBS to communicate is represented as Minimum Solutions. In general, the problem of finding this minimum solution vectors is the same as finding the vectors with the least numbers of ‘1’s such that the intersection of them with each of the row vectors that compose the availability matrix is not empty.

III. CONSIDERATIONS

Having m users, u_1, u_2, \dots, u_m , each of them able to use several of the n channels that a CRN presents, c_1, c_2, \dots, c_n , the idea is to find an array in which a base station CCBS is able to transmit to each user (u_i) utilizing the minimum number of channels.

The matrix that relates channel usability for each CRU is represented as $U_{m \times n}$. Each row vector defined by $U(i, :)$ is always different than 0, taking into account that each CRU must have at least one channel to communicate. So, not considering primary occupation, the problem can be defined as finding a vector $v \times n$ such that

$$\sum_1^n ((v \cdot *U(1,:)) \vee (v \cdot *U(2,:)) \dots \vee (v \cdot *U(m,:))) = n \quad (1)$$

in which the number of ‘1’s is minimum. This problem can be related to a satisfiability problem (SAT) which is known to be NP-complete [21]. This can be proved considering that

$$Z = \begin{bmatrix} (v \cdot *U(1,:)) \\ (v \cdot *U(2,:)) \\ \vdots \\ (v \cdot *U(m,:)) \end{bmatrix} = \begin{bmatrix} z_{11} & z_{12} & \dots & z_{1n} \\ z_{21} & & & \\ \vdots & & \ddots & \\ z_{m1} & & & z_{mn} \end{bmatrix}, \quad (2)$$

then

$$((v \cdot *U(1,:)) \vee \dots \vee (v \cdot *U(m,:))) \quad (3)$$

is equal to the vector

$$z' = \left[(z_{11} \vee \dots \vee z_{m1}) \quad \dots \quad (z_{1n} \vee \dots \vee z_{mn}) \right]. \quad (4)$$

Taking into account that

$$\sum z' = n \quad (5)$$

means that each

$$(z_{1i} \vee \dots \vee z_{mi}) \quad (6)$$

is ‘1’, so the problem is equal to find a vector v with minimum norm such that for every $j = 1:n$,

$$(z_{11} \vee \dots \vee z_{m1}) \quad (7)$$

is true, which is the definition of the n-satisfiability problem. This vector is defined in general for this paper as the vector of minimum solutions.

In the case when PUs are not considered, let’s assume that for an array consisting on m users and n channels, the minimum number k of broadcasting channels for the array has been found. As shown in Fig. 4, CRUs enter and leave the CRN dynamically. This means that the algorithm for finding the minimum solutions vectors must consider the dynamics of the network. For reducing the complexity of the algorithm, the property that this CRN has that only a new CRU can enter/leave at a specific time is used. If a new CRU enters the network, the minimum number of channels needed to broadcast signals to each of the CRU devices is at most k+1, and at least k. Similarly, if a CRU leaves the CRN, the minimum number for the broadcast signalling channels is at least k-1, and at most k.

However, as shown in Fig. 4, a channel is inoperative when used by a PU. The presence of PUs can be described by using the mask vector p containing the PU occupancy stored in the CCBS database. Considering that $U(i,:)$ is the usability vector for CRU i, the vector $A(i,:) = U(i,:) * p$ represents the availability vector for transmitting broadcast signals by the CCBS. When primary occupation is considered, in some specific moments a CRU i defined by $A(i,:)$ might be unavailable for communication.

IV. CASE STUDY

In this section, early results obtained when using low numbers of channels and CRUs in the network are presented. The number of channels was defined to be low in order to compare the results of the algorithm for obtaining the minimum number of channels to communicate with all the CRUs with the real minimum number.

For the first simulation, the number of channels n was defined as 8. The number of CRUs, m , was also defined as 8, due to the fact that the maximum number of users that can communicate in a specific moment is the number of channels available in the network. The number of time slots, t , is defined to be 10. CRU and PU presence in the CRN are defined as random, with probabilities 0.2 and 0.5, respectively. In Table I, the channel usability of all the possible CRUs in the CRN is shown.

TABLE I. CHANNEL USABILITY (CRU NUMBER = 8)

	f_1	f_2	f_3	f_4	f_5	f_6	f_7	f_8
CRU 1	1	0	0	0	0	0	1	0
CRU 2	1	1	0	0	0	0	1	1
CRU 3	1	0	0	1	0	0	1	0
CRU 4	1	0	1	1	0	1	0	0
CRU 5	0	0	0	0	1	0	0	1
CRU 6	0	1	0	0	1	0	0	0
CRU 7	1	0	0	1	0	0	0	0
CRU 8	1	0	0	1	0	0	1	1

As shown in Table I, the minimum number of channels needed to transmit to all CRUs in the network is 2, using f_1 and f_5, f_4, f_7, f_3 and f_5 .

An advantage of the broadcasting solution is that the base station, e.g. the CCBS, in theory is able to communicate with as many CRUs in the CRN as desired. This means that even idle CRUs can receive information from the CCBS. As a proof, we simulate this situation by doubling the number of CRUs. Results are shown in Table II.

TABLE II. CHANNEL USABILITY (CRU NUMBER = 16)

	f_1	f_2	f_3	f_4	f_5	f_6	f_7	f_8
CRU 1	1	0	0	0	0	0	1	0
CRU 2	1	1	0	0	0	0	1	1
CRU 3	1	0	0	1	0	0	1	0
CRU 4	1	0	1	1	0	1	0	0
CRU 5	0	0	0	0	1	0	0	1
CRU 6	0	1	0	0	1	0	0	0
CRU 7	1	0	0	1	0	0	0	0
CRU 8	1	0	0	1	0	0	1	1
CRU 9	0	1	0	0	1	0	0	0
CRU 10	0	0	0	0	0	0	0	1
CRU 11	0	0	0	0	1	0	0	0
CRU 12	0	1	0	0	1	0	0	0
CRU 13	0	0	0	0	1	0	0	1
CRU 14	1	0	0	0	0	0	0	0
CRU 15	0	0	0	0	1	1	0	0
CRU 16	0	0	1	0	0	0	0	0

Notice that the number of minimum channels for communicating with all CRUs is similar. In this case, this number is four, two more than in the previous situation. Besides, this is because CRU 10 and CRU 16 only have f_8 and

f_3 , respectively as their usable channels. A possible minimum solutions vector is then $v = [1\ 0\ 1\ 0\ 1\ 0\ 0\ 1]$. The similarity on the number is because the CRUs, while heterogeneous in frequency, are defined with similar characteristics.

The algorithm considered for solving the minimum number of channels is an adaptation of the Greedy Algorithm. The basic idea is that the channel that might be used the most by the CRUs is the first to be considered as a possible solution to communicate to all the CRUs. The next channel to be considered as a solution to the problem is the second that might be used the most by the CRUs. The vector is constructed by defining as '1' all these channels until all the possible channels are considered. An obvious improvement for this algorithm is to discard the CRUs that are covered with the channel in the previous step, and repeat the process until every CRU is able to receive communication from the CCBS. For reducing the calculations for the following time slots, the property that the difference between the minimum numbers of channels needed for broadcasting in consecutive time slots is at most one. Considering the patterns of entrance and departure of the CRUs, shown in Table III, the numbers of channels, defined by $mod(v)$, needed to broadcast to all active CRUs are presented in Table IV.

TABLE III. AVAILABILITY OF THE CRU ACCORDING TO THE TIME

	t_1	t_2	t_3	t_4	t_5	t_6	t_7	t_8	t_9	t_{10}
CRU 1	0	0	0	0	0	1	0	0	1	0
CRU 2	0	0	0	0	0	0	0	0	0	0
CRU 3	0	0	0	0	1	1	1	0	0	0
CRU 4	0	0	0	0	0	0	0	0	0	0
CRU 5	0	0	0	0	0	0	0	0	0	0
CRU 6	0	0	0	1	1	0	0	0	0	0
CRU 7	0	0	1	1	1	0	0	0	0	0
CRU 8	0	1	0	0	0	0	0	0	0	0

TABLE IV. MINIMUM SOLUTION VECTOR (WITHOUT PUS)

	t_1	t_2	t_3	t_4	t_5	t_6	t_7	t_8	t_9	t_{10}
$mod(v)$	0	1	1	2	2	1	1	0	1	0

Next, the presence of PUs is considered and shown in Table V. Results for a minimum solutions vector are shown in Table VI. The considerations were the same as for the case when PUs were not included, $m = 8, n = 8, t = 10$.

TABLE V. PRIMARY USER OCCUPATION (IN TIME)

	t_1	t_2	t_3	t_4	t_5	t_6	t_7	t_8	t_9	t_{10}
f_1	0	0	0	0	1	1	0	0	0	0
f_2	1	1	1	1	1	0	0	0	0	1
f_3	0	0	0	0	0	0	1	1	1	1
f_4	0	0	0	0	0	1	1	0	0	0
f_5	0	0	0	0	0	0	0	0	0	0
f_6	1	1	1	1	1	1	0	0	1	1
f_7	1	1	1	1	0	1	0	0	0	0
f_8	0	0	0	1	1	1	1	0	0	0

TABLE VI. MINIMUM SOLUTION VECTOR (WITH PUS)

	t_1	t_2	t_3	t_4	t_5	t_6	t_7	t_8	t_9	t_{10}
$mod(v)$	0	1	1	2	2	0*	1	0	1	0

As expected, CRUs might not receive information from the CCBS because the channels are occupied by the PUs. This can be seen when $t = t_6$. CRU1 and CRU3 are in the CRN but the CCBS cannot transmit information to any of them because their available channels are already in use by PUs. Another situation that might arise because of PUs' presence is the necessity for the CCBS to transmit through more channels to reach the same CRUs.

V. CONCLUSION AND FUTURE WORKS

The transmission of broadcasting signals is a necessity in a centralized network. In this manner, the base station can reach all its users, in this case CCBS and CRUs, respectively. This is in order for the CCBS to announce alarms, availability, among others. When broadcasting availability as a periodical beacon to heterogeneous frequency systems, reducing the number of broadcasting channels is a need for energy reasons.

The sole idea of analyzing a simple network for finding a vector composed of the minimum number of channels a cognitive radio base station needs to broadcast signals to all its users is a NP-complete problem as shown in section III. Different solutions might be found using diverse techniques. For easing the algorithm, characteristics of the proposed CRN model are used.

When considering primary occupation, some of those characteristics are not useful. This is the reason why a greedy approach was considered at first. The fact that both the number of CRUs and channels were considered to be low helped making the decision of choosing the greedy approach, which is known to be useful in those cases.

For future works, different techniques such as tree-based and genetic approaches, as well as satisfiability techniques will be considered, when expanding the number of channels and users. For deciding which technique to base the new minimum solution algorithm, three characteristics will be evaluated: complexity of the algorithm, time of execution and closeness to the optimal solution. In the energy reduction part, more strategies to reduce energy transmission, such as database use for PUs and low-energy transmission mechanisms, will be explored.

ACKNOWLEDGMENT

Part of this work was supported by the Department of Universities, Research and Information Society (DURSI) of the Government of Catalonia, European Social Funds (SGR-1202); by a FI Grant from the Government of Catalonia, in accordance with the Resolution IUE/2681/2008, and also by the Spanish Government (TRION MICINN TEC2009 – 10724).

REFERENCES

- [1] J. Mitola III and G.Q. Maguire, Jr., "Cognitive Radio: Making Software Radios More Personal," *IEEE Personal Communications (Wireless Communications)*, vol.6, no. 4, pp. 13-18, August 1999.
- [2] I. F. Akyildiz, W.Y. Lee, M.C. Buran, and S. Mohanty, "A survey on spectrum management in cognitive radio networks," *IEEE Communications Magazine*, vol. 46, no. 4, pp. 40-48, April 2008.
- [3] IEEE 802 LAN/MAN Standards Committee 802.22 WG on WRANs (Wireless Regional Area Networks). IEEE. <http://www.ieee802.org/22/>. Retrieved 2009-01-18.
- [4] J.Palicot, M.Katayama, A. Nafkna, G.Ravera, M.Massoth, J. Perez-Romero, "Challenges in Advanced Communications and Services," Panel AICT 2010, IARIA Panels, May 2010.
- [5] A. Yau, P. Komisarczuk, and P. D. Teal, "On Multi-Channel MAC Protocols in Cognitive Radio Networks," in *Australasian Telecommunication Networks and Applications Conference 2008, ATNAC 2008*, pp. 300-305, December 2008.
- [6] H. Wang, H. Qin, and L. Zhu, "A Survey on MAC Protocols for Opportunistic Spectrum Access in Cognitive Radio Networks," in *IEEE International Conference on Computer Science and Software Engineering 2008*, pp. 214-218, December 2008.
- [7] S-Y. Lien, C-C. Tseng, and K-C. Chen, "Carrier Sensing based Multiple Access Protocols for Cognitive Radio Networks," in *IEEE Conference on Communications 2008, ICC 2008*, pp. 3208-3214, May 2008.
- [8] End to end efficiency. E3. https://ict-e3.eu/project/technical_highlights/enablers/enablers.html. Retrieved 2009-10-11.
- [9] M. Filo, A. Hossain, A.R. Biswas, and R. Piesiewicz, "Cognitive Pilot Channel: Enabler for Radio Systems Coexistence," *Second International Workshop on Cognitive Radio and Advanced Spectrum Management 2009, CogART 2009*, pp. 17-23, May 2009.
- [10] End to End Reconfigurability II (E2R II) White Paper, "The E2R II Flexible Spectrum Management (FSM) Framework and Cognitive Pilot Channel (CPC) Concept – Technical and Business Analysis and Recommendations," pp. 1-52, November 2007. <http://smit.vub.ac.be/st/modules/stpubserver.aspx?pubid=410>. Retrieved 2009-10-11.
- [11] O. Sallent, J. Pérez-Romero, R. Agustí, P. Cordier, "Cognitive Pilot Channel Enabling Spectrum Awareness," in the *IEEE Conference on Communications Workshops 2009, ICC Workshops 2009*, pp. 1-6, June 2009.
- [12] N. Bolívar, J. L. Marzo and E. Rodríguez-Colina, "Distributed Control using Cognitive Pilot Channels in a Centralized Cognitive Radio Network," in the *Sixth Advanced International Conference in Telecommunications*, pp. 30-34, May 2010, ISBN: 978-0-7695-4021-4.
- [13] N. Bolívar and J. L. Marzo, "Energy Reduction for Centralized Cognitive Radio Networks with Distributed Cognitive Pilot Channels" in the *IEEE Latin-American Conference on Communications 2010, Latincom 2010*, September 2010.
- [14] C-Y. Chiu, E. H.-K. Wu, G.-H., Chen, "A Reliable and Efficient MAC Layer Broadcast (Multicast) Protocol for Mobile Ad Hoc Networks," in the *Global Telecommunications Conference 2004, GLOBECOM 2004*, pp. 2802 – 2807, vol. 5, Dec 2004.
- [15] M. Cagalj, J.-P., Hubaux and C. Enz, "Minimum Energy Broadcast in All Wireless Networks: NP-Completeness and Distribution Issues," in *Proceedings of the 8th annual international conference on Mobile computing and networking, MobiCom 02*, pp. 172-182, September 2002.
- [16] H.-P. Tsai, H.-P. Hung and M.-S. Cheng, "On Channel Allocation for Heterogeneous Data Broadcasting," *IEEE Transactions On Mobile Computing*, Vol. 8, No. 5, May 2009.
- [17] C. H. Hsu, G. Lee, and A. L. P. Chen, "An Efficient Algorithm for Near Optimal Data Allocation on Multiple Broadcast Channels," *Distributed and Parallel Databases*, vol. 18, no. 3, 2005.
- [18] K. Aardal, S. P. M. Van Hoesel, A. M. C. A. Koster, C. Mannino, and A. Sassano, "Models and solution techniques for frequency assignment problems," *Annals of Operations Research* 153, vol. 153, no. 1, pp. 79 - 129, 2007.
- [19] I. Katzela and M. Naghshineh, "Channel Assignment Schemes for Cellular Mobile Telecommunication Systems: A Comprehensive Survey," *IEEE Personal Communications Magazine*, vol. 3, no. 3, pp. 10 – 31, June 1996.
- [20] M. Davis and H. Putnam, "A Computing Procedure for Quantification Theory," in vol. 7, Issue 3, *Journal of the ACM*, July 1960.
- [21] S.A. Cook, "The complexity of Theorem-Proving Procedures," in *STOC '71, Proceedings of the third annual ACM symposium on Theory of computing*, pp. 151-158, May 1971.

A Flexible Bufferless H-ARQ Processor Based on Dataflow Scheduling

Pierre-Henri Horrein, Christine Hennebert
CEA, LETI, Minatec
Grenoble, France
Email: pierre-henri.horrein@cea.fr

Frédéric Pétrot
TIMA Labs
CNRS, Grenoble-INP, UJF
Grenoble, France
Email: Frederic.Petrot@imag.fr

Abstract—Flexible radio is a challenging way to implement communication standards. In these standards, Hybrid ARQ (H-ARQ) is admitted as a usual error control protocol. H-ARQ is a cross-layer protocol, offering a number of different possible versions, with multiple instantiations running concurrently. In this context, designing a flexible H-ARQ component is a necessity. This paper presents an H-ARQ processor able to cope with the possible versions of the protocol and any number of instantiations. Based on a modified hardware/software partitioning, it is able to dynamically reconfigure its operation mode. Data representation is used to create codewords, associated to an operation. A new buffer management scheme, based on software buffers and independent of the number of protocol instantiations, is proposed. The resulting architecture is able to process any H-ARQ protocol with no throughput penalty, in MIMO or SISO environments, and to support concurrent standards.

Keywords—H-ARQ; flexible radio; reconfigurable hardware.

I. INTRODUCTION

In the last few years, the flexible radio concept has become one of the major research field in wireless networks. Rapidly evolving standards, increased mobility, and technology advances are calling for adaptable and flexible solutions.

Traditional radio devices, while very efficient for those computational intensive applications, can not cope with the growing number of connection methods offered by the standards. These different standards evolve very quickly. This imposes a flexibility, to keep pace with the advances included in the standards (update flexibility). Telephone applications are very representative of this two-dimensional expansion. Smartphones usually offer personal, local and wide area network connection (PAN, LAN, WAN), through different standards. All these standards are also evolving, which, with traditional devices, means redesigning a new platform to support the updates.

At the same time, the increasing requirements for quality in wireless networks demand that error control through retransmission (in addition to Forward Error Correction - FEC) be an unavoidable part of new standards. The aim of error control is to guarantee a controlled error probability during transmissions. Hybrid Automatic Repeat and reQuest (H-ARQ), further described in Section II, is now used in many wireless standards, such as 3GPP HSPA, IEEE WiMax or 3GPP LTE.

Implementations of H-ARQ in a traditional (not flexible) radio device has been described in several patents. Yet, the design of a flexible H-ARQ processor usable in a flexible radio context has, to the best of the authors' knowledge, not been described before. The aim of this article is to describe a solution to implement such a H-ARQ processor.

This paper is organized as follows. First, H-ARQ and traditional solutions, along with the challenges due to flexibility are presented

in Section II. Then, the concepts underlying the proposed solutions are presented in Section III, while details on the actual solution are given in Section IV. Finally, use cases and practical results are presented in Section V, and the study concluded in Section VI.

II. H-ARQ DETAILS

The aim of this study is to describe a solution for flexible implementation of H-ARQ. This section presents usual H-ARQ schemes and existing implementations as well as challenges for a flexible implementation.

A. H-ARQ processing

H-ARQ is an error control protocol based on two types of error control methods:

- *proactive* methods, acting before transmission, basically using FEC, integrated in the PHY layer;
- *reactive* methods, taking place after errors occur, using Automatic Repeat reQuest (ARQ) protocols integrated in the MAC layer (or between MAC and PHY).

The use of these two types of techniques in a single protocol allows for enhanced error correction and reduced effect on performance. The original protocol, described in [1], was simply an ARQ protocol operating on FEC encoded packets. FEC was used as a solution to lower the retransmission probability, thus reducing the mean latency of a transmission, while ARQ was used to reduce the overhead of FEC methods, since it is not necessary to provide sufficient error correction for the worst case.

While the aim of the original H-ARQ protocol was to cope with the respective problems of FEC and ARQ, the cooperation of both methods is far more powerful. Several enhancements have been proposed, which make use of this cooperation. Incremental Redundancy [2] (IR) is a method used to further reduce the code overhead. In the first transmission, only the raw packet or a very high-rate code is sent. If errors occur, additional parity bits from the code are sent in the retransmissions, for error correction. This method is mainly used with punctured codes instead of the straightforward partitioning.

Chase Combining (or Code Combining, CC) [3] aims at a better efficiency of retransmissions, using confidence information on the previously received packet (from previous transmissions). In this scheme, no additional information is sent in retransmissions, but the receiver combines all the retransmissions, to obtain the most likely packet. This can be done at different levels. In this study, a slightly different combining scheme using soft bits average is used.

Finally, Partial Incremental Redundancy is a scheme using both approaches. Incremental Redundancy using punctured codes is the most complex but the most efficient version of the protocol, but

the retransmissions are not self-decodable. In Partial IR, the raw packet is always included in the transmissions, with only the parity bits changing.

Enhancements are also possible on the ARQ side but not necessarily thanks to the cooperation. H-ARQ benefits from the classical ARQ protocols, which mainly impact the way retransmissions are scheduled. This study focuses on the most commonly used protocol, N-Stop and Wait (N-SAW). SAW protocols are "send and wait" protocols, in which the transmitter is in a waiting state while waiting for the acknowledgement from the receiver. N-SAW protocols are SAW protocols using multiple instances, meaning that several SAW protocols can run concurrently. This increases the required buffering capacity, as well as the packet ordering complexity, but the available bandwidth is better used.

B. Integration and implementation

H-ARQ is a cross-layer operation. It must be integrated in the transmission layer of a communication chain (Layer 1), to implement the combining methods, as well as in the protocol layer (Layer 2), to manage acknowledgement transmission and retransmission scheduling. This study focuses on the layer 1 integration.

Two main operations must be implemented in the PHY layer part of the protocol: the packet rebuilding based on the different transmissions, and the buffering of received packets. Integration of H-ARQ in a baseband processing chain is presented in Figure 1. The H-ARQ block processes soft-bits (estimated value, along with confidence information) from the deinterleaving block, before decoding. Data processed in the decoder is the enhanced results from the H-ARQ protocol.

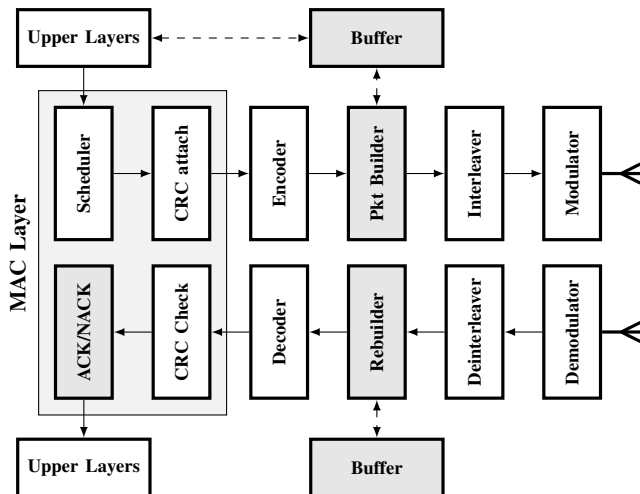


Figure 1. H-ARQ integration in a usual communication system

The rebuilding process uses several basic operations:

- a depuncturer to recover the punctured codes,
- a bit combiner for Code Combining, which can operate on retransmissions, on transmissions from multiple channels, or on repeated bits of a single transmission,
- retransmission concatenation for Incremental Redundancy, the most complex operation.

Possible enhancements to the protocol may require other operations to be implemented. These operations are simple. The

problem when dealing with the implementation of H-ARQ comes from the scheduling of these operations. Yet, traditional device usually implements a single version of the protocol. This reduces the scheduling complexity, since it is predefined, allowing the H-ARQ to be implemented as a part of the decoder, using hard-wired control to manage the scheduling.

The real problem in these architectures lies in the buffer management. In a N-SAW protocol, the H-ARQ processor is required to process up to N packets concurrently. This means that it must be able to store the N received packets and select the buffer corresponding to the packet being received. Several, mostly patented, solutions have been proposed to solve this issue. [4] presents a method based on dynamic computation of addresses in a buffer to manage memory, along with a method to decide whether a received packet must be combined with an already received packet or not. [5] presents a global method to process H-ARQ in a traditional communication device.

Finally the emergence of Multiple Input Multiple Output (MIMO) solutions, as opposed to Single Input Single Output (SISO) solutions has led to research on the use of H-ARQ in such environments. MIMO devices use several antennas for emission and reception, leading to truly time-concurrent transmissions. Two main possibilities are used for operation with H-ARQ. The first one uses the multiple transmission possibility to send several retransmissions concurrently. The second one sends different packets on each channels, thus increasing the throughput when compared to SISO solutions. The theoretical study of the different methods is out of the scope of this study.

C. Flexible radio constraints

A lot of flexible radio platforms have been described in the literature. This paper does not focus on pure software radio, but on hybrid architectures, based on reconfigurable hardware and on software. The study focuses on a dynamically reconfigurable implementation of the H-ARQ (the hardware does not need to be deployed with each configuration change). Figure 2 presents a possible architecture of a flexible system, which will be used as a reference in this study. A generic processor is available, used to process high layers algorithms (especially layer 2). The processing chain is implemented as a sequence of processing units, controlled through a configuration controller, connected to the system bus, and addressable by the processor.

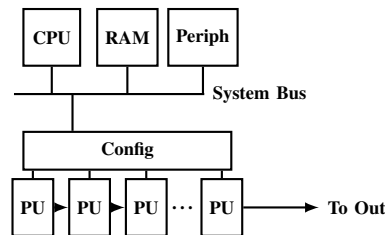


Figure 2. Reference system architecture

Flexible devices must meet constraints that can be avoided when dealing with more traditional, dedicated devices: in the development process, the design of the device is done before a standard is targeted, since the standard is dynamically chosen. While in traditional devices, it is possible to optimize the processing chain

since the precise implementation details are known, flexible devices must take into account all the possibilities.

In the case of a flexible H-ARQ processor, two main constraints appear.

- Any version of the protocol can be used, as well as mixed version, and they can exist concurrently. The design must be able to process any protocol based on a sequence of known operations, regardless of the sequence, and to switch from one to the other efficiently, meaning with minimal reconfiguration overhead. It must also be able to stand MIMO operations;
- Buffers can quickly become a bottleneck. While in traditional devices, the maximum number of buffers (usually around 8) is known before the implementation, in a flexible environment, this upper bound can not be known. Selecting the highest possible number is inefficient, since it can evolve with standard updates. Furthermore, flexible radio is also used to implement different standards concurrently, in order to reduce the required silicon area in multiply connected devices.

Resolving these constraints is unavoidable in order to use H-ARQ in a flexible radio environment. The next sections present an efficient solution based on hardware/software partitioning and configurable hardware.

III. DESIGN OF THE FLEXIBLE H-ARQ PROCESSOR

A. Hardware/Software partitioning

In order to meet the two flexibility constraints, the solution proposed as a result of this study follows the flexible radio philosophy:

- definition of an efficient hardware/software partitioning and
- design of an efficient reconfigurable hardware part to support the processing.

In a traditional implementation, H-ARQ partitioning between hardware and software usually follows the PHY/MAC partitioning. All the PHY elements are processed in hardware, offering pipelining capabilities and high processing power, and all the MAC protocols processed in software, offering the high level approach best fitted to MAC operations. The need for flexibility in the PHY elements (packet rebuilding) means that a new partitioning may be benefiting.

First of all, the management of the content of the transmissions is easier in software. While in a single standard, the sequence of retransmissions is usually based on a predefined sequence, which can be hard wired in the hardware part, this is not true in the flexible case, since each standard has its own sequence.

Secondly, buffer management also becomes a software part. In the presence of a single known standard, it is possible to manage the buffers through a simple round-robin algorithm. When several standards can be present at the same time, the algorithm is not so simple anymore, since the association between the standards and the buffers must be stored and controlled.

Thirdly, and to cope with the possibly high number of buffers, buffering itself is easier in software: any software system has memory. There are two main advantages to software buffering, apart from cost. Management of buffers is easier, since it is possible to use all the software mechanisms for buffers management. And secondly, locating the buffers in the software memory would make these buffers accessible to the processor, opening the door to more complex and possibly more efficient H-ARQ protocols.

B. Operation sequence representation

Given this modified partitioning when compared to the usual implementation, it is necessary to define the flexible hardware component as well as the control required to use it, and the integration of software buffers. The flexible H-ARQ processing presented here relies on a per-bit operation based on data representation.

In a practical communication protocol, different operations can be applied on the information. On the transmission part, the packet is encoded, and then prepared for the H-ARQ protocol before modulation for transmission. This preparation, made according to different parameters such as the current transmission index, the current estimated channel quality, or the H-ARQ protocol being used, is also called rate-matching. The rate-matching algorithm can:

- puncture, meaning delete information from the packet. The punctured information will not be transmitted.
- repeat, meaning send the same information any number of time in a single packet. This is often done to fill unused bandwidth.
- resend, meaning that information already sent in previous transmissions will be resend in this transmission.

Rate-matching can be a destructive operation, which needs to be reversed. To be able to use the received transformed packet, the receiver needs this packet, as well as information on the meaning of this packet: which operation has been applied to which part of the packet. This representation is sent along with the packet.

The representation can take different forms. It defines the association of each bits in the current transmission with the bits of the complete packet being transmitted. One of the most used representation is the puncturing pattern of the code. It is a binary matrix shared between the transmitter and the receiver, and in which a 1 means that the bit is present in the transmission, and a 0 means that it has been punctured. Another method is to use a shared parameterized algorithm, and to send only the parameters. Regardless of the method used, each information bit must be associated to the operation that was applied to it. When no repetition of bits in a single packet is possible, a single bit is sufficient, to signal whether a bit is present or not in the packet. If repetition is possible, several bits are required, to give the number of times the bit is sent. If a bit was punctured a neutral value must be inserted to replace the deletion. This neutral value usually is a "not trustworthy" value (meaning a soft-bit with the lowest possible confidence value).

This representation is the key to H-ARQ operation scheduling. It defines the sequence of operations to be executed by the H-ARQ component. This is better shown with the example of an Incremental Redundancy component, as in Figure 3. The control sequence is the concatenation of the matrices representing the current (new) and previous (prev.) transmissions. A neutral value is also possible if none of the transmissions contain a bit. If the scheme is Full Incremental Redundancy (no combination of bits), when the matrix for the new transmission gives a "1", data is consumed from the new transmission data source, else when the matrix for the previous transmissions gives a "1", data is consumed from the buffered data source, else when both matrices give a "0", data is consumed from the neutral data source.

This concatenation method can be extended as a complete scheduling method: when both matrices give a "1", data is read

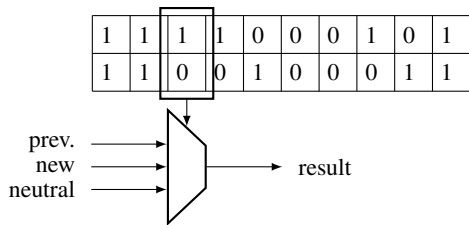


Figure 3. Dataflow operation

from both buffered and new data source, combined, and output. The combination of the representations of all transmissions of a packet creates a codeword, defining which operation must be applied to recover a given information bit.

Using this representation of packets, implementation of H-ARQ does not need prior knowledge of the version used. All inputs become data flows, as well as outputs. The representation is consumed by the component, which enables consumption of some input data, and production of some output data. For each possible representation value, a given input/output mapping is used.

The H-ARQ processor resulting from this hardware/software partitioning and from the per-bit operation principle presented is divided in three main parts, as shown on Figure 4, further presented in the next sections:

- a control part, which computes the operation associated to the current bit,
- an operating part processing data according to the operation associated to the current bit,
- a buffer part to store the transmissions associated to each instance of the protocol.

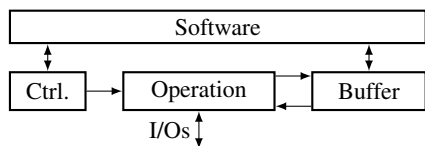


Figure 4. Dataflow scheduling architecture for H-ARQ

IV. IMPLEMENTATION DETAILS

A. Operating part

The operating part described in the previous section is responsible for the bit processing according to the control part instructions. Since the atomic operations used by the H-ARQ component are simple, each operation is implemented separately and a multiplexer is used for control. A simple mux is not sufficient, because of the possible number of inputs and outputs (especially in MIMO operation). A specific configurable data switch has been designed to implement the operation mux. It associates a specific input/output mapping to a given codeword (transmitted by the control part). The mappings may be dynamically modified if some standards require different operations. The modification is done by writing values to a look-up table, with a low latency. This latency is too high for modification during processing of a packet, but is negligible for reconfiguration between two packets.

The resulting architecture is presented in Figure 5. The operations are implemented between two data switches. The input switch

is sufficient to schedule any sequence of operations. It selects its inputs (buffered data, a given input stream if several are possible, or a neutral value), and maps them to the output corresponding to the desired operations. The output switch is used to manage the buffers, and the output streams if several are possible (for example, a Viterbi decoder or a block code decoder). As a result, all dataflow management, and thus all the configuration process, is performed using the switches.

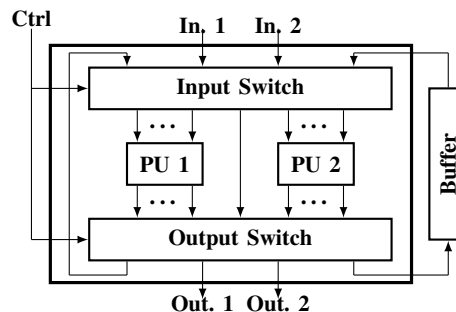


Figure 5. Dataflow scheduling architecture for H-ARQ

The configuration process only consists in giving the I/O mapping information to the switch, *ie.* associating a codeword (runtime control associated to each byte) to a I/O mapping.

B. Control

The second part in the component design is the control part. Control of H-ARQ processing, in this component, means sending to the operating part the sequence of operations needed to build the packet from all its transmissions. Different designs have been envisioned for this part.

Two main operations must be processed when controlling H-ARQ processing. First, recover the transmission representation, meaning the information required to recover the received packet based on the transmissions. This operation can be either very straightforward (known puncturing patterns, which are applied to the transmission), or they may require some computation (parameterized algorithm) in order to recover the complete transmission.

The second operation is the effective control of the operating part, meaning the processing of the representations in order to create the commands to be sent to the operating part. Once again, this can be very straightforward, like in the example in Section III-B, or it can require some computation when the rate-matching process becomes more complicated. For example, if repetition of information in a single transmission is allowed, the concatenation of representations may not be the best choice, since it would be necessary to add support for N-bits repetition in the operating part. It is better to have only a 1 bit repetition operation, and to let the control iterate the operation N times (iteration is typically control).

In order to support both control operations, different hardware/software limit have been experimented.

- An "all hardware" solution, in which everything is processed in hardware. This is an efficient solution for simple H-ARQ schemes, since it frees the processor, and since it avoids the need for synchronization between both targets. Yet, it substantially reduces the flexibility, since updates in processing

becomes difficult, and it limits the component capabilities to the implemented algorithms.

- A mixed solution, in which one operation is implemented in software, and the other in hardware. This is inefficient, since to avoid excessive data exchange between both domains, this solution makes sense only if the hardware operation is the second one, which benefits more from a software implementation.
- The most flexible solution is the "all software" solution. In this solution, everything is processed in software, and the only hardware element is an interface with all the operations to be processed by the operating part. This interface is a small memory, and the size of the sequence being stored. If the sequence is smaller than the packet being processed, the control part iterates the sequence (no control, only a counter), otherwise, the packet is fully represented in memory.

These experimentations are not shown in Section V, but the preferred solution is the software solution in terms of flexibility. The required processing is not time consuming for the processor, while it is complex in hardware. The all hardware solution is useful for a fast implementation of a non-flexible component.

C. Bufferless design

The previous design meets the first flexibility constraint, the protocol-independence. But the second constraint is still not met. The last part of the H-ARQ component is the buffer part. The goal of the buffer part is to manage the storage, as long as required, of received transmissions, which may still be used. This management means that, along with the required buffer space, a control of which information is stored, and where, is also required.

The buffer part, in an environment where the number of possible concurrent transmissions is known, can be implemented in hardware. The existing implementations of H-ARQ mostly uses small and fast memory, with the control responsible for managing the memory, and associating an address with a transmission number. In this study, experimentations have been conducted with FIFOs affected to a specific transmission through the use of a mux. The resulting simplification of multiple buffers management comes at the expense of increased single buffer size.

But with FIFOs or with addressable memory, the infinite buffer constraints is still not met. In order to offer to the device as much memory as required to store numerous transmissions, the hardware buffer has been replaced with a software buffer, located in the processor (software) memory, and managed by the software. This offers multiple advantages:

- more available memory for the component.
- easier to manage. Memory management is an important task in software, and all kernels offer a memory management API to the applications
- accessible buffer. More efficient H-ARQ algorithms could be used, through the use of software, since the buffer is made visible to the software.

This extended flexibility has a cost: data transfer to and from software must not be a blocking point. Figure 6 shows the buffer part details. FIFOs are inserted at the input and at the output to avoid stalling the transfer, and thus be able to use the burst capacity of most RAM. These FIFOs are used as a local cache for

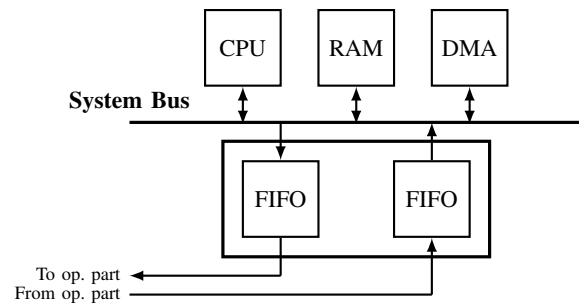


Figure 6. HW/SW interface for bufferless H-ARQ

buffer data. In order to avoid overloading the processor, a DMA is required to implement the software buffers. The size of the FIFOs depends on the bus throughput.

V. PRACTICAL RESULTS

A. Environment

Validation of the proposed architecture means validation of the flexibility as well as validation in terms of performance (impact on the global system, and reconfiguration overhead). In order to experiment on both aspects, the proposed architecture has been implemented and integrated in a complete communication chain, and compared with non-flexible devices implementations of Chase Combining and Incremental Redundancy.

The targeted communication environment is the Magnet high data-rate communication chain [6], supporting up to 40 Mbps. The hardware platform is based on an ATMEL AT91 (a System on Chip integrating an ARM processor), and a Xilinx Virtex 4 (XC4VSX55). The maximum packet size allowed has been fixed to 2kb per packet. The convolutive code used for FEC is a rate $\frac{1}{3}$ code, leading to up to 6kb per encoded packet. The reception chain uses soft bits to add confidence information to the received packet. In the considered implementation, a soft bit is coded on 3 bits words, meaning 4 levels of confidence for each possible hard bit value. All these choices are coherent with existing standards, even if the size is rather smaller than usual.

Based on this implementation, two main lines have been followed when conducting the experiments. First, the flexibility of the platform is studied. While it is difficult to prove that any H-ARQ variation can be implemented, extensive experimentations are conducted in order to validate at least some flexibility. The second point studied is the cost of flexibility. Both points are studied in the next sections.

B. Flexibility: configuration examples

The implementation of the proposed architecture uses two possible processing units:

- a combiner, which combines the information coming from two inputs selected according to the codeword. This combiner outputs the resulting combined symbols.
- a voter, which outputs the most probable value among the two selected inputs.

The voter has been implemented in order to validate the feasibility of multiple dataflow operations management in the device. When combining was required in a version of the protocol, both

operations could be used. Based on these two units, several configurations have been produced in order to process the different versions.

When operating in Chase Combining mode, the output stream is the result of the combination of previous and current transmissions, which adds the need for a combining operation, applied on previous and current transmissions. Incremental Redundancy operation adds complexity, since data can be present in current or in previous transmissions only. Combining of multiply received bits is optional in Incremental Redundancy, but it comes at no cost using the proposed component.

The most challenging operation in this architecture is the repetition of bits. Two possibilities are used. In the first one, a loop is introduced after the first switch, and after the last one, thus adding two possible inputs for the component. Repetition of a bit is then just a matter of selecting the corresponding input. In this case, a delay is introduced during the processing if a bit is repeated more than once, since the two first repetition must be combined before combining with the third one. The second method uses a special processing unit, able to accumulate the inputs, as long as the output is not read.

In order to validate the flexibility of the architecture, experimentations have been conducted on the physical platform. The purpose of these experimentations is to evaluate the ability of this new component to deal with numerous, concurrent and independent instantiations of the H-ARQ protocol. For a given instantiation, either a known version of the protocol is used, from existing standard, or versions built using randomly generated puncturing/repeating patterns may be chosen. While this is not sufficient to guaranty that the proposed component is usable for any possible H-ARQ scheme, it offers a good coverage of the possible cases.

This scenario has been used for big files transfers (1GB each). The switch time from one instance to the others corresponds to the time of two memory write. The component is able to stand high data rates (up to 40Mb/s in simulation, the platform is not able to stand more than 20Mb/s), including reconfiguration latency between each packet. These results make this component fit for real-time applications.

C. Performance and configuration overhead

The precedent section showed that the flexibility constraint is met by the architecture. But it is important to study the cost of the architecture, since flexibility usually means overhead.

In terms of slices cost in the FPGA, the addition of the H-ARQ component and its control interface adds around 300 slices, which means about 1% additional slices in the reference reception chain. As a comparison, this cost is similar to the cost of an Incremental Redundancy only component. In terms of buffer space, the proposed H-ARQ component requires 64 bits of local buffer. With a total available memory of 32MB, and a usable DMA engine, the platform has been used to implement a 10-SAW adaptive H-ARQ protocol. This implementation requires 18kb of free memory for each protocol instance, but this memory is located in the system memory, and no buffers are required in the hardware device, leading to an important gain in silicon area requirements.

In terms of performance, the component processes 1 input bit per clock cycle with no repetition. When there is repetition in the scheme, with the accumulator solution, the throughput stays the

same, but control becomes more complicated because of the need for synchronization at the output. If the loopback solution is used and if a bit can be repeated only once, there is no overhead either. If more repetition can occur, a delay is introduced in the processing. This delay is equal to the length of the pipeline, *ie.* 6 clock cycles, once every two repetitions. The configuration time, which is the time required to change the codeword/mapping association, is negligible, since it is only a write to a look-up table.

VI. CONCLUSION AND FUTURE WORK

An implementation of a H-ARQ processor fit for flexible radio devices has been presented in this paper. Thanks to its design, this component is able to cope with current and future envisioned versions of the protocol. The buffer is virtually unlimited, and the control management is flexible. The choice of operations, implemented between the switches in the operative part, is open. Managing multiple inputs or outputs, when parallel transmissions are possible (OFDMA, MIMO, ...) is intuitive thanks to the dataflow view.

The component is based on a specific software/hardware partitioning:

- memory and scheduling of required operations are managed through software,
- actual computation is done in hardware, using configurable codewords to describe the operation to be processed.

The codewords used to describe the different operations are based on the representation of the different dataflow. The component is able to use the sequence of operations applied on the original packet and on the already received transmissions, and associate to each combination an operation to process.

The resulting component is fast, small (about the same size as other dedicated H-ARQ devices used for a single version of the protocol), and flexible enough that any H-ARQ protocol can be configured and processed. In the continuation of this work, power consumption measures are planned, as well as a study of new protocols using the flexibility property to enhance the error correction capacity.

REFERENCES

- [1] J. Wozencraft and M. Horstein, "Coding for Two-Way Channels," Research Laboratory of Electronics, MIT, Tech. Rep., 1961.
- [2] D. M. Mandelbaum, "An Adaptive-Feedback Coding Scheme Using Incremental Redundancy," *IEEE Transactions on Information Theory (corresp.)*, vol. 33, pp. 388-389, 1974.
- [3] D. Chase, "Code Combining - A Maximum-Likelihood Decoding Approach for Combining an Arbitrary Number of Noisy Packets," *IEEE Transactions on Communications*, vol. Vol. COM-33, pp. 385-393, 1985.
- [4] B. Franovici, "Method and system for memory management in a HARQ communication system," European Patent 2 093 921 A1, 2009.
- [5] M.-C. Tsai, W. Chowdiah, and W. Jing, "Packet decoding for H-ARQ transmission," World Patent 2009/108 516 A2, 2009.
- [6] R. Prasad, *My personal Adaptive Global NET (MAGNET)*. Springer, 2010.

Optimal Pilot Placement in Cognitive Radio Systems for Wiener Filtered MMSE Channel Estimation

Boyan V. Soubachov

Department of Electrical Engineering
University of Cape Town
Rondebosch, Cape Town, South Africa
e-mail: boyan@crg.ee.uct.ac.za

Neco Ventura

Department of Electrical Engineering
University of Cape Town
Rondebosch, Cape Town, South Africa
e-mail: neco@crg.ee.uct.ac.za

Abstract—Non-contiguous Orthogonal Frequency Division Multiplexing (NC-OFDM) Cognitive Radios (CRs) pose an intriguing situation for optimal pilot-pattern generation. It has been proposed that in order to attain the lowest possible Mean Squared Error (MSE) of a channel estimator, the pilots should be placed adjacent to an interfering Primary User (PU) to allow for the highest pilot to data symbol cross-correlation and the lowest pilot auto-correlation. In past research, this has been shown to provide a significant decrease in the channel estimator's MSE; moreover the optimal power loading required such that the PU does not experience interference above a certain threshold from the Secondary User (SU) is not taken into account. This leads to a contradiction between the optimal power loading and the optimal pilot pattern. In this paper, the relationship between these two concepts is investigated with the implementation of a Minimum Mean Squared Error (MMSE) Wiener filter and the optimal pilot positioning is derived.

Keywords—OFDM; cognitive radio; MMSE estimation; power loading

I. INTRODUCTION

Bearing in mind the practical limits of higher frequency ranges, spectrum scarcity has become a great issue. This is further exacerbated by the immense growth of services and protocols which demand an ever increasing link speed. It has thus become of great importance to achieve as high a spectral efficiency as possible when engineers design the next generation wireless communications systems and standards.

A solution widely accepted as a spectrally efficient and practical alternative to spectrum re-arrangement is cognitive radio. Cognitive radio works on the basis of an intelligent software-defined radio (SDR) where a CR user (also known as the secondary user) transmits in licensed (or primary user) frequency bands when the licensed user themselves are not transmitting [1]. This solution promises to be an almost ideal alternative since, in a perfect implementation, the entire usable spectrum would be fully utilised.

The call for cognitive radios is further backed by research and surveys done on spectral usage in typical geographic areas. It has been noted that even though much of the usable spectrum has been occupied and licensed, it is only used anywhere from 15% to 85% of the time in a wide geographic

and time dispersion [2]. This can be even lower in certain situations such as sub-urban environments where frequency utilisation from 100 MHz to 3 GHz can be utilised as little as 7% of the time [3]. An interpretation which can be derived from this is that much of the usable spectrum is reserved for licensed operation but is only used by its licensees a very small percentage of the time or that its actual licensed use is limited to a relatively small geographical area.

It is commonly proposed that a non-contiguous OFDM system be used to implement a CR system. This allows the sub-channels of an OFDM system which interfere with the primary user to be switched off. This means that the NC-OFDM system would comply with one of the principles of CR such that any CR-compliant communications are transparent to, and need not be considered by, non CR-compliant systems.

In this paper, the related work in the fields of optimal power loading and optimal pilot patterns is described in Section II. The system model used to derive the proposed solution is described in Section III and the proposed solution itself is derived in Section IV. The simulation results are shown and discussed in Section V and a conclusion is drawn in Section VI.

II. RELATED WORK

In related work, two aspects of CR research focus on the optimal pilot patterns and the optimal power loading for secondary users. In [4] the optimal power loading is investigated for CR users such that power loaded to the individual sub-channels (which are then assigned to SUs) is such that interference to PUs, which are adjacent to the SUs, is kept below a threshold value as specified by design. It found in [4] that the optimal power loading profile which maintains interference to the PU below a threshold is that of a 'step' profile, meaning that less power is allocated to sub-channels closer to the PU and more power is allocated to sub-channels farther away from a PU.

The optimal pilot pattern for the SU in a cognitive radio environment is investigated in [5]. It was found that when a PU initially starts transmitting it is optimal to convert the sub-channels adjacent to the PU's transmission band to pilot sub-channels. This is such that the cross-correlation between pilot and data symbols is maximised (as the addition of an

extra pilot sub-channel can only increase the cross-correlation) and the auto-correlation between pilot sub-channels is decreased. It is also noted that the MSE of the estimator also depends on the signal-to-noise ratio (SNR) of the received pilot symbols [5].

These two aspects are both optimal in their own sense but it was found that they crucially fail to consider their common dependence. While the optimal pilot pattern proposes that an extra pilot be placed adjacent to the PU (with MSE decreasing as the pilot sub-channel is moved closer to the PU) it is not considered that the SNR of the pilot symbols in the sub-channel may only decrease due to the decrease in transmission power for the pilot bearing sub-channel as necessitated by the optimal power loading algorithm. This contradiction is further exacerbated by the fact that a PU would, in most practical situations, be non-orthogonal to the SU and therefore the SU would have a higher noise floor on sub-channels closer to the PU, additionally reducing the SNR available for pilot sub-channels.

A further addition to the problem is the principle of boosting the power for pilot symbols. This is characterised as the pilot-to-data power ratio (PDPR) and the point behind it being that a lower estimator MSE can be achieved by allocating more power to pilot symbols than which is normally allocated to data symbols.

Research done on this contradiction, as presented in this paper, has led to the development of a solution where the optimal pilot pattern is achieved while maintaining the optimal power loading profile such that interference to the PU is kept below a desired threshold. The channel estimation method used is the MMSE criterion implemented as the Wiener finite impulse response (FIR) filter.

III. SYSTEM MODEL

The model used to simulate the CR system is that of an OFDM transmission of N sub-channels having N_d carriers disabled due to an interruption caused by a PU. This allows spectrum to be fully utilised since there would be no guard-bands between the PU's and the SU's signal.

The system is considered to have allocated a total of N_p sub-channels for the sole purpose of transmitting pilots. For the sake of simplicity, the system is analysed using a 1-dimensional pilot pattern in frequency only. As prescribed in [6], the system differentiates between PU-to-SU and SU-to-PU interference for the purposes of optimal power loading.

A. Power density spectrum of signals

The transmitted signals in the system model are assumed, for the sake of simplicity, to be shaped by a rectangular pulse shaping function. The power density spectrum of the rectangular pulse shaping function can be represented as [4]

$$\phi_i(f) = P_i T_s \left(\frac{\sin(f \cdot \pi \cdot T_s)}{f \cdot \pi \cdot T_s} \right)^2. \quad (1)$$

In (1), P_i represents the transmit power of the i_{th} sub-carrier and T_s represents the symbol duration of that same sub-carrier. It would serve well to note that the equation is only applicable to a rectangular pulse-shaping function and is used for simplicity. Other equations may be substituted for (1) but the contradiction (and therefore solution) will still hold since all non-ideal filters have some form of spectral roll-off and therefore present interference to adjacent frequency bands.

B. Interference from PU to SU

The signals between PU and SU are assumed to be non-orthogonal and therefore the interference imposed on a SU by a PU is effectively 'smeared' due to the Fast Fourier Transform (FFT) performed by the SU [6]. The expected value of the power density spectrum of the PU's signal after an FFT of size M is performed can be described as [6]

$$E\{I_M(\omega)\} = \frac{1}{2\pi M} \int_{-\pi}^{\pi} \phi_{PU}(e^{j\omega}) \left(\frac{\sin(\omega - \psi)M/2}{\sin(\omega - \psi)/2} \right)^2 d\psi \quad (2)$$

where ω represents the angular frequency which has been normalised to the sampling frequency and $\phi_{PU}(e^{j\omega})$ represents the power density spectrum of the PU's pulse-shaping filter.

The interference from the PU to the SU can then be described as the integral of the expected value of the power spectral density, which may be expressed as

$$I_{PU}(d_i, P_i) = \int_{d_i - \Delta f / 2}^{d_i + \Delta f / 2} E\{I_M(\omega)\} d\omega \quad (3)$$

In (3), d_i represents the spectral distance between the considered sub-carrier and the PU and Δf represents the width of one sub-channel of the SU (equivalent to the inverse of the OFDM symbol duration).

C. Interference from SU to PU

The interference from the secondary user to the primary user is modelled using simpler mathematics due to the assumption that we do not have any information about the PU's modulation scheme and other transmission properties, only the bandwidth and signal power.

The interference caused by spectral roll-off from the SU can then be simply modelled as the integration of the power density spectrum of the signal, represented as (1) for the rectangular pulse shaping filter case. The interference from the SU can therefore be modelled as [4]

$$I_{SU}(d_i, P_i) = \int_{d_i-B/2}^{d_i+B/2} \phi_i(f) df. \quad (4)$$

It should be noted that B denotes the bandwidth occupied by the PU's signal such that the integration is performed over the PU's bandwidth with an added frequency 'offset' introduced by the spectral distance between the considered sub-channel and the PU's signal.

D. Optimal power loading

The optimal power loading algorithm is specified in [4]. It is important to note that the same power loading algorithm is derived at the boundary level where the interference to the PU is equal to the interference threshold parameter such that transmission power is maximized and, consequently, so is channel capacity.

It is noted in [4] that this is indeed the optimal point for the power loading algorithm since the channel capacity of a sub-channel is proportional to the power loaded to said sub-channel. The interference equation at the threshold was therefore used such that the equation is formulated as

$$P_i^* = \frac{I_{th}}{\frac{\partial I_{SU}}{\partial P_i}}. \quad (5)$$

where I_{th} is the power threshold of the interference introduced into the primary user's band by the secondary user.

E. Estimator correlation and Wiener filter MMSE

One of the ways in which a channel frequency response (CFR) can be estimated and interpolated is through the use of a Wiener FIR filter [7]. The optimal Wiener filter allows us to achieve the MMSE criterion for the channel estimator by utilizing statistics about the channel, specifically the channel's auto- and cross-correlation data.

The frequency cross-correlation between pilot and data symbols where a rectangular Doppler spectrum is assumed is given as [7], [8]

$$\theta_{\Delta f}(d_{dp}) = \frac{\sin(2\pi\tau_{\max}\Delta f d_{dp})}{2\pi\tau_{\max}\Delta f d_{dp}}. \quad (6)$$

In equation (6), τ_{\max} represents the maximum expected delay of the channel, Δf represents the sub-channel width or carrier spacing and d_{dp} represents the integer distance between the pilot and the data sub-channel to which the cross-correlation needs to be calculated.

The auto-correlation function between different pilot symbols is also needed to compute the optimal Wiener FIR filter coefficients. The auto-correlation function for the pilot symbols is given as [7], [8]

$$\phi(d_{pp'}) = \theta_{\Delta f}(d_{pp'}) + \frac{\sigma_n^2}{E\{|S(n_{p'})|^2\}}, \quad (7)$$

where $d_{pp'}$ represents the integer distance (sub-channel multiples) between two neighbouring pilot symbols in the frequency dimension, σ_n^2 represents the mean noise variance between pilot symbols and $E\{|S(n_{p'})|^2\}$ represents the mean energy of the pilot symbols.

For the implementation of the MMSE filter, the derivative of the MSE function needs to be set to zero such that we achieve the filter coefficients which achieve the minimum possible MSE. The MMSE for the Wiener filter is derived as [7]

$$J_{n,i} = E\{|H_{n,i}|^2\} - \boldsymbol{\theta}_{n,i}^T \boldsymbol{\phi}^{-1} \boldsymbol{\theta}_{n,i}^* \quad (8)$$

where $\boldsymbol{\theta}$ and $\boldsymbol{\phi}$ represent the cross- and auto-correlation matrices respectively. However, since we are dealing with the single dimensional estimator (frequency only) the cross- and auto-correlation matrices reduce to vectors [7] and therefore can be simplified to element-wise multiplication and inversion.

IV. OPTIMAL SOLUTION

In order to obtain the optimal pilot placement, the pilot needs to be placed in the sub-channel which allows for the lowest MMSE out of the possible sub-channels for pilot placement. Given that the MMSE is defined as always positive [7] it would mean that the pilot placement needs to be found where

$$\boldsymbol{\varepsilon} = -\boldsymbol{\theta}_n \boldsymbol{\phi}^{-1} \boldsymbol{\theta}_n \quad (9)$$

is a maximum. It should be noted that, in (9), since the estimator is 1-dimensional for these purposes and the filter coefficients are strictly real [7], the error vector $\boldsymbol{\varepsilon}$ is obtained without any conjugation and using only element-wise multiplication and inversion.

The optimisation problem can therefore be written as

$$\min \boldsymbol{\varepsilon} = -\frac{[\theta_{\Delta f}(d_{dp})]^2}{\theta_{\Delta f}(d_{pp'}) + \frac{2(\sigma_n^2 + I_{PU})}{P_i^*}}. \quad (10)$$

The error function as specified by (9) and (10) is used to determine where the optimal placement of the new pilot would be. The functions are chosen such as to represent the change in MSE relative to the SU's system without adding a new pilot. The MSE change in (10) is evaluated only over 2 pilot sub-channels, therefore MSE difference is only compared to the nearest pilot instead of all pilots. This is due to the linear scaling of the MSE difference between a localised, 2-pilot model and an evaluation over all pilots and so the optimal calculation is done over the nearest, unmoved pilot and the proposed positioning of the new pilot. Since the SNR expression in (7) represents the average SNR over all

pilots, the term is then adjusted in (10) so that the SNR contribution added by the new pilot is divided by a factor of two. This allows the error function value to be either positive or negative in that a negative error function value would represent a decrease in the overall estimation MMSE whereas a positive value would represent an overall increase in the estimation MMSE.

The proof to this logical decision is simple in that the MMSE of the Wiener filter as demonstrated in (8) depends on the auto-correlation of pilot symbols (ϕ). For a two-dimensional system, the matrix depends on the nearest pilot symbols in both time and frequency but in the one-dimensional case (be it either time or frequency) the matrix becomes a vector and the values are then only dependent on the two nearest pilot symbols on either side of the pilot symbol concerned.

It would serve well to note that the function described in (10) is transcendental in nature and therefore has no algebraic form solution for its derivative. Techniques such as the Karush-Kuhn-Tucker (KKT) conditions cannot be used to find an equation for the optimal position. The solution, therefore, has to be found using enumeration over the problem space or through a numerical solution.

At first thought, it would seem computationally expensive to search for the optimal pilot positioning (where the MMSE error function is lowest) by brute-force enumeration. This is however not the case since the error function is bound to a problem space which is single dimensional (vector space) and, at most, has a length equal to the pilot interval of the original pilot pattern. Another advantage is that the pilot auto-correlation values can be pre-computed and stored after the first iteration for obtaining the optimal error function since the pilot symbols are of a known sequence.

V. SIMULATION PARAMETERS AND RESULTS

In order to simulate the system an NC-OFDM cognitive radio receiver was simulated using the parameters as described in Table 1. It should be noted that the narrowband and wideband PU interference parameters are specified as a percentage of the PU's power.

The system was simulated by averaging the results over 10000 runs such that a statistically significant sample was achieved and an appropriate conclusion could be inferred. The system simulated first was that of a wideband system where the PU's spectrum was set to be 20 times the bandwidth of a single SU sub-channel.

It was noted that due to the mathematical formulation of the SU-to-PU interference, the width of the PU plays a large role in determining the optimal pilot positioning. This is due to the summation caused by the integral, effectively meaning that PUs with a larger bandwidth are more sensitive to interference effects and spectral roll-off introduced by the SU. This meant that in implementing the error function and obtaining the optimal pilot placement, lower interference

thresholds could be used for the narrowband case (where the PU's band is assumed to be of the same bandwidth as 1 pilot sub-channel).

TABLE I. SIMULATION PARAMETERS

Parameter	Value
PU transmit power	1 mW
Maximum delay spread (τ_{\max})	10 μ s
FFT size	512
PU bandwidth	625 ($20 \Delta f$) kHz
SU transmit power	1 mW
SU sub-channel bandwidth (Δf)	31.25 kHz
Noise floor	-90 dBm
Pilot spacing (sub-channels)	9
Wideband interference thresholds	[25; 10; 5; 1] %
Narrowband interference thresholds	[0.25; 0.1; 0.05; 0.01] %

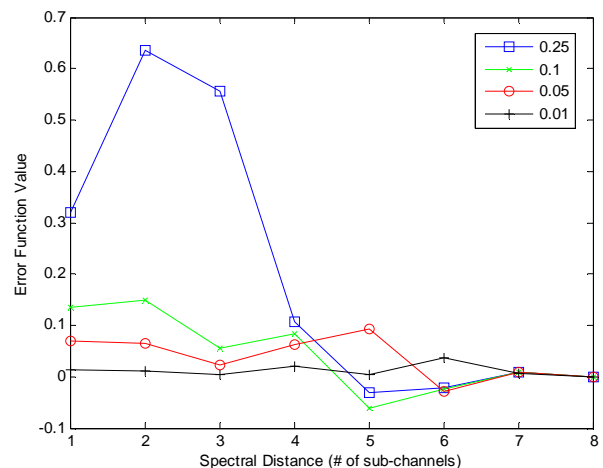


Figure 1. This figure demonstrates the error function value of a pilot sub-channels for all possible placement positions. The model of interference from the PU is that of a wideband one where the PU's bandwidth is equivalent to 20 times of that of the SU's sub-channel bandwidth.

Fig. 1 shows the error function values for possible sub-channel positions of the pilot sub-channel. The different graphs also represent the different interference thresholds in Table 1. This is done for the wideband PU case.

It is noted that in Fig. 1 the optimal pilot position shifts farther away from the PU as the interference threshold decreases. This can be attributed to the stringency of the threshold constraint forcing the pilots to be placed farther away due to the needed reduction of spectral roll-off from the pilot sub-channels.

Another interesting observation which can be noted in Fig. 1 is that for sub-channels 7 and 8, the error function value is almost identical for all 4 interference threshold parameter values and it seems to converge to a point. This

can be attributed to the optimal power loading algorithm and the finite, maximum transmission power which can be loaded per sub-channel. Since the power loading algorithm has reached the point where power assigned to the sub-channel is capped, the whole factor of power loading has effectively been removed from the error function's equation and the power at those points assumes a uniform loading profile (or a water-filling profile for data sub-channels). This means that the error function's value from sub-channels 7 and onwards purely depend on the auto-correlation between pilot symbols and the cross-correlation between pilot symbols and data symbols such that the algorithm becomes irrelevant and the values at any further positions need not be computed so as to save on computational time.

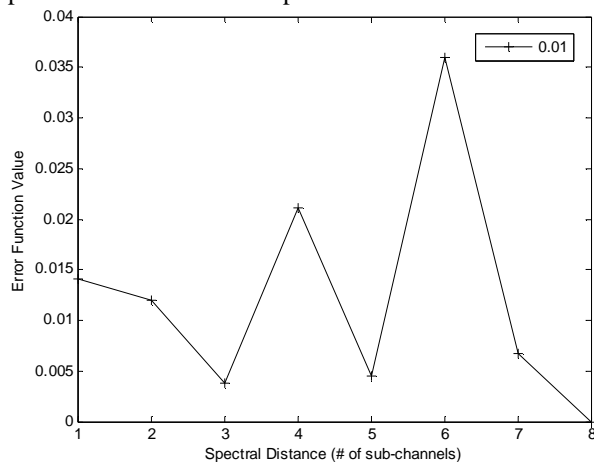


Figure 2. This figure represents the error function value for all possible pilot sub-channel placement positions for an interference threshold of 1%. The graph is zoomed in for the threshold value from Fig. 1.

Fig. 2 demonstrates the error function value as seen in Fig. 1 for 1% interference threshold while zoomed in on the graph. The graph shows how the optimal pilot position is at sub-channel 6 (5 sub-channels away from the PU where sub-channel 1 is adjacent to the PU). This graph shows an interesting result in that while there is a clear, optimal position, the numeric difference in values of the error function between the best and second best position is relatively small when compared to the rest of the graphs.

This can be attributed to the low interference threshold parameter as defined for the optimal power loading algorithm. This means that the pilot sub-channel has a lower power assigned to it throughout the possible placement positions such that a placing the pilot anywhere in the solution space will provide a relatively small decrease in MSE.

In a practical implementation scenario, this phenomenon can reach a point where it could be debated as to whether a pilot should be added or whether the decrease in MSE is negligible compared to the loss in data rate for when the sub-channel is converted to a pilot-bearing sub-channel.

In Fig. 3 the system is simulated for the case where a narrowband primary user is transmitting. Upon first

inspection, one can easily notice that the interference threshold parameter values are much lower, this is due to the decreased bandwidth of the PU which in turn leads to integration over a smaller period to compute the interference introduced to the PU from the SU. The reduced integration period means that for a fixed threshold value, the total sum of the interference will be less than the wideband scenario due to the smaller area of integration. This means that the pilots will tend to be placed farther away the higher the PU's bandwidth is.

Another observation made from Fig. 3 is the convergence to the same error function value occurring from a distance of 6 sub-channels and greater. This can be attributed to the same reason as explained for Fig. 1.

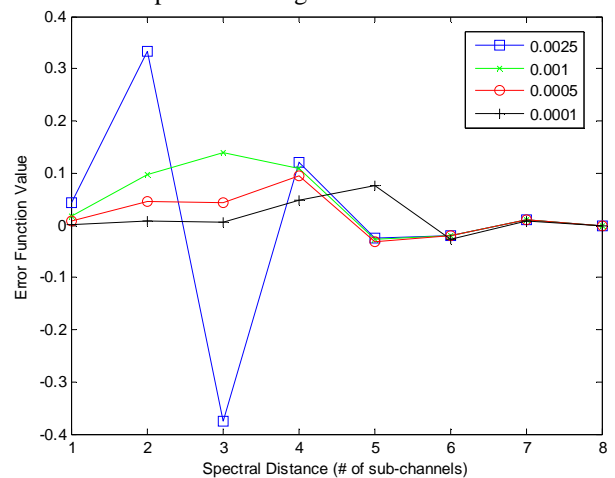


Figure 3. This figure represents the error function value for all possible pilot sub-channel placement positions for the narrowband PU case. The threshold values used are the same as those described in Table 1.

VI. CONCLUSION

The hypothesis investigated in this paper has shown that for the successful implementation of a cognitive radio system, the optimal power loading algorithms and optimal pilot patterns cannot be implemented independently without considering either of them.

It was found that the sub-channels adjacent to the PU cannot simply be converted to pilot sub-channels without any consideration to the optimal power loading algorithms. An error function was therefore derived which allows for the optimal placement of pilots which satisfy interference thresholds while achieving the lowest possible MSE.

The error function was used to compute the optimal pilot placement and was simulated accordingly. It was found that in many cases it is impractical to place the pilot sub-channel adjacent to the PU since the reduction of power required to keep interference to the PU below a threshold mandated a very low SNR on the pilot symbols, leading to a very noisy channel estimate.

It was also found that the interference threshold mandated for the optimal power loading played a big role in

determining the optimal position for the optimal pilot sub-channel position. It was observed that, trivially, as the interference threshold decreased, the pilot sub-channel needed to be placed farther away from the PU such that the threshold condition still is satisfied.

An observation also made was that the error function value for all thresholds converged due to the maximum power which could be allocated per sub-channel due to the power loading algorithm. This meant that the error value did not need to be computed for sub-channels farther than the convergence point.

ACKNOWLEDGMENT

The authors would like to thank Telkom SA, the National Research Foundation (NRF), Technology and Human Resources for Industry Programme (THRIP), the Department of Trade and Industry (DTI), Nokia Siemens Networks and TeleSciences, for supporting this research project.

REFERENCES

- [1] J. Mitola III and G. Q. Maguire Jr., "Cognitive radio: making software radios more personal," *Personal Communications, IEEE*, vol. 6, pp. 13-18, 1999.
- [2] I. F. Akyildiz, W. Lee, M. C. Vuran, and S. Mohanty, "NeXt generation/dynamic spectrum access/cognitive radio wireless networks: A survey," *Computer Networks*, vol. 50, pp. 2127-2159, 9/15, 2006.
- [3] V. Valenta, Z. Fedra, R. Marsalek, G. Baudoin and M. Villegas, "Towards cognitive radio networks: Spectrum utilization measurements in suburb environment," in *Radio and Wireless Symposium, 2009. RWS '09. IEEE, 2009*, pp. 352-355.
- [4] G. Bansal, M. J. Hossain and V. K. Bhargava, "Optimal and Suboptimal Power Allocation Schemes for OFDM-based Cognitive Radio Systems," *Wireless Communications, IEEE Transactions on*, vol. 7, pp. 4710-4718, 2008.
- [5] I. Rashad, I. Budiarjo and H. Nikookar, "Efficient pilot pattern for OFDM-based cognitive radio channel estimation - part 1," in *Communications and Vehicular Technology in the Benelux, 2007 14th IEEE Symposium on*, 2007, pp. 1-5.
- [6] T. Weiss, J. Hillenbrand, A. Krohn and F. K. Jondral, "Mutual interference in OFDM-based spectrum pooling systems," in *Vehicular Technology Conference, 2004. VTC 2004-Spring. 2004 IEEE 59th*, 2004, pp. 1873-1877 Vol.4.
- [7] S. Kaiser. (1998, *Multi-carrier CDMA mobile radio systems - analysis and optimization of detection, decoding, and channel estimation*.
- [8] I. Budiarjo, H. Nikookar and L. P. Ligthart, "Performance evaluation of OFDM based cognitive radio system with wiener filter channel estimation using frequency hopping GSM channel model at 900 MHz," in *Wireless Technologies, 2007 European Conference on*, 2007, pp. 74-77.

Deriving the Key Electrical Specifications for a Multi-Standard Radio Receiver

Silvian Spiridon, Florentina Spiridon, Claudius Dan and Mircea Bodea

Faculty of Electronics, Telecommunications and Information Technology

“POLITEHNICA” University of Bucharest, Romania

e-mail: silvian.spiridon@gmail.com, florentina.spiridon@gmail.com, claudius.dan@gmail.com, mirceabodea@yahoo.com

Abstract—This paper focuses on finding the key electrical specifications for a multi-standard radio receiver compatible with the major commercial wireless standards. By developing a standard independent methodology, the paper addresses systematically the large amount of information comprised in the envisaged standards. Based on the systematic approach, the multi-standard receiver main electrical requirements are defined and their values determined. The presented results constitute the starting point in building a multi-standard wireless receiver.

Keywords—software defined radio; receiver electrical specifications.

I. INTRODUCTION

At the beginning of the mobile Internet age, it becomes clear there is a strong need of mobile equipment able to maximize its wireless connectivity.

There are several reasons that make extremely attractive the usage of multi-standard radio transceivers to enable the wireless interoperation of such mobile equipment.

First of all, a multi-standard solution is efficient as only one design is required to handle the mobile device wireless communication. Thus the number of different dedicated ICs or IP blocks inside a large SoC is reduced. This simplifies the overall communication platform integration. Secondly, since only one design is required to cover for the all the targeted wireless standards all cost related to the IP development and testing are minimized.

The ideal multi-standard receiver was proposed by Mitola in [1]. The Software Defined Radio Receiver (SDRR) shown in Fig. 1.a is the optimal choice from system level perspective, as it comprises only an ADC. In reality, due to practical implementation constrains, a multi-standard receiver requires a signal conditioning path in between the antenna and the ADC. The SDRR concept shown in Fig. 1.b relaxes the ADC specifications by ensuring for the wanted signal additional selectivity and amplification.

A possible SDRR implementation is shown in Fig. 1.c, [2]. The receiver is based on the direct conversion architecture, the optimum choice for a multi-standard enactment, [3]. Also, the homodyne receiver is embedding a full signal conditioning path. The received signal is amplified by the Low Noise Amplifier (LNA) and then downconverted to baseband.

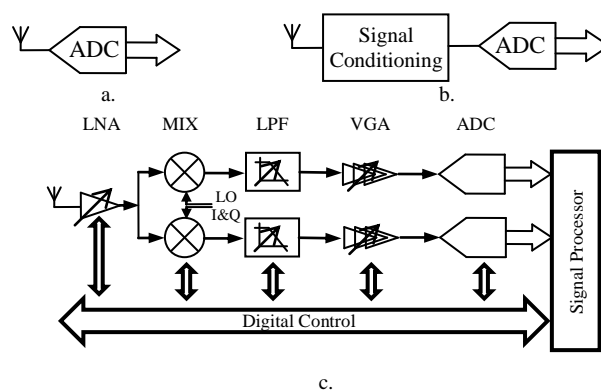


Figure 1. a. Mitola SDRR Concept, b. SDRR embedding signal conditioning and c. SDRR with complete analog signal conditioning

The blockers and interferers are removed by the channel selection Low Pass Filter (LPF) and then the Variable Gain Amplifier (VGA) boosts the useful signal to optimally load the Analog to Digital Converter (ADC).

Through digital control the SDRR blocks main characteristics (e. g., bandwidth, noise, and linearity) can be changed dynamically depending on the particular standard requirements or even on the particular communication burst necessities.

The paper's main goal is to identify the key electrical requirements and their values for a SDRR based on the Fig. 1.c concept targeting compatibility to the major commercial wireless standards listed in Table I. Based on a systematic approach, the paper introduces a standard independent methodology for evaluating the SDRR performance.

Section II defines the SDRR receiver sensitivity, NF and gain requirements, while Section III analyses the blocker and interferers impact on the SDRR linearity requirements. Section IV concludes the paper.

II. DEFINING THE SDR SENSITIVITY, NOISE FIGURE AND GAIN REQUIREMENTS

A. Sensitivity and Noise Figure

One of the most important parameters of a wireless receiver is its sensitivity, S_{RX} . The sensitivity is defined as the minimum input signal the receiver must be able to demodulate within a specified Bit Error Rate (BER).

TABLE I. TARGETED MAJOR COMMERCIAL WIRELESS STANDARDS KEY SPECIFICATIONS

Wireless Standard	Frequency Plan [MHz]		Modulation Type	SNR ₀ [dB]	RF Signal BW / Channel Spacing [MHz]	Specified Sensitivity [dBm]	Sensitivity @ NF _{RX} = 3 dB [dBm]	
	Downlink	Uplink						
GSM, [4]	GSM 850	869 ÷ 894.8	824 ... 849.8	GMSK	9	0.2	-102	-109
	GSM 900	935 ÷ 960	890 ... 915					
	DCS 1800	1805 ÷ 1880	1710 ... 1785					
	PCS 1900	1930 ÷ 1990	1850 ... 1910					
UMTS, [5]	I	2110 ÷ 2170	1920 ÷ 1980	QPSK	-18 (@ 12.2kbps)	3.84 / 5	-117	-123
	II	1930 ÷ 1990	1850 ÷ 1910					
	III	1805 ÷ 1880	1710 ÷ 1785					
Bluetooth, [6]	2402 ÷ 2480		GFSK	16	1	-70	-94	
DECT, [7]	1880 ÷ 1980, 2010 ÷ 2035		GFSK	13	1.2 / 1.736	-83	-97	
WLAN IEEE 802.11b (DSSS), [8]	1 / 2 Mbit/s	2400 ÷ 2485		DBPSK / DQPSK	-4 / -2	14 / 5	-80	-104 / -102
	5.5 / 11Mbit/s			CCK	9 / 11		-76	-91 / -89
WLAN IEEE 802.11a,g (OFDM), [8]	6 / 9 Mbit/s	5150 ÷ 5350 & 5725 ÷ 5825 (a)		BPSK	4 / 5	16.6 / 20	-82 / -81	-95 / -94
	12 / 18 Mbit/s			QPSK	7 / 9		-79 / -77	-92 / -90
	24 / 36 Mbit/s			16QAM	12 / 16		-74 / -70	-87 / -83
	48 / 54 Mbit/s			64QAM	20 / 21		-66 / -65	-79 / -78

Thus, the Signal-to-Noise Ratio at the RX output, SNR_{out} , has to be above a minimum value SNR_0 . SNR_0 value is set by the received useful signal modulation characteristics and it incorporates the digital demodulator non-idealities.

Based on the analysis presented in [9], the SNR_0 as a function of the BER has been determined for the basic modulation schemes. Table I notes the targeted standards signal modulation and the corresponding SNR_0 values. The SNR_0 has a negative value for UMTS and WLAN 802-11 standards, as it accounts the processing gain specific to direct sequence spread spectrum systems, [10].

The usage of SNR_0 facilitates the finding of the multi-standard receiver key electrical parameters by enabling a standard independent approach.

As each standard specifies a sensitivity level, given the useful signal RF bandwidth, BW_{RF} , the receiver NF, NF_{RX} , is calculated as:

$$NF_{RX} \leq S_{RX} - 10 \log BW_{RF} - SNR_0 - N_0, \quad (1)$$

where $N_0 = k_B T = -174$ dBm/Hz represents the noise power spectral density at the antenna output for $T = 290$ °K.

In practice, an overhead to SNR_0 should be considered in (1), since the overall receiver SNR is degraded by multiple factors, not only by noise (e. g., imperfect impedance matching, multipath channel).

The receiver NF specifications for all the wireless standards can be calculated with (1) by accounting the specified sensitivity levels from Table I.

A NF as the one derived by (1) can be obtained at the expense of larger power consumption of thy receiver.

In order to maximize the link budget, most commercially available dedicated receivers push their sensitivity level towards smaller and smaller values by decreasing NF_{RX} .

Hence, a true re-configurable multi-standard solution must embed a receiver with a small NF (typically < 3 dB) in order to be able to achieve a low enough sensitivity for all the targeted standards. Table I also comprises the required sensitivity levels, assuming $NF_{RX} = 3$ dB, for all the envisaged wireless standards.

B. Maximum gain requirements

In general, the receiver signal conditioning path gain is constraint by the received signal strength.

Any wireless receiver with an analog signal conditioning path embeds at least one variable gain block (for example VGA in Fig. 1.c). Thus, for each communication burst an Automated Gain Control loop (AGC) measures the Receiver Signal Strength Indicator (RSSI) and changes the receiver gain accordingly, in order to avoid the ADC overloading and to optimally load it.

The receiver maximum gain requirements are constraint by the ADC full scale level, FS_{ADC} , and the specified receiver sensitivity.

In order to optimally load the ADC, the receiver signal conditioning path maximum gain, G_{RX} , is given by:

$$G_{RX} = \frac{k \cdot FS_{ADC}}{S_{RX}}, \quad (2)$$

where $k < 1$ accounts the head room taken to avoid the ADC overloading.

TABLE II. THE MULTI-STANDARD RECEIVER MAXIMUM GAIN REQUIREMENTS

Wireless Standard		G_{RX} [dB]
GSM		115
UMTS		129
Bluetooth		100
DECT		103
WLAN IEEE 802.11 b,g (DSSS)	1 / 2 / 5.5 / 11 Mbit/s	110 / 108 / 97 / 95
WLAN IEEE 802.11 a,g (OFDM)	6 / 9 / 12 / 18 24 / 36 / 48 / 54 Mbit/s	101 / 100 / 98 / 96 93 / 89 / 85 / 84

For a multi-standard receiver embedding analog signal conditioning (see Fig. 1.c), k is set by the Variable Gain Amplifier (VGA) gain step (e. g., 6 dB, [11]). Equation (2) assumes all interferers and blockers have been totally filtered out before the ADC. This corresponds to the case of complete analog channel selection.

Table II presents the receiver signal conditioning path maximum gain requirement for all the envisaged standards calculated based on equation (2) for a 1 V FS ADC and for a receiver matched to 100Ω with $k = 0.9$; the NF_{RX} of the receiver was assumed to be 3 dB. For direct sequence spread spectrum systems (e. g., WLAN 802.11b) the gain requirement is smaller, as in practice other signals will be present as well inside the received bandwidth.

Nonetheless, we can conclude, based on Table II data, that the low sensitivity levels of the targeted wireless standards require a large maximum gain for the multi-standard receiver.

III. BLOCKERS AND INTERFERERS IMPACT ON THE MULTI-STANDARD RECEIVER CHARACTERISTICS

Besides the useful signal, other interferers and blockers can be present at the antenna input. The list comprising all interferers and blockers under which influence the receiver must still be able to properly demodulate the wanted signal represents the receiver blocker diagram. For each wireless standard such a receiver blocker diagram is specified.

Based on the targeted standards blockers diagrams analysis it results there are two major issues due to blockers and interferers:

- the receiver output clipping, due to the large receiver gain requirements and to the large difference between the useful signal and the blocker levels (i. e., typically $> +40$ dBc);
- intermodulation distortions that fall in-band, due to the receiver not perfectly linear transfer characteristic.

The receiver output clipping can be handled by making the LNA and VGA blocks gain variable. Through

On the other hand intermodulation distortions are unwanted products that potentially fall in-band and cannot be disseminated from the useful signal. Thus the wanted signal demodulation is affected due to the SNDR degradation. Further on the analysis presented in this Section focuses on

finding the values for the Figures of Merit (FOMs) used in evaluating the radio receiver linearity performance: the $IIP2$ and $IIP3$.

A. Finding the SDR $IIP2$

While receiving the RF input power may change significantly because of the reception of unwanted blockers/interferers. Due to the receiver even order distortions, the received signal DC offset component will change. This *dynamic offset* effect upsets the received signal demodulation, especially if the envisaged modulation concentrates a large part of the symbol spectral power at low frequencies. This is the case for older standards like GSM, as the latest wireless standards use modulation schemes that do not carry information at low frequencies.

The figure of merit quantizing the analog front-end second order distortions is the second order intercept point, $IIP2$. The SDRR input referred $IIP2$, $IIP2_{RX}$, is given by, [12]:

$$iIIP2_{RX} = 2 \times P_{blocker} - P_{in} + SNR_0, \quad (3)$$

where $P_{blocker}$ is the blocker level and P_{in} is the wanted signal level.

Based on the targeted standards analysis, it results the worst case scenario is met for the GSM standard that requires $IIP2_{RX} = +46$ dBm, [2].

B. Finding the SDR $IIP3$

For most wireless receivers, given the fully differential circuit implementation, the dominant non-linear contribution comes from the third order coefficient of power series expansion of their transfer characteristic. The maximum in-band level of the third-order intermodulation product, P_{IM3} , must be smaller than the useful RF signal level with SNR_0 :

$$P_{IM3} \leq P_{in} - SNR_0 \quad (4)$$

In practice, a supplementary head room to SNR_0 should be considered, since the overall receiver SNR is degraded by multiple factors, not only by the down-converted spurs.

Given (4), the receiver $IIP3$, $IIP3_{RX}$, must meet the condition specified by the equation:

$$IIP3_{RX} \geq P_{interferer} + \frac{P_{interferer} - P_{IM3}}{2} \quad (5)$$

where $P_{interferer}$ is the power per interferer of two interferers that cause the in-band third order distortion.

A special case is represented by OFDM Signals. An OFDM signal comprises frequency orthogonal sub-carriers, [9]. Receiver non-linearity leads to formation of bogus signals in-band due to sub-carrier intermodulation. The figure of merit in evaluating the third order intermodulation products thus formed is the Composite Triple Beat (CTB).

As is pointed out in [13] the worst case for the CTB products level is found in the centre band of the OFDM signal spectrum:

TABLE III. MULTI-STANDARD RECEIVER IIP3 REQUIREMENTS

Standard	Intermodulation conditions	RX IIP3[dBm]	
		Eq.	Value
GSM	$P_{\text{interferer}} @ -49 \text{ dBm}, P_{\text{in}} @ -99 \text{ dBm}$	(5)	-19
UMTS	$P_{\text{interferer}} @ -46 \text{ dBm}, P_{\text{in}} @ -114 \text{ dBm}$	(5)	-21
Bluetooth	$P_{\text{interferer}} @ -39 \text{ dBm}, P_{\text{in}} @ -64 \text{ dBm}$	(5)	-18.5
DECT	$P_{\text{interferer}} @ -47 \text{ dBm}, P_{\text{in}} @ -80 \text{ dBm}$	(5)	-24
WLAN IEEE 802.11b,g (DSSS)	$P_{\text{interferer}} @ -35 \text{ dBm}, P_{\text{in}} @ -70 \text{ dBm}$ CCK - 11 Mbit/s	(5)	-12
W-LAN IEEE 802.11g (OFDM @ 2.4 GHz)	Interferer intermodulation: $P_{\text{interferer}} @ \text{Sensitivity},$ $P_{\text{in}} @ +32 \dots +15 \text{ dBc} (6 \dots 54 \text{ Mbit/s})$	(5)	-32
	Blocker intermodulation: $P_{\text{blocker}} @ -10 \text{ dBm}, P_{\text{in}} @ -42 \text{ dBm},$ BPSK - 6 Mbit/s	(5)	+8.5
	Sub-carrier intermodulation: $P_{\text{in}} @ -20 \text{ dBm}, N = 52 \text{ carriers},$ 64QAM - 54 Mbit/s	(9)	+10
W-LAN IEEE 802.11a (OFDM @ 5 GHz)	Sub-carrier intermodulation: $P_{\text{in}} @ -30 \text{ dBm}, N = 52 \text{ carriers},$ 64QAM - 54 Mbit/s	(9)	+5

$$CTB[\text{dB}] \leq -2(IIP3_{\text{RX}} - P_{\text{in}}) + 1.74, \quad (7)$$

where P_{in} is the OFDM signal power in all the carriers.

Hence, in order for the digital back-end to be able to still demodulate properly the wanted signal, the CTB level must be smaller than the useful RF signal level per carrier with SNR_0 :

$$CTB \leq P_{\text{in}} - 10 \log N - SNR_0, \quad (8)$$

where N represents the number of OFDM sub-carriers.

In (8) SNR_0 represents the corresponding SNR headroom of the OFDM sub-carrier modulation.

Given (7) and (8), it results that in order to avoid destructive inter-carrier intermodulation, the $IIP3_{\text{RX}}$ must meet the following condition:

$$IIP3_{\text{RX}} \geq \frac{1}{2}(P_{\text{in}} + 10 \log N + SNR_0 + 1.74) \quad (9)$$

Each wireless standard specifies a set of particular intermodulation conditions. Table III summarises the power per interferer of two interferers that cause the in-band distortion and the input signal power. By analysing all the targeted standards, the receiver $IIP3$ specifications were derived using (5) or (9) and noted in Table III. The large variations in the $IIP3$ requirements are a reflection of the extreme reception conditions specific to the wireless environment. In [12] it is shown a versatile receiver is able

to mitigate all presented scenarios, by adjusted dynamically its linearity and noise performance with the received power.

IV. CONCLUSIONS AND FUTURE WORK

This paper conducted an analysis for finding the main requirements for a SDRR targeting compatibility with the major commercial wireless standards (see Table I).

Thanks to the standard independent systematic approach the presented analysis found the values for the key SDRR electrical specifications (i. e., NF_{RX} , $IIP2_{\text{RX}}$ and $IIP3_{\text{RX}}$) that ensure its compatibility with the envisaged standards.

Of course, a true SDRR has to be versatile and robust, such as it can adjust dynamically its performance (e. g., NF_{RX} , $IIP3_{\text{RX}}$) depending on the communication burst particularities. Nonetheless if a SDRR targets compatibility with the standards from Table I, it must meet the electrical specifications determined in this analysis.

So, the presented analysis constitutes the starting point in building the SDRR. Further on, the SDRR electrical specifications must be partitioned over its building blocks. The optimal specification partitioning must account the limitations due to the physical implementation (i. e., CMOS process) for each of the SDRR building blocks.

ACKNOWLEDGMENT

The authors would like to express their acknowledgment to Dr. F. Op't Eynde for the fruitful discussions on the topic.

REFERENCES

- [1] J Mitola, "Software radios - survey, critical evaluation and future directions," IEEE Nat. Telesystems Conf., 1992, pp. 13/15 - 13/23.
- [2] S. Spiridon, Monolithic Wide-band Multi-Standard Re-Configurable Transceiver Architectures, PhD Thesis Progress Report, "POLITEHNICA" University of Bucharest, December 2005.
- [3] T. H. Lee, *The Design of CMOS Radio-Frequency Integrated Circuits*, Cambridge University Press, 2nd Ed., 2004, pp. 710-713.
- [4] "ETS 300 577, GSM: Digital Cellular Telecommunications System (Phase 2); Radio Transmission and Reception," European Telecommunication Standard Institute (ETSI), 1997.
- [5] "3GPP, Technical Specification 25.101, v.6.10.0," Third Generation Partnership Project, Dec. 2005.
- [6] "IEEE Std 802.15.1™-2005," IEEE Computer Society, 2005
- [7] "ETS 300 175, DECT: Digital Enhanced Cordless Telecommunications," European Telecommunication Standard Institute (ETSI), 1995.
- [8] "IEEE Std 802.11g-2003," IEEE Computer Society, 2003.
- [9] A. Tarniceriu, B. Iordache, and S. Spiridon, "An Analysis on Digital Modulation Techniques for Software Defined Radio Applications," Proc. of the Annual Intl. Semiconductor Conf. CAS 2007, October 2007, vol. 2, pp. 451-454.
- [10] A. J. Viterbi, *CDMA: Principles of Spread Spectrum Communication*, Addison-Wesley, 1995.
- [11] S. Spiridon and F. Op't Eynde, "Low power CMOS fully differential variable-gain amplifier," in Proc. of the Annual Intl. Semiconductor Conf. CAS 2005, October 2005, vol. 2, pp 383-386.
- [12] F. Op't Eynde, "Direct-Conversion Radio Transceivers," RF IC Design Course Slides, EPFL, Switzerland, October 2005.
- [13] The Relationship Of Intercept Points Composite Distortions And Noise Power Ratios, <http://www.matrixtest.com/literat/mtn109.pdf>, Matrix Technical Notes, October 2005

Cyclostationarity Detection of DVB-T Signal: Testbed and Measurement

Matthieu Gautier¹, Marc Laugeois¹ and Philippe Hostiou²

¹CEA, LETI, Minatec, Grenoble, France,

²TeamCast, Centre Espace Performance, F35769 Saint-Grégoire, France,
matthieu.gautier1@cea.fr, marc.laugeois@cea.fr, philippe.hostiou@teamcast.com

Abstract—In this paper, realistic performance of Digital Video Broadcasting - Terrestrial (DVB-T) spectrum sensing are investigated for cognitive radio applications. To this end, an implementation of a cyclostationarity detector is proposed as an efficient means for signal detection under low Signal to Noise Ratio (SNR) conditions. This paper focuses on the design of a hardware testbed that performs the cyclostationarity detection, and introduces a measurement campaign that has been performed in order to have a realistic validation of the proposed solution. Measurement results show that SNR down to -6 dB could be detected by our hardware demonstrator.

Keywords—TV White Spaces, Cyclostationarity detection, FPGA, Measurement.

I. INTRODUCTION

The performance of sensing algorithms is fundamental in establishing the opportunistic communication of a cognitive radio (CR) system [1]. Many scenarios have been investigated in the context of CR network. The most likely to occur in the short term is the unlicensed usage of TV bands often referred to as the TV White Space (TVWS) scenario. This scenario was made possible by the FCC in the US in 2008, with some restrictions which include high-sensitivity requirements for primary user detection [2]. In the context of this scenario, standardization has been very active, especially under the IEEE802.22 banner [3].

In Europe, the TV bands primary user is the DVB-T transmitters and cyclostationarity detector has been proposed as the most promising technique for DVB-T signal sensing. By using cyclostationary features induced by the Cyclic Prefix (CP), it allows OFDM (Orthogonal Frequency Division Multiplexing) based signals detection at low SNR.

If the theoretical aspect of this detector has been thoroughly addressed in literature [4][5][6], solutions need to be proposed for its hardware implementation in order to achieve a good architecture-performance tradeoff. Indeed, in an operational system, the sensing block has to be implemented on a real hardware platform. Then, all theoretical functions have to be expressed as logical blocks and an explicit dimensioning of all links between blocks and data format must be carefully performed. In [7], an efficient implementation of a cyclostationarity detector was proposed by our team. The *a priori* knowledge of the DVB-T signal nature helps avoid the implementation of a large FFT operator as used in the state of the art architectures [8][9].

This paper focuses on the design of a testbed that performs the hardware architecture introduced in [7] that performs the detection of DVB-T signals for the TVWS scenario. Some spectrum sensing testbeds have already been developed: most of them concern the energy detection [10][11] or collaborative sensing [10][12] and those that deal with cyclostationarity detection are high level demonstration [13] or dedicated to other bands (802.11n [14] and 802.11g [15]), not dedicated to the TVWS scenario.

The other objective of this paper is to achieve realistic performance of the cyclostationarity detector using the proposed testbed. To this end, a measurement campaign has been performed with the platform and results from these measurements are given in this paper.

This paper consists of 5 parts. Following this introduction, Section II introduces the cyclostationarity detector and its hardware implementation dedicated to DVB-T signals. In Section III, the platform used for the demonstration is described. Section IV details the experimental validation of the detector by giving some measurement results. Finally, conclusions are drawn and outlook is provided.

II. CYCLOSTATIONARITY DETECTOR FOR DVB-T SIGNALS

This section derives the theoretical equation used by cyclostationarity detector and introduced the hardware architecture (presented in [7]) suitable to DVB-T signals.

A. Cyclostationarity based OFDM detector

For the DVB-T signal sensing, the proposed technique is based on the *a priori* knowledge of the OFDM modulation based DVB-T physical layer. The algorithm, described in [6] aims at detecting the cyclostationarity of the DVB-T signal through the analysis of the Fourier decomposition of its second order momentum. It exploits the structure of the OFDM symbols which contains the same pattern at its beginning and end; the so called cyclic prefix. By computing the autocorrelation of the incoming signal with a lag corresponding to the symbol duration, the cyclic prefix is emphasized while the rest of the correlation tends to zero. This is due to the fact that the data portion of the OFDM symbols is uncorrelated over consecutive symbols. Thus, the mathematical expectation of the correlation signal is time periodic, also referred to as the cyclostationary nature of the OFDM signal $s[n]$.

Let us now consider the autocorrelation of this signal:

$$R_s(u, m) = E \{ s[u + m]s^*[u] \}. \quad (1)$$

Under the condition that all subcarriers are used, the autocorrelation of an OFDM signal is written as [6]:

$$R_s(u, m) = R_s(u, 0) + R_s(u, N)\delta(m - N) \dots \\ \dots + R_s(u, -N)\delta(m + N), \quad (2)$$

with N being the number of subcarriers and δ being the Dirac function.

The first term of (2) is the power of the received signal. Energy detectors, derived only from this term, provide poor performance at low SNR. To increase the performance of the detector at low SNR, we focus on the last two terms of (2) to build a cost function. The terms $R_s(u, N)$ and $R_s(u, -N)$ correspond to the correlation induced by the cycle prefix. It can be shown [16] that $R_s(u, N)$ is a periodic function of u which characterizes the signal s . $R_s(u, N)$ has a period $\alpha_0^{-1} = N + D$ with D being the length of the cyclic prefix. As this function depends on u in a periodic way, the signal is not a stationary but a cyclostationary signal. Its autocorrelation function can be written as a Fourier series:

$$R_s(u, N) = R_s^0 + \sum_{k=-\frac{N+D}{2}, k \neq 0}^{\frac{N+D}{2}-1} R_s^{k\alpha_0}(N) e^{2i\pi k\alpha_0 u}. \quad (3)$$

In (3), $R_s^{k\alpha_0}$ is the cycle correlation coefficient at cycle frequency $k\alpha_0$ and at time lag N . This term can be estimated as follows:

$$R_s^{k\alpha_0}(N) = \frac{1}{U} \sum_{u=0}^{u-1} s(u + N)s^*(u) e^{-2i\pi k\alpha_0 u}, \quad (4)$$

where U is the observation time.

The basic idea behind the cyclostationarity detector is to analyze this Fourier decomposition and assess the presence of the signal by setting a cost function related to one or more of these cyclic frequencies. This cost function is compared to some reference value. This technique was introduced in a more general context in the early 90s by Gardner [17][16]. Recent papers have applied this approach to the opportunistic radio context [4][5][6]. They mainly differ in the way the harmonics are considered. In our study, the proposed cost function exploits both the fundamental and several harmonics as expressed in (5):

$$J_s(K_s) = \frac{1}{2K_s + 1} \sum_{k=-K_s}^{K_s} |R_s^{k\alpha_0}(N)|^2, \quad (5)$$

where K_s is the number of harmonics that are considered.

It can be observed that the cost function is only built upon $R_s(u, N)$, while $R_s(u, -N)$ is omitted. Indeed, it is quite easy to prove that $|R_s^{k\alpha_0}(N)|^2 = |R_s^{k\alpha_0}(-N)|^2$ [6].

Introduced in [7], the hardware integration of this algorithm is presented in the following chapter.

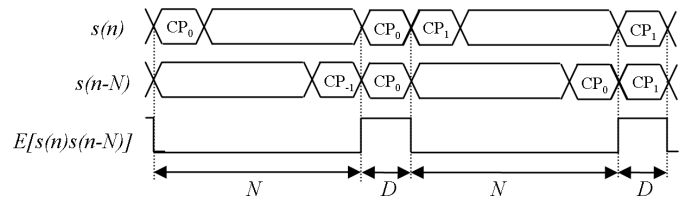


Figure 1. Ideal autocorrelation signal of an OFDM symbol burst.

B. Hardware architecture for DVB-T detector

The DVB-T standard defines three FFT sizes: $N=2048$, 4096 or 8192 for a channel bandwidth B_s of 8MHz. The cyclic prefix over FFT size ratio D/N can also vary: 1/32, 1/16, 1/8, 1/4. Considering all the configurations leads to very highly complex hardware architecture. However, in practice, deployment considers a smaller set of parameters depending on the country. For instance, in France, the set of parameters used is $N=8192$ and $D/N=1/32$, only this set will be used to design our architecture.

A key characteristic that will be exploited in the architecture design stems from the broadcast nature of the DVB-T signal. This means that detector sensitivity can be increased significantly by very long integration time. This is a relevant feature since sensitivity requirements for primary user detection are very challenging (typically SNR=-10dB [18]). It also changes the way that the reference signal is used to define the decision variable. When undertaking this calibration phase, the secondary system needs to consider a reference noise value which is independent of the signal presence.

When considering long (ideally infinite) integration time, the autocorrelation function defined in previous section tends to a rectangular signal as depicted in Fig. 1, the cyclic ratio being $\frac{D}{N+D}$. In this case, the Fourier coefficient is written as:

$$R_s^{k\alpha_0}(N) = \frac{A}{2\pi k} \left\{ \sin\left(\frac{2\pi k D}{N+D}\right) + j \left(1 - \cos\left(\frac{2\pi k D}{N+D}\right)\right) \right\}, \quad (6)$$

Each coefficient power is given by:

$$|R_s^{k\alpha_0}(N)|^2 = \begin{cases} \left(\frac{AD}{N+D}\right)^2, & k = 0, \\ 2 \left(\frac{A}{2\pi k}\right)^2 \left(1 - \cos\left(\frac{2\pi k D}{N+D}\right)\right), & k \neq 0. \end{cases} \quad (7)$$

Decision variable computation:

First, a reference noise level has to be computed from the observation in order to be compared with the signal cost function $J_s(K_s)$. It is obvious from equation (7) that $R_s^{k\alpha_0}(N) = 0$ when $k = l \left(\frac{N}{D} + 1\right)$, $l = \{1, 2, \dots + \infty\}$. The Fourier harmonics $l \left(\frac{N}{D} + 1\right)$ are not impacted by the presence of the signal and can thus be used for calibration purpose to define the reference noise level. Similarly to (5), a cost function J_n could be defined in order to compute the noise level:

$$J_n(K_n) = \frac{1}{2K_n} \sum_{l=-K_n, l \neq 0}^{K_n} \left| R_s^{l \left(\frac{N}{D} + 1\right) \alpha_0}(N) \right|^2, \quad (8)$$

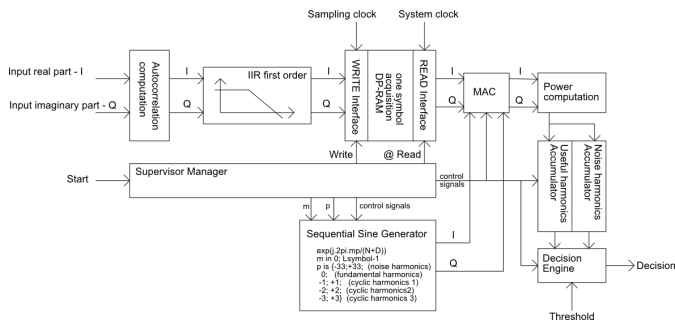


Figure 2. Cyclostationarity detector for DVB-T signals.

with K_n being the number of harmonics that are considered. For example, considering the French set of parameters ($D/N=1/32$) and considering the first 4 signal harmonics $-3;+3$ and one noise harmonic (i.e., $K_s=3$ and $K_n=1$), the decision variable V can be expressed as follows:

$$V = \frac{J_s(K_s)}{J_n(K_n)} = \frac{2}{7} \frac{\sum_{k=-3}^3 |R_s^{k\alpha_0}(N)|^2}{|R_s^{-33\alpha_0}(N)|^2 + |R_s^{33\alpha_0}(N)|^2}. \quad (9)$$

Hardware architecture:

Introduced in [7], the proposed cyclostationarity detector hardware architecture is shown in Fig. 2 for the parameters $K_s = 3$ and $K_n = 1$.

First, the autocorrelation is computed on the I/Q complex samples. The IIR (Infinite Impulse Response) integrator then averages over a number of symbols tuned by setting the integration time parameter to achieve the required sensitivity. The supervisor, a Finite State Machine (FSM), then triggers the writing into a buffer that stores 8192 filter output samples (equivalent to the length of an OFDM symbol). Then, using a faster clock, the Fourier harmonics are computed sequentially. The sine generator computes sequentially the required sine function of the Fourier taps of interest. The Multiply ACCumulate (MAC) function enables the Fourier coefficient to be obtained for these taps. The sequence is as follows. First the reference harmonics $-33; +33$ are generated to compute the noise reference power. Then the harmonics of interest for the DVB-T signal $0;-1;+1;-2;+2;-3;+3$ are calculated. The power of each harmonic is summed up to obtain the cyclostationarity estimator value. Finally the decision engine gives the final result by comparing the estimated value to the decision value according to (9), which provides a hard decision output of the detector.

This technique holds theoretically for infinite integration time to guarantee the rectangular shape of the autocorrelation estimator. Whenever a finite integration is performed, detection performance is improved by increasing the integration ability

	Complexity			Latency
	Slices	RAM blocks of 18kbits	Mult	
Detector	1600	122	23	Depends on n
Total	25280	232	128	

TABLE I. COMPLEXITY EVALUATION OF THE DVB-T DETECTOR.



Figure 3. Platform overview.

of the filter. The integration ability of the filter depends on the length of the filter denoted n .

The complexity of such a detector hardware implementation is determined on a Xilinx Virtex 4 target technology using the ISE XST synthesis tool. Results are provided in Table I. The complexity is compared with the total resource available in the FPGA. Table I shows that 6% of the slices, 52% of the RAM blocks and 17% of the multipliers have been used to perform the detection. If the final implementation will integrate this detector and a PHY layer for the opportunistic communication, this complexity seems quite high (especially the memory blocks) and a new version of Xilinx FPGA should be used for the final implementation.

III. TESTBEDS DESCRIPTION AND SPECIFICATIONS

A. Overview of the demonstrator

Fig. 3 shows the testbed used to validate the detection of DVB-T signal. The testbed consists of two parts:

- The modulator is a standard TeamCast DVB-T products [19]. A video stream is pulse shaped and transposed in the TV channel according to the DVB-T standard. It emulates a base station broadcast of the DVB-T network.
- The receiver performs two functions: the "sensing block" and the "DVB-T demodulator". It then provides a video stream and the decision variable provided by the detector.

A PC controls and supervises the testbeds using RS232 links. Three software Human-Machine interfaces have been developed, one to control the setting of the DVB-T modulator, one for the DVB-T demodulator and one that controls the detector characteristics and supervises the measurements.

A measurement consists in scanning a 8MHz UHF channel and then in detecting if this channel is vacant. The detection is based on the decision variable as defined by (9).

B. Hardware specification of the receiver

Fig. 4 provides an overview of the architecture of the receiver used to test the proposed architecture. The receiver is composed of two parts: a RF board that performs the translation of the RF UHF signal to IQ baseband signal and a digital board that executes the baseband algorithms.

The RF board is composed of an analog part and a digital part. The analog Downconverter block allows the transposition of the UHF band (470 - 860MHz) to an Intermediate Frequency (IF) of 240MHz. An Analog to Digital Converter (ADC) then converts the signal into samples. The sampling frequency is 73.4 Mhz corresponding to 8 times the symbol

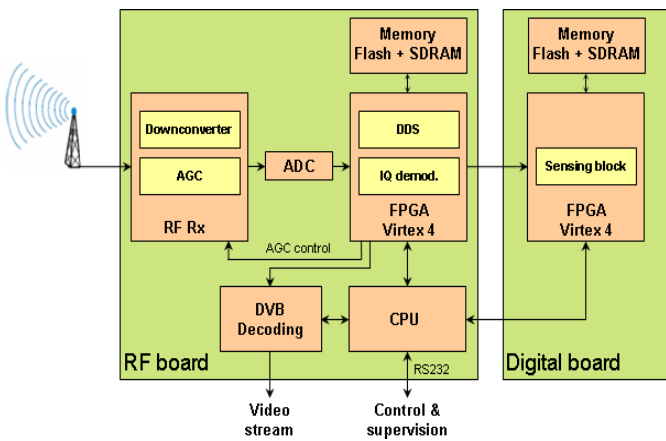


Figure 4. Receiver architecture.

frequency F_s . To ensure a constant level at the input of the ADC, two automatic gain control (AGC) loops are implemented, one at RF and one at IF.

The digital IF signal is then processed by an FPGA that performs the baseband transposition. The different elements are: a bandpass filter that attenuates the adjacent channels, an I/Q demodulation, a Direct Digital Synthesizer (DDS) that performs the baseband translation and finally decimators to switch from $8F_s$ to F_s .

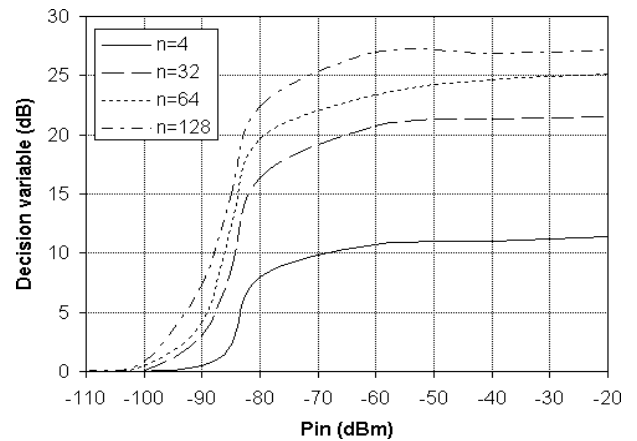
The IF and RF AGC guarantee the level of the digital signal into the range between -75 dBm and -35 dBm. The power is computed using the outputs of the ADC. The gain of the AGC is linear within this range, thus ensuring no distortion of the input signal. The RF board also contains a specific chip that performs the DVB-T decoding.

This I/Q stream is then transmitted to the Digital board via a high-speed serial link. The I/Q samples are received at the frequency F_s of 64/7 MHz. The digital board is composed of an FPGA Xilinx Virtex-4 FX60 and memories (both SDRAM and flash). The hardware architecture of the detector detailed in Section II is implemented on this board.

An important remark is that the IF AGC has not been integrated in the platform reducing the range of the input signal. Under this condition, the thermal noise of the receiver P_{Th} has been measured at -80 dBm.

IV. EXPERIMENTAL MEASUREMENTS

In this section, realistic performance results of the proposed detector are given from a measurement campaign. In this campaign, the channel is considered to be an AWGN (Additive White Gaussian Noise) one as Line of Sight conditions are performed. In our scenario, the primary system is the French DVB-T (i.e., FFT size of 8192 and a cyclic prefix of 1/32). First, the false alarm are induced by the thermal noise and, then, by a secondary system that already communicates in the channel.

Figure 5. Mean of decision variable versus P_{in} for different filter length n .

A. Decision variable distribution

First, we observed the distribution of the decision variable V according to (9) as a function of the receiver input power P_{in} . In practice, the power of noise harmonic comes from two sources: the thermal noise P_{Th} , which is constant, and the autocorrelation noise which is proportional to the input power $P_A = k_A P_{in}$. The power of useful harmonics is also proportional to the input power. Assuming that, in the useful harmonics, the power of the thermal noise is negligible relative to the power of the signal, the decision variable V can be written:

$$V = \frac{kP_{in}}{P_{Th} + k_A P_{in}} = \frac{k}{\frac{1}{SNR} + k_A}, \quad (10)$$

with k and k_A constant, $SNR = P_{in}/P_{Th}$ and $kP_{in} \gg P_{Th}$.

Fig. 5 shows the mean of decision variable V versus P_{in} for different filter length $n=4, 32, 64$ and 128 .

According to the curves of Fig. 5, three ranges of receiver input power can be distinguished:

- Range 1: When the input received power is lower than -100 dBm, (10) is no longer valid, and the noise becomes dominant compared to the signal. The harmonics are only noise harmonics and $V=0$ dB.
- Range 2: P_{in} for between -100 dBm and -80 dBm, the curve is approximately linear, and V is proportional to P_{in} .
- Range 3: For powers higher than -70 dBm, V is constant and only depends on n .

Finally, we note the influence of the filter length n . The larger n is, the higher the decision variable is. For high input powers (range 3), V is 11 dB for $n=4$ and 27 dB for $n=128$.

B. Detection probability

The detection probability p_D is the probability that the system detects the DVB-T signal when it is present in the channel. These probabilities are obtained (leading to a false alarm probability of 10%) when the detector is matched with the transmitter (i.e., FFT size of 8192 and a cyclic prefix of 1/32). Measurements are performed for different received power levels of the primary signal ($-90 \text{ dBm} < P_{in} < -70 \text{ dBm}$).

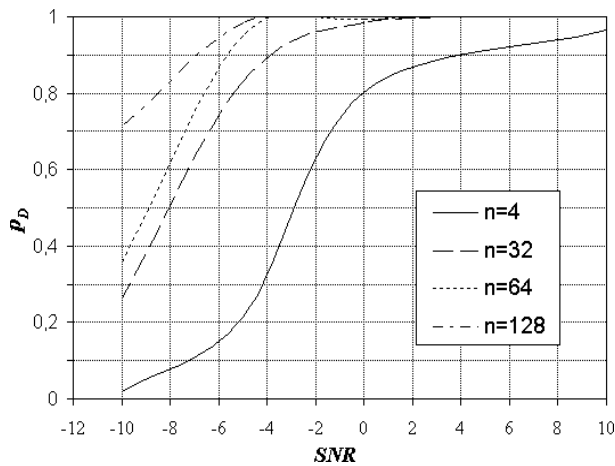
Figure 6. Detection probability versus SNR for different filter length n .

Fig. 6 shows the performance of the algorithm for different filter length $n = 4, 32, 64$ and 128 .

Thus, for the detection of a DVB-T signal (8k, 1/32) and a target of 95% of successful detection, the measurement results show that the detection of SNR down to 10 dB could be achieved with a filter length $n=4$, SNR down to -2 dB with $n=32$, SNR down to -5 dB with $n=32$ and SNR down to -6 dB with $n=128$.

C. False alarm: Another DVB-T signals

So far, the false alarms correspond to the case where the detector detects a signal while no signal is present at the receiver input. In this part, we analyse another kind of false alarms: when a secondary transmitter uses the same channel with a DVB-T signal having different characteristics than the primary transmitter DVB-T.

The detector is set on an FFT of 8192, a cyclic prefix of 1/32 and a filter size $n=64$. To test the influence of the size of the cyclic prefix, the false alarm probability is computed for a secondary transmitter using cyclic prefix of 1/16, 1/8 and 1/4 (with a given FFT size of 8192). To test the influence of the size of the FFT, the false alarm probability is computed for a secondary transmitter using FFT sizes of 4096 and 2048 (with a given cyclic prefix of 1/32).

The measurements are performed under high SNR conditions (input power P_{in} of -40 dBm). The detection probability p_D is plotted versus the false alarm probability p_{FA} for different sizes of cyclic prefix (Fig. 7) and for different sizes of FFT (Fig. 8).

The measurement results show that the size of the cyclic prefix has more influence on the number of false alarm than the length of the FFT. Thus, when the secondary transmitter uses an FFT of 8192 and a cyclic prefix different from the one of the detector, the detection probability is decreasing, the detection being impossible for $CP=1/16$. However, if the secondary transmitter uses an FFT size different than the one used by the detector, the number of false alarm is low and the detection is feasible.

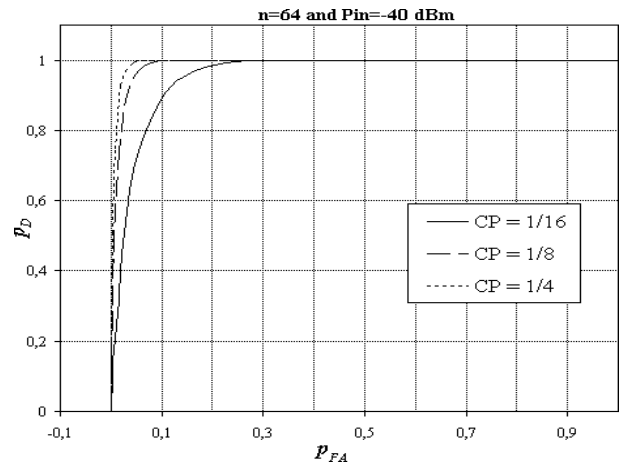


Figure 7. Detection probability versus false alarm probability for different sizes of cyclic prefix.

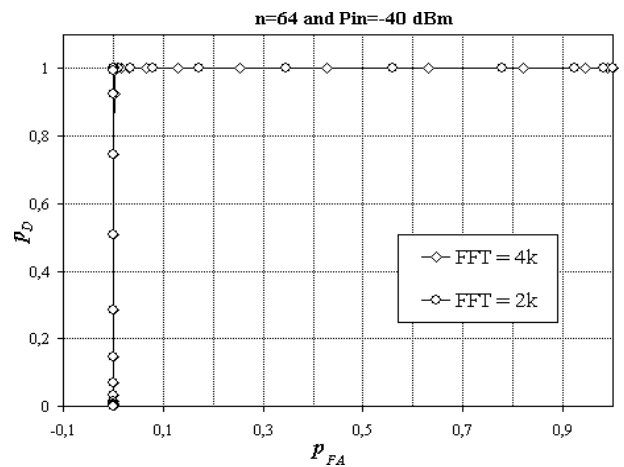


Figure 8. Detection probability versus false alarm probability for different sizes of FFT.

V. CONCLUSIONS AND FUTURE WORKS

Scenarios have a strong influence on architecture and its performance tradeoffs. In the secondary spectrum usage of licensed TV bands, interference is not allowed, and much attention must be paid to sensitivity. In this paper, DVB-T signal sensing has been addressed using the cyclostationarity detector. The motivation of this study is to achieve realistic performance of this detector for the TVWS scenario. This paper focuses on the design of a hardware testbed that performs the cyclostationarity detection and introduces a measurement campaign.

The receiver could not reach very low sensitivity because only one AGC has been implemented. However, this limitation is not prohibitive in the use of the algorithm. We have shown that, with a thermal noise of -80 dBm, the architecture could achieve the detection of SNR down to -6 dB.

The influence of the filter length has been highlighted with a 16 dB sensitivity gain between $n=4$ and $n=128$. Finally, the false alarm and detection performance will help the setting of the detection threshold according to the desired strategy of detection.

Future work is to update the RF board of the receiver with the integration of the IF AGC and to perform measurements with realistic broadcast channel conditions [20] with both multipaths and frequency dispersive characteristics.

ACKNOWLEDGMENT

The research leading to these results was derived from the French national project ANR-INFOP.

REFERENCES

- [1] J. Mitola III and G. Q. Maguire Jr, "Cognitive radio: making software radios more personal," *IEEE Personal Communications*, vol. 6, no. 4, pp. 13–18, 1999.
- [2] Official announcement of FCC, "FCC adopts rules for unlicensed use of television white spaces," available from <http://www.fcc.gov>, 15.03.2011, November 2008.
- [3] IEEE 802.22, "Wireless Regional Area Networks ("WRANs")," available from <http://www.ieee802.org/22/>, 15.03.2011.
- [4] M. Ghozzi, M. Dohler, F. Marx, and J. Palicot, "Cognitive Radio: Methods for Detection of Free Bands," *Elsevier Science Journal, Special Issue on Cognitive Radio*, vol. 7, Sept 2006.
- [5] J. Lunden, V. Koivunen, A. Huttunen, and H. Vincent Poor, "Spectrum Sensing in Cognitive Radios Based on Multiple Cyclic Frequencies," <http://arxiv.org/abs/0707.0909>, 15.03.2011, July 2007.
- [6] P. Jallon, "An algorithm for detection of DVB-T signals based on their second order statistics," *EURASIP journal on wireless communications and network*, 2008.
- [7] Dominique Noguét, Lionel Biard, and Marc Laugeois, "Cyclostationarity Detectors for Cognitive Radio: Architectural Tradeoffs," *EURASIP Journal on Wireless Communications and Networking*, 2020.
- [8] V. Turunen, M. Kosunen, A. Huttunen, S. Kallioinen, P. Ikonen, A. Pärssinen, and J. Ryyänen, "Implementation of cyclostationary feature detector for cognitive radios," *IEEE International Conference on Cognitive Radio Oriented Wireless Networks and Communications (CROWNCOM09)*, June 2009.
- [9] Y. Tachwali, M. Chmeiseh, F. Basma, and H. H. Refai, "A frequency agile implementation for IEEE 802.22 using software defined radio platform," *IEEE Globecom 2008*, December 2008.
- [10] D. Cabric, A. Tkachenko, and R. W. Brodersen, "Experimental study of spectrum sensing based on energy detection and network cooperation," *ACM 1st Int. Workshop on Technology and Policy for Accessing Spectrum (TAPAS06)*, August 2006.
- [11] J.Y. Xu and F. Alam, "Adaptive energy detection for cognitive radio: An experimental study," *IEEE International Conference on Computers and Information Technology (ICCIT09)*, December 2009.
- [12] S.M. Mishra, D. Cabric, C. Chang, D. Willkomm, B. Van Schewick, S. Wolisz, and B.W. Brodersen, "A Real Time Cognitive Radio Testbed for Physical and Link Layer Experiments," *IEEE New Frontiers in Dynamic Spectrum Access Networks (DySPAN05)*, Nov. 2005.
- [13] M. Ghozzi, B. Zayen, and A. Hayar, "Experimental Study of Spectrum Sensing Based on Distribution Analysis," *18th ICT-MobileSummit Conference*, June 2000.
- [14] S. Kandeepan, G. Baldini, and R. Piesiewicz, "Experimentally detecting IEEE 802.11n Wi-Fi based on cyclostationarity features for ultra-wide band cognitive radios," *IEEE International Symposium on Personal, Indoor and Mobile Radio Communications (PIMRC09)*, Sept. 2009.
- [15] L. Biard, D. Noguét, T. Gernandt, P. Marques, and A. Gameiro, "A hardware demonstrator of a cognitive Radio system using temporal opportunities," *IEEE International Conference on Cognitive Radio Oriented Wireless Networks and Communications (CROWNCOM09)*, June 2009.
- [16] W. A. Gardner and M. Spooner, "Signal Interception: Performance Advantages of Cyclic-Feature Detectors," *IEEE Transactions on Communications*, vol. 40, no. 1, Jan 1992.
- [17] W. A. Gardner and G. Zivanovic, "Degrees of cyclostationary and their application to signal detection and estimation," *IEEE Signal Processing*, vol. 22, no. 3, March 1991.
- [18] S. J. Shellhammer, "Spectrum sensing in IEEE 802.22," *IAPR Workshop on Cognitive Information Processing*, June 2008.
- [19] TeamCast, "Description of DVB-T modulator," available from <http://www.teamcast.com/en/maj-e/c2a2i19508/>, 15.03.2011.
- [20] TeamCast, "Description of RF Channel Simulator," available from <http://www.teamcast.com/en/maj-e/c1a2i19493/>, 15.03.2011.

A Censored and Ordered Sequential Collaborative Spectrum Sensing Scheme based on Evidence Theory for CRAHN

Nhan Nguyen-Thanh
 School of Electrical Engineering
 University of Ulsan
 Ulsan, S. Korea
 Email: ntnhan.vaa@gmail.com

Insoo Koo
 School of Electrical Engineering
 University of Ulsan
 Ulsan, S. Korea
 Email: iskoo@ulsan.ac.kr

Abstract—This paper proposes a censored and ordered sequential collaborative spectrum sensing scheme for cognitive radio ad hoc network (CRAHN). The scheme uses the ordered of the sensing data reliability for enabling the Dempster Shafer theory of evidence sequential combination. A preceding censored process removes the nodes having insignificant sensing data to the broadcasting sensing result process. The advantage of ordered sequential and censored mechanism will help to reduce communication resources (the energy consumption, the coordination and overhead in control channel and the sensing result collecting time) while keeping the same sensing performance compared with the conventional centralized cooperative spectrum sensing.

Index Terms—cognitive radio, spectrum sensing, collaborative, sequential fusion, censoring, Dempster Shafer theory

I. INTRODUCTION

In recent years, Cognitive Radio (CR) which enables opportunistic access to underutilized licensed spectrum band has been considered as a promising technology. Spectrum sensing (SS) plays an essential role in CR. Among various spectrum sensing techniques, energy detection is an engaging method due to its easy implementation and admirable performance. However, its major disadvantage is that the receiver signal strength can be seriously weakened at a particular geographical location due to multi-path fading and shadow effect [1]. In order to overcome the hidden node problem in which a single sensing node cannot distinguish between an idle or a deep fade band, the collaborative SS scheme has been considered in many literatures (see [2]-[8] for examples).

By utilizing the diversity of distributed sensing data resources based on a fusion rule such as “And rule,” “Or rule,” “ k out of n ,” etc. [2][3], cooperative spectrum sensing (CSS) can simultaneously decrease both the miss detection and the false-alarm probability of a single sensing node. A data fusion scheme for CR network based on Dempster-Shafer theory of evidence (D-S theory) was first proposed in [4]. This scheme shows a significant improvement in the detection probability as well as considerable reduction in the false alarms probability without any requirement of prior primary system’s activity information. Nguyen Thanh and Koo [5] enhanced the D-S theory based fusion scheme in [4] to

obtain a very high gain of combination by utilizing available primary signal’s SNR. However, such above advantages of data fusion schemes are at the cost of overhead traffic of control signaling and sensing results transmission, which consumes more communication resources such as reporting time delay, control channel bandwidth and transmission energy. The requirement resources will be extremely large when the number of CR User (CU) increases. However, only a few works have considered this problem. Yeelin and Su [6] proposes a sequential test for CSS to control the average number of the reporting bits and reduce the mean detection time and bandwidth. In [7], a data fusion scheme which utilizes a D-S theory based ordered sequential test for higher efficiency (i.e., lower reporting resources requirement) and faster detection is proposed. However, all of these sequential fusion schemes not only do not take advantage of removing the low reliability data from reporting by a censoring method as proposed in [8] but also can be only applied for centralized CR networks which require a data fusion center to control the process of sequential test.

For the case of CR ad hoc network (CRAHN), due to the lack of central controller, each CU is responsible for determining its actions based on its local observation. Since the CU cannot predict the influence of its actions on the entire network only with its local observation, collaboration schemes, in which the observed information can be exchanged among devices are essential [9]. Therefore, it is necessary to consider an effective mechanism for sequential fusion in such the case.

In this paper, we propose a collaborative SS scheme for CRAHN based on censored and ordered sequential D-S theory combination. The censored and ordered collaborative mechanism enables the sensing data sequentially to be combined in a descending sequence of reliability. This will help to reduce the number of reporting data and the sensing time.

The rest of the paper is organized as follows. Section 2 describes the system model. Section 3 introduces the collaborative spectrum sensing based on D-S theory. Section 4 proposes the censored and ordered collaborative mechanism. Section 5 develops the censored and ordered sequential D-S

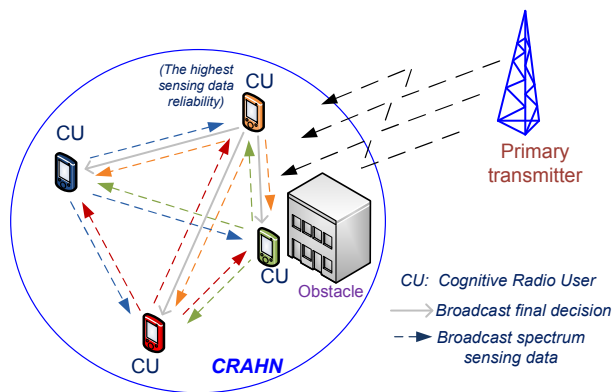


Fig. 1. System model

theory based collaborative SS scheme. Section 5 shows the simulation results. Finally, Section 6 concludes the paper.

II. SYSTEM DESCRIPTION

We consider a single-hop CRAHN with a dedicated common control channel (CCC) and multiple CUs sharing the same frequency band with a licensed system as shown in Fig. 1. In order to increase the reliability of the licensed user (LU) protection, the CUs, after sensing the spectrum band, exchange their SS information each other. Therefore, the collaborative SS model which does not require a central controller will be adopted into our CRAHN. As a result, the whole process of SS includes two phase: the individual SS phase and the collaborative phase. The individual SS for detecting the LUs signal is essentially a binary hypotheses testing problem as follows:

$$\begin{cases} H_0 : x(t) = n(t) \\ H_1 : x(t) = h(t) s(t) + n(t) \end{cases} \quad (1)$$

where H_0 and H_1 are the hypotheses of the absence and presence of the LU's signal, respectively, $x(t)$ represents the received data at the CU, $h(t)$ denotes the gain of the channel between LU and CU, $s(t)$ is the signal transmitted from the primary user and $n(t)$ is the additive white Gaussian noise. The spectrum sensing method is energy detection. The output of energy detector is the received signal power which is given by

$$x_E = \sum_{n=1}^N |x_n|^2 \quad (2)$$

where x_n is the n -th sample of the received signal and $N = 2TW$. T and W denote the detection time and signal bandwidth, respectively. When N is relatively large (e.g. $N > 200$), x_E can be well approximated as a Gaussian random variable under both hypotheses H_1 and H_0 , with mean μ_1 , μ_0 and variance σ_1^2 , σ_0^2 , respectively [10], such that

$$\begin{cases} \mu_0 = N & \sigma_0^2 = 2N \\ \mu_1 = N(\gamma + 1) & \sigma_1^2 = 2N(2\gamma + 1) \end{cases} \quad (3)$$

where γ is the SNR of the LU's signal at the CU.

III. THE D-S THEORY BASED COLLABORATIVE SPECTRUM SENSING

A. Basic probability assignment estimation

In order to apply D-S theory of evidence to the collaborative spectrum sensing scheme, the frame of discernment A is defined as $\{H_1, H_0, \Omega\}$, where Ω , called ignorance hypothesis, denotes either hypotheses is true. After sensing time, each CU will estimate its self-assessed decision credibility which is equivalent to Basic Probability Assignment (BPA) for these hypotheses. The BPA function is defined as a form of the cumulative density function similar to those in [5] as follows:

$$m_i(H_0) = \int_{x_{E_i}}^{+\infty} \frac{1}{\sqrt{2\pi}\sigma_{0i}} \exp\left(-\frac{(x - \mu_{0i})^2}{2\sigma_{0i}^2}\right) dx \quad (4)$$

$$m_i(H_1) = \int_{x_{E_i}}^{+\infty} \frac{1}{\sqrt{2\pi}\sigma_{1i}} \exp\left(-\frac{(x - \mu_{1i})^2}{2\sigma_{1i}^2}\right) dx \quad (5)$$

$$m_i(\Omega) = 1 - m_i(H_1) - m_i(H_0) \quad (6)$$

where $m_i(H_0)$, $m_i(H_1)$ and $m_i(\Omega)$ are the BPA of hypotheses H_0 , H_1 and Ω of the i -th CU, respectively. Using these functions, the BPA of hypotheses H_0 and H_1 are unique for each test statistics value x_{E_i} and vary in such a way that the larger x_{E_i} is the larger $m_i(H_1)$ and the smaller $m_i(H_0)$ are and vice versa. These values are broadcasted from various CUs and combined at each CUs to obtain a final decision.

B. D-S theory based combination

According to the D-S theory of evidence, the combination of the BPAs from n sources can be obtained via the following equations [11]:

$$m(H_0) = \sum_{A_1 \cap A_2 \cap \dots \cap A_n = H_0} \prod_{i=1}^n m_i(A_i) / (1 - K) \quad (7)$$

$$m(H_1) = \sum_{A_1 \cap A_2 \cap \dots \cap A_n = H_1} \prod_{i=1}^n m_i(A_i) / (1 - K) \quad (8)$$

where

$$K = \sum_{A_1 \cap A_2 \cap \dots \cap A_n = \emptyset} \prod_{i=1}^n m_i(A_i)$$

and A_i can be one element of the set $\{H_1, H_0, \Omega\}$.

A simple decision strategy is chosen; and the global decision is made while considering the following numerical relationships:

$$\log\left(\frac{m(H_1)}{m(H_0)}\right) \underset{H_1}{\overset{H_0}{\leq}} 0 \quad (9)$$

where the ratio $\frac{m(H_1)}{m(H_0)}$ is considered as the global combination ratio.

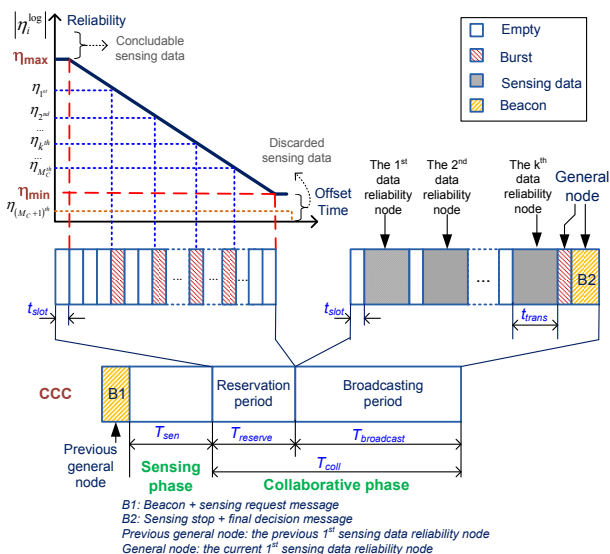


Fig. 2. The censored and ordered collaborative mechanism

IV. THE CENSORED AND ORDERED COLLABORATIVE MECHANISM

As mentioned above, the main problem of D-S theory based collaborative spectrum sensing as well as other schemes is the large communication resource requirement for reporting sensing results, particularly, in a large cognitive radio network. For this reason, in order to reduce the overhead, the total processing time and the energy consumption for spectrum sensing, we propose an censored and ordered sensing data reliability broadcasting mechanism in which nodes with higher current sensing datas reliability will broadcast earlier and nodes with sensing datas reliability lower than a censored threshold will not report as shown in Fig. 2. The highest sensing data reliability node, which is free after first broadcasting its sensing data, becomes the general node and makes the final decision.

The proposed ordered collaborative mechanism includes the reservation period and the broadcasting period. In the first period, the CUs make a reservation by utilizing a short burst signal according to a reservation timeslot R_T . Since every CU can listen to the CCC, the broadcasting time slot position can be determined according to the reservation burst order.

In details, the reservation period $T_{reserve}$ is divided into κ reservation timeslots ($\kappa \geq M$, i.e., number of CUs). Each timeslot length t_{slot} is equal to a slot time, i.e., the time required by the radio layer for functioning carrier sensing.

After sensing the spectrum band, each CU estimates its data reliability and conducts a censored process. This means that the CU will take no action if the sensing data reliability is smaller than a minimum reliability threshold η_{min} . The selection of the minimum threshold has to guarantee that the discarded, i.e. lower reliability than η_{min} , sensing data have less significant in the contribution to final decision if it is used.

After the censored process, the CU whose sensing data reliability is larger than η_{min} will calculate the reservation

timeslot R_T according to the data reliability as follows:

$$R_T = \left\lfloor \frac{\eta_{max} - \eta_i^{\log}}{\eta_{max} - \eta_{min}} \kappa \right\rfloor \quad (10)$$

where $\lfloor \cdot \rfloor$ is a round-down operator and η_{max} is the maximum reliability threshold. The η_{max} is selected large enough such that a reliable final decision can immediately be concluded if the data reliability is a larger than that value.

In broadcasting period, CUs will transmit their sensing data at the corresponding reserved data timeslot if the first part of the data timeslot, equivalent to a slot time, is empty. In contrast, if the first part of the data timeslot is occupied by a burst signal, the nodes have to wait for the followed beacon message which includes the stop broadcasting request and final decision result from the general node.

V. THE CENSORED AND ORDERED SEQUENTIAL D-S THEORY BASED COLLABORATIVE SPECTRUM SENSING SCHEME

For broadcasting the sensing result in the sequence of the data reliability, the i -th CU will make its self-assessed credibility ratio which is defined by:

$$\eta_i^{\log} = \left| \log \frac{m_i(H_1)}{m_i(H_0)} \right|. \quad (11)$$

At the general node, the broadcasted BPA is immediately combined in the sequence as follows:

$$m_{combined}^k(H_j) = m_{combined}^{k-1}(H_j) \oplus m_k(H_j) \quad j = 0, 1 \quad (12)$$

where $k = 1, \dots, M_C$, $m_{combined}^{k-1}(H_j)$ and $m_{combined}^k(H_j)$ are the $(k-1)$ -th and (k) -th combined BPA of hypothesis H_j , respectively, M_C is the total number of CUs joined in the broadcasting process after censoring and \oplus is the combination operator defined based on DS-theory as follows:

$$m_a \oplus m_b(H_j) = \frac{m_a(H_j)m_b(\Omega) + m_a(H_j)m_b(H_j) + m_a(\Omega)m_b(H_j)}{1 - [m_a(H_j)m_b(H_{1-j}) + m_a(H_{1-j})m_b(H_j)]} \quad (13)$$

$$m_a \oplus m_b(\Omega) = 1 - m_a \oplus m_b(H_1) - m_a \oplus m_b(H_0), \quad (14)$$

where $j = 0, 1$, and a and b denote the two arbitrary combining sources.

Due to the commutative and associative properties of the D-S theory combination operator \oplus , the combined result of the sequential CSS scheme will be equal to that of the non-sequential one as in (7) and (8) when all nodes' sensing data are combined as the same time. Therefore, instead of using the 0 as a threshold for the final decision making as in (9), the general node adopts a couple thresholds $\pm \delta$ where $\delta > 0$ for comparing the combination ratio. The value of δ is selected large enough so that the cooperative gain is equivalently maintained though the number of combined sensing data is lower. The proposed sequential fusion scheme is based on the following final decision making strategy:

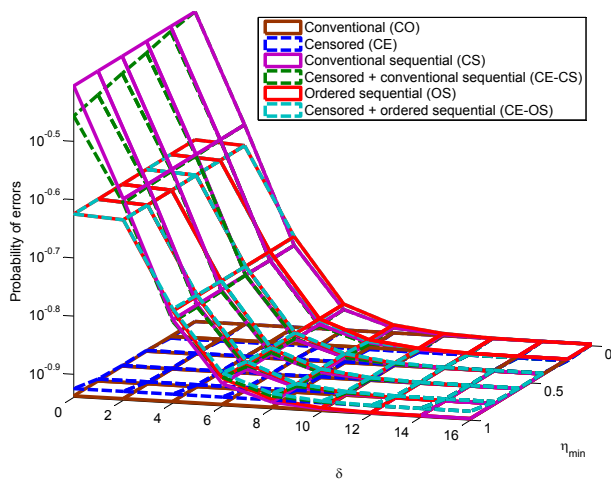


Fig. 3. The error probabilities of different fusion schemes vs. both the censoring threshold η_{min} and the sequential test's threshold δ under the LUs signal SNR = -15 dB at all 20 CUs.

- If $k < M_C$ then

$$D_{final} = \begin{cases} H_1 & \text{if } \eta_{combined}^k > \delta \\ \text{no decision} & \text{if } -\delta < \eta_{combined}^k < \delta \\ H_0 & \text{if } \eta_{combined}^k < -\delta \end{cases}$$

where D_{final} denotes the global decision, M is the total number of CUs in the network and $\eta_{combined}^k$ represents the global decision credibility ratio at the k -th report which is given by:

$$\eta_{combined}^k = \log \frac{m_{combined}^k(H_1)}{m_{combined}^k(H_0)}. \quad (15)$$

In the case that $-\delta < \eta_{combined}^k < \delta$ the general node will wait for the next data report.

- If $k = M_C$ then the truncated process is applied as follows:

$$D_{final} = \begin{cases} H_1 & \text{if } \eta_{combined}^k > 0 \\ H_0 & \text{if } \eta_{combined}^k < 0 \end{cases}.$$

VI. SIMULATION RESULTS

For simulation, we assume that the LU signal is DTV signal whose bandwidth is 6 MHz. 20 sensing nodes with the same LU signals SNR are in the network. The local sensing time is 50 μ s. Firstly, we consider the influence of the censoring threshold η_{min} and the sequential test's threshold δ on the collaborative SS performance, i.e. the global error probability as shown in Fig.3. In the figure, the *conventional* (CO), the *conventional sequential* (CS), the *censored* (CE), the *censored and conventional sequential* (CE-CS), the *ordered sequential* (OS) and the *censored and ordered sequential* (CE-OS) DS-theory based data fusion are simulated under the same LUs signal SNR as -15 dB at all 20 CUs. As shown in the figure, the error probabilities of all others fusion scheme are converged to that of CO DS-theory based one when the value threshold δ is adequate enough (i.e. $\delta \geq 8$). Furthermore, when the threshold δ is large the increasing of threshold η_{min} in the range [0, 1] softly reduces the sensing performance.

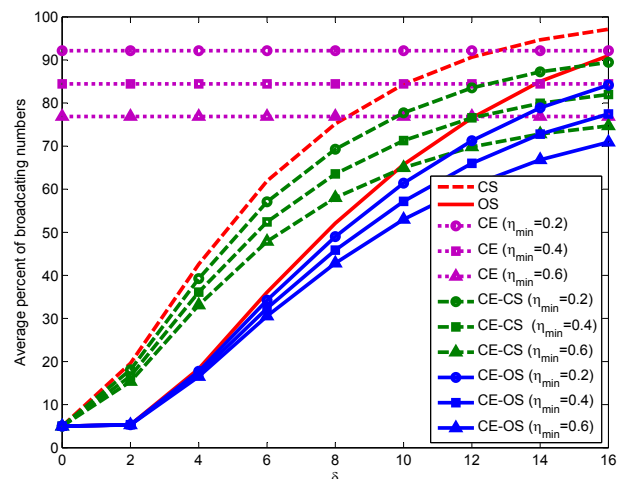


Fig. 4. The average percent of broadcasting number of different fusion schemes vs. the threshold value of sequential test δ with different values of censoring threshold η_{min} under the LUs signal SNR = -15 dB at all 20 CUs.

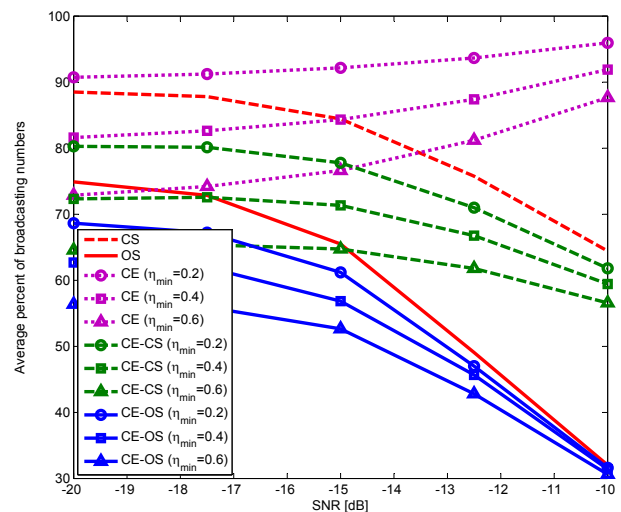


Fig. 5. The average percent of broadcasting number of different fusion schemes vs. the LU's signal SNR values with different δ values of censoring threshold η_{min} under the sequential test's threshold $\delta = 10$.

Fig. 4 shows the average percent of broadcasting number of CS, CE, OS, CE-CS and CE-OS fusion schemes according to δ with different values of η_{min} under the LU's signal SNR = -15 dB at all 20 CUs. The figure indicates that the number of broadcasting nodes is low when the threshold δ is low. Therefore, the selection of threshold δ is a tradeoff between performance and network overhead. Beside, as shown in the Fig.4, the average percent of broadcasting number for the same fusion scheme will decrease when we increase the value of η_{min} . In the case of our proposed CE-OS scheme, at $\delta = 10$, for example, the average percent of broadcasting number is 65% for $\eta_{min} = 0$ (i.e., OS scheme), 60% for $\eta_{min} = 0.2$ and 52% for $\eta_{min} = 0.6$. This result is fully significant if we note that the SS performance is almost unaffected in the range from 0.2 to 0.6 of the threshold η_{min} at $\delta = 10$ in Fig. 3. Above all, compared with other schemes, our proposed CE-OS

fusion outperforms the other schemes in the same threshold condition. Indeed, as shown in the Fig. 4, at $\delta = 10$ and $\eta_{min} = 0.6$, the average broadcasting number percent is 77% for CE fusion, 62% for CE-CS fusion and 52% for our proposed CE-OS fusion.

For further consideration, the five above schemes are simulated with different SNR conditions and different threshold η_{min} values while keeping $\delta = 10$. As shown in the Fig.5, for CE fusion, the broadcasting number increases when the SNR increases. This can be explained by the fact that the sensing data reliability will be improved when the SNR increases. For both CE-CS and CE-OS fusion, however, the broadcasting numbers is reduced when the SNR value increases. Similarly to previous results the same best performance is obtained by our proposed CE-OS scheme.

VII. CONCLUSIONS

In this paper, a censored and ordered sequential D-S theory based collaborative SS scheme for CRAHN has been proposed. The preceding censored process and the followed ordered sequential fusion not only maintain the same sensing performance compared with the conventional cooperative centralized spectrum sensing scheme but also strongly reducing the collaborative resource requirements such as the overhead of control channel, the energy and the collecting sensing data time. For future works, the detail protocol for coordination between CUs and the timing for making the proposed scheme precisely work in practice require more research.

ACKNOWLEDGEMENT

“This research was supported by Basic Science Research Program through the National Research Foundation of Korea (NRF) funded by the Ministry of Education, Science and Technology (KRF-2010-0017144)”

REFERENCES

- [1] I. F. Akyildiz, W. Lee, M. C. Vuran, and S. Mohanty, “NeXt generation/dynamic spectrum access/cognitive radio wireless networks: a survey,” in *Computer Network*, Vol.50, no.13, pp.2127-2159, Sep. 2006.
- [2] A. Ghasemi and E. S. Sousa, “Collaborative spectrum sensing for opportunistic access in fading environments,” in *New Frontiers in Dynamic Spectrum Access Networks, 2005. DySPAN 2005. 2005 First IEEE International Symposium on*, 2005, pp. 131-136.
- [3] G. Ganesan and Y. G. Li, “Agility improvement through cooperative diversity in cognitive radio,” in *Proc. IEEE GLOBECOM 2005*, pp.2505-2509, Nov. 2005.
- [4] Q. Peng, K. Zeng, J. Wang, and S. Li, “A distributed spectrum sensing scheme based on credibility and evidence theory in cognitive radio context,” in *IEEE 17th Int. Symposium on Personal, Indoor and Mobile Radio Communications*, Sept. 2006, pp.1-5.
- [5] N. Nguyen-Thanh and I. Koo, “An enhanced cooperative spectrum sensing scheme based on evidence theory and reliability source evaluation in cognitive radio context,” *Communications Letters, IEEE*, vol. 13, pp. 492-494, 2009.
- [6] S. Yeelin and Y. T. Su, “A sequential test based cooperative spectrum sensing scheme for cognitive radios,” in *Personal, Indoor and Mobile Radio Communications, 2008. PIMRC 2008. IEEE 19th International Symposium on*, 2008, pp. 1-5.
- [7] N. Nguyen-Thanh and I. Koo, “An Efficient Ordered Sequential Cooperative Spectrum Sensing Scheme Based on Evidence Theory in Cognitive Radio,” *IEICE Transactions on Communications*, vol. E93-B, pp. 3248-3257, 2010.

- [8] T. Kieu-Xuan and I. Koo, “A Censor-Based Cooperative Spectrum Sensing Scheme Using Fuzzy Logic for Cognitive Radio Sensor Networks,” *IEICE Transactions on Communications*, vol. E93-B, pp. 3497-3500, 2010.
- [9] I. F. Akyildiz, W.-Y. Lee, and K. R. Chowdhury, “CRAHNS: Cognitive radio ad hoc networks,” *Ad Hoc Networks*, vol. 7, pp. 810-836, 2009.
- [10] H. Urkowitz, “Energy detection of unknown deterministic signals,” *Proceedings of the IEEE*, vol.55, no.4, pp. 523-531, April 1967.
- [11] Z. Wentao, F. Tao, and J. Yan, “Data Fusion Using Improved Dempster-Shafer Evidence Theory for Vehicle Detection,” in *4th Int. Conf. on Fuzzy Systems and Knowledge Discovery*, vol.1, Aug. 2007, pp.487-491.

DVB-T Receiver Performance Measurements Under Secondary System Interference

Jussi Kerttula and Riku Jäntti
 Communications and Networking Department
 Aalto University, School of Electrical Engineering
 Espoo, Finland
 jussi.kerttula@aalto.fi, riku.jantti@aalto.fi

Abstract—Interest to allow secondary use on television frequency bands has been growing and recently Federal Communications Commission (FCC) opened vacant TV channels for unlicensed use. Many countries, especially in Europe, are using DVB-T standard for providing terrestrial digital television transmissions, whereas countries like U.S. rely on ATSC standard. When assessing the impact and potential of secondary use, primary system's tolerance to interference must be known. In this paper we provide essential interference tolerance measurement results for DVB-T system that illustrate how secondary use could impact its performance. We show how DVB-T receivers BER behaves under interference and how bursty interference signal affects compared to continuous interference. We also calculate example protection distances for different secondary transmitters.

Keywords—DVB-T; interference; secondary use; measurements

I. INTRODUCTION

Development of new wireless services and technology is forcing us to rethink the methods how radio spectrum is allocated. Static and exclusive allocations are able to provide high protection for the licenced service, but often fail to be efficient and flexible. The inefficient use of allocated spectrum can be seen from many measurement campaigns [1] [2], but it is obvious that utilization also depends on the band. Bands such as cellular phone bands and industrial, scientific and medical (ISM) bands, are already now highly utilized. Some radio bands that seem to be underutilized may be used by aviation or safety related services that require high reliability and therefore cannot in practice be used by secondary system.

Secondary use of inefficiently used bands is an interesting possibility to improve spectrum utilization. Secondary system operates on a non-interfering basis in the same band with licenced primary system. Secondary use might be allowed to certain group of secondary users or open to every user that is willing to obey the given rules. TV frequencies have especially been under investigation in many recent studies. Switchover from analog to digital TV broadcasting has taken place in many countries already and most of the remaining countries will do it within few years. This switchover results to so called digital dividend due to increased efficiency. Digital dividend can be used to carry more channels or it can be released to some other use, such as secondary system.

When exploring the secondary use of TV bands, the effects it causes to TV reception and how it should be taken

into account in network planning process must be carefully assessed. In previous studies, interference tolerance limits for digital signal on adjacent channels are measured in [3] [4] for Advanced Television Systems Committee (ATSC) receivers and in [5] for Digital Video Broadcasting Project's terrestrial (DVB-T) receivers. These clearly show that there is significant difference in performance between different standards but also between different receivers. These measurements use Threshold Of Visibility (TOV) as a limit for the interference. TOV is in practice the same as Quasi Error Free (QEF) limit defined later in this paper. In [6] Bit Error Rate (BER) measurements have been done for DVB-T reception when interfering signal is analogue PAL-G TV-signal, but this is not comparable to digital multicarrier interference signal due to different waveform. BER is able to provide more information about the impact of interference, than simple TOV limit. Interference impact on much lower interference levels than the TOV limit is reached and BER can show this. The aim of this paper is to give an overview of DVB-T as a primary system and provide relevant interference tolerance measurement results, mostly in terms of BER, that can be used when analyzing the potential and effects of secondary use of TV-bands.

This paper is organized as follows. Section II briefly explains main features of DVB-T system that affects to secondary use. In Section III we introduce our measurement setup and methodology. Measurement results are presented in Section IV. In Section V we calculate what kind of protection distances are needed to protect the primary users. Finally, Section VI concludes our work.

II. DVB-T AS A PRIMARY SYSTEM

Television frequency band is often considered to be the most attractive part of radio spectrum for use. Television broadcasting uses relatively low frequency range that enables long link distances. Transmitter locations are static and usually they have continuous transmission with fixed channels. This information is publicly available and can be used when deciding which channels are available in specific location by using geolocation database [7]. Generally, secondary systems have to estimate spectrum availability in time, frequency and temporal domains. However, TV transmissions are usually so static and continuous that the time domain assessment can be left out, which makes the situation much simpler.

DVB-T is a widely adopted terrestrial digital television standard that is being used e.g. in most European countries. It uses orthogonal frequency division multiplexing (OFDM), where transmitted data is carried by large number of closely spaced orthogonal subcarriers. DVB-T system can utilize different combinations of parameters depending on the given performance requirements. Number of subcarriers, guard interval, modulation and code rate can be modified and these affect to the net bitrate, required carrier-to-noise ratio (C/N), mobility and possible single frequency network use. System parameters that are used in our measurements are presented in Table I. This set of parameters is used for example in Finland and Sweden and it gives 22.21 Mbit/s net bitrate [8].

When analyzing the interference tolerance limits of DTV, error correction coding plays a significant role. DVB-T system uses a kind of concatenated structure that consists of inner and outer coding. The outer code uses Reed-Solomon coding which is very robust against bursty errors, while an inner code uses convolutional coding which is good against random-type errors. In addition to these coding methods, interleaving and energy dispersal are used to improve the received video quality. DVB-T systems use MPEG-2 or MPEG-4 video compression. As a result even small bit error likely produces noticeable and irritating flaw in the video stream. Therefore the target is to produce virtually error-free bitstream after errordecoding at the receiving end. Evaluating the quality of experience, or video quality is not so relevant, since the transition from perfect to unacceptable quality is very rapid.

In practice the maximum acceptable error rate is decided to be one uncorrected error event per hour, meaning BER of 10^{-11} at the input of MPEG-2 demultiplexer, and 2×10^{-4} after inner Viterbi decoding. This error level is also called Quasi Error Free (QEF) level. Measurement results presented in this paper maps this QEF limit to about 1.5×10^{-2} BER before Viterbi decoding. For the parameters given in Table I, the minimum C/N requirements to achieve QEF level are given in [8] for Gaussian, Rician and Rayleigh channels, being 16.7dB, 17.3dB and 20.3dB, respectively. Rician channel is modeling fixed reception and Rayleigh channel model portable reception. Based on these we can estimate the minimum required power level by using following formula:

$$P_{min}(dBm) = 10 \log(kT_0BF(C/N)_{min}) + 30 \quad (1)$$

where $k = 1.3 \times 10^{-23} J/K$ is the Boltzmann's constant, $T_0 = 290K$ is the temperature, $B = 7.6MHz$ is the receiver's noisebandwidth, F is receiver's noise figure and C/N_{min} is the minimum signal quality to achieve QEF level. Result is scaled from dBW to dBm by adding 30dB. When we expect noise figure to be 8dB and Rician channel, the minimum required signal power becomes $-79.9dBm$.

Protection ratios for adjacent channel and co-channel interference are usually defined as a function of power levels between wanted TV-signal and interferer. This is also known as Desired-to-Undesired ratio (D/U). Organizations such as ITU-R, Nordig, DIGITALEUROPE/EICTA and Digital TV

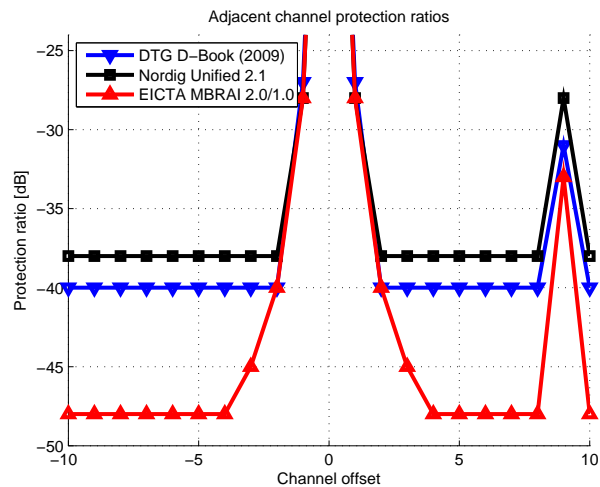


Fig. 1. DVB-T protection ratio specifications

TABLE I
DVB-T PARAMETERS

Parameter	Value
Channel bandwidth	8 MHz
FFT size	8192 (8K)
Number of subcarriers	6817
Modulation	64-QAM
Code rate	2/3
Carrier spacing	1116 Hz
Useful symbol duration	896 μ s
Guard interval	1/8

Group (DTG) provide protection ratio requirements and recommendations for receiver manufacturers and network planning purposes. Most of these specifications are presented in Figure 1. These protection ratios are given against other DVB-T transmissions. It can be seen that there is a large difference between them. Requirements are generally looser for first adjacent channels $N \pm 1$ and image channel $N + 9$ interference tolerance than other adjacent channels.

A. DVB-T coverage and network planning principles

Compared to analog TV-system, the network planning process is somewhat different for DVB-T system. This is due to the fact that in DVB-T there either is or is not coverage at certain time, whereas with analog system the coverage edge is softer. Digital coverage rapidly changes from perfect reception to no reception at all which make coverage area predictions and network planning challenging.

DVB-T coverage area definition includes time and location probabilities [9]. Receiving location is covered if service can be perfectly received some wanted percentage of time. This means that carrier-to-noise and carrier-to-interference relations are above required threshold. Next level is so called "small area" typically 100m x 100m and within this area the percentage of covered receiving locations is defined. Coverage is "good" when 95% of receiving locations are covered and "acceptable" if the number is 70%. The total coverage area that is achieved by using one or multiple transmitters consists

of a sum of these small areas that fulfill the given coverage requirements.

Theoretical propagation models are used to estimate transmitter coverage and to help network planning. Often used model for broadcast networks is the ITU-R P.1546. It gives relatively good results by taking into account e.g. terrain topography with decent amount of complexity. This model is commonly used when planning and coordinating TV-frequencies. More complex models that are based on diffraction also exist, and they can potentially provide more accurate results. These models are often used by network operators that want to optimize their network.

DVB-T networks are already now usually interference limited. In a typical implementation, interference reduces the coverage radius of a broadcast station by up to few kilometers when compared to noise limited case. The interference is caused by other TV-transmitters that are using the same channel, despite that they are usually several hundred kilometers apart. High-power transmitters in high masts and the relatively low frequencies cause that the interference distances are long. This means that it is not enough to allocate these frequencies domestically, but in many cases also international coordination is needed.

It is evident that if secondary use of TV-channels is allowed, it will cause additional interference towards TV-services. The important question is that how much additional interference should be tolerated? The effect of this additional interference could be assessed in many ways, for example in terms of coverage probability degradation.

III. INTERFERENCE MEASUREMENTS

When exploring the opportunities for secondary use, the tolerance limits for interference should be carefully determined. Tolerance limits are naturally different for different systems and different parameter sets, but limits can vary between different manufacturers significantly. In the case of DVB-T system, most of the previous interference measurements only provide the hard QEF or TOV threshold, but we see that there is a need for more detailed measurements as well.

A. Measurement setup

Measurement setup is shown in Fig. 2. DVB-T signal is first received via directional roof-top antenna. Adjustable attenuator is used to change the DVB-T signal strength down to desired level. Interfering signal is created with matlab and R&S SMJ100A signal generator. Interference signal is then summed to DVB-T signal and then split to receiver and to spectrum analyzer. Tektronix RSA6114A spectrum analyzer is used to measure all the power levels, taking the impedance match into account. Finally, the signal is fed to DVB-T receiver. The measured commercial receiver is able to give BERs before and after Viterbi decoding. Therefore it is connected to computer that records these values for later use and analysis. Also visual quality of the received video stream can be analyzed via television. QEF limit can also be found by visual assessment with about $\pm 1dB$ accuracy.

TABLE II
INTERFERENCE SIGNAL PARAMETERS

Parameter	Value
Bandwidth	8 MHz
FFT size	2048 (2K)
Used subcarriers	1728
Modulation	QPSK
Carrier spacing	4464 Hz
Symbol duration	224 μ s

B. Measurement methodology

Measurements are conducted at about 10 km distance from a large DVB-T broadcast station. Channel #32 (558-566 MHz) was used as a desired channel and signal strength at the receiver's input is $-57dBm$ without added attenuation. Interference signal for all measurements is OFDM-signal and its detailed parameters are shown in Table II. During each interference measurement, the DVB-T signal strength is constant and interference signal is changed.

Our measurements consisted of three different cases. First receiver sensitivity and co-channel interference tolerance were measured. The second case measured adjacent channel interference tolerance for channels $N \pm 1$ and $N \pm 2$. Third case examined how the effects of a non-continuous bursty interference signal differ from a continuous interference signal. In real scenario it is likely that secondary users don't have constant transmissions, but they can be timevariant. Bursty signal is created by switching the same interference signal between ON and OFF states. Our focus is not to provide only TOV or QEF limit but to show in more detailed manner how the BER behaves when interference is present. Most of our measurements are done with Receiver-1, which is able to give the BER numbers, but for comparison we also tested visually the interference tolerance limits with two other commercial receivers referred as Receiver-2 and Receiver-3.

IV. MEASUREMENT RESULTS

This section presents and analyzes the obtained measurement results.

A. Sensitivity and co-channel interference

Sensitivity of the DVB-T receiver was measured by attenuating the received signal level. Since we used fixed roof-top antenna, the radio channel is expected to be Rician. Figure 3 shows the BERs before and after Viterbi decoding as a function of signal power. It can be seen that the Viterbi decoding can correct all the errors when received power is over $-75dBm$. The QEF limit is then reached at power level of $-79dBm$. This is close to the simulated power limit presented earlier in this paper. This $-75dB$ limit is also chosen to be used in most of the measurements in this paper, because it can be considered to be the power level close to cell border.

Co-channel interference tolerance was measured with $-75dBm$ desired DVB-T power level. Results are shown in Figure 4. It can be seen that interference does not cause noticeable effect when D/U ratio is more than $28dB$. The QEF limit is achieved at $22dB$ D/U ratio. ITU-R BT.1368-8 gives

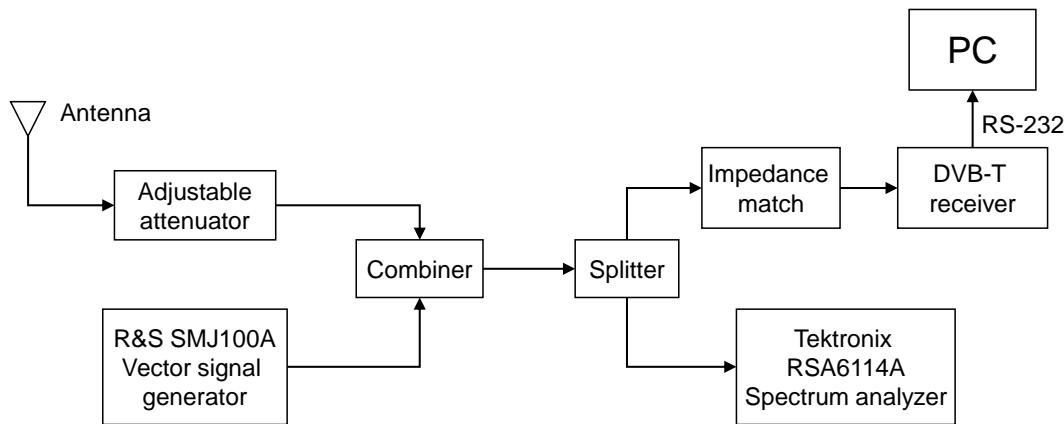


Fig. 2. Measurement setup

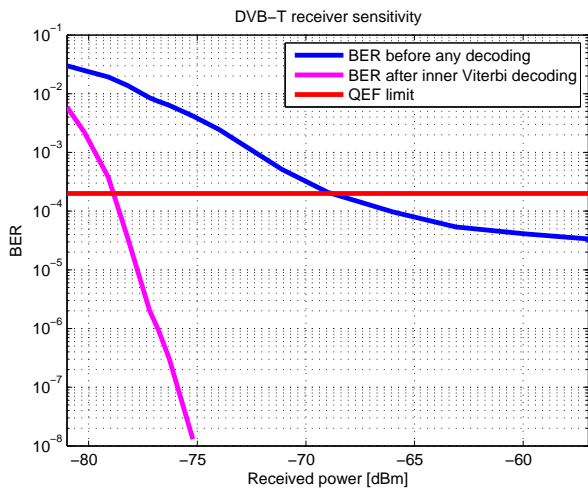


Fig. 3. DVB-T receiver sensitivity

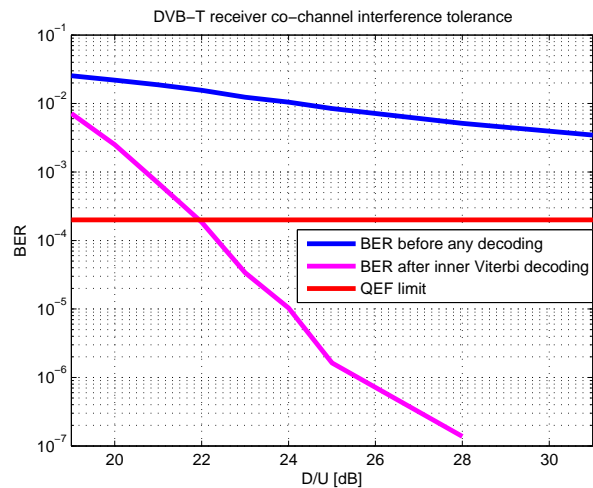


Fig. 4. Co-channel interference tolerance

protection ratios between two interfering DVB-T signals. For these used parameters the ratios are 19dB, 20dB and 23dB for Gaussian, Rician and Rayleigh channels, respectively.

B. Adjacent channel interference

Adjacent interference tolerance determines whether a guard channel is needed between the primary and secondary user or what kind of guard distance should separate them. Measured results for $N \pm 1$ are shown in Figure 5. It can be seen that $N + 1$ interference starts to degrade the BER when D/U is less than $-20dB$. For $N - 1$ interference the performance is better and the interference begins to affect when D/U is less than $-30dB$. However the QEF limits are reached with D/U ratios $-30dB$ and $-35dB$, for $N + 1$ and $N - 1$, respectively. ITU-R BT.1368-8 gives $-30dB$ protection ratios for both $N \pm 1$ channel interference. Tolerance for $N \pm 2$ channel interference are presented in Figure 7. Again it can be seen that $N - 2$ channel tolerates more interference than

$N + 2$. The QEF limits for $N \pm 2$ channels are about 12dB lower D/U level than for $N \pm 1$. Protection ratios for all the measured receivers are presented in Table III. It can be observed that Receiver-2, which is an USB-stick type receiver, have significantly worse tolerance for interference on adjacent channels beyond $N \pm 1$ and it does not even meet the loosest Nordig specification. Receiver-1 and Receiver-3 are both set-top boxes, and also their interference tolerance is much better, meeting more stringent EICTA MBRAI requirements.

In order to see how desired power level affects to the interference tolerance, we also measured $N+1$ channel interference using different desired power levels. These results are shown in Figure 6 where only BERs before Viterbi decoding is plotted. As seen from the other figures, the QEF limit is approximately 1.5×10^{-2} and this is also plotted in the figure. The impact of noise naturally decreases when desired power is stronger. Due to this, the QEF limits, in terms of D/U ratio, are not the same for every desired signal strength. Stronger desired

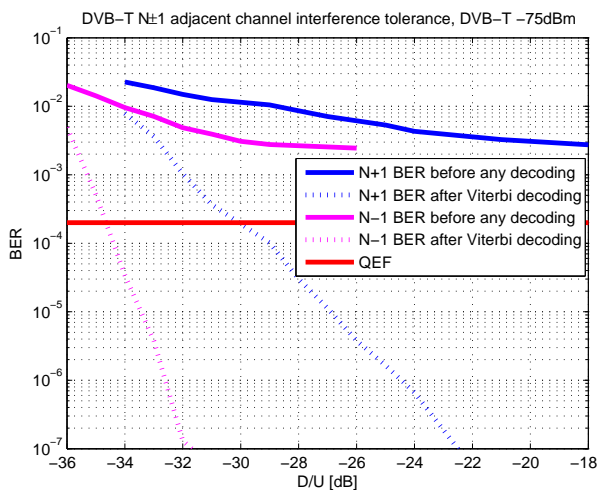


Fig. 5. $N \pm 1$ Adjacent channel interference tolerance

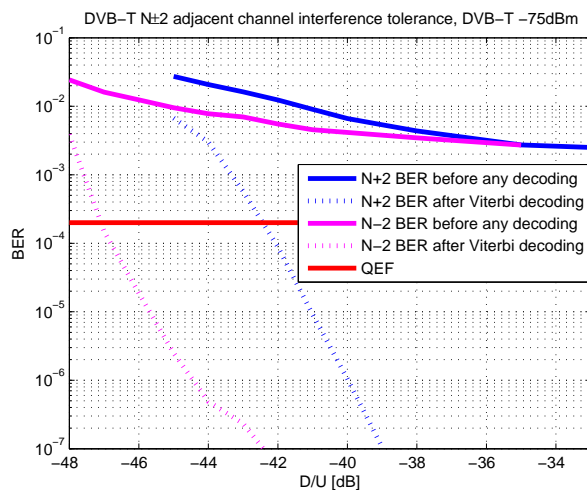


Fig. 7. $N \pm 2$ Adjacent channel interference tolerance

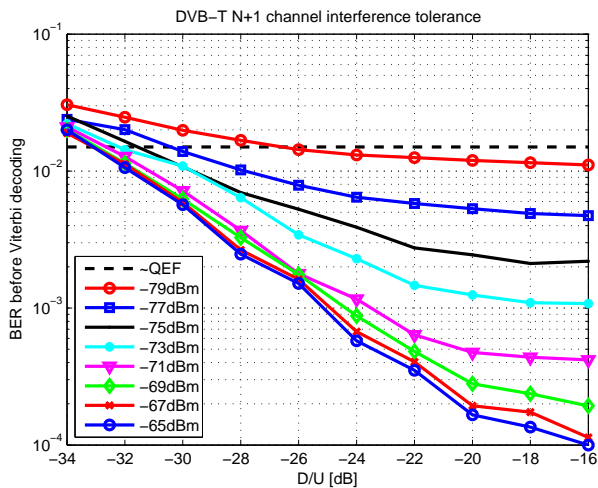


Fig. 6. $N + 1$ Adjacent channel interference tolerance with different desired power levels

TABLE III
MEASURED D/U PROTECTION RATIOS, DVB-T POWER $-75dBm$

	N-3	N-2	N-1	N	N+1	N+2	N+3
Receiver-1	-50	-47	-34.5	22	-30	-42.5	-48
Receiver-2	-24	-26	-25	21	-30	-31	-32
Receiver-3	-45	-40	-34	21	-36	-46	-52

signals can tolerate more interference even in terms of D/U ratio. However, with this change is not significant when desired signal is stronger than $-75dBm$, as seen from this figure.

C. Bursty interference

Bursty interference tolerance is measured by visually determining the QEF limit, because bursty interference causes the BER to vary significantly and therefore these values don't give reliable results. Four bursty signals with different transmit/silence ratios were used, and then also continuous signal were measured for comparison. Shortest transmission

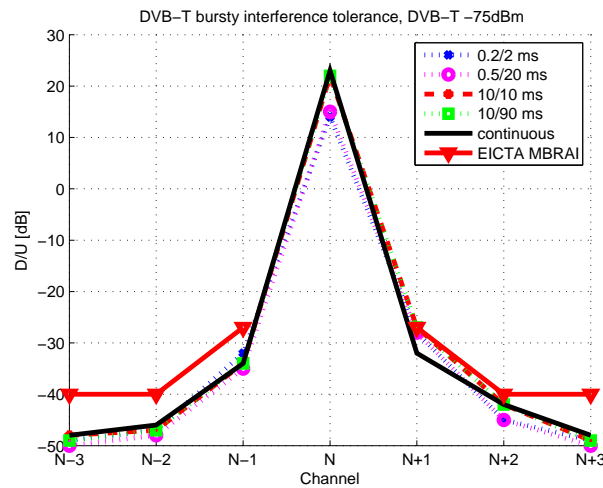


Fig. 8. Bursty interference tolerance, QEF limits

bursts were $0.2ms$ long and longest were $10ms$. The results are presented in Figure 8 along with the EICTA MBRAI protection ratios. It can be seen that on co-channel the very short bursts could operate about at about $6dB$ higher power level. This improvement disappears or reduces on adjacent channels. This receiver also fulfils the EICTA MBRAI specification. The average BER is normally slightly lower with bursty interference signal compared to equal strength continuous one, but BER during the burst determines whether errors occur or not. Overall it can be said that there is no significant difference between the bursty and continuous signal tolerances.

V. PROTECTION DISTANCES

Interference tolerance levels of the primary systems is one of the parameter that determines what kind of secondary use is possible and how long the protection distances should be between secondary transmitter and primary receiver. The limits are difficult to put into right perspective as plain dB values,

but based on them and by assuming something about the secondary system, we can calculate example cases about the protection distances.

Let us assume that we have a DVB-T receiver with fixed antenna at 10m height, located at the edge of the coverage area. According to the Reference Planning Configurations (RPC) defined in [10], the corresponding minimum field strength E is $56dB\mu V/m$. Now receiver input power can be calculated if we know possible losses and antenna gain to transmitter direction by using following equation

$$P[dBm] = E[dB\mu] + G + 10 \log\left(\frac{\lambda^2}{4\pi}\right) - 10 \log(120\pi) - 90 \quad (2)$$

where antenna gain G also includes the losses. Assuming that $G = 1.7dB$ to the direction of wanted signal and $600MHz$ frequency, minimum input power becomes $-75dBm$.

Let us use three different type of secondary transmitters, representing Wireless Regional Area Network (WRAN), Wireless Local Area Network (WLAN) and Wireless Personal Area Network (WPAN) -type transmitters with Effective Radiated Powers (ERPs) of $26dBm$, $20dBm$ and $10dBm$, respectively. Propagation loss $L(d)$ is calculated using modified Hata model given in [11] for suburban environment. If the transmitting antenna is located indoors, we assume that the indoor-outdoor propagation causes additional $6dB$ attenuation. Now we can calculate the minimum protection distance d from equation

$$P_{DVB} - PR = P_{sec} - L(d) \quad (3)$$

where P_{DVB} is the received DVB-T power, PR is the protection ratio for secondary interference and P_{sec} is the ERP power of secondary transmitter. We assume that DVB-T receiver antenna is located at 10m height and it has $0dB$ gain to the direction of interfering secondary transmitter. Protection distances for different secondary transmitters are presented in Table IV. It can be seen that co-channel use requires several hundreds of meters protection distances even with small power devices. Adjacent channel protection distances range from less than meter up to 190 meters, but still $20dBm$ WLAN-type secondary transmitter can interfere neighbors TV. Now we assumed that DVB-T uses almost isotropic antenna and there is only one secondary interferer. In practice, DVB-T reception is often done with directive roof-top antennas with gains of $10 - 15dB$ for the main lobe and less than $0dB$ gains elsewhere. This reduces the interference in most cases, but if the interferer hits the main lobe when being between DVB-T receiver and transmitter, interference increases significantly. This is difficult to avoid. We might also have multiple interferers on different adjacent channels, causing cumulative effect.

VI. CONCLUSION

In this paper we have presented measurement results of DVB-T receiver performance when single transmitter is causing interference. We use BER as a performance metric that provides more information than visual error free assessment. Visual errors begins to occur when BER after inner Viterbi

TABLE IV
PROTECTION DISTANCES

Channel (PR)	Secondary ERP and antenna location			
	26dBm out 10m	20dBm out 5m	10dBm in 5m	10dBm in 2m
$N(22dB)$	5800m	950m	640m	310m
$N \pm 1(-30dB)$	190m	50m	40m	21m
$N \pm 2(-42dB)$	90m	20m	8m	< 1m

decoding reaches 2×10^{-4} . Conducted measurements show that interference begins to degrade BER several dBs before errors can be visually seen. Tolerance for bursty interference is almost similar compared to continuous interference and therefore same limits can be used for both. However, deciding the protection limits against secondary use is a challenge since different organizations have difference in their specifications and in practice the interference tolerance varies significantly between receivers. From calculated protection distances it can be concluded that in most cases WLAN-type or smaller transmitter can operate on adjacent channels without causing too much interference, especially if secondary transmitter is located indoors and one guard channel is left between it and TV-channel.

ACKNOWLEDGMENT

The research leading to these results has received funding from the European Union's Seventh Framework Programme FP7/2007-2013 under grant agreement no. 248303.

REFERENCES

- [1] M. Lopez-Benitez, A. Umbert, and F. Casadevall, "Evaluation of spectrum occupancy in Spain for cognitive radio applications," in *Proc. IEEE 69th Vehicular Technology Conf. VTC Spring 2009*, 2009, pp. 1-5.
- [2] M. A. McHenry. (2005) Nsf spectrum occupancy measurements projects summary. Shared Spectrum Company. [Online]. Available: <http://www.sharedspectrum.com/measurements/>
- [3] G. L. Stuber, S. M. Almalfouh, and D. Sale, "Interference analysis of tv-band whitespace," *Proc. IEEE*, vol. 97, no. 4, pp. 741-754, 2009.
- [4] K. Salehian, Y. Wu, and G. Gagnon, "Performance of the consumer atsc-dtv receivers in the presence of single or double interference on adjacent/taboo channels," *IEEE Trans. Broadcast.*, vol. 56, no. 1, pp. 1-8, 2010.
- [5] B. Randhawa and S. Munday, "Conducted measurements to quantify dvb-t interference into dtb receivers," ERA Tech./Ofcom, Tech. Rep., October 2007.
- [6] M. M. Velez, P. Angueira, D. De La Vega, A. Arrinda, and J. L. Ordiales, "Dvb-t ber measurements in the presence of adjacent channel and co-channel analogue television interference," *IEEE Trans. Broadcast.*, vol. 47, no. 1, pp. 80-84, 2001.
- [7] M. Nekovee, "Cognitive radio access to tv white spaces: Spectrum opportunities, commercial applications and remaining technology challenges," in *Proc. IEEE Symp. New Frontiers in Dynamic Spectrum*, 2010, pp. 1-10.
- [8] ETSI EN 300 744, "Digital video broadcasting (dvb); framing structure, channel coding and modulation for digital terrestrial television," Jan 2009.
- [9] ETSI TR 101 190, "Digital video broadcasting (dvb); implementation guidelines for dvb terrestrial services; transmission aspects," Oct 2008.
- [10] ITU-R, "Final acts of the regional radiocommunication conference for planning of the digital terrestrial broadcasting service in parts of regions 1 and 3, in the frequency bands 174-230 mhz and 470-862 mhz (rrc-06)," 2006.
- [11] ITU-R SM.2028-1, "Monte carlo simulation methodology for the use in sharing and compatibility studies between different radio services or systems," 2002.

Efficient Mid-end Spectrum Sensing Implementation for Cognitive Radio Applications based on USRP2 Devices

Daniel Denkovski, Vladimir Atanasovski and Liljana Gavrilovska

Faculty of Electrical Engineering and Information Technologies
Ss Cyril and Methodius University in Skopje
Skopje, Macedonia
{daniel, vladimir, liljana}@feit.ukim.edu.mk

Abstract—Spectrum sensing is a cornerstone task in cognitive radio environments supporting dynamic spectrum access by spectrum opportunities discovery. It must be reliable and accurate in order not to harm the primary system by incorrect spectrum opportunities decisions. Mid-end spectrum sensing devices are spectrum sensing devices with satisfactory signal detection performances and reasonable price. This paper presents an efficient and flexible mid-end spectrum sensing solution (an USRP2 based spectrum sniffer implementation) that offers many sensing functionalities and detection capabilities by implementing several sensing modes of operation and detector types. Additionally, the paper presents several usage possibilities of this USRP2 spectrum sniffer implementation proving its efficient employment in various spectrum sensing applications.

Keywords- spectrum sensing, cognitive radio, USRP2 based sniffer implementation, detector, operation mode.

I. INTRODUCTION

Dynamic spectrum access is an increasingly popular networking paradigm aiming to resolve frequency spectrum scarcity problems that come from the traditional fixed frequency resources reservation policies. Cognitive radios incorporate the dynamic spectrum access functionality striving to access and use the temporary available frequency bands and dynamically adapt to changing environment conditions.

Spectrum sensing is a crucial aspect in cognitive radio since it enables the secondary users to be spectrum aware and facilitates the spectrum opportunities discovery process. There are various and numerous spectrum sensing implementations that can be generally classified into three groups: high, low and mid-end sensing devices. High-end spectrum sensing devices mainly refer to spectrum analyzers and these devices' main characteristic is their high precision in terms of signal detection. However, the high accuracy reflects in high price, which may make them inappropriate for certain cognitive radio applications. On the other hand, the low-end spectrum sensing devices are cheap solutions having low precision and, thus, limited applicability in different applications. They often result in false conclusions about the spectrum opportunity. The mid-end spectrum sensing devices are a trade-off between price and accuracy.

They are cheaper sensing solutions than the high-end spectrum analyzers and offer solid detection performances. All spectrum sensing solutions may employ various spectrum sensing techniques [1]. However, energy detection is most commonly used technique due to its simplicity and satisfactory detection capabilities.

The spectrum sensing devices can be used in many spectrum related applications. Besides their main function to detect spectrum opportunities in cognitive radios, they can be also used in long and medium term spectrum measurements [2, 3]. Furthermore, different cooperative sensing [4, 5] and data fusion techniques can be implemented to achieve better detection capabilities in the cognitive environment. The input from the sensing devices can be also used for planning of medium and long term spectrum sharing strategies, either between primary and secondary users or between the secondary users in the cognitive network.

This paper presents an efficient and flexible mid-end USRP2 based spectrum sensing (i.e., sniffer) implementation. The developed sniffer implementation extends the spectrum sensing capabilities of the basic GNU radio USRP2 sensing implementation (used in [6]) introducing several detector types and different modes of operation of the sniffer. This sensing implementation can be used to perform wideband and band-specific spectrum measurements and can be utilized in various cognitive radio applications.

The paper is organized as follows. Section II presents the spectrum sniffer implementation based on USRP2 hardware with all comprising GNU radio based and extended processing blocks and the functionalities and possibilities of the sniffer. Section III presents several possible sensing relevant applications of the USRP2 based sniffer implementation. Section IV concludes the paper and presents directions for the future work.

II. USRP2 BASED SPECTRUM SNIFFER IMPLEMENTATION

This section elaborates on a custom design and development of a versatile USRP2 based spectrum sensing (i.e., sniffer) implementation using the off-the-shelf available USRP2 hardware and accompanying GNU Radio software.

Universal Software Radio Peripheral 2 (USRP2) [7] is a hardware platform for development of various radio applications. Its motherboards are enabled to use various daughterboards covering different frequency ranges. The USRP2 hardware supports fast and high precision analog-to-digital and digital-to-analog conversion and Ethernet interface for connection to host computers. This results in wider band signals support, as well as increased dynamic range of the system. GNU Radio [8] is an open source software development toolkit that provides the basic signal processing blocks required to make the USRP2 hardware a software defined radio (SDR) programmable platform. GNU Radio applications are primarily written in python with the performance-critical signal processing written in C++.

The USRP2 based sniffer implementation is developed as a C++ application that includes the GNU Radio basic and USRP2 specific blocks. This sensing implementation is based on the logic of the original GNU radio python based implementation *usrp_spectrum_sense.py*, with extended functionalities and support of several additional features. Moreover, the C++ realization of the sniffer eliminates the C++ to/from python parsing resulting in better sensing performances. This subsection presents the sniffer architecture and the possibilities provided by the sniffer, i.e., the supported detector types and modes of operation.

1) USRP2 based sniffer architecture

The sensing-relevant input parameters in the developed USRP2 C++ based sniffer implementation are: *starting and end frequency*, *decimation factor*, *FFT size*, *gain*, *detection type*, *tune time* (if switching between frequencies is required) and *dwel time* (time spent at a measurement frequency point). More details on the detection types of the sniffer and the modes of operation are given in subsections 2) and 3), respectively.

The developed USRP2 C++ sniffer implementation architecture along with all the included GNU Radio basic and extended blocks is depicted on Figure 1. The architecture consists of seven processing blocks: *usrp2_source_32fc*, *gr_stream_to_vector*, *gr_fft_vcc*, *gr_fft_vfc*, *gr_complex_to_mag_squared*, *gr_complex_to_mag* and the custom made *gr_energy_detector_f* processing block. Their key characteristics are:

- *usrp2_source_32fc* is a GNU radio USRP2 specific block that creates the USRP2 source and has the control of the hardware (it sets up the decimation rate and performs the tuning of the center frequency).
- *gr_stream_to_vector* is a GNU radio block that converts the input from the *usrp2_source_32fc* from stream of complex samples to vector of complex samples with size *fft_size*.
- *gr_fft_vcc* is a GNU radio processing block that transforms the vector of time samples with size *fft_size* into frequency domain vector of complex samples with size *fft_size*.
- *gr_complex_to_mag* is a GNU radio processing block that converts the complex vector of time samples with size *fft_size* into amplitudes vector with the same size.
- *gr_fft_vfc* is a GNU radio block that converts the vector of amplitudes per time to frequency domain complex vector with size *fft_size*.
- *gr_complex_to_mag_squared* is a GNU radio processing block that converts the complex vector (sample) in power vector (sample) summing the magnitude squared I and Q values and passing the output to *gr_energy_detector_f* block.
- *gr_energy_detector_f* is a custom made C++ processing block that performs the actual preprocessing of the measurement data. On initialization of this block the detection type, dwell and tune times are specified. This block constantly receives the vectors' samples from the *gr_complex_to_mag_squared* block and performs the chosen preprocessing (detection type) during the specified *dwel time*. The output of this block is packed into a message queue variable of type *gr_msg_queue*, timely read and post-processed by the main function. The output of the main function is the decisions vector for the occupancy in the inspected frequency span. The *gr_energy_detector_f* also initiates the tuning between sequential frequencies if required.

Figure 1 illustrates the possibilities and features that the current USRP2 C++ sniffer implementation can offer. Several flow graphs are possible, based on the selection of the detection type and the mode of operation of the sniffer (subsections 2) and 3)). The current implementation of the sniffer also provides possibilities for *remote control*.

2) Detector types

The current USRP2 based sniffer implementation allows selection of *five energy-based detector types*. The main enabler of the different detection types is the custom made *gr_energy_detector_f* block. Besides the maximum hold detector as the basic implementation in GNU radio, it enables the following four other detection types to be used: minimum hold, mean hold, Higher-Order-Statistics Energy Detection (HOSED) type, as well as FFT Averaging Ratio (FAR) detection type.

The *minimum hold detector* saves and returns the minimum value of the received power during the inspection time (dwell time) on a specific frequency band. Oppositely, the *maximum hold detector* returns the maximal value of the received power during the examination time. The *mean hold detector* calculates and gives at the output the average received power during the inspection time. When the previous three detection types are in use, the occupancy decision on frequency band of interest is based on comparisons with predefined threshold values. The *higher order statistics energy detector*, besides the average received power, calculates important higher order statistics such as *skewness* and *kurtosis* [9] of the received power during the inspection time. This valuable statistical

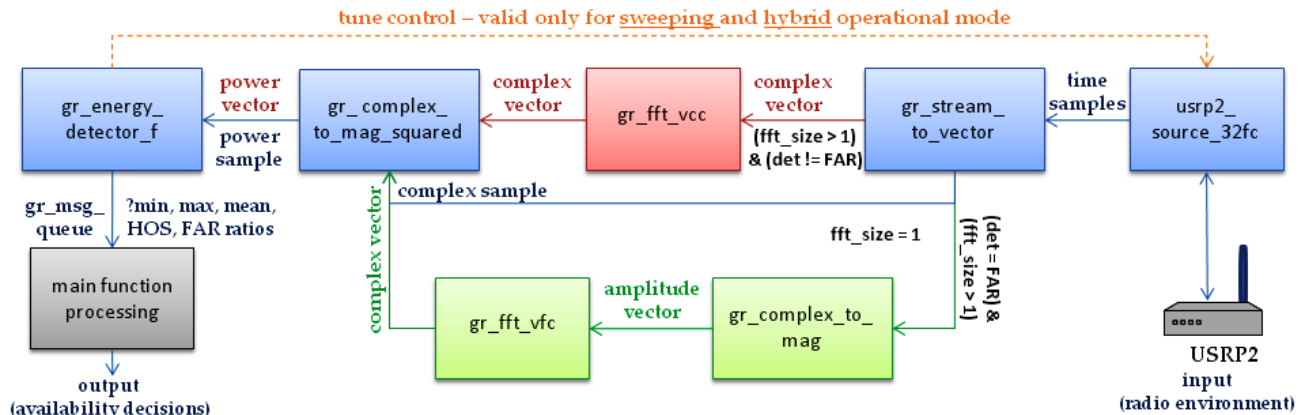


Figure 1. USRP2 based sniffer application architecture

information can be helpful in the detection process since it reflects some characteristics of the distribution of the receiving power and has proved to offer better detection performance than the classical average energy detector. The decision on the occupancy of the inspected frequency band in the case of HOS detection is made by comparison of the calculated statistics values with the statistics values of the system noise. The *FFT averaging ratio detector* [10] is a detector utilizing FFT analysis on the amplitude of the received time samples. The output of this energy detector type is the average PSD (Power Spectral Density) ratio of each frequency bin in the FFT analysis. Based on these output values, a decision is made whether a frequency band is occupied or not by comparing the referred with predefined threshold values.

When using the first four detection types, the flow graph of the sniffer is consisted of the following five blocks: *usrp2_source_32fc*, *gr_stream_to_vector*, *gr_fft_vcc*, *gr_complex_to_mag_squared* and *gr_energy_detector_f* block, if using FFT. If FFT is not used (*fft_size=1*), the *gr_fft_vcc* is excluded from the previous flow graph (Figure 1). When FAR detection is selected the sniffer flow graph consists of the following six blocks: *usrp2_source_32fc*, *gr_stream_to_vector*, *gr_complex_to_mag*, *gr_fft_vfc*, *gr_complex_to_mag_squared* and *gr_energy_detector_f* blocks, as the FFT analysis is performed on the amplitude of the time samples (Figure 1).

3) Modes of operation

The custom made C++ sniffing implementation enables the USRP2 hardware to work in *three modes of operation*: real-time measurement mode, sweeping measurement mode and hybrid measurement mode.

The *real-time measurement mode* supports real-time measurements on 25 MHz of bandwidth at most. The samples gathered from the USRP2 hardware are post-processed in the GNU radio host computer environment, employing FFT (Fast Fourier Transform) analysis of the received data. This allows various frequency resolutions, but high FFT size values (higher than 1024) are not recommended since the number of operations to calculate FFT transform increases exponentially as the FFT size rises.

This can cause disturbance of the operation of the USRP2 due to the higher processing requirements and the inability of the host computer to process in-time all data coming from the USRP2. Before the actual FFT analysis of the samples, time windowing is performed in order to reduce the spectral leakage (a side-effect coming from the time restrictions). The current implementation uses the Hamming Window. In addition, FFT overlapping is used and the overlapping frequency points are dropped to reduce the non linear response of the DDC at the edges of the FFT analysis. The real-time measurement mode utilizing FFT is consisted of five processing blocks (Figure 1) This mode of operation can be also performed without FFT analysis of the data, excluding the use of *gr_fft_vcc* block.

The *sweeping mode of operation* of the sniffer enables particular values for the resolution bandwidth in the range 195.3125 KHz – 25 MHz, corresponding to the respective decimation factors of the digital-down-conversion process. Here, the USRP2 periodically switches the center frequency between sequential frequency bands, with the chosen resolution bandwidth size, to cover the full requested frequency span. This mode of operation is employed when the required frequency span is higher than the largest possible receiving bandwidth size of 25 MHz. When using this mode of operation, only four blocks are connected in the flow graph: *usrp2_source_32fc*, *gr_stream_to_vector*, *gr_complex_to_mag_squared* and *gr_energy_detector_f*, where the *gr_energy_detector_f* initiates the switching between the sequential frequency bands, when the dwell time at a frequency band is expired.

The sweeping mode of operation can be jointly combined with FFT analysis to multiplicatively increase the resolution bandwidth of the USRP2 hardware, resulting in *hybrid mode of operation* of the sniffer. This mode of operation can offer higher sensing performances due to the increased frequency resolution as well as reduced sweep time requirements. When targeting a particular resolution bandwidth size, the number of sweeps (consequently the sweep time) to cover the full span of interest can be reduced by the usage of the highest receiving bandwidth (lowest possible decimation factor) and specific FFT size to support

the resolution bandwidth requirement. This mode of operation utilizes five processing blocks (Figure 1): *usrp2_source_32fc*, *gr_stream_to_vector*, *gr_fft_vcc*, *gr_complex_to_mag_squared* and *gr_energy_detector_f*, where the last is in charge of initiating the switching between frequency bands.

The following section presents several sensing related applications of the previously elaborated USRP2 sniffer implementation. It shows its versatility and potentials for practical usage.

III. USRP2 SNIFFER APPLICATIONS

The basic application of the developed USRP2 based sniffer implementation is in the area of assisting the dynamic spectrum access process, i.e., to serve for detection and localization of secondary spectrum access opportunities. Several applications engaging the USRP2 based sniffing have been included in part of the authors' previous work. The applications are classified in two types: *energy detector based applications* and *HOS detector based applications*, each elaborated in more details in the subsequent subsections.

A. Applications based on energy detector

The classical energy detection technique employed by the USRP2 based sniffer implementation is consisted of the minimum hold, maximum hold and the mean hold detector types. This subsection presents two applications of the USRP2 based energy detector, the first focusing on frequency spectrum measurements, the second on data fusion and dynamic radio environmental maps (REMs) derivation.

1) Medium and long term spectrum measurements

The classical energy detector in the USRP2 sniffer implementation can be included in medium and long term spectrum measurement campaigns. Wideband measurements can mainly employ the sweeping and hybrid mode of operation of the sniffer, while band-specific measurements can be performed with the real-time measurement mode of the sniffer (if the bandwidth of interest does not surpass the USRP2 hardware limitations, i.e., the maximal bandwidth of 25 MHz).

Ref. [11] shows the usage of the USRP2 sniffer implementation for the 2.4 GHz ISM band inspection. The measurement setup includes the USRP2 hardware comprising the RFX2400 daughterboards. The focus on the campaign was on the definition of the measurement methodology for the referred frequency band. The USRP2 based sniffer implementation is used mainly in the sweeping and hybrid operational mode with maximum hold energy detection type. The results prove that this USRP2 sniffer implementation offers sensing and detection performances comparable to high end-devices performances. Moreover, it has been verified that the hybrid mode of operation of the sniffer offers significantly better performances than the classical sweeping operational mode (Figure 2 [11]).

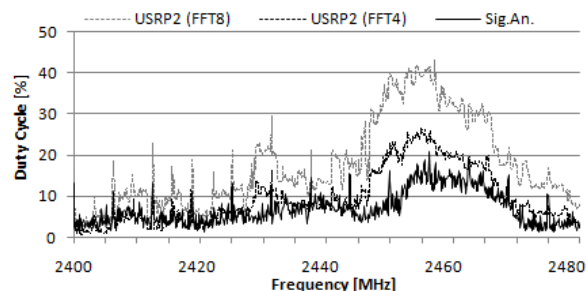


Figure 2. 2.4 GHz ISM duty cycle results of the USRP2 sniffer in hybrid mode and spectrum analyzer, RBW = 100KHz and sweep=1s

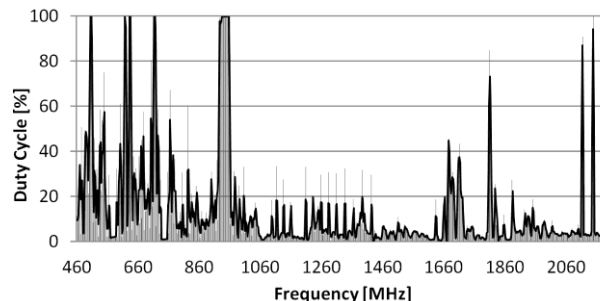


Figure 3. Wideband (460–2200 MHz) duty cycle results in working day busy hour (12:00–18:00 hours) gathered using the USRP2 sniffer in hybrid mode

Wideband measurements have been also performed with the energy detector of the USRP2 based spectrum sniffer implementation using WBX daughterboards [7]. The USRP2 sniffer implementation is used in hybrid operational mode with mean hold detection for these measurements employing FFT with size 16 and receiving bandwidth of 1 MHz, resulting in resolution bandwidth of 62.5 KHz. Figure 3 plots the duty cycle results for the spectrum usage gathered in this campaign.

B. Dynamic Radio Environmental Maps Creation

Additional application of classical energy detection option of the USRP2 spectrum sniffer implementation can be to provide input to the process of dynamic derivation of radio environmental maps (REMs). The USRP2 sniffers can be distributed on various locations in the observed environment and can report received power levels at specific frequency bands to a centralized fusion center. The fusion center gathers the spectrum data from the scattered USRP2 based sniffers and combines the information into REMs. This process can be performed in a dynamic fashion and can impact the discovery of the spatial distribution of the primary users in cognitive network. Therefore, it can facilitate the secondary system spectrum opportunities detection.

Figure 4 depicts the results of a real-time REM calculation demo. The demo scenario consists of two WLAN signal sources, one access point and one laptop computer as a source. Four USRP2 sniffers are placed in an indoor environment and a fusion center dynamically interpolates (with modified IDW interpolation [12]) the data

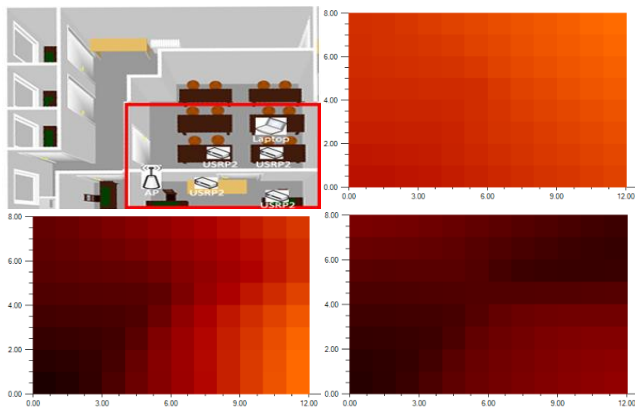


Figure 4. Real-time REM calculation demo: no source (upper right plot), one source (lower left plot), two sources (lower right plot)

from the scattered USRP2 sniffers. As seen on Figure 4, the interpolation data is able to roughly localize both signal sources.

C. Applications based on HOS detector

This part presents two applications of the HOS detector option of the USRP2 sniffer implementation in cognitive environments, i.e., a *channel selection application* and *cooperative channel selection application*. Both applications utilize the USRP2 sniffer implementation in sweeping measurement mode with HOS detection type.

1) Channel selection based on HOS detection

The HOS detector of the USRP2 sniffer implementation can be useful in cognitive radios in order to serve the channel selection process. Namely, the consideration of the higher order statistics values in the channel selection improves the decisions for the best channel. The impact of the HOS detection has been tested on USRP2 devices in a demo based on real environment conditions. The channels width in the demo is chosen to be 2.5 MHz and the center frequencies of the channels are chosen in the manner to include the WiFi channels center frequencies. The demo is focused on the full 2.4GHz ISM band (due to hardware limitations, RFX2400 daughterboards) and Figure 5 plots the environment conditions during the tests. The channel classification criteria is based on average, skewness and kurtosis values of the received power, each of the referred considered with utility factors a , b and c , respectively. The target is to select a channel with statistics closest to the system noise. Figure 6 plots the dependence of the channel selection probability and the utility factors settings. As can be noticed (considering the environment conditions), the worse results are gained when the channel selection depends mostly on the average received power. Predefined frequencies are chosen due to the USRP2 hardware non-idealities – it has different noise power levels and different variations at different frequencies. The decisions on the best channel are more confident when the channel decision depends more on the skewness and kurtosis of the received

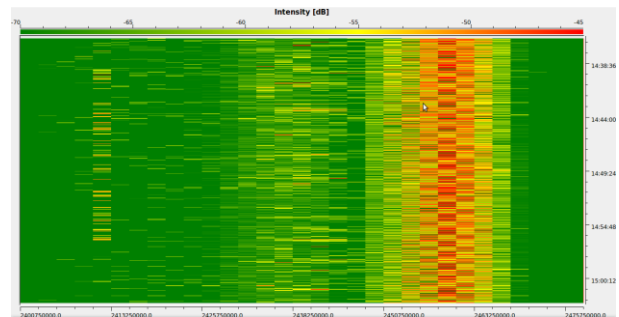


Figure 5. 2.4 GHz ISM spectrum conditions during USRP2 HOS detector demo

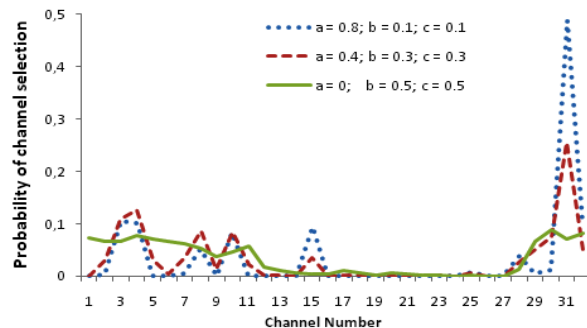


Figure 6. HOS channel selection based on different utility factors settings

power. The best performances in terms of channel selection are gained when the decision depends equally on the skewness and kurtosis of the received power, i.e., $b=c=0.5$. This result reflects the actual environment conditions (illustrated on Figure 5).

The dependence of the channel selection with the sensing time duration is presented in Table I. Here, a channel is considered as free if the duty cycle of the channel occupancy is lower than 5% (5 dB above noise level criteria, inspection time 30 min), and the maximum received energy does not exceed 10 dB above average noise (the most green channels in Figure 5). The channel selection decision improves as the sensing period is higher and sensing period of 3.2 s yields a free channel selection probability of 1 (thus resulting in successful avoidance of busy channels, Table I).

TABLE I. HOS DETECTION: CHANNEL SELECTION PROBABILITY

Sensing period	Busy channel selection probability	Free channel selection probability
800 ms	0.226037	0.773963
1600 ms	0.118825	0.881175
3200 ms	0	1

2) Cooperative channel selection based on HOS data

The HOS detection option of the USRP2 based sniffer implementation has also been included in a cooperative demo comprising USRP2 based cognitive nodes. The cooperative nodes exchange their mean power, skewness and

kurtosis values in distributed fashion according to the RAC²E [13] rendezvous protocol for cognitive ad-hoc networks. After a simple fusion (with averaging) of the gathered data, a source USRP2 based cognitive radio finds the best channel available and starts the communication with a destination USRP2 node. The targeted band in the cooperative demo is the 2.4 GHz ISM band and the environment conditions are the same as in the demo presented in the previous part (the tests were run simultaneously). The demo aims to prove how the cooperative exchange and fusion of the HOS data among the cooperative nodes improves the best channel decision.

TABLE II. COOPERATIVE HOS DETECTION: CHANNEL SELECTION PROBABILITY

Sensing period	Cooperative nodes	Busy channel selection probability	Free channel selection probability
800 ms	1	0.226037	0.773963
	2	0.138968	0.861032
	3	0.071736	0.928264
1600 ms	1	0.118825	0.881175
	2	0.029412	0.970588
	3	0.014706	0.985294

The results (Table II) prove that, as the number of cooperative nodes increases, the channel selection process is more reliable (free channels are most probably to be chosen, whereas busy channels are effectively avoided). As can be noticed, with sensing period of 1600 ms and three cooperative nodes, the probability of selection of a busy channel is 1.5%, and the probability of selection of a free channel is 98.5%.

IV. CONCLUSION AND FUTURE WORKS

Future wireless networks will focus on dynamic and flexible usage of spectrum resources. The importance of spectrum sensing is crucial in such cognitive environments. It provides support for spectrum awareness and dynamic spectrum opportunities detection. Therefore, providing simple and cheap spectrum sensing solutions with good accuracy is an important research challenge. The mid-end devices can be an efficient tool for spectrum sensing, but must be carefully configured and used depending on the actual application.

This paper presents a flexible and efficient USRP2 based spectrum sniffer implementation. The main advantages of the developed C++ sniffer implementation are the support of different modes of operation and detection types, as well as better timing performances than the original python based GNU radio implementation. This enables the developed sniffer implementation to be implemented in various cognitive radio applications. Several of them were presented in the paper and they demonstrate the applicability potential of the USRP2 sniffer implementation in cognitive environments.

Future work will focus on additional detector types implementation, as well as comparative analysis of the

different detectors' performances. The spectrum sniffer will be implemented in additional cognitive radio applications, i.e. different cooperative sensing and fusion methods can be tested in applications comprising the referred sniffer implementation. Furthermore, the USRP2 sniffer implementation can be included in derivation of secondary spectrum usage strategies, such as spectrum driven policy derivation and integration into a policy based system [14].

ACKNOWLEDGMENT

Parts of this work were funded by the EC through the FP7 project FARAMIR (248351) [15]. The authors would like to thank everyone involved.

REFERENCES

- [1] T. Ycek and H. Arslan, "A survey of spectrum sensing algorithms for cognitive radio applications," *IEEE Communications Surveys & Tutorials*, vol. 11, no. 1, pp. 116–160, 2009.
- [2] M. Lopez-Benitez et al, "Performance of spectrum sensing for cognitive radio based on field measurements of various radio technologies," in *Proceedings of the 16th European Wireless Conference (EW) 2010, Special session on Cognitive Radio*, Lucca, Italy, April 12-15, 2010.
- [3] M. Wellens and P. Mähönen, "Lessons Learned from an Extensive Spectrum Occupancy Measurement Campaign and a Stochastic Duty Cycle Model", *Springer Mobile Networks and Applications*, 2009.
- [4] Z. Quan et al, "An Optimal Strategy for Cooperative Spectrum Sensing in Cognitive Radio Networks", *IEEE Global Communications Conference (GLOBECOM) 2007*, Washington, DC, USA, November, 2007.
- [5] J. Unnikrishnan et al, "Cooperative Spectrum Sensing and Detection for Cognitive Radio", *IEEE Global Communications Conference (GLOBECOM) 2007*, Washington, DC, USA, Nov. 2007.
- [6] R. Vuyyuru et al, "Evaluation of Energy Based Spectrum Sensing Algorithm for Vehicular Networks, SDR Forum Technical Conference 2009, December 2009.
- [7] Universal Software Radio Peripheral 2 (USRP2). Information available at: www.ettus.com.
- [8] GNU Radio software development toolkit. Information available at: <http://gnuradio.org/redmine/wiki/gnuradio>.
- [9] D. N. Joanes, C. A. Gill, "Comparing measures of sample skewness and kurtosis", *Journal of the Royal Statistical Society: Series D (The Statistician)*, Volume 47, Issue 1, pages 183–189, April 1998.
- [10] Z. Chen et al, "Demonstration on Real time Spectrum Sensing for Cognitive Radio", *IEEE Communications Letters*, vol.14, no.10,2010.
- [11] D. Denkovski, M. Pavloski, V. Atanasovski and L. Gavrilovska, "Parameter settings for 2.4GHz ISM spectrum measurements," *3rd International Symposium on Applied Sciences in Biomedical and Communication Technologies (ISABEL) 2010*, Rome, Italy, 7-10 November, 2010.
- [12] R. J. Renka, "Multivariate interpolation of large sets of scattered data," *ACM Transactions on Mathematical Software* 14, 2, 139–148, 1988.
- [13] V. Pavlovska, D. Denkovski, V. Atanasovski and L. Gavrilovska, "Novel Rendezvous Protocol for Asynchronous Cognitive Radios in Cooperative Environments", *the 21st Annual IEEE International Symposium on Personal, Indoor and Mobile Radio Communications (PIMRC) 2010*, Istanbul, Turkey, 26-30 September, 2010.
- [14] D. Denkovski, V. Pavlovska, V. Atanasovski and L. Gavrilovska, "Novel Policy Reasoning Architecture for Cognitive Radio Environments", *IEEE Global Communications Conference (GLOBECOM) 2010*, Miami, USA, 6-10 December, 2010.
- [15] EC FP7 project FARAMIR, Information available at: <http://www.ict-faramir.eu>.